DEVELOPMENT OF ELECTROCHEMICAL AND OPTICAL SENSORS FOR SOME FOOD ADDITIVES AND PHARMACEUTICALS

Thesis submitted to

Cochin University of Science and Technology

in partial fulfilment of the requirements

for the award of the degree of

Doctor of Philosophy

in

Chemistry

by

Soumya T. Cyriac

Department of Applied Chemistry

Cochin University of Science and Technology

Kochi – 22

October 2017

Development of Electrochemical and Optical Sensors for some Food Additives and Pharmaceuticals

Ph.D. Thesis under the Faculty of Sciences

By

Soumya T. Cyriac
Research Fellow
Department of Applied Chemistry
Cochin University of Science and Technology
Kochi, India 682022
Email: soumyatc@gmail.com

Supervising Guide

Dr. K. Girish Kumar
Professor & Head
Department of Applied Chemistry
Cochin University of Science and Technology
Kochi, India 682022
Email: giri@cusat.ac.in

Department of Applied Chemistry
Cochin University of Science and Technology
Kochi, India 682022

October 2017

DEPARTMENT OF APPLIED CHEMISTRY
COCHIN UNIVERSITY OF SCIENCE AND TECHNOLOGY
KOCHI - 682022, INDIA

Dr. K. Girish Kumar
Professor & Head

Tel: 0484 - 2575804
E-mail: chem.@cusat.ac.in

Date: 30 October 2017

Certificate

Certified that the work entitled **"Development of Electrochemical and Optical Sensors for Some Food Additives and Pharmaceuticals"**, submitted by Ms. Soumya T. Cyriac, in partial fulfilment of the requirements for the degree of Doctor of Philosophy in Chemistry to Cochin University of Science and Technology, is an authentic and bonafide record of the original research work carried out by her under my supervision at the Department of Applied Chemistry. Further, the results embodied in this thesis, in full or in part, have not been submitted previously for the award of any other degree. All the relevant corrections and modifications suggested by the audience during the pre-synopsis seminar and recommended by the Doctoral committee have been incorporated in the thesis.

K. Girish Kumar
(Supervising Guide)

Declaration

I hereby declare that the work presented in this thesis entitled **"Development of Electrochemical and Optical Sensors for some Food Additives and Pharmaceuticals"** is based on the original work carried out by me under the guidance of Dr. K. Girish Kumar, Professor & Head, Department of Applied Chemistry, Cochin University of Science and Technology and has not been included in any other thesis submitted previously for the award of any degree.

Kochi-22
30/10/2017

Soumya T. Cyriac

Dedicated to

My Parents…

Acknowledgement

Completion of this work was possible with the support extended by several people. I would like to acknowledge and thank each one of them for their help and guidance during this amazing journey.

Words are deserting my thoughts to express my thanks and gratitude to Dr. K. Girish Kumar, Professor & Head, Department of Applied Chemistry, Cochin University of Science and Technology, Kochi, who has given me values of sincerity, perseverance, tolerance, patience to life and personality. I am extremely grateful to him for providing resolute guidance and valuable advice which always came with faith and confidence in my abilities during my research programme. I also remain indebted for his fatherly support during the times when I was really down. Without his support, it would have been very difficult to complete this research work successfully.

It is my privilege to have Dr. K. Sreekumar, Professor, Department of Applied Chemistry, Cochin University of Science and Technology, Kochi, as my Doctoral Committee Member. I am thankful to him for resolute guidance, constructive counsel, critical appreciation and continuous help during course of this study for which I shall remember him with great respect for all the time to come.

I take this opportunity to express my extreme thanks to all faculty members of Department of Applied Chemistry, CUSAT for their inspiration and timely help. I also acknowledge help of various non – teaching staff members who rendered me a lot of support.

At this point, special mention must be made about Dr. Anitha I, Principal, Government College, Kongad, Palakkad, for her keen interest in all my matters with extreme gratefulness in my mind.

I express my gratefulness to Manager Rev. Fr. Nelson Thaiparambil, Principal Dr. Mathew V and Management of St. Michael's college, Cherthala for

all the supports given to me. I acknowledge my colleagues at St. Michael's college, Cherthala, Dr. Manoj, Seena miss, Dr. Peral, Liya miss, Libin sir, Dr. Beena and Dr. Saranya for their help and good wishes.

Research scholars often talk about loneliness during their course of study but this is something which I never experienced in our lab. Very special thanks to all my lab mates for imparting a lot of help by sharing professional skills and knowledge. During my initial period of research, my seniors Dr. Rema, Dr. Sindhu, Dr. Renjini, Dr. Leena, Dr. Laina, Dr. Sobhana, Dr. Theresa, Dr. Divya and Dr. Anuja had given me valuable tips that made my research to go unhindered. My dear lab mates, Jesny chechi, Dr. Jintha, Dr. Monica, Zafna, Unni, Ammu, Ambily, Sheela Miss, Shalini, Sanu and Manna have all extended their support in a very special way, and I gained a lot from them, through their personal and scholarly interactions.

I am greatly indebted to Unni and Ammu for their untiring assistance during preparation of thesis. No appropriate word could be traced in the lexicon of heart for affection, moral support and constant inspiration bestowed upon me by my friends Sreejith, Ajith, Sruthy, Meera, Shanty and Gopika. I would like to extend my gratefulness to all my friends in polymer, biochemistry, physical, organic and inorganic labs. A special thanks to Dr. Rakesh and Dr. Rethikala, my M.Sc. classmates, for their help, support and well wishes.

I owe a lot to my parents, who encouraged and helped me at every stage of my personal and academic life and longed to see this achievement come true. I deeply miss my father, who is not with me to share this joy. Words cannot express how much I am grateful to my mother, sisters and in-laws for all the sacrifices that you've made on my behalf. I am also grateful to my uncles, aunties and cousins who have supported me all way along.

I am very much indebted to my in-laws who supported me in every possible way to see completion of this work. Your prayer has been the force which sustained me this far. I fondly recall with love, emotional support and consistent encouragement exhibited by my husband and son.

For the financial services rendered, I thank Council of Scientific and Industrial Research (CSIR), India for fellowship, Directorate of Extramural Research and Property Rights, DRDO, New Delhi and Kerala State Council for Science, Technology and Environment, Kerala for the funding assistance in the form of projects.

I am happily acknowledging help extended by scientists at STIC, CUSAT, Department of Photonics, CUSAT and Amrita Center for Nanosciences, Amrita University, Kochi for analyzing various samples.

Above all, I bow myself in front of the ***almighty*** *for all blessings showered upon me throughout my life.*

Soumya T. Cyriac

Preface

Sensors have found extensive applications in diverse fields such as medicine, agriculture, industry, defence and transport. They offer attractive means to solve concerns related to everyday life of man. Sensors and sensing devices are increasingly captivating the attention of scientists across globe. Chemical sensors are miniaturised devices that can deliver information in presence of specific compounds or ions, even in complex biological samples. Chemical sensing consists of two major steps: recognition and transduction. Based on their signal transduction methods, chemical sensors can be categorized into electrochemical sensors, optical sensors, mass sensitive sensors and heat sensitive sensors.

Electrochemical and optical sensors are developed for the determination of food additives and pharmaceuticals during the course of present study. Based on excellent electrochemical properties of glassy carbon electrodes (GCE), chemically modified with polymers and gold nanoparticles, four voltammetric sensors were developed for food additives, propyl gallate, *tert*-butylhydroquinone, ponceau 4R and acid green 50. Nanostructured gold nanoparticles were used for colorimetric determination of tetracycline, a pharmaceutical and ethylenediamine passivated carbon dots were used as fluorescent probes for food colorant, sunset yellow.

Thesis entitled "Development of electrochemical and optical sensors for some food additives and pharmaceuticals" is divided into nine chapters. A brief outline of chapters is given below.

Chapter 1 outlines a brief introduction to different types of chemical sensors and discusses in detail about voltammetric, colorimetric and fluorescent sensors. Detailed reviews on research work in the field of above sensors are also incorporated in this chapter.

Chapter 2 gives a brief description of materials and methods used for fabrication of various sensors. Instruments used for different studies are also mentioned. Preparations of different kinds of buffer solutions and description of reference methods for validating applicability of developed sensors are also included in this chapter.

Chapter 3 reports development of gold nanoparticle/poly(*p*-aminobenzenesulphonic acid) composite modified glassy carbon electrode (AuNP/poly(*p*-ABSA)/GCE) for electrochemical determination of propyl gallate (PG). Experimental parameters such as effect of pH, number of cycles of electrodeposition, number of cycles of electropolymerization and scan rate were optimized. Fundamental kinetic parameters for electrochemical oxidation of PG were also optimized. A plausible two electron mechanism was suggested for electrochemical oxidation of PG. Suitability of developed sensor for determination of PG in vegetable oil samples have also been dealt in detail.

Chapter 4 presents electrochemical sensing of *tert*-butylhydroquinone (TBHQ), a synthetic phenolic antioxidant using poly bromophenol blue modified GCE. Optimization studies of developed sensor and response characteristics are also explained in this chapter. TBHQ undergoes a two electron oxidation to corresponding quinone involving a two-step mechanism. Analytical application of developed sensor was demonstrated by successful determination of TBHQ in coconut and sunflower oil samples.

Chapter 5 details electrochemical oxidation of ponceau 4R (P4R) using poly (L-cysteine) modified glassy carbon electrode [poly (L-Cys)/GCE]. Modified electrode was characterized by scanning electron microscopy, atomic force microscopy, electrochemical impedance spectroscopy and cyclic voltammetry. Experimental conditions for sensor fabrication were optimized. Kinetic parameters of electrochemical reaction such as heterogeneous rate constant, charge transfer coefficient, number of electrons transferred and diffusion

coefficient were determined. Proposed method has been successfully applied for determination of P4R in soft drink samples.

Chapter 6 describes development of an electrochemical sensor for quantification of acid green 50 (AG) using poly glycine modified GCE. Optimization studies of developed method are discussed in detail in this chapter. Various kinetic parameters such as standard heterogeneous rate constant, number of electrons exchanged and diffusion coefficient were calculated. Practical applications of proposed sensor are also discussed in this chapter.

Chapter 7 focuses application of citrate capped gold nanoparticles (AuNPs) as a colorimetric probe for quantification of tetracycline (TET), a polyketide antibiotic. Proposed assay is based on distance dependent optical properties of AuNPs and TET triggered self-assembly of AuNPs in the presence of Cu^{2+}. Aggregation of AuNPs, induces a color change from red-to-blue (or purple). Developed colorimetric sensor exhibits good analytical figures of merit and shows promising practical applications.

Chapter 8 details green synthesis of ethylenediamine (EDA) passivated carbon dots (CDs) using Hibiscus leaves as carbon source, via microwave irradiation process. Eventually, optical sensing aspects of CDs have been evaluated on food colorant, sunset yellow (SY). Fluorescence intensity of EDA passivated CDs quenched dramatically in presence of SY. Based on this, an efficient turn off sensor was developed for quantification of SY. Developed fluorescence assay was employed for selective and sensitive determination of SY in soft drink samples.

Chapter 9 gives objectives, summary and future outlook of research work.

Contents

Chapter 1

INTRODUCTION.....01 - 45

1.1 Chemical sensors..... 02
1.2 Electrochemical sensors 03
1.3 Voltammetric sensors..... 03
1.4 Voltammetric cell set up..... 04
1.4.1 Working electrode..... 04
1.4.1.1 Glassy carbon electrode..... 05
1.4.2 Reference electrode 05
1.4.3 Auxiliary electrode/Counter electrode..... 06
1.5 Techniques for electrochemical analysis..... 06
1.5.1 Cyclic voltammetry (CV) 07
1.5.2 Linear sweep voltammetry (LSV)..... 07
1.5.3 Differential pulse voltammetry (DPV) 08
1.5.4 Square wave voltammetry (SWV) 08
1.5.5 Chronoamperometry (CA)..... 08
1.5.6 Chronocoulometry (CC)..... 09
1.5.7 Electrochemical impedance spectroscopy (EIS) 10
1.6 Electrode double layer..... 11
1.6.1 Different forms of mass transport 12
1.6.1.1 Diffusion..... 12
1.6.1.2 Convection..... 13
1.6.1.3 Migration..... 13
1.6.2 Kinetics of electrode reaction 14
1.6.2.1 Reversible systems 14
1.6.2.2 Irreversible systems..... 15
1.6.2.3 Quasi-reversible systems..... 16
1.6.2.4 Heterogeneous rate transfer constant..... 16
1.7 Chemically modified electrodes 17
1.7.1 Polymer film modified electrodes 18
1.7.2 Gold nanoparticles..... 19
1.8 Literature review of electrochemical sensors based on polymer film and gold nanoparticles modified electrodes..... 20
1.9 Optical sensors..... 29
1.10 Colorimetric sensors..... 31
1.10.1 Gold nanoparticles as colorimetric sensors..... 31
1.10.2 Literature review of colorimetric sensors based on gold nanoparticles probes 33
1.11 Fluorescence sensors 35

1.11.1 Quenching of fluorescence 37
1.11.1.1 Dynamic or collisional quenching 37
1.11.1.2 Static or contact quenching 38
1.11.1.3 Inner filter effect 38
1.11.2 Fluorophores or fluorescent probes 39
1.11.2.1 Stokes shift 40
1.11.2.2 Fluorescence quantum yields and life time 40
1.11.3 Carbon dots 41
1.11.3.1 Surface passivation and functionalization of CDs 42
1.11.3.2 Synthesis of CDs 42
1.11.3.3 Green synthesis of CDs 42
1.11.4 Literature review of fluorescence sensors based on green synthesis of CDs 43
1.12 Scope of present investigation 44

Chapter 2

MATERIALS AND INSTRUMENTATION ..... 47 -52

2.1 Reagents 47
2.2 Instruments 48
2.3 Cleaning of GCE 49
2.4 Preparation of buffer solutions 49
2.4.1 Preparation of acetate buffer solutions (ABS) 49
2.4.2 Preparation of phosphate buffer solutions (PBS) 50
2.5 Reference methods for sample analysis 50
2.5.1 Reference method for antioxidant, propyl gallate 50
2.5.2 Reference method for antioxidant, *tert*-butylhydroquinone 50
2.5.3 Reference method for food colorants 51

Chapter 3

VOLTAMMETRIC SENSOR FOR PROPYL GALLATE BASED ON GOLD NANOPARTICLE/POLY (*P*-AMINOBENZENESULPHONIC ACID) COMPOSITE MODIFIED GLASSY CARBON ELECTRODE ..... 53 - 80

3.1 Introduction 54
3.2 Experimental 56
3.2.1 Preparation of AuNP/poly(*p*-ABSA)/GCE 56
3.2.2 Experimental procedure 58
3.2.3 Treatment of vegetable oil samples 59
3.3 Results and discussion 59
3.3.1 Characterisation of electrode surface 59
3.3.1.1 Surface morphology of bare GCE and AuNP/poly(*p*-ABSA)/GCE 59

3.3.1.2 Surface area study 60
3.3.1.3 Electrochemical impedance spectroscopic studies 61
3.3.2 Electrochemical behavior of PG on bare and modified GCE 62
3.3.3 Effect of Supporting electrolyte and pH 64
3.3.4 Effect of poly(*p*-ABSA) film thickness on electrochemical response of PG 66
3.3.5 Effect of number of cycles of electrodeposition 67
3.3.6 Effect of scan rate 68
3.3.7 Analytical parameters 70
3.3.8 Evaluation of kinetic parameters 72
3.3.9 Chronoamperometric measurements 75
3.3.10 Interference study 77
3.3.11 Reproducibility and stability 77
3.3.12 Application study 78
3.4 Conclusions 78

Chapter 4

VOLTAMMETRIC SENSOR FOR TERTIARY BUTYLHYDROQUINONE BASED ON POLY BROMOPHENOL BLUE MODIFIED GLASSY CARBON ELECTRODE ..... 81 - 105

4.1 Introduction 82
4.2 Experimental 85
4.2.1 Preparation of poly BPB film modified GCE 85
4.2.2 Experimental procedure 86
4.2.3 Treatment of edible vegetable oil samples 86
4.2.4 HPLC-UV as the standard method 86
4.3 Results and discussion 87
4.3.1 Characterisation of electrode surface 87
4.3.1.1 Surface morphology of bare GCE and poly(BPB)/GCE 87
4.3.1.2 Surface area study 88
4.3.1.3 Electrochemical impedance spectroscopic studies 90
4.3.2 Electrochemical behaviour of TBHQ on bare and modified GCE 90
4.3.3 Optimizing the variables of developed method 92
4.3.3.1 Influence of supporting electrolyte and pH 93
4.3.3.2 Effect of number of cycles of electropolymerization 94
4.3.4 Influence of scan rate 95
4.3.5 Determination of TBHQ 97
4.3.6 Evaluation of kinetic parameters 99
4.3.7 Chronoamperometry 100
4.3.8 Interference study 102
4.3.9 Reproducibility, repeatability and stability 102

4.3.10 Analytical performance 103
4.4 Conclusions 103

Chapter 5

VOLTAMMETRIC SENSOR FOR PONCEAU 4R BASED ON POLY L-CYSTEINE MODIFIED GLASSY CARBON ELECTRODE ..... 107 - 133

5.1 Introduction 108
5.2 Experimental 110
5.2.1 Preparation of poly(L-Cys)/GCE 110
5.2.2 Analytical procedure 111
5.2.3 Sample treatment 112
5.3 Results and discussion 112
5.3.1 Characterisation of electrode surface 112
5.3.1.1 Surface morphology of bare GCE and poly(L-Cys)/GCE 112
5.3.1.2 Surface area study 113
5.3.1.3 Electrochemical impedance spectroscopic studies 115
5.3.2 Electrochemical behaviour of P4R on bare and poly(L-Cys) film modified electrode 116
5.3.3 Optimization of experimental parameters 118
5.3.3.1 Influence of supporting electrolyte and pH 118
5.3.3.2 Influence of accumulation time 119
5.3.3.3 Influence of number of cycles of electropolymerization 120
5.3.4 Influence of scan rate 121
5.3.5 Calibration plot and limit of detection 123
5.3.6 Number of electrons 125
5.3.7 Reaction mechanism 125
5.3.8 Evaluation of kinetic parameters 126
5.3.9 Chronocoulometric studies 128
5.3.10 Repeatability, reproducibility and stability of poly(L-Cys)/GCE 130
5.3.11 Interference study 130
5.3.12 Application study 131
5.4 Conclusions 131

Chapter 6

VOLTAMMETRIC SENSOR FOR ACID GREEN 50 BASED ON POLY GLYCINE MODIFIED GLASSY CARBON ELECTRODE ..... 135 - 159

6.1 Introduction 136
6.2 Experimental 139

6.2.1 Preparation of poly Gly/GCE 139
6.2.2 Analytical procedure 140
6.2.3 Sample treatment 140
6.3 Results and discussion 140
6.3.1 Characterisation of electrode surface 140
6.3.1.1 Surface morphology of bare GCE and poly Gly/GCE 140
6.3.1.2 Surface area study 142
6.3.1.3 Electrochemical impedance spectroscopic studies 143
6.3.1.4 Electrochemical behaviour of AG on poly Gly/GCE 144
6.3.2 Optimization of experimental conditions 145
6.3.2.1 Influence of supporting electrolyte 145
6.3.2.2 Influence of pH 146
6.3.2.3 Effect of number of cycles of electropolymerization 146
6.3.2.4 Influence of accumulation time 147
6.3.3 Effect of scan rate 148
6.3.4 Calibration plot and limit of detection 150
6.3.5 Number of electrons 151
6.3.6 Evaluation of kinetic parameters 152
6.3.7 Chronocoulometric studies 154
6.3.8 Repeatability, reproducibility and stability of poly Gly/GCE 156
6.3.9 Interference study 157
6.3.10 Application study 157
6.4 Conclusion 157

Chapter 7

COLORIMETRIC SENSOR FOR TETRACYCLINE BASED ON GOLD NANOPARTICLE PROBE ..... 161 - 180

7.1 Introduction 162
7.2 Experimental 164
7.2.1 Preparation of AuNPs 164
7.2.2 Colorimetric determination of TET 164
7.2.3 Analysis of pharmaceutical formulations 164
7.3 Results and discussion 165
7.3.1 Characterisation of AuNPs 165
7.3.2 Colorimetric assay of TET 167
7.3.3 Influence of reaction media 168
7.3.4 Effect of various metal ions as cross-linking agents 169
7.3.5 Effect of concentration of Cu^{2+} on the absorbance of AuNPs 170
7.3.6 Influence of time on the absorption ratio of AuNPs 170
7.3.7 Colorimetric determination of TET 171
7.3.8 Mechanism of colorimetric assay 174
7.3.9 Selectivity 178

7.3.10 Application study 179
7.4 Conclusions..... 179

Chapter 8

CARBON DOTS BASED FLUORESCENCE SENSOR FOR SUNSET YELLOW..... 181 - 206

8.1 Introduction..... 182
8.2 Experimental..... 184
8.2.1 Synthesis of EDA passivated CDs 184
8.2.2 Analytical procedure 186
8.2.3 Analysis of real samples 186
8.3 Results and discussion..... 186
8.3.1 Optimization of synthetic condition of CDs 186
8.3.1.1 Influence of microwave irradiation time on formation of CDs 186
8.3.1.2 Influence of amount of passivating agent on CDs..... 187
8.3.2 Characterization of CDs 188
8.3.3 Measurement of quantum yield 195
8.3.4 Optimization of experimental parameters 197
8.3.4.1 Effect of medium..... 197
8.3.4.2 Effect of pH 197
8.3.4.3 Effect of irradiation time on fluorescence intensity..... 198
8.4 Fluorescence quenching of CDs by SY..... 199
8.5 Mechanism of fluorescence quenching 201
8.6 Selectivity 204
8.7 Application in real samples 205
8.8 Conclusion 206

Chapter 9

SUMMARY ..... 207 - 209

9.1 Objectives of work 207
9.2 Summary of work done 208
9.3 Future outlook 209

REFERENCES ..... 211 - 233

LIST OF PUBLICATIONS..... 235 - 236

List of Tables

Table 2.1: Preparation of 0.1 M acetate buffer solution 51
Table 2.2: Preparation of 0.1 M phosphate buffer solution 52
Table 3.1: Comparison of different modified electrodes for detection of PG 79
Table 3.2: Comparison of different PG sensors 79
Table 3.3: Effect of possibly interfering species on the signal of 1×10^{-4} M PG 79
Table 3.4: Determination of PG in food samples 80
Table 4.1: Comparison of different modified electrodes for detection of TBHQ 104
Table 4.2: Comparison of different TBHQ sensors 104
Table 4.3: Effect of possibly interfering species on the signal of 5×10^{-6} M TBHQ 104
Table 4.4: Determination of TBHQ in food samples 105
Table 5.1: Comparison of different modified electrodes for detection of P4R 132
Table 5.2: Comparison of different P4R sensors 132
Table 5.3: Effect of possibly interfering species on signal of 1.0×10^{-5} M P4R 132
Table 5.4: Determination of P4R in soft drink samples 133
Table 6.1: Comparison of different modified electrodes for detection of AG 158
Table 6.2: Comparison of different methods for determination of AG 158
Table 6.3: Effect of possibly interfering species on the signal of 5.0×10^{-5} M AG 158
Table 6.4: Determination of AG in soft drink samples 159
Table 7.1: Comparison of different methods for determination of TET 180
Table 7.2: Determination of TET in pharmaceutical formulation 180
Table 8.1: Comparison of different methods for determination of SY 206

List of Figures

Figure 1.1: Jablonski diagram..... 36

Figure 3.1: Structure of PG..... 54

Figure 3.2: Cyclic voltammograms obtained for electropolymerization of *p*-ABSA on GCE..... 57

Figure 3.3: Cyclic voltammograms obtained for electrodeposition of AuNPs on poly(*p*-ABSA)/GCE 58

Figure 3.4: SEM images of (a) bare GCE (b) AuNP/poly(*p*-ABSA)/GCE 60

Figure 3.5: (a) Overlay of cyclic voltammograms of 2.0×10^{-3} M $K_3[Fe(CN)_6]$ on bare GCE at various scan rates (b) plot of current *vs* square root of scan rate for bare GCE 61

Figure 3.6: (a) Overlay of cyclic voltammograms of 2.0×10^{-3} M $K_3[Fe(CN)_6]$ on AuNP/poly(*p*-ABSA)/GCE at various scan rates (b) plot of current *vs* square root of scan rate for AuNP/poly(*p*-ABSA)/GCE..... 61

Figure 3.7: EIS spectra of (a) bare GCE (b) AuNP/poly(*p*-ABSA)/GCE in 5.0×10^{-3} M $[Fe(CN)_6]^{3-/4-}$ in 0.1 M KCl at a frequency range 1 -10^5 Hz..... 62

Figure 3.8: Cyclic voltammograms of 1.0×10^{-4} M PG at bare GCE, AuNP/GCE, poly(p-ABSA)/GCE and AuNP/poly(*p*-ABSA)/ GCE in 0.1 M PBS of pH 7.0 63

Figure 3.9: Differential pulse voltammograms of 1.0×10^{-4} M PG at bare GCE (a) and AuNP/poly(*p*-ABSA)/GCE in 0.1 M PBS of pH 7.0..... 64

Figure 3.10: Influence of pH on oxidation peak current and peak potential of 1.0×10^{-4} M PG..... 65

Figure 3.11: Influence of cycle number of electropolymerization on peak current of 1.0×10^{-4} M PG..... 67

Figure 3.12: Influence of cycle number of electrodeposition on peak current of 1.0×10^{-4} M PG..... 68

Figure 3.13a: Overlay of linear sweep voltammograms of PG on AuNP/poly (*p*-ABSA)/GCE at various scan rates 69

Figure 3.13b: Plot of anodic peak currents *vs* square root of scan rate of PG..... 69

Figure 3.14: Plot of log i *vs* log υ 70

Figure 3.15a: Overlay of differential pulse voltammograms for oxidation of PG at various concentrations..... 71

Figure 3.15b: Plot of peak current *vs* concentrations of PG in the range 1.0×10^{-4} to 9.0×10^{-6} M..... 71

Figure 3.16: Tafel plot 72
Figure 3.17: Variation of E_{pa} with ln υ 74
Figure 3.18: Variation of E_{pa} with scan rate 75
Figure 3.19a: Chronoamperograms obtained at AuNP/poly(*p*-ABSA)/GCE in 0.1 M PBS (pH 7.0) for different concentrations of PG 76
Figure 3.19b: Plots of current *vs* $t^{-1/2}$ derived from the chronoamperograms of Fig. 3.19a 76
Figure 3.19c: Plot of slope of straight lines against variousconcentration of PG 77
Figure 4.1: Structure of TBHQ 83
Figure 4.2: Cyclic voltammograms obtained for electropolymerization of BPB on GCE 85
Figure 4.3: SEM images of (a) bare GCE (b) poly BPB/GCE 87
Figure 4.4: AFM images of (a) bare GCE (b) poly BPB/GCE 88
Figure 4.5: (a) Overlay of cyclic voltammograms of 2.0×10^{-3} M $K_3[Fe(CN)_6]$ on bare GCE at various scan rates (b) plot of current *vs* square root of scan rate for bare GCE 89
Figure 4.6: (a) Overlay of cyclic voltammograms of 2.0×10^{-3} M $K_3[Fe(CN)_6]$ on poly BPB/GCE at various scan rates (b) plot of current *vs* square root of scan rate for poly BPB/GCE 89
Figure 4.7: EIS spectra of (a) bare GCE (b) poly BPB/GCE in 5.0×10^{-3} $[Fe(CN)_6]^{3-/4-}$ in 0.1 M KCl at the frequency range 1 -10^5 Hz 90
Figure 4.8: Cyclic voltammograms of 1.0×10^{-3} M TBHQ at (a) bare GCE (b) poly BPB/GCE in PBS of pH 7.0 91
Figure 4.9: Differential pulse voltammograms of 1.0×10^{-3} TBHQ at (a) bare GCE (b) poly BPB/GCE 92
Figure 4.10: Influence of pH on oxidation peak current and peak potential of 5.0×10^{-6} M TBHQ 93
Figure 4.11: Influence of cycle number of electropolymerization on the peak current of 5.0×10^{-6} M TBHQ. 95
Figure 4.12: Overlay of cyclic voltammograms of TBHQ on poly BPB/GCE at various scan rates. 96
Figure 4.13: Plot of anodic and cathodic peak currents *vs* square root of scan rate for TBHQ 97
Figure 4.14: Plot of log i *vs* log υ 97
Figure 4.15a: Overlay of differential pulse voltammograms for oxidation of TBHQ at various concentrations 98

Figure 4.15b: Calibration curve for TBHQ in the concentration range $1.0 \times 10^{-5} – 1.0 \times 10^{-6}$ M 98
Figure 4.16: Variation of E_{pa} and E_{pc} with log υ..... 100
Figure 4.17a: Chronoamperograms obtained at poly BPB/GCE in 0.1 M PBS (pH 7.0) for different concentrations of TBHQ..... 101
Figure 4.17b: Plots of I *vs* $t^{-1/2}$ derived from the chronoamperograms of Fig. 4.17a 101
Figure 4.17c: Plot of slope of the straight lines against the concentration of TBHQ 102
Figure 5.1: Structure of P4R..... 108
Figure 5.2: Cyclic voltammograms obtained for electropolymerization of L-Cys on GCE..... 111
Figure 5.3: SEM images of (a) bare GCE (b) poly(L-Cys)/GCE..... 113
Figure 5.4: AFM images of (a) bare GCE (b) poly(L-Cys)/GCE 113
Figure 5.5: (a) Overlay of cyclic voltammograms of 2.0×10^{-3} M $K_3[Fe(CN)_6]$ on bare GCE at various scan rates (b) plot of current *vs* square root of scan rate for bare GCE 114
Figure 5.6: (a) Overlay of cyclic voltammogram of poly(L-Cys)/GCE at different scan rates (b) plot of current vs square root of scan rate for poly(L-Cys)/GCE..... 115
Figure 5.7: EIS spectra of (a) bare GCE (b) poly(L-Cys)/GCE in 5.0×10^{-3} M $[Fe(CN)_6]^{3-/4-}$ in 0.1 M KCl at the frequency range 1 - 10^5 Hz 116
Figure 5.8: Cyclic voltammograms of 1.0×10^{-4} M P4R at (a) bare GCE (b) poly(L-Cys)/GCE in 0.1 M PBS of pH 7.0 117
Figure 5.9: Square wave voltammograms of 1.0×10^{-4} M P4R at (a) bare GCE (b) poly(L-Cys)/GCE in 0.1 M PBS of pH 7.0 117
Figure 5.10: Influence of pH on oxidation peak potential and peak current of 1.0×10^{-5} M P4R..... 119
Figure 5.11: Influence of accumulation time on anodic peak current of 1.0×10^{-5} M P4R..... 120
Figure 5.12: Influence of number of cycles of electropolymerization on anodic peak current of 1.0×10^{-5} M P4R..... 121
Figure 5.13: Overlay of cyclic voltammograms of 1.0×10^{-4} M P4R on poly(L-Cys)/GCE at various scan rates 122
Figure 5.14: Variation of anodic and cathodic peak currents of 1.0×10^{-4} M P4R with scan rate 122
Figure 5.15: Plot of log i *vs* log υ..... 123

Figure 5.16a: Overlay of square wave voltammograms for electrooxidation of P4R on poly(L-Cys)/GCE at various concentrations in 0.1 M PBS of pH 7.0 124
Figure 5.16b: Calibration curve of P4R in the concentration range $1.0 \times 10^{-5} – 1.0 \times 10^{-6}$ M 124
Figure 5.17: Variation of E_{pa} and E_{pc} with log υ..... 126
Figure 5.18a: Chronocoulograms obtained at poly(L-Cys)/GCE in 0.1 M PBS (pH 7.0) in the concentration range 1.1×10^{-3} - 4.0×10^{-4} M 129
Figure 5.18b: Plot of Q *vs* $t^{1/2}$ derived from the chronocoulograms of Fig. 5.18a..... 129
Figure 5.18c: Plot of slope of Q *vs* $t^{1/2}$ graph against concentration of P4R..... 130
Figure 6.1: Structure of AG 136
Figure 6.2: Cyclic voltammograms obtained for electropolymerization of Gly on GCE 139
Figure 6.3: SEM images of (a) bare GCE (b) poly Gly/GCE..... 141
Figure 6.4: AFM images of (a) bare GCE (b) poly Gly/GCE..... 141
Figure 6.5: (a) Overlay of cyclic voltammograms of 2.0×10^{-3} M $K_3[Fe(CN)_6]$ on bare GCE at various scan rates (b) plot of current *vs* square root of scan rate for bare GCE 142
Figure 6.6: (a) Overlay of cyclic voltammograms of 2.0×10^{-3} M $K_3[Fe(CN)_6]$ on poly Gly/GCE at various scan rates (b) plot of current vs square root of scan rate for poly Gly/GCE 143
Figure 6.7: EIS spectra of (a) bare GCE (b) poly Gly/GCE in 5.0×10^{-3} M $[Fe(CN)_6]^{3-/4-}$ in 0.1 M KCl at the frequency range 1 -10^5 Hz..... 143
Figure 6.8: Cyclic voltammograms of 1.0×10^{-3} M AG at (a) bare GCE (b) poly Gly/GCE in PBS of pH 7.0 145
Figure 6.9: Influence of pH on the oxidation peak current and peak potential of 5.0×10^{-5} M AG 146
Figure 6.10: Influence of cycle number of electropolymerization on the peak current of 5.0×10^{-5} M AG. 147
Figure 6.11: Influence of accumulation time on the peak current of 5.0×10^{-5} M AG 148
Figure 6.12a: Overlay of linear sweep voltammograms of 1.0×10^{-4} M AG on poly Gly/GCE at various scan rates 149
Figure 6.12b: Plot of anodic peak currents *vs* scan rate of 1.0×10^{-4} M AG..... 149
Figure 6.13a: Overlay of square wave voltammograms for oxidation of AG at various concentrations 150
Figure 6.13b: Plot of concentrations of AG *vs* peak current in the range 1.0×10^{-4} to 9.0×10^{-6} M 151

Figure 6.14: Variation of E_{pa} with ln υ 153
Figure 6.15: Variation of E_{pa} with υ 153
Figure 6.16a: Chronocoulograms obtained at poly Gly/GCE in 0.1 M PBS (pH 7.0) for different concentrantions of AG 155
Figure 6.16b: Plots of Q *vs* $t^{1/2}$ derived from the chronocoulograms of Fig. 6.16a 155
Figure 6.16c: Plot of the slope of the straight line against the concentration of AG 156
Figure 7.1: Structure of TET 162
Figure 7.2: Absorption spectrum of AuNPs 166
Figure 7.3: (a) TEM images of AuNPs (b) Selected area electron diffraction (SAED) pattern of AuNPs 166
Figure 7.4: DLS spectrum of aqueous suspension of AuNPs 167
Figure 7.5: Zeta potential of AuNPs 167
Figure 7.6: Absorption spectra of AuNPs solutions containing 2.5×10^{-5} M Cu^{2+} (a) in the absence and (b) presence of 1.0×10^{-4} M TET. Inset image shows corresponding colorimetric response..... 168
Figure 7.7: Effect of addition of various metal ions (Ca^{2+}, Co^{2+}, Mn^{2+}, Ba^{2+}, Pb^{2+}, Mg^{2+} and Cu^{2+}) on the absorption ratio of (A_{630}/A_{520}) AuNPs solution in presence of 1×10^{-4} M TET 169
Figure 7.8: Effect of concentration of Cu^{2+} on absorption intensity of AuNPs..... 170
Figure 7.9: Absorption ratio (A_{630}/A_{520}) profiles of AuNPs solutions containing 2.5×10^{-5} M Cu^{2+} in the absence and presence of different concentrations of TET 171
Figure 7.10a: Absorption spectra of AuNPs in the presence of 2.5×10^{-5} M Cu^{2+} and different concentration of TET in the range of $9.0 \times 10^{-6} – 9.0 \times 10^{-7}$ M 172
Figure 7.10b: A plot of ($A_{630/520}$) versus concentration of TET in the range of $9.0 \times 10^{-6} – 9.0 \times 10^{-7}$ M in presence of 2.5×10^{-5} M Cu^{2+} 173
Figure 7.11: Photographs of a solution of (1) AuNPs + 1×10^{-4} M TET, (2) AuNPs + 5×10^{-5} M TET, (3) AuNPs + 1×10^{-5} M TET, (4) AuNPs + 5×10^{-6} M TET, (5) AuNPs + 1×10^{-6} M TET and (6) AuNPs in the presence of 2.5×10^{-5} M Cu^{2+} (from left to right) 173
Figure 7.12: TEM images of AuNPs (a) in the absence and (b) presence of 1×10^{-4} M TET and 2.5×10^{-5} M Cu^{2+}..... 175
Figure 7.13: DLS spectra of AuNPs (a) in the absence and (b) presence of 1.0×10^{-4} M TET and 2.5×10^{-5} M Cu^{2+}..... 175

Figure 7.14: Absorption spectra of AuNPs in the absence and presence of 2.5×10^{-5} M Cu^{2+} 176
Figure 7.15: Zeta potential of AuNPs (a) in the absence and (b) presence of 1×10^{-4} M TET and 2.5×10^{-5} M Cu^{2+} 177
Figure 7.16: Selectivity of developed sensor 178
Figure 7.17: Effect of various drugs on absorption ratio of AuNPs for the determination of 5.0×10^{-6} M TET 179
Figure 8.1: Structure of sunset yellow 182
Figure 8.2: Effect of microwave irradiation time on the fluorescence intensity of CDs 187
Figure 8.3: Effect of volume of EDA on the fluorescence intensity of CDs 188
Figure 8.4: (a) Absorption and (b) emission spectrum of synthesized CDs 189
Figure 8.5: Solution of CDs under (a) visible and (b) UV light 189
Figure 8.6: Fluorescence spectra of (a) bare CDs (b) EDA passivated CDs 190
Figure 8.7: TEM image of synthesized CDs. Inset: Lattice spacing of one particle 191
Figure 8.8: DLS spectrum of aqueous suspension of CDs 191
Figure 8.9a: XPS survey spectrum of CDs 192
Figure 8.9b: High resolution C1s region of CDs 193
Figure 8.9c: High resolution O1s region of CDs 193
Figure 8.9d: High resolution N1s region of CDs 194
Figure 8.10: FTIR spectrum of CDs 195
Figure 8.11a: Fluorescence spectra of different concentrations of CDs 196
Figure 8.11b: Absorption spectra of different concentrations of CDs 196
Figure 8.11c: Linear relationship between integrated fluorescence intensities and absorbance of CDs 197
Figure 8.12: Effect of pH on fluorescence intensity 198
Figure 8.13: Effect of time on the fluorescence intensity of (a) CDs (b) CDs + 7.0×10^{-6} M SY (c) CDs+ 1.5×10^{-5} M SY 199
Figure 8.14a: Effect of concentration of SY on the fluorescence intensity of CDs (2.5×10^{-5} to 2.0×10^{-6} M SY) 200
Figure 8.14b: The linear relationship between the ratio of fluorescence intensities and concentrations of SY in the range 1.0×10^{-5} to 2.0×10^{-6} M 200

Figure 8.15: Overlay of (a) fluorescence spectrum of CDs (b) absorption spectrum of SY 201
Figure 8.16: Fluorescence decay curves of CDs in the absence and presence of SY 203
Figure 8.17: Absorption spectra of SY in the (a) presence and (b) absence of CDs 203
Figure 8.18: Selectivity of the developed sensor 204
Figure 8.19: Effect of various substances on the fluorescence spectrum of CDs for the determination of 5.0×10^{-6} M SY 205

List of Schemes

Scheme 3.1: Schematic representation of modification procedure of GCE 56

Scheme 3.2: Mechanism of electrooxidation of PG 73

Scheme 4.1: Redox reaction of TBHQ on poly (BPB)/GCE 84

Scheme 4.2: Mechanism of electrooxidation of TBHQ 94

Scheme 5.1: Mechanism of electrochemical oxidation of P4R 125

Scheme 7.1: (A) Cu^{2+} induced cross-linking recognition between citrate and TET. (B) Schematic representation of colorimetric detection of TET using citrate modified gold nanoparticles (AuNPs) cross-linked by Cu^{2+} 177

Scheme 8.1: Schematic illustration depicting one pot synthesis of CDs from hibiscus leaves 185

.....ꕥ.....

Chapter 1

INTRODUCTION

Contents

1.1 Chemical sensors
1.2 Electrochemical sensors
1.3 Voltammetric sensors
1.4 Voltammetric cell set up
1.5 Techniques for electrochemical analysis
1.6 Electrode double layer
1.7 Chemically modified electrodes
1.8 Literature review of electrochemical sensors based on polymer film and gold nanoparticles modified electrodes
1.9 Optical sensors
1.10 Colorimetric sensors
1.11 Fluorescence sensors
1.12 Scope of present investigation

Sensors offer a variety of applications for improving quality of life and have played a decisive role in monitoring the concerns associated with health, industry, agriculture and ecology. There is a growing societal need to develop rapid, sensitive and cost effective methods for identification of wide range of analytes. Researches based on sensor technologies have experienced exponential growth over the past three decades and different sensing concepts are being developed to quantify various chemical or biological processes. Continuous research and development in the field of analytical chemistry has resulted in development of better chemical sensing devices.

1.1 Chemical sensors

No information without interaction[1] is the principle behind all sensing technologies. Each interaction has two components; first one is target or analyte, which has to be determined and second one is sensor, which is designed for determination of a particular analyte. According to "Cambridge definition", "*Chemical sensors are miniaturised devices that can deliver real time and on-line information on presence of specific compounds or ions in even complex samples".*[2] Major parts of a chemical sensor include sample, transduction platform and signal-processing step.

Based on the principle of transduction, chemical sensors can be classified into

i) Electrochemical sensors: It transforms electrochemical interaction, stimulated either electrically or due to spontaneous interaction at zero-current condition, between analyte and electrode into a useful signal. Based on mode of operation, they are subdivided into voltammetric/amperometric, potentiometric and conductometric sensors.

ii) Optical sensors: It monitors changes in optical properties resulting from interaction between analyte and receptor. Optical sensors cover different region of electromagnetic spectrum. They are further divided based on optical properties such as absorbance, reflectance, luminescence, fluorescence, refractive index and light scattering.

iii) Mass sensitive sensors: It measures changes in mass caused by accumulation of analyte at specially modified surface. Such devices are of two types (i) piezoelectric devices (ii) surface acoustic wave devices. In piezoelectric devices, mass of analyte adsorbed on a quartz oscillator plate is measured as a function of frequency shift in oscillation. Surface acoustic wave devices measure changes in propagation velocity of an acoustical wave due to accumulation of definite mass of analyte.

iv) Heat sensitive sensors: It measures heat effects associated with chemical reactions or adsorption involving analyte. Heat sensitive sensors are usually known as calorimetric sensors.

1.2 Electrochemical sensors

Electrochemical sensors have found wide applications in diverse fields such as medicine, industry and environmental science. Field of electrochemical sensing technology have become very attractive due to its outstanding detectability, procedural simplicity and cost effectiveness.

1.3 Voltammetric sensors

Voltammetry is an important electroanalytical technique where current is monitored as a function of applied potential. Polarography, invented by Czech chemist Jaroslav Heyrovsky in early l920's has led to development of voltammetry. Even though, significance of voltammetry as a tool for determining certain organic and inorganic species diminished in late 1950's due to number of experimental difficulties, improvisation of classical voltammetric techniques in mid of 1960's enhanced its selectivity and

sensitivity leading to renaissance in field of electrochemistry. Unique properties of voltammetric techniques such wide linear range of concentration (10^{-12} to 10^{-1} M), excellent sensitivity, rapid analysis time (in seconds), ability to quantify various analytes simultaneously, workability in a range of solvents and temperatures have made this method superior over other conventional techniques. This technique has been widely used to study kinetic and mechanistic parameters involved in a large number of electrochemical processes. In addition to this, voltammetric methods have also been used for electrochemical characterisation and calculation of band gap of materials such as polymers, nanoparticles and quantum dots.

1.4 Voltammetric cell set up

Voltammetric cell consists of three electrodes – working electrode, auxiliary/counter electrode and reference electrode. Electrodes are immersed in an excess of non-reactive supporting electrolyte, which furnish electrical conductivity between electrodes.

1.4.1 Working electrode

In voltammetry, generally polarizable microelectrode is used as working electrode and it forms the interface in which electrochemical process being take place. An ideal working electrode should have large potential range appropriate for electrochemical phenomena (reduction or oxidation) that occur at surface of electrode. It should also possesses reproducible chemical, physical and electronic properties, good chemical inertness, microstructural and morphological stability over wide potential range as well as reproducible surface.

Frequently used working electrodes in voltammetry includes those based on various forms of carbon (glassy carbon, graphite and carbon paste), noble metals (Au and Pt) and mercury (dropping mercury electrode and hanging mercury drop electrode).[3-5] Electrochemical sensors discussed in subsequent chapters are based on chemically modified glassy carbon electrodes.

1.4.1.1 Glassy carbon electrode

Glassy carbon electrode (GCE) or vitreous carbon electrode, with variety of architectures including disks, plates and rods is the most commonly employed carbon based electrodes for electroanalysis.[6] Glassy carbon material is prepared by heat treatment of polyacrylonitrile or phenolic resin at temperatures between 1000 and 3000°C, under pressure.[7] GCE has properties of both ceramic and glassy materials and is impermeable to liquids and gases. Characteristics of GCE such as high electrical conductivity and chemical resistance, reasonable mechanical and dimensional stability, micro structurally isotropic and widest potential range among all carbonaceous electrodes made it particularly valuable material for electrochemical measurements.[8-10]

1.4.2 Reference electrode

It is an electrode of known potential that approaches ideal non polarisability.[11] Potential of an ideal reference electrode is independent of time and temperature and is unaffected by composition of solution under study. Electrochemical reaction at reference electrode is reversible with Nernstian behaviour. Standard hydrogen electrode is the most commonly employed primary reference electrode. However, difficulty in construction and maintenance limits its wide use in voltammetric measurements.

Consequently, secondary reference electrodes such as Ag/AgCl or calomel electrode is often employed for voltammetric studies. Compared to calomel electrodes, Ag/AgCl electrodes can withstand temperatures greater than 60°C. Ag/AgCl electrode is made up of Ag wire, coated with AgCl and is dipped in a solution having chloride ions.

1.4.3 Auxiliary electrode/Counter electrode

Auxiliary electrodes allow passage of current through it without producing substances by electrolysis. In voltammetric studies, current is measured between counter electrodes and working electrodes. They are often composed of electrochemically inert materials such as platinum, gold or carbon. Generally, surface area of counter electrode is larger than that of working electrodes to support the current generated at working electrode. Owing to its distinctive properties such as inertness and speed, electrodes made of platinum wire are often used as counter electrodes in electrochemical measurements.

1.5 Techniques for electrochemical analysis

Various techniques used for electrochemical analysis explore diverse phenomena such as kinetics, reaction mechanisms and chemical status of analytes in solution. Among various electrochemical techniques, cyclic voltammetry (CV), differential pulse voltammetry (DPV), square wave voltammetry (SWV), linear sweep voltammetry (LSV), chronoamperometry (CA), chronocoulometry (CC) and electrochemical impedance spectroscopy (EIS) have been employed for present study.

1.5.1 Cyclic voltammetry (CV)

It is one of the most widely employed techniques for obtaining qualitative information about electrochemical processes. CV may be considered as the starting point of electrochemical studies, because it often forms the first experiment performed during an electrochemical analysis.[12] In particular, CV provides an insight on various aspects of an electrochemical process which include behaviour of a redox couple (Nernstian or non-Nernstian), reaction mechanisms, electron transfer kinetics and number of electrons transferred in electrochemical process.[13] However, it is seldom used for quantitative evaluation, since the measurement of peak current in CV is imprecise.[11]

In CV, potentiostat applies a triangular potential sweep to working electrode, wherein potential is varied in both forward and reverse directions while observing current. At switching potential, direction of scan is reversed and potential is returned to its initial value. Resultant graph obtained by plotting current *vs* potential is termed cyclic voltammogram. Development of diffusion layer near electrode surface results in formation of characteristic peaks in cyclic voltammograms. Important variables in a cyclic voltammogram are cathodic peak potential (E_{pc}), anodic peak potential (E_{pa}), cathodic peak current (i_{pc}) and anodic peak current (i_{pa}).

1.5.2 Linear sweep voltammetry (LSV)

Linear sweep voltammetry is very similar to CV. In LSV, working electrode is subjected to linear potential sweep, at constant rate throughout scan. Potential in LSV is swept between initial and final without reversal of scan, compared to CV. Faradaic current in LSV increases with scan rates,

resulting in increased signal to noise ratio. Additionally, capacitive current also increases with increase in scan rate. As a result, contribution of capacitive current to total current is scaled up. Consequently, signal to noise ratio is decreased with increase in scan rate for LSV experiments.[14-16]

1.5.3 Differential pulse voltammetry (DPV)

Differential pulse voltammetry is one of the most popular and sensitive method employed for electrochemical measurements. In DPV, current is measured immediately before and after application of pulsed potential and the difference in current is plotted as a function of potential. DPV can be used to probe redox properties of small amounts of chemicals with high sensitivity because effect of charging current is minimized and only faradaic current is extracted.

1.5.4 Square wave voltammetry (SWV)

In SWV, potential is linearly swept between reference and working electrodes and net current, obtained by difference between forward and reverse currents, is measured.[17] Potential waveform in SWV consists of regular square wave superimposed on a staircase. Since SWV is a pulsed technique, it can efficiently remove charging current. Thus, it possess several advantages such as wide dynamic range, faster measurements and high sensitivity.[18]

1.5.5 Chronoamperometry (CA)

It is an excellent electroanalytical technique used for probing mechanisms and kinetics of electrode process and determining diffusion coefficients. In CA, potential is stepped in a square-wave fashion from E_1, at

which no electrochemical reaction occurs to E_2, where concentration of electroactive species on electrode surface decreases to zero and resulting current is monitored as a function of time. When potential is varied, current increased instantaneously and then decreases as a function of time. Variations in current occur due to expansion or reduction of diffusion layer at electrode.[19] CA provides a better signal to noise ratio in comparison to other amperometric techniques because current is integrated over relatively longer time intervals.[11,20] Chronoamperometric measurements are either single potential step, where current resulting from forward step is recorded or double potential step in which potential is returned to a final value (E_f), following a time period (τ) at a given step potential (E_s).

In CA, response of current *vs* time can be predicted by the following equation[21]

$$\boldsymbol{I = nFAD^{1/2}C\pi^{-1/2}t^{-1/2}}$$

where D is diffusion coefficient, F is Faraday's constant, A is surface area of electrode, n is number of electrons involved in reaction and C is concentration of electroactive species, respectively.

1.5.6 Chronocoulometry (CC)

Chronocoulometry is considered as an outgrowth of chronoamperometric technique and is particularly valuable for the studies on adsorption of electroactive substances.[21] It is preferred for measurement of electrode area (A), diffusion coefficients (D) and kinetics of electrode process. In CC, integral of current i.e. amount of charge passed is recorded as a function of time. It is performed under same conditions as that of CA. There are many

advantages for CC over CA. CC offers enhanced signal to noise ratio compared to CA, because charge often grows with time in CC, as a result latter parts of transient are least biased by non-ideal potential rise. Additionally, in CC, charge arising as a result of various processes such as double layer charging, adsorption on electrode surface and diffusion into electrode surface can be distinguished and studied accordingly. Above peculiarities of CC is especially valuable in studies on adsorption of electroactive substances.[11,22] On integrating Cottrell equation and adding corrections for double layer charge and interfacial interactions, charge at any time can be estimated using following equation,[23]

$$\boldsymbol{Q = \frac{2nFAC(Dt)^{1/2}}{\pi^{1/2}} + Q_{dl} + nFA\Gamma}$$

where Γ is surface excess, D is diffusion coefficient of analyte, n is number of electrons, Q_{dl} is double layer charge, C is bulk concentration, A is effective surface area of electrode and other symbols have their standard meanings.

Plot of Q *vs* $t^{1/2}$ is termed as Anson Plot and intercept of which is equal to,

$$\boldsymbol{Q_{dl} + nFA\Gamma}$$

On subtracting back ground current Q_{dl}, it is possible to calculate surface excess (Γ) of electroactive species.

1.5.7 Electrochemical impedance spectroscopy (EIS)

Electrochemical impedance spectroscopy has received significant attention in past few years due to its ability to explain physical and electronic properties of electrochemical systems such as diffusion coefficients, electron

transfer rate constants, adsorption mechanisms, charge transfer resistances, capacitances and pore sizes.[24] Complex impedance (Z), which is sum of real (Z') and imaginary (-Z") components, is estimated by changing excitation frequency (f) of applied potential over wide range of frequencies. Consequently, EIS combines real and imaginary components of impedance.[25]

EIS data is graphically represented by Nyquist and Bode plots. Among these, Nyquist plot is most commonly used. In Nyquist plot, imaginary impedance obtained from double-layer capacitance is plotted against real impedance, which is equivalent to resistance of the cell.[11] Imaginary and real components of impedance can be used to extract information about electron transfer kinetics and mass transport properties of electrochemical process. In the impedance spectra, semicircular portion observed at higher frequency is related to electron transfer limited process. Diameter of semicircle provides charge transfer resistance at electrode surface (R_{ct}) and for sluggish electron transfer, semicircle of larger diameter is observed.[26] Linear part of impedance spectrum observed at lower frequency denotes diffusion limited process. At higher frequencies, charge transfer resistance and double layer capacitance become more prominent and diffusion of electroactive species (to and from electrode) become irrelevant.

1.6 Electrode double layer

It can be defined as array of charged particles and/or oriented dipoles that exist at electrode/solution interface. 'Electrode double layer' model was proposed in 1850's by Helmholtz. Electrode double layer consists of compact layer and diffuse layer. Compact layer is formed by inner and outer Helmholtz planes. Inner Helmholtz plane contains specifically adsorbed

ions and solvent molecules. Locus of centres of solvated ions are non-specifically adsorbed to surface by coulombic force in outer Helmholtz plane. Diffuse layer which extends from outer Helmholtz plane into bulk solution, is formed by scattering of non-specifically adsorbed ions in a three dimensional region due to thermal agitation.

Flow of current at electrode-solution interface can be due to either faradaic or non-faradaic processes. In faradaic process, transfer of electrons across interface causes oxidation or reduction and is governed by Faraday's laws. Under certain conditions, processes such as adsorption and desorption can change potential area of electrode or solution composition which in turn change structure of electrode-solution interface. Such processes are called non-faradaic processes. Current produced by faradaic and non-faradaic processes are called faradaic current and non-faradaic currents, respectively. In electrode reaction, faradaic processes are preferred and it depends on mass transport of electroactive species and kinetics of electrode reaction.

1.6.1 Different forms of mass transport

Overall reaction at electrode can be influenced by different forms of mass transport. The three general forms of mass transport processes include diffusion, convection and migration.

1.6.1.1 Diffusion

Spontaneous movement of chemical species from a region of higher concentration to a region of lower concentration to minimise the difference in concentration gradient is termed as diffusion. Fick proposed two laws to predict rate of movement of analyte by diffusion.

According to Fick's first law, rate of movement of electroactive species by diffusion (J_o) is related to concentration gradient ($\frac{\partial Co}{\partial x}$) and diffusion coefficient (D_o).

$$\boldsymbol{J_o = -D_o \frac{\partial C_o}{\partial x}}$$

Fick's second law predict variation in concentration of different electroactive species as a function of time within the electrochemical cell.

$$\boldsymbol{\frac{\partial Co}{\partial t} = \frac{\partial^2 C_o}{\partial x^2}}$$

From the above relation, it is clear that greater the change in concentration, higher will be the rate of diffusion. Mass transport in voltammetry usually depends only on diffusion.

1.6.1.2 Convection

It occurs due to movement of chemical species either by density gradient (natural convection) or by mechanical means (stirring or rotating solution - forced convection). Influence of convection can be minimized by using unstirred electrolyte solutions.

1.6.1.3 Migration

It is the movement of charged species under the influence of a potential difference caused due to an electric field. Effect of migration can be eliminated by adding higher concentration of supporting electrolyte into the solution.

1.6.2 Kinetics of electrode reaction

1.6.2.1 Reversible systems

An electrochemical system is considered to be reversible when electron transfer kinetics at the surface of electrode is much faster than the rate of mass transport at all potentials. In reversible systems, concentration of electroactive species is given by the following Nernst equation,

$$E_e = E_e^o + \frac{RT}{nF} ln \frac{C_o}{C_R}$$

where C_o, C_R, E_e, E_e^o and n are surface concentrations of oxidized and reduced species, equilibrium potential, standard potential and number of electrons involved, respectively. R, T and F have their standard meaning.

Peak current (i_p) for a reversible system (at 25°C) is given by Randles-Sevcik equation,

$$i_p = (2.69 \times 10^5) n^{3/2} A D^{1/2} C v^{1/2}$$

where A, D, C and υ refers to surface area of electrode (cm^2), diffusion coefficient ($cm^2\ s^{-1}$), concentration of chemical species ($mol\ cm^3$) and scan rate ($V\ s^{-1}$), respectively. As shown in above equation, peak current varies linearly with concentration and increases with square root of scan rate. For a simple reversible redox couple, ratio of reverse to forward current $(i_{p,r}/i_{p,f})$ is unity.

For a reversible process, formal potential (E^o) is centred between anodic (E_{pa}) and cathodic peak potentials (E_{pc}) and the peak potential is independent of scan rate.

$$E^0 = \frac{E_{pa} + E_{pc}}{2}$$

The peak potential separation (ΔE) can be used to calculate number of electrons transferred during a reversible reaction and it function as a criteria for evaluating Nernstian behaviour.

Peak potential is given by,

$$\Delta E_p = E_{pa} - E_{pc} = \frac{0.059}{n} \text{ V}$$

Calculated value of ΔE_p at 298 K for one electron process is around 0.059 V.

1.6.2.2 Irreversible systems

A system is considered to be irreversible when the electron transfer kinetics at electrode surface are slower (sluggish electron exchange) than rate of mass transport. In this regime, equilibrium between concentration of oxidized and reduced species is not retained. Additionally, individual peaks are widely separated and are reduced in magnitude. Ratio of peak currents and peak potential separation are dependent of scan rate and peak potential increases with scan rate. For an irreversible process, peak potential is expressed as,

$$E_p = E^0 - \frac{RT}{\alpha F}[0.780 + ln(\frac{D_0^{1/2}}{k_0}) + ln(\frac{\alpha F v}{RT})^{1/2}]$$

where 'α' is transfer coefficient

The peak current for totally irreversible process is given by,

$$i_p = (2.99 \times 10^5)\alpha^{1/2} A C_o D^{1/2} v^{1/2}$$

which is about 80% of peak current for reversible process, when value of α is 0.5.

1.6.2.3 Quasi-reversible systems

When the electron transfer kinetics is comparable with rate of mass transfer, system is considered as quasi-reversible. Peak current in a quasi-reversible process is controlled by both mass transfer and charge transfer ($\boldsymbol{i_p^{quasi}}$) and is given by Randles-Sevcik equation[27]

$$\boldsymbol{i_p^{quasi} = \pm(2.65 \times 10^5) n^{3/2} A C D^{1/2} v^{1/2}}$$

where A, D and C are area (cm^2), diffusion coefficient ($cm^2\ s^{-1}$) and concentration (M), respectively. Compared to reversible systems, quasi-reversible system shows larger separation in peak potentials and on increasing the scan rate, peak potential also increases.

1.6.2.4 Heterogeneous rate transfer constant

Knowledge on reaction kinetics at the electrode surface is of great significance for understanding heterogeneous electron transfer reactions. To explain kinetics of electrode reaction, Butler-Volmer formulation was employed, which describes relationship between electrode potential and peak current.[11]

$$\boldsymbol{i = A\ .\ i_0 \left[\frac{(1-\alpha) nF}{RT} (E - E_{eq}) \right] - \left[\exp - \frac{\alpha nF}{RT} \ (E - E_{eq}) \right]}$$

where i and i_o are current and exchange current density respectively. E_{eq} is equilibrium potential and other symbols have their usual meanings. First and second part of above equation denotes current density for anodic and cathodic processes, respectively.

For a reversible reaction,

$$O + ne^{-} \rightleftharpoons R$$

Anodic (k_a) and cathodic (k_b) rate constants are given by Butler – Volmer equation,

$$\boldsymbol{k_a = k_0 exp[\alpha_a nF(E - E^{0\prime})/RT]}$$

$$\boldsymbol{k_b = k_0 exp[\alpha_c nF(E - E^{0\prime})/RT]}$$

where k_0 represents standard rate constant, α_a and α_c corresponds to anodic and cathodic charge transfer coefficients. $E^{0\prime}$ indicates formal potential.

Among various techniques employed for determination of heterogeneous rate constant, CV provides a simple and systematic approach, based on separation of peak potential.

1.7 Chemically modified electrodes

Chemically modified electrodes (CME) have received wide attention and have opened up new possibilities in field of electroanalysis since 1970's when Murray and co-workers introduced idea of immobilizing foreign molecules on the surface of electrodes.[28]

IUPAC has defined CME as, *an electrode made of a conducting or semiconducting material that is coated with a selected monomolecular, multi molecular, ionic or polymeric film of a chemical modifier and that by means of faradaic (charge-transfer) reactions or interfacial potential differences (no net charge transfer) exhibits chemical, electrochemical, and/or optical properties of the film.* [29]

Concept of CME has emerged to solve the difficulties faced by electrochemists while working with bare electrodes. Generally, bare electrodes encounter challenges such as higher over potential, surface fouling, slow electron transfer kinetics, surface passivation and poor sensitivity, which limit their practical utility.[30] By changing chemical nature of electrode surface through surface modification, above mentioned limitations can be reduced to a greater extent. CME offers several advantages such as improved selectivity, sensitivity and better reproducibility. Additionally, it also accelerates electron transfer rate of analyte and reduces its over potential. These unique features of CME have been exploited in fields of sensing, electrocatalysis, electrochromic display devices and fuel cells. Strategies used for chemical modification of electrode surface include covalent attachment, electro deposition, irreversible adsorption and electropolymerization.

Sensors that have been developed for present investigation include glassy carbon electrodes modified with several chemical modifiers such as gold nanoparticles and conducting polymers of *p*-aminobenzenesulphonic acid, bromophenol blue, L-cysteine and L-glycine.

1.7.1 Polymer film modified electrodes

Conducting polymers (CPs), which integrates electronic features of metals and inorganic semiconductors,[31] have drawn extensive interest because of their cost effectiveness, good electrical conductivity, strong adherence to electrode surface, homogeneity in electrochemical deposition and environmental stability.[32-34] Electrical conductivity of polymer film arises from the delocalized π electrons of polymer backbone. During the electropolymerization process, initially, a radical cation is formed from

monomer, followed by dimerization process, ensued by subsequent oxidation and coupling reactions.[11]

Generally, potentiodynamic (cyclic or pulse voltammetric techniques), potentiostatic (constant potential) and galvanostatic (constant current) methods are employed to achieve electropolymerization. To get a clear knowledge about redox process that takes place during initial stages of electropolymerization, CV is often used.[35] By varying applied current and potential, properties of polymer films such as charge transfer characteristics, permeation and thickness can be controlled. Moreover, tailoring of functional groups (–COOH or $–NH_2$) to polymer, impart selective molecular interactions between polymer modified electrode and target molecule.[36] Thus, use of CPs as electrode modifiers has resulted in comprehensive development of sensing technology.

Additionally, non-conducting polymer films, resulting from electropolymerization can also be used for fabrication of electrodes. Materials that form non-conducting polymers include phenol and its derivatives, phenylenediamines, and electroinactive polypyrrole.[37] Merits of non-conducting polymer film also include good selectivity, fast response and high reproducibility, which makes them suitable candidates for fabrication of electrodes.[38,39]

1.7.2 Gold nanoparticles

Gold has received several accolades throughout the history for its rarity, attractiveness and perpetuity. Rapid advances in nanoscience have encouraged its use and applications as nanomaterial in different branches of

science. Among various metal nanoparticles, gold nanoparticles (AuNPs) have become most widely explored nanostructures,[40] which offer several practical applications in sensing, catalysis, diagnosis and treatment. Owing to unique physicochemical attributes such as good conductivity, high surface to volume ratio, good electrocatalytic ability, interface dominated property and biocompatibility, they have been used as excellent scaffold for development of electrochemical sensors.[41-43]

Various strategies adopted for synthesis of AuNPs include chemical synthesis,[44,45] electron beam irradiation,[46] magnetron sputtering and electrodeposition.[47,48] Due to ease of synthesis and ability to control morphology and distribution of nanoparticles, electrochemical deposition method is preferred over other methods.[49,50] Based on morphology, AuNPs have been categorized as nanowires, nanospheres, nanorods, nanoshells and nanocages.[51] Furthermore, AuNPs modified electrodes offer benefits such as improved rate of mass transport, more effective surface area and enhanced electrocatalysis over bare electrodes.[52,53]

1.8 Literature review of electrochemical sensors based on polymer film and gold nanoparticles modified electrodes

A novel biosensor was fabricated for electroanalysis of NADH and NAD^+ using composites of conducting poly [*p*-aminobenzenesulphonic acid (*p*-ABSA)] and flavins [flavin adenine dinucleotide (FAD), flavin mononucleotide (FMN), riboflavin (RF)] films on GCE (poly(*p*-ABSA)/ FAD/GCE) by Kumar and Chen.[54] Modified electrode was characterized by techniques such as atomic force microscopy (AFM), scanning electron microscopy (SEM), CV and ultraviolet visible (UV–vis) spectroscopy.

Addition of flavins significantly altered morphology of polymer materials and adsorption of flavins occurs in order of RF < FMN < FAD on poly (*p*-ABSA) films. Developed sensor showed excellent electrocatalytic activity for oxidation of NADH and for reduction of NAD^+. Proposed method exhibited linear response to NADH in the concentration range 3.0×10^{-4} to 1.0×10^{-5} M. Developed biosensor could also observe NAD^+/NADH reversible reaction at physiological condition.

Zhang *et al.* fabricated a GCE modified with composite film of polyaniline (PAN)/*p*-ABSA modified GCE (PAN-ABSA/GCE) for simultaneous determination of uric acid (UA) and ascorbic acid (AA) in a mixture.[55] The PAN-ABSA composite film was characterized by techniques such as spectroscopy, microscopy and electroanalysis. Simultaneous determination of UA and AA was achieved by resolving overlapped voltammetric response of UA and AA into two well-defined peaks with both CV and DPV. Peak currents at modified electrode were linearly dependent on concentrations in the range 2.5×10^{-4} to 5.0×10^{-5} M for UA and 1.8×10^{-4} to 3.5×10^{-5} M for AA, respectively. Detection limits for UA and AA were 1.2×10^{-5} M and 7.5×10^{-6} M, respectively. Developed sensor exhibits good stability, reproducibility, sensitivity and selectivity. Practical applicability of the modified electrode was also verified by real sample analysis.

Simultaneous determination of methotrexate (MTX) and calcium folinate (CF) by electroanalysis is reported by Zhu *et al.*[56] Modified electrode was prepared by electropolymerization of *p*-ABSA on quaternary amine functionalized multiwalled carbon nanotubes (Q-MWNTs) modified GCE (poly-ABSA/Q-MWNTs/GCE). Voltammetric behavior of MTX and

CF were evaluated by CV. Electrochemical performance of poly-ABSA/ Q-MWNTs/GCE was much better than that of bare GCE, *p*-ABSA/GCE and Q-MWNTs/GCE. Sensor exhibited a linear relationship between anodic peak current and concentration of MTX in the linear range 8.0×10^{-6} to 1.0×10^{-7} M in presence of 8.0×10^{-6} M CF, with a detection limit of 1.5×10^{-8} M. Similarly, anodic peak current for concentration of CF also showed a linear behavior in the range 6.5×10^{-6} to 1.0×10^{-7} M with a detection limit of 2.0×10^{-8} M in presence of 8.0×10^{-6} M MTX. Modified sensor exhibited advantages such as good reproducibility and stability. Practical utility of *p*-ABSA/Q-MWNTs/GCE was demonstrated by direct determination of MTX and CF in urine samples.

Li *et al*. established an electrochemical method to detect Sudan I, a synthetic chemical colorant using poly(*p*-ABSA) film modified GCE.[57] Electrochemical behavior of Sudan I at poly(*p*-ABSA)/GCE was evaluated by anodic stripping voltammetry. Compared to bare GCE, modified electrode showed better electrochemical oxidation for Sudan I. Experimental parameters were optimized and under optimized conditions, anodic stripping voltammetry showed linear range for concentration of Sudan I from 2.0×10^{-6} to 4.0×10^{-9} M. Limit of detection offered by fabricated electrode for Sudan I was 1.2×10^{-9} M. Application of proposed method was confirmed in hot chili and ketchup samples with satisfactory results.

Simultaneous determination of xanthine, its methyl derivatives (theophylline and caffeine) and its oxidation product (uric acid) on a GCE modified with *p*-PABSA (*p*-PABSA/GCE) is reported by Jesny and Girish Kumar.[58] Well defined and well separated peaks were obtained for above

purines on *p*-PABSA/GCE in square wave mode. LSV was employed to study mechanistic aspects of polymer modified electrode. Diffusion coefficients of xanthines were determined by chronoamperometry. Sensor exhibited electrochemical oxidation, free of interferences in the range 1.0×10^{-4} to 9.0×10^{-7} M for xanthine and 1.0×10^{-4} to 1.0×10^{-5} M for theophylline and caffeine. Limit of detection for xanthine, theophylline and caffeine were estimated to be 3.50×10^{-7}, 7.02×10^{-6} and 1.20×10^{-5} M, respectively. Developed sensor was effective for simultaneous determination of xanthine, theophylline and caffeine in body fluids and commercially available beverages. Additionally, it was also employed for individual determination of theophylline and caffeine in pharmaceutical formulations.

Yang and coworkers developed an electrochemical method for estimation of trace amounts of Cu^{2+} using poly bromophenol blue fabricated glassy carbon electrode (PBPB/GCE) by anodic stripping voltammetry.[59] Characterization and growth mechanism of synthesized PBPB films were done by techniques such as in situ electron spin resonance (ESR) spectro electrochemistry, attenuated total reflection (ATR)-FTIR spectroscopy, electrochemical methods and also by qualitative analysis. Developed system exhibited linear concentration in the range $1.0 \times 10^{-5} - 1.0 \times 10^{-8}$ M. Minimum detectable limit of Cu^{2+} using this method was 3.5×10^{-9} M. Modified electrode showed advantages such as good sensitivity, stability and reproducibility for determination of Cu^{2+} in H_2SO_4 solution (pH 2.0). Application of the developed system was validated by determining concentration of Cu^{2+} in water samples.

Simultaneous determination of hydroquinone, catechol and resorcinol was achieved by Yang *et al.* using poly-BPB/MWNT/GCE.[60] Electrochemical behavior of analytes were investigated by CV. Linear range of 10^{-4} to 10^{-6} M was reported, with limit of detection of 3×10^{-7} M for hydroquinone, catechol and resorcinol. Modified electrode showed excellent reproducibility and stability. Application study of developed sensor was conducted by evaluating amount of each compound in water samples collected from a photo studio.

Simultaneous determination of 5-hydroxyindoleacetic acid (5-HIAA) and 5-hydroxytryptamine (5-HT) was reported by Xu *et al.* using PBPB film modified electrode (PBPB/CME).[61] Electroanalytical behavior of 5-HIAA and 5-HT were investigated by CV and DPV. Limit of detection for 5-HIAA and 5-HT were 5.0×10^{-10} and 2.5×10^{-10} M, respectively. Proposed method was successfully applied for simultaneous determination of analytes in urine samples of patients suffering from acute appendicitis.

An electrochemical microsensor for nitric oxide (NO) was fabricated by Peng *et al.* using PBPB coated carbon fiber microelectrodes (CFME).[62] Electrochemical activity of PBPB modified CFME towards NO was studied by SWV and amperometry. Developed microsensor showed better electrocatalytic activity towards oxidation of NO in the linear range 8.9×10^{-5} to 3.6×10^{-8} M, with limit of detection of 3.6×10^{-9} M. Proposed method displayed good sensitivity, reproducibility and stability. Practical applicability of developed microsensor for NO monitoring was validated using biological samples.

Yang *et al*. demonstrated development of an anodic stripping voltammetric method for determination of Sn^{2+} using GCE modified with Bi and poly(BPB) (Bi/poly(BPB)/GCE).[63] Codeposition of Bi and Sn on Bi/poly(BPB)/GCE has improved sensitivity and repeatability of modified electrode. Linear concentration range of 2.0×10^{-5} to 2.0×10^{-8} M was found using Bi/poly(BPB) modified GCE, with a limit of detection of 7.0×10^{-9} M for Sn^{2+}. Proposed method was successfully used for measurement of Sn^{2+} in juices of canned orange, mango, grape and pineapple.

A voltammetric sensor has been developed for determination of uric acid (UA) using PBPB/AuNPs composite modified GCE by Sivasankaran *et al*.[64] Surface morphology of modified electrode was characterized using AFM, SEM and by various electrochemical techniques. Modification of GCE with PBPB and AuNPs has resulted in reduction of oxidation potential and increased peak current. Developed method showed good repeatability and reproducibility. Linear concentration range and limit of detection of PBPB/AuNPs/GCE were estimated to be 1.0×10^{-3} to 2.0×10^{-5} M and 2.2×10^{-6} M respectively. Practicability of developed sensor was confirmed using artificial blood serum and urine samples analysis and recoveries were in good agreement with spectrophotometric analysis.

Gu and coworkers reported development of an electrochemical sensor for metronidazole, an anti-protozoal drug using β-cyclodextrin-functionalized gold nanoparticles/poly(L-cysteine) modified glassy carbon sensor (β-CD-AuNPs/poly(L-Cys)/GCE).[65] Modified electrode showed better electrocatalytic activity towards metronidazole. Under optimized conditions, linearity between concentration of metronidazole and logarithm of peak currents was

observed within the range 6.0×10^{-4} to 1.0×10^{-7} M, with a detection limit of 1.4×10^{-10} M. Performance of developed sensor was confirmed by analysis of metronidazole in an injection sample.

Electrochemical determination of sunset yellow (SY) based on poly L-Cys modified GCE was reported by Zhang *et al.*[66] Electrocatalytic property of modified electrode and kinetics involved in electrode reaction were investigated using techniques such as CV, EIS and CC. Linear relationship between peak current and concentration of SY was observed within the range of $7.0 \times 10^{-7} – 8.0 \times 10^{-9}$ M. Minimum detectable level of SY was found to be 4.0×10^{-9} M. Reported electrochemical sensor exhibited advantages such as simplicity, reproducibility, good sensitivity and stability. Modified sensor was successfully applied for the determination of SY in commercial soft drink samples.

Thomas and coworkers fabricated a poly (L-Cys) film modified GCE for determination of artificial antioxidant, butylated hydroxyanisole (BHA).[67] Developed sensor exhibited good electrocatalytic activity and showed linear response in the range 1.0×10^{-5} to 1.0×10^{-6} M. Limit of detection, heterogeneous electron transfer rate (k_s) and charge transfer coefficient (α) involved in electrochemical oxidation of BHA on poly (L-Cys/GCE) were found to be 4.1×10^{-7} M, 1.20 s^{-1} and 0.575, respectively. Practical utility of developed sensor was confirmed by estimating concentration of BHA in vegetable oils.

Two electrochemical sensors were developed for determination of antiparasitic drug, tinidazole (TIN) using GCE modified with L-Cys (L-Cys/GCE) and a double layer of L- Cys/AuNPs (AuNP/L-Cys/GCE) by

Jos *et al*.[68] Surface morphology of modified electrodes was studied using SEM. Developed sensors showed advantages such as good stability and nano molar detection limit. TIN showed well-defined reduction peaks at – 0.581 and -0.487 V on L-Cys/GCE and AuNP/L-Cys/GCE, respectively. Linearity for both modifications were ranged between 1.0×10^{-5} to 7.0×10^{-7} M. Developed sensors were utilized for estimation of TIN concentration in spiked urine samples and pharmaceutical formulations.

Ferraz *et al.* developed a voltammetric sensor for simultaneous quantification of anti-tuberculosis drugs, pyrazinamide (PZA) and ethionamide (ETO) using poly(L-Cysteine) film-modified GCE.[69] Electrochemical behavior of sensor was studied using techniques such as CV, SWV, EIS and SEM. Under optimized experimental conditions, linear response was observed within the range of 5.1×10^{-5} to 4.8×10^{-7} M, with limit of detection of 1.1×10^{-7} M for PZA and 2.5×10^{-4} to 2.4×10^{-6} M, with limit of detection of 5.3×10^{-7} for ETO. Developed sensor was successfully used for determination of PZA and ETO in human serum and urine samples.

Yu *et al.* explored electrocatalytic activity of polyglycine modified GCE (poly Gly/GCE) towards oxidation of ascorbic acid (AA).[70] Conditions for efficient polymerization process such as voltage range, electrolyte pH, monomer concentration and cyclic numbers were optimized. Linear range and limit of detection recorded by modified electrode for AA was 2.5×10^{-4} to 6.0×10^{-8} M and 4.0×10^{-8} M, respectively. Developed sensor possessed good stability and selectivity and was applied for determination of AA in oranges. Results obtained by developed sensor were in good agreement with those estimated by amperometry and iodimetry.

Electrochemical behavior of quinine isomers, hydroquinone (HQ) and catechol (CC) were investigated using poly Gly/GCE by Wang *et al*.[71] Modified electrode was found to be resistant to fouling of electrode surface by oxidization products and was employed for simultaneous determination of HQ and CC. Limit of detection for HQ and CC was found to be 1.0×10^{-6} M (in presence of 1.0×10^{-4} M CC) and 5.0×10^{-7} M (in presence of 1.0×10^{-4} M HQ), respectively. The as-prepared electrode showed better sensitivity and selectivity and was applied for determination of HQ and CC in water samples.

Narayana *et al*. fabricated a polymer-nanocomposite modified GCE by two step process, which include electropolymerization of glycine (Gly), followed by drop casting of multi-walled carbon nanotubes (MWCNTs).[72] Modified electrode (MWCNTs/poly(Gly)/GCE) was used for electrochemical sensing of anti-inflammatory drug, paracetamol (PC) in presence of folic acid (FA) and dopamine (DA). Characterization of developed sensor was done using EIS. Developed sensor showed better selectivity and sensitivity. Linearity recorded for modified electrode was within the range 1×10^{-5} to 5×10^{-7} M, with limit of detection 5.0×10^{-7} M. Developed electrode was successfully used for determination of PC in human serum and drug samples.

Ferraz and coworkers reported the use of poly Gly modified GCE for determination of anti-tuberculosis drug, pyrazinamide (PZA) using SWV.[73] Electroanalytical behavior of PZA on modified electrode (poly(Gly)/GCE) was investigated using CV and SWV. PZA was found to undergo a diffusion controlled redox reaction on modified electrode. Under optimized

conditions, linear dependency in concentration of PZA was recorded within the range 6.2×10^{-6} to 4.7×10^{-7} M. Limit of detection and limit of quantification were calculated to be 3.5×10^{-8} M and 1.2×10^{-7} M, respectively. Developed sensor exhibited excellent sensitivity and repeatability and was applied for quantification of PZA in human urine and pharmaceutical samples.

Zhang and coworkers reported development of a novel electrochemical method for simultaneous determination of uric acid (UA), ascorbic acid (AA) and dopamine (DA).[74] The as prepared poly(glycine)/carbon nanohorns composite modified GCE (CNHs/PGLY/GCE) was characterized by techniques such as CV, DPV and EIS. Developed sensor exhibited good sensitivity, stability and selectivity. Modified electrode showed linear behavior between oxidation peak current and concentrations of UA, AA and DA in the range 3.5×10^{-4} - 2.0×10^{-6}, 4.5×10^{-4} - 3.0×10^{-6} and 2.8×10^{-4} - 1.0×10^{-6} M, respectively. Minimum detectable levels of UA, AA and DA that can be found by present sensor were calculated to be 1.8×10^{-7}, 3.4×10^{-7} and 3.0×10^{-8} M, respectively. Proposed method was successfully applied for determination of UA, AA and DA in human urine samples, with satisfactory results.

1.9 Optical sensors

Developments in visual indicators have opened up the field of optical sensors, as a substitute to mechanical and/or electronic sensors. Optical sensing technology is rapidly growing and it integrates benefits of optical fibres with selectivity and specificity of chemical transduction systems. Optical sensors are a class of chemical sensors, which depend on optical

transducers for measurement of analytical signal. Chemical transducer forms the heart of such sensors. Concentration of an analyte is determined by measuring chemically encoded optical signals generated by interaction of electromagnetic radiation with analyte. Various methods in optical sensing such as absorbance, fluorescence and reflectance function under different regions of electromagnetic spectrum. As a result, optical sensors allow measurement of life time, scattering, polarization and refractive index in addition to intensity of light.[75,76] Distinguishing features of optical sensors over conventional sensors includes sensitivity, selectivity and non-invasive character. Among various optical sensing methods, those based on absorption (colorimetric sensors) and emission of lights (fluorescence sensors) are most commonly employed techniques.

Over past few decades, researchers have increasingly exploited advances in fabrication of micro and nanostructured materials for improving utility of prevailing sensing techniques. Concept of nanotechnology was presented by Richard Feynman in 1959 during his famous lecture called 'There's plenty of room at the bottom'. He proposed idea that new functionalities and possibilities arise when size of materials reduced into nanometres range. Notion proposed by Richard Feynman has become a reality today and gold nanoparticles (AuNPs) and carbon dots (CDs) represent a significant section among nanomaterials. Use of nanoparticles produces most intuitive effects in sensor characteristics such as fast response time and better selectivity. This is because when size is decreased, surface to volume ratio is also increased dramatically resulting in increased surface phenomena of nanomaterials over bulk. Among nanomaterials, AuNPs and CDs have been used as sensing platforms in the present study.

1.10 Colorimetric sensors

Presently, there is an enthusiastic pursuit for colorimetric sensors in many areas and disciplines. High sensitivity, online throughput readouts and ease of operation form major attractions of colorimetric sensors, making them one of the most promising candidates in field of sensing. Colorimetric sensing process is based on quantitative measurement of absorbance and absorption takes place from ultraviolet to visible region of spectrum. Concentration of analyte can determined by following the Beer-Lambert's law,

$$\boldsymbol{A = \varepsilon\, b\, c}$$

where A and c are absorbance and concentration of absorbing species, respectively. b is path length and ε is molar absorptivity.

On absorbing ultraviolet or visible radiations, molecules undergo electronic transitions. Of the four possible electronic transitions, π-π*, n-π*, σ-σ* and n-σ*, energy required for electronic transitions, n–π* and π –π* corresponds to energy in near-UV and visible region. So, absorption spectroscopy is found to be very useful for determination of conjugated systems.[77]

1.10.1 Gold nanoparticles as colorimetric sensors

History of using colloidal gold can be traced back to fourth century AD, when it was used as a pigment to stain legendary 'Lycurgus cup'.[78] In 1857, Michael Faraday published first scientific report on production of colloidal gold nanoparticles and he found that carbon disulfide can stabilize "fine particles" that formed during aqueous reduction of gold chloride by

phosphorus, resulting in formation of "beautiful ruby fluid".[79] Currently, gold nanoparticles are also synthesized by following similar approach in which surface capping ligands inhibit aggregation of particles by physical and/or electrostatic repulsion. Particle size of AuNPs can be adjusted by altering ratio between gold ions to reducing agent/stabilizer. Thus, larger sized AuNPs are obtained when the above ratio become higher.

Colorimetric sensors based on AuNPs have received considerable attention for past decade since molecular events are easily identifiable due to changes in colour. Moreover, colour changes can be observed by naked eye examination, without need of any sophisticated instruments. AuNPs based colorimetric sensors have been developed for biomolecules (DNA/proteins), ions and organic molecules.[80] However, changes in colour is dependent on factors such as morphology, aggregation state of AuNPs and refractive index of medium.[81] Generally, well-dispersed AuNPs (diameter of 10–50 nm) solutions exhibits ruby red colour, while aggregates of smaller AuNPs or larger AuNPs (>50 nm) show blue or purple colour. Colour change related with aggregation or dispersion of AuNPs is correlated to inter particle plasmon coupling, generated due to a band shift in visible region of electromagnetic spectrum.[82,83] Mechanisms involved in aggregation of AuNPs can be either non cross linking aggregation (stabilizing ligands removed from surfaces of AuNPs) or inter particles cross linking aggregation (binding of modified ligands with target analytes on AuNPs). Due to their extremely high extinction coefficients, minimum detectable levels of analyte can be as low as nanomolar levels in AuNPs based colorimetric sensors.[84]

AuNPs based optical probes have become valuable tools for detecting analytes related to disease diagnosis, monitoring of ecological contaminants and for ensuring the quality and safety of food stuffs. Unique properties of AuNPs could be attributed to its ability to absorb or scatter light at its surface plasmon resonance (SPR) wavelength[85] and by changing morphology of AuNPs, SPR wavelength can be altered from visible to near IR region.[86] Optical properties of AuNPs at visible region make them easily detectable by naked eye and the prospect of tuning them to near IR region makes them attractive sensors for bio imaging.[87] Additionally, optical sensing property of AuNPs is also related to its surface chemistry as well as inter-particle interactions. Localized surface plasmon resonance (LSPR) is the combined oscillation of nanostructure's conduction band electrons in tune with incident electromagnetic field.[88] Dipolar LSPR is the simplest form of LSPR. LSPR spectrum is dependent on morphology of nanostructure, dielectric constant of nanomaterial and its surrounding medium.[89] The Mie theory examines contribution of various parameters to total extinction of metal nanoparticles.[90]

1.10.2 Literature review of colorimetric sensors based on gold nanoparticles probes

Highly sensitive and selective colorimetric sensing method for Hg^{2+} was reported by Tan *et al.* using AuNPs probes, functionalised with both mercaptopropionic acid and homocysteine.[91] Unlike conventional colorimetric methods, they followed a cloud point extraction procedure in presence of 2,6-pyridinedicarboxylic acid and triton X-114, where small sized, colourless AuNPs were converted to corresponding red coloured ones upon interaction with Hg^{2+}. Developed system exhibited better sensitivity and selectivity for sensing trace amounts of Hg^{2+}.

Cao and coworkers reported a sensitive colorimetric method for determination of melamine, an industrial chemical.[92] Synthesis of AuNPs were achieved at room temperature using 3,5-dihydroxybenzoic acid (DBA) as reducer, without adding gold nanoparticle seeds. It was reported that in presence of melamine, color of DBA capped AuNPs changes from purple to yellowish green due to strong H-bonding formation between DBA and melamine. Developed method allowed detection of melamine at nanomolar level during formation of AuNPs. Linear relationship existed between absorbance and concentration of melamine in the range from 1×10^{-5} to 1×10^{-9} M, with limit of detection as 8×10^{-10} M.

A colorimetric method was reported for on-site determination of melamine in raw milk samples using citrate capped AuNPs as probes by Li *et al*.[93] When melamine was added into unmodified AuNPs solution, a color change from red to blue was observed. Proposed method allows detection of melamine by naked eye, without need of any sophisticated instruments. Additionally, developed method offers other advantages such as simplicity, fast reaction time and cost effectiveness. Detection limit of proposed method was 3.2×10^{-6} M. Practical utility of developed method was validated using analysis of spiked raw milk samples.

Tripathy and coworkers studied design of non-aggregation based colorimetric sensing system for selective detection of HCl in aqueous environments using unlabeled AuNPs probes.[94] Developed system exploits ability of chloro species to induce rapid leaching of AuNPs in aqueous dispersion containing strong oxidizing agents, leading to marked damping of surface plasmon resonance peak of AuNPs dispersion. Proposed method

exhibited better selectivity for HCl over common acids, salts, and anions. Developed sensing system was useful for detection of HCl in natural water systems at concentrations as low as 500 ppm.

AuNPs based colorimetric assay was reported for rapid detection of 1-hydroxypyrene (1-OHP) by Hu *et al*.[95] Developed sensing method relied on non-cross linking aggregation of AuNPs induced by 1-OHP in presence of formic acid, with a change in color from red to violet blue. Developed sensor exhibited a wide linear range from 1.0×10^{-6} to 1.0×10^{-8} M and minimum detectable limit was 3.3×10^{-9} M. Practical utility of developed assay was confirmed by detecting 1-OHP in urine samples and results were consistent with values obtained from HPLC.

1.11 Fluorescence sensors

Fluorescence sensing is one of the most sensitive methods employed in analytical chemistry, with their sensitivity reach absolute limit of single molecules.[96] Sensing based on fluorescence is poised to solve challenges and constraints associated with many branches of science. Fluorescence is a phenomenon in which emission of a photon occurs from a fluorophore after electronic excitation during absorption of light. Generally, emission of fluorescence is observed at higher wavelength than excitation. In light emission phenomenon, photons having well specified energies can be absorbed and emitted.

Jablonski diagram (Fig. 1.1) is used to demonstrate the photo-physical processes that occur in electronically excited molecules. On absorption of light, transition of molecules take place from ground singlet state (S_0) to excited state (S_n) and it follows Frank-Condon principle. Molecules in

excited state may undergo different relaxation process including vibrational relaxation and internal conversion. Vibrational relaxation is a non-radiative transition from highest energy excited state (S_n) to lowest energy vibration state. During vibrational relaxation, energy is transferred from molecules to its surrounding, through collisions[92] and it occurs very rapidly. Internal conversion is also a non-radiative transition from vibrational level of excited electronic state to lowest energy vibration level of lower electronic state. The above process is mechanistically identical to vibrational relaxation and takes place in 10^{-12} s or less. Molecules in S_1 electronic state can experience a transition to first triplet state (T_1) and process is termed as intersystem crossing. It occurs as a relatively slow process (10^{-8} s). Emission of photons from T_1 to S_0 is termed phosphorescence and is a spin forbidden process.

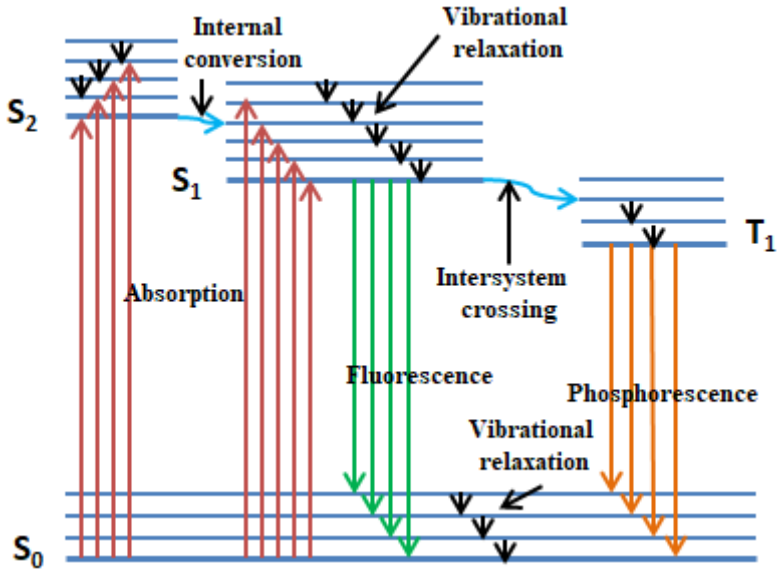

Figure 1.1: Jablonski diagram

1.11.1 Quenching of fluorescence

Different processes which reduce fluorescence intensity of a given sample are collectively termed as quenching. Quenching measurements provide vital information about type of molecular interactions and ease of access of fluorophore to target species. It can occur by various molecular interactions such as energy transfer, molecular rearrangements and excited state reactions. Additionally, quenching can also occur by non-molecular mechanisms, such as reduction in amplitude of incident light by fluorophore itself or by other species. Dynamic and static quenching are usually encountered mechanisms involved in fluorescence quenching. Dynamic or collisional quenching takes place when excited-state fluorophore and quencher in solution undergo collisional encounter, resulting in deactivation of fluorophore. Static quenching occurs when a non-fluorescent stable complex is formed between ground state fluorophore and quencher.

1.11.1.1 Dynamic or collisional quenching

During collisional quenching, fluorophore undergoes diffusive encounter with quencher in excited state and then returned to ground state without any chemical alternation of molecules during the process. Reduction in fluorescence intensity associated with collisional quenching is given by Stern-Volmer equation,[97]

$$\frac{\boldsymbol{F_0}}{\boldsymbol{F}} = \mathbf{1} + \boldsymbol{k_q \tau_0}[\boldsymbol{Q}] = \mathbf{1} + \boldsymbol{K_D}[\boldsymbol{Q}]$$

where F and F_0 represents fluorescence intensity in presence and absence of quencher, k_q denotes bimolecular quenching constant, [Q] is concentration of quencher and K_D is Stern-Volmer constant in dynamic quenching.

1.11.1.2 Static or contact quenching

Static quenching does not depend on molecular collision or diffusion, because it takes place in the ground state. Relationship between concentration of quencher and fluorescence intensity is given by the following equation,

$$K_s = \frac{[F - Q]}{[F][Q]}$$

where K_s is association constant for complex formation, [F] and [Q] represents concentration of uncomplexed flurophore and quencher, respectively. [F-Q] denotes concentration of complex.

Dynamic and static quenching can be primarily differentiated on basis of life time measurements and also with their differing rely on viscosity and temperature. In static quenching, life time remain unchanged because only uncomplexed fluorophore will give observed fluorescence. On contrary, life time of fluorophore is perturbed in collisional quenching since quenching is an additional rate process that depopulate excited state without fluorescence emission.[97] As temperature increases, diffusion coefficients also increases, resulting in larger amount of collisional quenching. On the other hand, increase in temperature decrease the stability of weakly bound non fluorescent complexes with subsequent decrease in static quenching.

1.11.1.3 Inner filter effect

Fluorescence sensors based on dynamic and static quenching are found to be more complicated and time consuming because they involve intermolecular connection between fluorophore and target molecule. Additionally, they also demand complementary geometry and works only if

they are located at a particular distance. These constraints limit practical applications of fluorescent sensors. In this context, sensors based on inner filter effect (IFE) assume considerable significance. IFE is usually considered as an annoying source of error in fluorescent sensing, but it is beneficial for development of highly sensitive fluorescent assay.[98-101] IFE refers to absorption of excitation and/or emission light of fluorophores by absorbers (quenchers) in detection system. [97,102] It is interesting to note that IFE takes place only if the excitation and/or emission bands of fluorophore overlap with absorption band of absorber. Compared to other mechanisms, IFE possesses enhanced sensitivity because changes in absorbance of target molecule is transformed into exponential changes in intensity of fluorophore. Nowadays, IFE has gained much interest in field of sensors,[103-108] which can be attributed to its simplicity, flexibility and selectivity.

1.11.2 Fluorophores or fluorescent probes

Fluorophore can be defined as a luminescent chemical species that can re-emits photons at excited state. Main features of fluorescent probe include quantum yield, life time, stokes shift, excitation coefficient and emission wavelength. An ideal fluorophore possess high quantum yield and molar absorption coefficients. It should be stable upon continuous illumination and is measureable with conventional instrumentation. However, inherent properties of fluorophore get altered with changes in environment of surrounding medium. Molecular interaction between fluorophore and target molecules is transformed into a fluorescence signal. In present study, carbon dots were used as fluorophore for determination of food additive, sunset yellow.

1.11.2.1 Stokes shift

Fluorescence emission takes place at lower energy/longer wavelength compared to absorption. Stokes shift refers to difference between spectral positions of band maxima of absorption and emission, arising from same electronic transition[109] and the term is named after Irish physicist George G. Stokes.[110] It occurs mainly due to two reasons[111] (i) vibrational relaxation (ii) solvent reorganisation. Vibrational relaxation arises from rapid decay of fluorophore to lowest vibrational level of S_1 or higher vibrational level of S_0. Furthermore, complex formation, and/or energy transfer and excited state reactions can also account for stoke shift of fluorophores. Fluorophores with large stokes shift values are found to be more suitable for sensing applications.

1.11.2.2 Fluorescence quantum yields and lifetime

Most imperative attributes of fluorophores include its quantum yields and lifetime. Fluorescence quantum yield (ϕ) is ratio of number of photons emitted to number of photons absorbed.[97]

$$\boldsymbol{\phi} = \frac{\Gamma}{\Gamma + \boldsymbol{k_{nr}}}$$

where Γ is emissive rate of fluorophore and k_{nr} is non-radiative decay rate to S_0. Value of quantum yield varies between zero and one and it is close to unity when $k_{nr} < \Gamma$. The ϕ of a fluorophore is usually measured with respect to a dye of known quantum yield and is estimated using following equation,

$$\frac{\boldsymbol{\phi_S}}{\boldsymbol{\phi_R}} = \frac{\boldsymbol{A_S\, I_R\, \eta_R^2}}{\boldsymbol{A_R\, I_S\, \eta_S^2}}$$

where ϕ_S and ϕ_R represents quantum yield of standard and reference, respectively. I, A and η denotes integrated fluorescence intensity, absorbance

and refractive index, respectively. Subscripts S and R refers to sample and reference.

For a fluorophore, lifetime (τ) denotes a short period of time that the molecules remain in excited state before it returns to ground state and is given by equation,

$$\boldsymbol{\tau = \frac{1}{\Gamma + k_m}}$$

Lifetime of a fluorophore usually vary from nanoseconds to picoseconds.

1.11.3 Carbon dots

Carbon dots (C-dots or CDs) or carbon quantum dots (CQDs), is a type of nanostructured material with average size below 10 nm.[112] It was discovered by Xu *et al.* in 2004, during preparative electrophoresis of single walled carbon nanotubes.[113] CDs have received considerable attention from researchers owing to their unique optical properties. CDs are considered as better fluorescent probes compared to prevailing quantum dots and organic dyes[114,115] due to their advantages like easy availability, water solubility, chemical inertness, photoluminescence, low toxicity, biocompatibility and high resistance to photobleaching.[116] Distinctive and novel proprieties of CDs have found diverse applications in various fields such as biology (bioimaging, biosensing, drug delivery, nanomedicine), chemical sensing, and optoelectronics.[117-119] However, exact mechanisms responsible for fluorescence emission of CDs are debatable even today.[120] Suggested mechanisms include band gap transitions caused by conjugated π-domains[121,122] or through surface related defective sites.[123,124]

1.11.3.1 Surface passivation and functionalization of CDs

Surface passivation is employed as an effective strategy to stabilize fluorescence and to improve fluorescence quantum yields of CDs.[116] Surface passivation of CDs can be achieved using organic polymers or with inorganic salts or heteroatoms (S or N).[125] During surface passivation, groups like amine, hydroxy and carboxyl are introduced on surface of CDs, which impart better water solubility, good dispersibility and specific chemical reactivity to prepared CDs.[126]

Surface functionalization impart certain defects in surface of CDs, which act as excitation energy traps and lead to large variations in fluorescence emissions.[127,128] Chemical groups such as amines, carboxylic acid and hydroxyls are introduced onto surface of CDs for functionalization treatment. Surface passivating agents usually act as functionalizing agents also.[125]

1.11.3.2 Synthesis of CDs

Synthetic approaches of CDs can be broadly classified into two categories, *viz* 'top-down' method and 'bottom-up' method.[112,125] Top-down method involves breaking down of larger carbon structures by methods like electrochemical oxidation, arc discharge and laser ablation and bottom-up approaches include synthesis of CDs from molecular precursors through combustion/thermal treatments and microwave assisted synthetic routes.

1.11.3.3 Green Synthesis of CDs

Recently, green synthesis has gathered much interest among researchers for production of CDs. Microwave assisted green synthetic procedures offer

advantages such as simplicity, cost effectiveness, robustness and capability for development of materials with high quantum yield.[129-131] Present investigation focuses on microwave assisted green synthesis of CDs from leaves of Hibiscus plant and its use as a fluorescence probe for the determination of synthetic food colorant, sunset yellow.

1.11.4 Literature review of fluorescence sensors based on green synthesis of CDs

Prasannan and Imae demonstrated synthesis of fluorescent CDs from bio waste of orange peels through one-step hydrothermal carbonization process.[130] Synthesized CDs showed spherical morphology (2-7 nm diameter) and yellow fluorescence, with a quantum yield of 12.7%. Developed method revealed its great potential as fluorescent marker.

Zhou *et al*. reported a synthetic method for large scale production of water soluble CDs from watermelon peel.[132] CDs were synthesized through low-temperature pyrolysis and filtration, without any complex or post-treatment process. Developed CDs showed strong blue luminescence, good aqueous solubility and good pH stability (pH range of 2.0–11.0). Practical applicability of developed CDs was demonstrated in live cell imaging.

Synthesis of CDs by nitric acid oxidation of plant soot was reported by Tan *et al*.[133] Prepared CDs were soluble in water and average size recorded was 3.1 nm. Strong photoluminescence was revealed under UV light. Synthesised CDs had good photostability when compared to organic dyes such as rhodamine and fluorescein. Effectiveness of various ligands such as 4,7,10-trioxa-1,13-tridecanediamine (TTDDA), poly-L-lysine (PLL), cysteine and

chitosan as passivating groups were also investigated. Practical applicability of CDs was evaluated in cell imaging.

A green method for synthesis of CDs via hydrothermal process has been reported by Xu *et al.* using aloe as carbon source.[134] Prepared CDs were characterized by AFM, TEM, fluorescence spectroscopy, UV-vis absorption spectroscopy as well as by FTIR. CDs were spherical in shape and average diameter was 5 nm. The as-synthesized CDs display bright yellow fluorescence with a quantum yield of 10.4%. Surface of as-prepared CDs were rich in hydroxyl groups, which results in better quantum yield, good photostability and improved solubility. Synthesized CDs were used to probe tartrazine in food samples.

Yuan *et al.* developed a method to detect food colorant, sunset yellow in soft drink samples using fluorescent CDs.[135] CDs were prepared using non-fluorescent chelating ligand N-(2-Hydroxyethyl) ethylenediaminetriacetic acid (HEDTA) as carbon source. CDs were synthesized by heating HEDTA in air. As-prepared CDs were water soluble with an average size of 5.9 nm and exhibited strong blue fluorescence. The synthesised CDs were used for determination of sunset yellow in soft drinks.

1.12 Scope of present investigation

Recognition and quantification of analytes has become major priority of researchers to address the concerns related with food quality, clinical diagnosis and clean environment. Great efforts have been put forwarded to develop simple, sensitive and cost effective methods for determination of these analytes. Increased sophistication of instruments in analytical chemistry

have brought breakthrough in field of sensing and sensors based on voltammetric and optical methods have become an undisputed choice for determination of target species.

Based on our proficiency in developing sensors in diverse fields,[136-145] present investigation aims to develop sensitive and reliable methods for determination of food additives and pharmaceuticals. Sensors based on voltammetry are very well suited to achieve these goals. Present study includes development of four voltammetric sensors for determination of food additives such as propyl gallate, *tert*-butylhydroquinone, ponceau 4R and acid green 50. In addition to effect of various experimental parameters and analytical figures of merit, kinetic parameters of each developed system were also explored.

Additionally, two optical sensors were also developed during the course of study. Among two optical sensors developed, one is a colorimetric sensor for determination of tetracycline, a pharmaceutical and other is a fluorescence sensor employed for determination of sunset yellow, a commercially available synthetic food colorant. Practical utility of developed sensors were confirmed by determining concentration of target species in commercially available samples.

.....ꕥ.....

Chapter 2

MATERIALS AND INSTRUMENTATION

Contents

2.1 Reagents
2.2 Instruments
2.3 Cleaning of GCE
2.4 Preparation of buffer solutions
2.5 Reference methods for sample analysis

This chapter provides brief account about materials and instruments used for development of voltammetric and optical sensors for analysis of food additives and pharmaceuticals. Cleaning of glassy carbon electrode (GCE) and preparation of different buffer solutions are also discussed.

2.1 Reagents

Analytical grade chemicals and solvents were used throughout studies, without further purification. Millipore water was obtained from Millipore Direct-Q instrument. Propyl gallate, *tert*-butylhydroquinone, L-cysteine, tetracycline, oxytetracycline and chloroauric acid were purchased from Sigma Aldrich, India. Reagents such as *p*-aminobenzenesulphonic acid, bromophenol blue, acid green 50, glycine, sunset yellow, ethylenediamine, sodium citrate, copper nitrate, cobalt nitrate, potassium nitrate, lead nitrate, manganese chloride, magnesium chloride, disodium hydrogen orthophosphate,

sodium dihydrogen orthophosphate, potassium ferricyanide, sodium chloride and sodium sulphite were purchased from SD Fine chemicals, Mumbai, India. Acetic acid, ascorbic acid, aspartic acid, citric acid, sodium acetate, sulphuric acid, glucose, fructose and saccharin were purchased from Merck specialities Pvt. Ltd, India. Fluorescein from Loba Chemie Pvt Ltd, India was used.

Pure grade pharmaceuticals such as penicillins (ampicillin), amoxicillin, ceftriaxone sodium, cephalexin, metronidazole, tinidazole and sulfamethoxazole were obtained as gift samples.

Samples for application studies such as vegetable oils (sunflower and coconut oils), soft drinks and tetracycline tablets were procured from local market.

2.2 Instruments

Electrochemical studies consisting of cyclic voltammetry, linear sweep voltammetry, differential pulse voltammetry, square wave voltammetry, electrochemical impedance spectroscopy, chronoamperometry and chronocoulometry were carried out in a conventional three electrode system using CH instruments (USA) and BAS Epsilon electrochemical analyzer (USA) coupled with a personal computer. Nanoparticles and polymer film modified GCE were used as working electrodes. Platinum wire and Ag/AgCl electrodes were served as auxiliary and reference electrodes, respectively. Cleaning of working electrode was performed using an ultrasonicator (Oscar Ultrasonics, Pvt. Ltd. Mumbai). Scanning electron microscopic images were taken on a JOEL 6390 LV. Atomic force microscopic images were obtained on

a composite desktop AFM/STM-Nanosurf AG, Switzerland. pH measurements were recorded in metrohm digital pH meter.

Fluorescence spectroscopic studies were performed with JAZ-EL-200-X spectrofluorimeter using a quartz cuvette of 1 cm path length and UV- visible spectra were taken using Thermo scientific, Evolution 201, China. TEM images were recorded using JEM-2100 HRTEM. Zeta potential and particle size were measured using ZetasizerNano ZS series, Malvern instruments. Fourier transform infrared (FTIR) studies were performed on JASCO 4100 spectrometer using KBr discs. Surface functional properties were done by X-ray photoelectron spectroscopy (Thermo Fischer Scientific Co., USA). Fluorescence lifetime was measured using a HORIBA fluorescence lifetime system (Helteapro tm, USA). Morphology and size of nanoparticles were characterized by transmission electron microscopy (Hitachi H600). Photographs were taken with Sony DSC-290 digital camera.

2.3 Cleaning of GCE

Prior to use, GCE was mechanically polished with alumina powder (0.05 micron) on a polishing pad and was cleaned thoroughly with millipore water. It was then sonicated with methanol, 1:1 HNO_3 solution, acetone and millipore water each for 5 minutes, respectively.

2.4 Preparation of buffer solutions

2.4.1 Preparation of acetate buffer solutions (ABS)

Sodium acetate trihydrate and acetic acid were weighed in different amounts as detailed in table, dissolved in water and diluted to 100 mL for preparing ABS of different pH values (Table 2.1).

2.4.2 Preparation of phosphate buffer solutions (PBS)

By mixing monosodium dihydrogen phosphate and disodium hydrogen phosphate in different amounts, PBS of different pH values was prepared. Amounts of monosodium dihydrogen phosphate and disodium hydrogen phosphate used for preparation of PBS are enlisted in Table 2.2.

2.5 Reference methods for sample analysis

Reference methods employed for analysis of various samples are detailed below.

2.5.1 Reference method for antioxidant, propyl gallate

Spectrophotometric determination of propyl gallate (PG) was performed using the procedure described in AOAC.[146] Stock solution of PG was prepared using methanol as solvent. Working standards were prepared by adding suitable volume of stock solution into 25 mL standard flask, followed by addition of 2.5 mL of 10% NH_4OAc solution to each standard flask. Resultant solutions were diluted to 24 mL with water. Subsequently, 1.0 mL of ferrous tartarate solution was also added to each standard flask. Mixed solution was allowed to stand for $\geq$ 3 minutes. Optical density of each sample was measured at 540 nm and calibration graph was plotted by absorbance against concentration. Using standard curve, concentrations of antioxidants in vegetable oil samples were calculated.

2.5.2 Reference method for antioxidant, *tert*-butylhydroquinone

Chromatographic determination of *tert*-butylhydroquinone (TBHQ) was performed by adopting procedure proposed by Lin *et al.*, [147] with some minor modifications. HPLC instrument equipped with UV–visible detection

at 280 nm was used. Mobile phase was a mixture of (A) methanol and (B) 1% orthophosphoric acid. Flow rate and sample injection volume were 1 mL minute^{-1} and 20 μL respectively. Peak area ratios were used for calculation of concentrations of TBHQ in edible vegetable oils.

2.5.3 Reference method for food colorants

Spectrophotometric determination of food colorants such as ponceau 4R (P4R), acid green 50 (AG) and sunset yellow (SY) was performed using procedure described in AOAC.[148] Stock solutions of food colorants were prepared using suitable solvents. Working standards were prepared by serial dilution of stock solution. Optical density of each sample was measured at wavelength of maximum absorption (i.e., at wavelength of 507, 633 and 482 nm for P4R, AG and SY, respectively). Calibration graph was plotted by absorbance against concentration. Using standard curve, concentrations of food colorants in soft drink samples were calculated.

Table 2.1: Preparation of 0.1 M acetate buffer solution

pH	CH_3COOH (in grams/100 mL)	$CH_3COONa.3H_2O$ (in grams/100 mL)
2	0.5994	0.0024
3	0.5900	0.0237
4	0.5098	0.2054
5	0.2161	0.8711
6	0.0319	1.2885
7	0.0036	1.3534
8	0.0034	1.3602
9	0.0038	1.3609
10	0.0000	1.3609

Table 2.2: Preparation of 0.1 M phosphate buffer solution

pH	NaH_2PO_4 (in grams/100 mL)	Na_2HPO_4 (in grams/100 mL)
2	1.3799	0.0001
3	1.3790	0.0003
4	1.3780	0.0036
5	1.3615	0.0360
6	1.2143	0.3218
7	0.5836	1.5466
8	0.0940	2.4970
9	0.0100	2.6605
10	0.0010	2.6781

.....ഠോര.....

Chapter 3

VOLTAMMETRIC SENSOR FOR PROPYL GALLATE BASED ON GOLD NANOPARTICLE/POLY (*P*-AMINOBENZENESULPHONIC ACID) COMPOSITE MODIFIED GLASSY CARBON ELECTRODE

Contents

3.1 Introduction
3.2 Experimental
3.3 Results and discussion
3.4 Conclusions

This chapter reports application of gold nanoparticle (AuNP)/poly(p-aminobenzenesulphonic acid) [poly(p-ABSA)] composite modified glassy carbon electrode (GCE) for electrochemical determination of propyl gallate (PG). The AuNP/poly(p-ABSA) composite showed excellent electron transfer ability for oxidation of PG by lowering oxidation potential and remarkably enhancing current response. Experimental parameters such as effect of pH, number of cycles of electrodeposition, thickness of polymer film and scan rate were optimized. The calibration curve showed that oxidation peak current was proportional to concentration of PG in the range 1.0×10^{-4} *to* 9.0×10^{-6} *M, with a correlation coefficient of 0.997 and limit of detection of* 1.9×10^{-7} *M. Diffusion coefficient of* 2.3×10^{-6} $cm^2\ s^{-1}$ *was calculated from chronoamperometric measurements. Designed sensor shows excellent reproducibility and stability and it was successfully used to determine PG in edible vegetable oils (coconut oil and sunflower oil), with recoveries between 98.9 and 101.3 %.*

3.1 Introduction

Antioxidants are a group of food additives which play an important role in food industry due to their ability to protect food stuffs from loss of nutritive value and discoloration caused by oxidative rancidity.[149] These can also be used to prevent degradation of foodstuffs during processing, packaging and storage. Antioxidants work by suppressing chain initiation or break chain propagation during peroxidation of unsaturated fatty acids.[150] Among various antioxidants, PG (Fig. 3.1) has been widely used as a food additive owing to its high performance, stability and wide availability. However, studies have indicated that excessive use of synthetic antioxidants can result in potential health risk associated with their intake.[151,152] Following recommendation of International organization, JECFA (Joint FAO/WHO Expert Committee on Food Additives), use of synthetic phenolic antioxidants is regulated by legal authorities and for PG, acceptable daily intake recommended by JECFA is 0 – 2.5 mg kg^{-1} of body weight.[153]

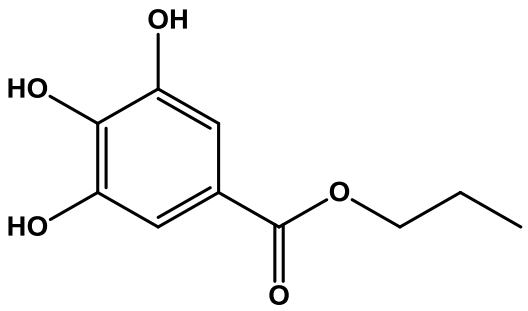

Figure 3.1: Structure of PG

So far, several methods such as chromatography,[154-156] spectrophotometry[157,158] and electrochemical methods[159,160] have been developed for determination

of PG in food stuffs. Among these, electrochemical methods are one of the most favorable techniques due to its rapid and sensitive detection procedures, good miniaturization potential, less cost, thus making it suitable for faster analysis.[161]

Chemically modified electrodes have attracted considerable attention as important analytical tool for electrochemical determination of various analytes. Unique properties of polymer films such as good stability, reproducibility, more active sites, strong adherence to electrode surface and homogeneity in electrochemical deposition makes them an excellent material for modification of electrodes.[162-164] Due to above mentioned properties, researchers have focused their interest on electrically conducting polymers especially polyaniline and its derivatives.[165] Sulfonated polyaniline such as *p*-ABSA is found to have better physical properties and environmental stability than its parent polyaniline.[166]

In recent years nanoparticles have been extensively used in construction of electrochemical sensors owing to their unique physiochemical characteristics that significantly differ from those of bulk materials.[167,168] Among metal nanoparticles, AuNP have been in the forefront of electrode sensor technology due to their high surface to volume ratio, outstanding electrocatalytic activity, good stability and biocompatibility.[169-171] They function as "electron antennae" efficiently channelizing electrons between electrode and analyte.[172] AuNP supported on conducting polymers enhance sensitivity of electrochemical sensor due to their synergistic chemical and physical properties.[173,174]

Present study is intended to develop an electrochemical sensor for selective and sensitive determination of PG using AuNP and poly(*p*-ABSA) composite modified GCE (Scheme 3.1). For the determination of PG, we have tried various chemical modifications on different electrodes (Table 3.1). From Table 3.1 it is clear that maximum peak current and lowest overpotential were obtained with AuNP/poly(*p*-ABSA)/GCE and the choice is justified. The composite structure increased electrocatalytic activity of modified electrode towards oxidation of PG. Suitability of present method was demonstrated by applying this method for determination of PG in vegetable oils.

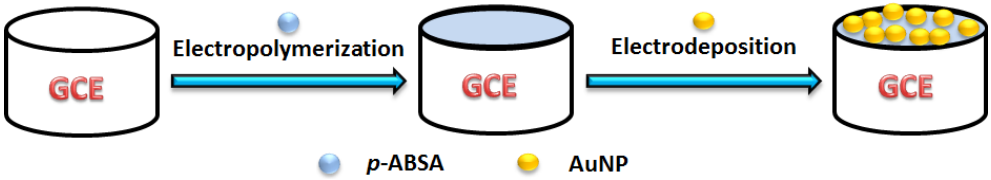

Scheme 3.1: Schematic representation of modification procedure of GCE

3.2 Experimental

3.2.1 Preparation of AuNP/poly(*p*-ABSA)/GCE

Prior to use, GCE was mechanically polished with alumina powder (0.05 micron) on a polishing pad and was cleaned thoroughly with double distilled water. Then it was sonicated with methanol, 1:1 HNO_3 solution, acetone and double distilled water each for 5 minutes respectively. After being cleaned, poly(*p*-ABSA)/GCE electrode was prepared according to literature (Fig. 3.2).[54]

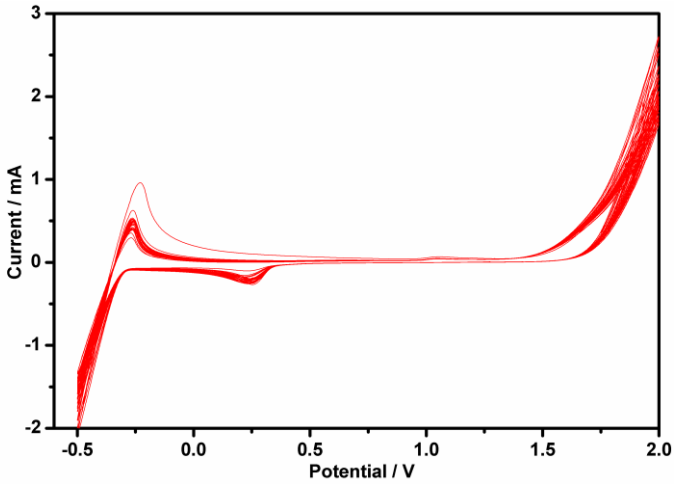

Figure 3.2: Cyclic voltammograms obtained for electropolymerization of *p*-ABSA on GCE

The cleaned GCE was immersed in an aqueous solution of 0.1 M HNO_3 containing 2.0×10^{-3} M *p*-ABSA and the electrochemical deposition of poly(*p*-ABSA) film was carried out by cyclic sweep between -0.5 and 2.0 V at 0.1 V s^{-1} for 30 cycles. The resulting film was washed with doubly distilled water before analysis. Finally, the modified electrode poly(*p*-ABSA)/GCE was electroactivated by cyclic scans from -0.75 to 0.65 V in 0.1 M PBS (pH 7.0). The mechanism of electrochemical polymerization of *p*-ABSA on GCE was comparable to previous report. [27] In the first anodic scan a peak observed at 1.05 V which results from oxidation of *p*-ABSA to its free radical. In the reverse scan, a cathodic peak appeared at 0.26 V, which could be ascribed to hydrazobenzene sulphonic acid resulting from combination of free radicals. From second cycle onwards, an anodic peak appeared at 0.27 V, which might be due to oxidation of hydrazobenzene sulphonic acid to azobenzene sulphonic acid. On continuous scanning, larger peaks were observed due to continuous growth of polymer film.

Electrodeposition of AuNP on polymer modified electrode was carried out by potential cycling between 0 to 1.3 V (vs Ag/AgCl) at a scan rate of 0.1 V s^{-1} for a total of 20 cycles in 5.0 × 10^{-2} M H_2SO_4 solution containing 1.0 × 10^{-3} M $HAuCl_4$ (Fig. 3.3).[175] The gold nanoparticle modified GCE (AuNP/GCE) was prepared by the same procedure.

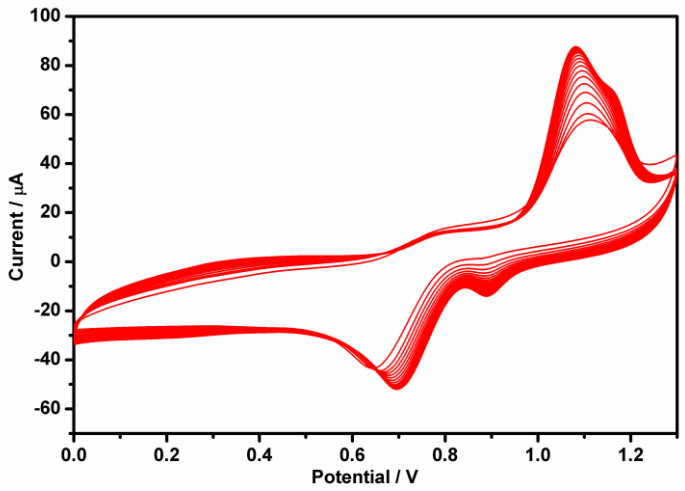

Figure 3.3: Cyclic voltammograms obtained for electrodeposition of AuNP on poly(*p*-ABSA)/GCE

3.2.2 Experimental procedure

Before taking electrochemical measurements, the solution was degassed with N_2. Electrochemical experiments were done using a conventional electrochemical cell containing suitable amount of PG in 10 mL of 0.1 M PBS (pH 7.0). Differential pulse voltammetry (DPV) was used to determine PG in 0.1 M PBS, recorded from -0.1 to 0.4 V with pulse amplitude of 0.5 V, pulse period of 0.5 s, pulse width of 0.2 s and a potential step of 0.004 V. The peak current for oxidation of PG at a potential of 0.106 V was measured.

3.2.3 Treatment of vegetable oil samples

5.0 mL of pure methanol was added into an Erlenmeyer flask (with a screw cap) containing 5.0 g of vegetable oil sample. After mixing on a laboratory shaker for 5 minutes, it was transferred to a centrifuge tube and centrifuged at 3000 rpm for 5 minutes. The extraction procedure was repeated twice; and the resulting solution was made up to 25 mL using methanol.[176] 1.0 mL aliquot of this sample solution was analyzed using voltammetric technique.

3.3 Results and discussion

3.3.1 Characterisation of electrode surface

Scanning electron microscopy (SEM), cyclic voltammetry (CV) and electrochemical impedance spectroscopy (EIS) were used to investigate the surface characteristics of bare and modified GCE.

3.3.1.1 Surface morphology of bare GCE and AuNP/poly(*p*-ABSA)/GCE

The SEM images (Fig. 3.4) display surface morphology of the bare GCE (a) and AuNP/poly(*p*-ABSA)/GCE (b). Since the surface morphology goes in hand with those reported for porous material like polyaniline,[177] highly porous nature of polymer film on surface of GCE is ascertained. From Fig. 3.4b, it could be clearly seen that AuNP are well fixed and uniformly dispersed on porous polymer film. The surface coverage (Γ) of AuNP was estimated to be 1.8×10^{-10} mol cm^{-2} from the integrated charge passed through working electrode during electrodeposition of AuNP based on Laviron equation, $Q = nFA\Gamma$.[178]

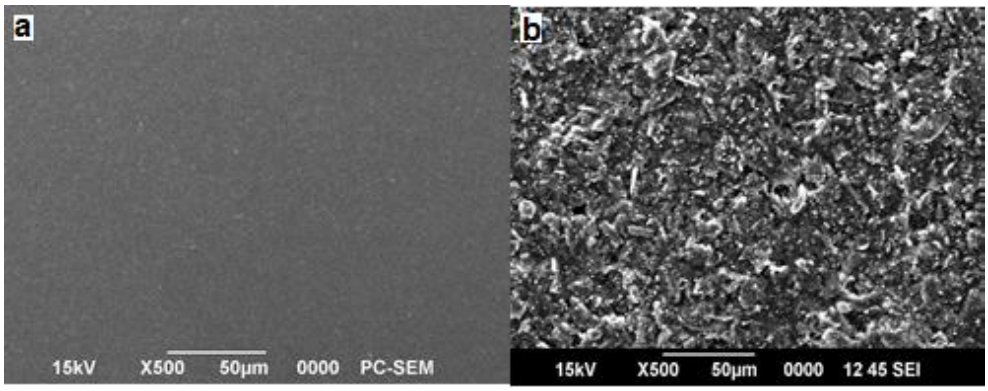

Figure 3.4: SEM images of (a) bare GCE (b) AuNP/poly(*p*-ABSA)/GCE

3.3.1.2 Surface area study

Effective surface area of bare (Fig. 3.5) and modified GCE (Fig. 3.6) were studied by recording the cyclic voltammograms of 2.0×10^{-3} M potassium ferricyanide solution at different scan rates. The apparent electroactive surface area of the different electrodes was calculated using Randles - Sevcik equation for reversible systems.[179]

$$I_p = 2.69 \times 10^5 A D_R^{1/2} n^{3/2} \nu^{1/2} C$$

where n is number of electrons transferred, A is electroactive surface area of electrode, D_R is diffusion coefficient, C refers to concentration of redox probe and ν is scan rate. According to the above equation, apparent electroactive surface area of GCE and AuNP/poly(*p*-ABSA)/GCE were found to be 0.027 and 0.155 cm^2 respectively. All these results imply that AuNP/poly(*p*-ABSA)/GCE has a higher electroactive surface area which in turn results in a relatively better electrochemical reaction ability of modified electrode.

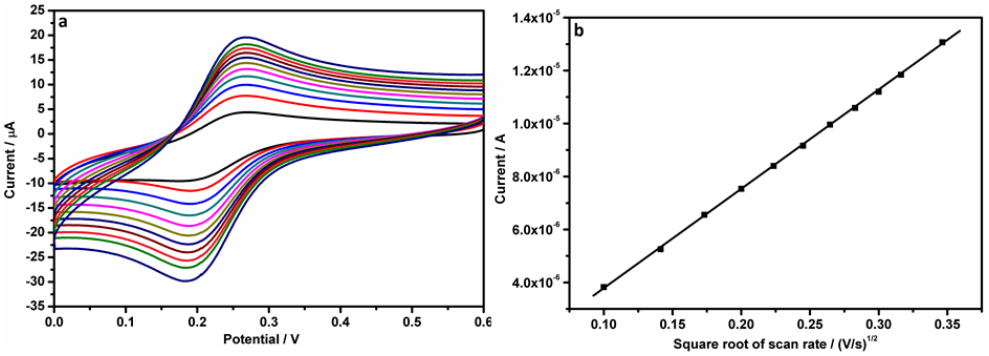

Figure 3.5: (a) Overlay of cyclic voltammograms of 2.0 × 10^{-3} M $K_3[Fe(CN)_6]$ on bare GCE at various scan rates (b) plot of current *vs* square root of scan rate for bare GCE

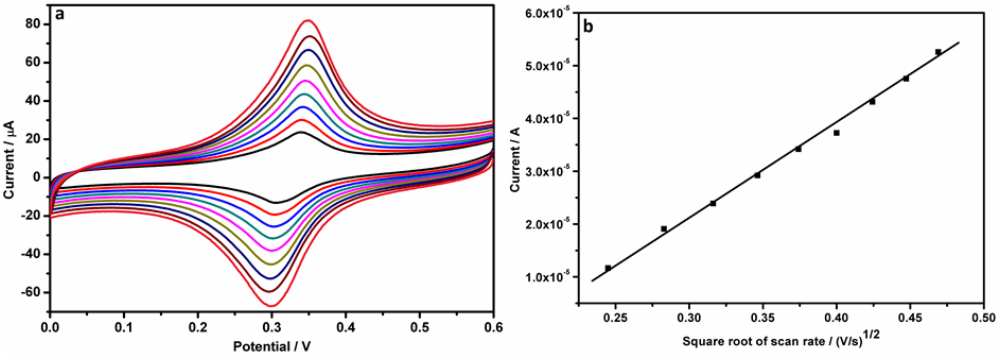

Figure 3.6: (a) Overlay of cyclic voltammograms of 2.0 × 10^{-3} M $K_3[Fe(CN)_6]$ on AuNP/poly(*p*-ABSA)/GCE at various scan rates (b) plot of current *vs* square root of scan rate for AuNP/poly(*p*-ABSA)/GCE

3.3.1.3 Electrochemical impedance spectroscopic studies

The EIS was used to characterize the electron transfer properties of bare and modified GCE. Fig. 3.7 shows Nyquist plots of bare GCE (a) and AuNP/poly(*p*-ABSA)/GCE (b). Compared with bare GCE, a small semicircle at high frequencies was observed for AuNP/poly(*p*-ABSA)/GCE, indicating that AuNP/poly(*p*-ABSA) composite on GCE improved the electron transfer properties of AuNP/poly(*p*-ABSA)/GCE.

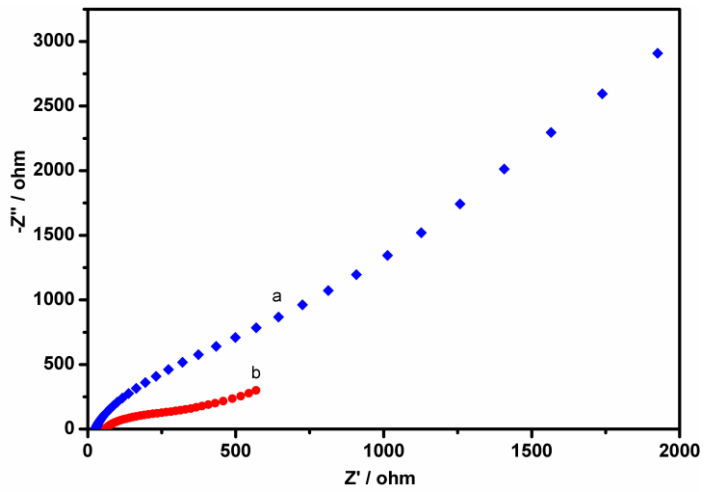

Figure 3.7: EIS spectra of (a) bare GCE (b) AuNP/poly(*p*-ABSA)/ GCE in 5.0×10^{-3} M $[Fe(CN)_6]^{3-/4-}$ in 0.1M KCl at a frequency range 1 -10^5 Hz

3.3.2 Electrochemical behavior of PG on bare and modified GCE

The electrocatalytic properties of modified GCE were initially investigated by CV. Fig. 3.8 shows a comparison of the cyclic voltammograms of 1.0 $\times10^{-4}$ M PG on bare GCE (a), poly(*p*-ABSA)/GCE (b), AuNP/GCE (c) and AuNP/poly(*p*-ABSA)/GCE (d), in 0.1 M PBS (pH 7.0). Absence of a peak in backward scan indicates that the oxidation process is irreversible on both bare and modified GCE. It is evident from obtained cyclic voltammograms that the oxidation of PG at modified electrodes produced better electrochemical response than bare GCE (0.258 V, 5.8 µA).

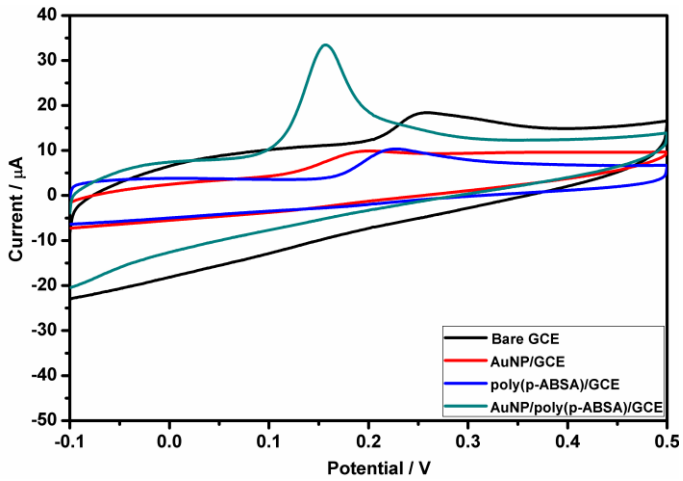

Figure 3.8: Cyclic voltammograms of 1.0 × 10^{-4} M PG at bare GCE, AuNP/GCE, poly(*p*ABSA)/GCE and AuNP/poly(*p*-ABSA)/ GCE in 0.1 M PBS of pH 7.0

The oxidation peak potential at poly(*p*-ABSA)/GCE (0.229 V) and AuNP/GCE (0.201 V) shift towards lower potential compared with bare GCE, but a remarkable increase in oxidation peak current was not observed. At the same time, AuNP/poly(*p*-ABSA)/GCE displays significantly lower oxidation potential (0.157 V) as well as much greater oxidation peak current (24 µA) than poly(*p*-ABSA)/GCE and AuNP/GCE. Moreover, oxidation peak current of PG at AuNP/poly(*p*-ABSA)/GCE has increased almost five fold and oxidation potential is lowered nearly by 100 mV compared to that of bare GCE. All these results illustrate that oxidation of PG can be efficiently catalyzed by AuNP/poly(*p*-ABSA) composite due to synergic effect of poly(*p*-ABSA) film and AuNP. The porous polymer film on GCE provides a template for growth of AuNP and offers an increase in effective surface area and also enhances the electronic conductivity of the composite. Additionally, no electrochemical response could be observed at modified

electrode when control experiment was performed under same condition, in the absence of PG.

Since oxidation of PG occurs at a lower potential of 0.106 V (35 µA) using DPV compared to CV, further studies were carried out using DPV technique. Fig. 3.9 shows corresponding differential pulse voltammograms of PG at bare GCE (a) and AuNP/poly(*p*-ABSA)/GCE (b). PG at modified GCE exhibited a very sharp and well defined oxidation peak in the potential range -1.0 to 0.4 V.

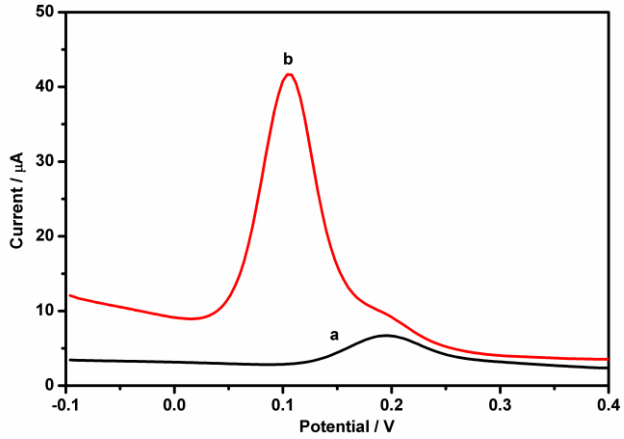

Figure 3.9: Differential pulse voltammograms of 1.0 × 10^{-4} M PG at bare GCE (a) and AuNP/poly(*p*-ABSA)/GCE (b) in 0.1 M PBS of pH 7.0

3.3.3 Effect of Supporting electrolyte and pH

The effect of pH on oxidation process of PG was studied by recording differential pulse voltammograms for 1.0 × 10^{-4} M at pH values ranging from 4.0 to 9.0.

Various electrolytes such as phosphate buffer, acetate buffer, hydrochloric acid, sulphuric acid, potassium nitrate and sodium hydroxide were tested.

Results indicated that lower oxidation potential and higher peak current were obtained with phosphate buffer solution for PG. Therefore, 0.1 M PBS was chosen as supporting electrolyte.

Effect of pH on the oxidation process of PG was determined by recording differential pulse voltammograms for 1.0×10^{-4} M PG at pH values ranging from 4.0 to 9.0 (Fig. 3.10). At constant scan rate, plot of E_p *vs* pH showed that the oxidation peak potential of PG shifted towards lower potential when pH has increased from 4.0 to 9.0. Relationship between oxidation peak potential and pH was linear with regression equation, $E_p(V) = -0.062\, p^H + 0.055$ ($R^2 = 0.997$). Value of slope was comparable with theoretical value (0.059 V pH^{-1}), indicating that the uptake of electrons is accompanied by an equal number of protons.[180]

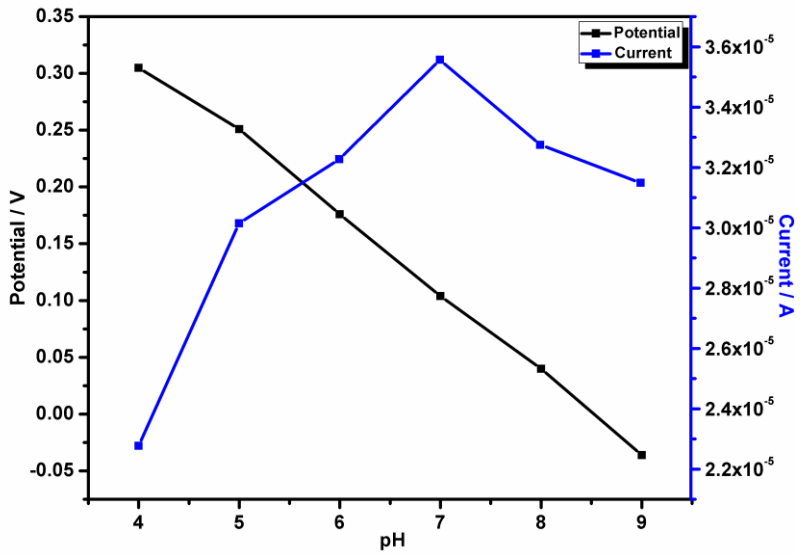

Figure 3.10: Influence of pH on oxidation peak current and peak potential of 1.0×10^{-4} M PG

In addition, with increase in pH value from 4.0 to 7.0, oxidation peak current increases and when pH exceeds above 7.0, peak current decreases (Fig. 3.10). Consequently, pH 7.0 was chosen as optimum value for analysis of this antioxidant.

3.3.4 Effect of poly(*p*-ABSA) film thickness on electrochemical response of PG

Thickness of poly(*p*-ABSA) film on oxidation peak current of 1.0×10^{-4} M PG is a critical parameter and experiments were carried out to study the thickness of polymer film. A series of AuNP/poly(*p*-ABSA)/GCE were prepared by CV and the thickness of polymer film was controlled by varying the number of cycles during polymerization. As shown in Fig. 3.11, oxidation peak current of PG increased with the polymer film thickness at first up to 30 cycles and then decreased. A higher peak current response indicates that AuNP are more scattered on the electrode surface when thickness of film increases. As a result, when specific surface area of AuNP has increased, it will result in increase of active catalytic sites on electrode surface. When the number of cycles of cyclic voltammetric scan was more than 30, peak current was decreased. This may be due to the fact that higher resistance of electrochemical process caused by increased polymer film thickness hindering the electronic exchange between PG and AuNP/poly(*p*-ABSA)/GCE, leading to a decrease in electrode sensitivity. So, 30 cycles of cyclic voltammetric scans were used to prepare the modified electrode.

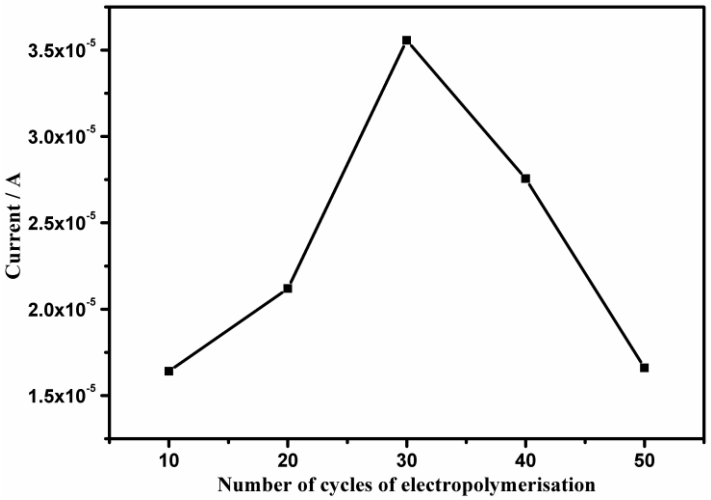

Figure 3.11: Influence of cycle number of electropolymerization on peak current of 1.0 × 10^{-4} M PG

3.3.5 Effect of number of cycles of electrodeposition

In order to evaluate the effect of number of cycles of electrodeposition of AuNP on oxidation of PG, DPV technique was used to detect the oxidative peak current on AuNP/poly(*p*-ABSA)/GCE. Fig. 3.12 shows the influence of number of cycles on oxidation peak current of PG. It was observed that when the amount of AuNP was too less at the electrode surface, peak current was also less, since film possesses only few catalytically active sites. As can be seen from Fig. 3.12, irreversible oxidation peak current of PG increased at first up to 20 cycles and when cycle number of electrodeposition was more than 30, peak current decreased. This may be attributed to decrease in effective surface area of electrode by virtue of increase in size of AuNP on electrode surface. As a result, electrocatalytic activity of electrode is decreased which in turn lead to decrease in oxidation

peak current of PG and sensitivity of electrode. Therefore, the optimal number of cycle of electrodeposition was taken as 20.

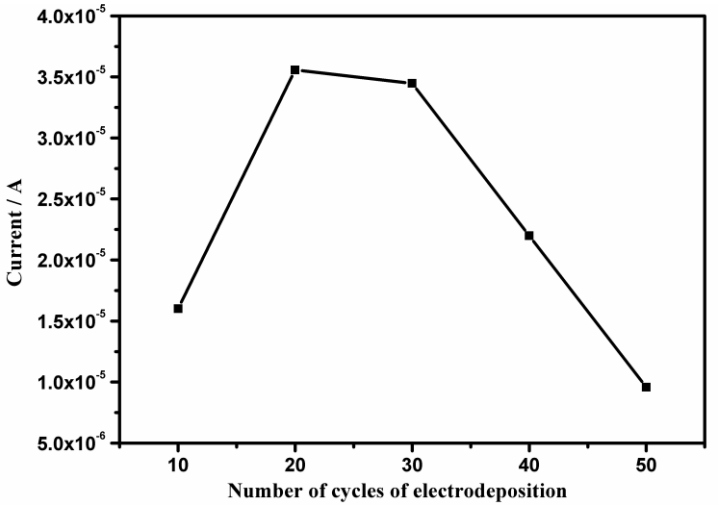

Figure 3.12: Influence of cycle number of electrodeposition on peak current of 1.0 × 10^{-4} M PG

3.3.6 Effect of scan rate

The effect of scan rate on oxidation of PG (1.0 × 10^{-4} M), in 0.1 M PBS (pH 7.0) on AuNP/poly(*p*-ABSA)/GCE was explored by linear sweep voltammetry (LSV). The LSV results demonstrate that when scan rate is increased, peak current as well as the peak potential increased (Fig. 3.13a). This clear shift of E_p as a function of scan rate indicates that the electrochemical oxidation of PG on AuNP/poly(*p*-ABSA)/GCE is a totally irreversible electrode process. On the other hand, Fig 3.13b indicates that, oxidation peak current of PG is directly linear with square root of scan rate in the range 0.02 to 0.18 V s^{-1}. The calibration equation was $I_p(A) = 2 \times 10^{-4}\ \nu^{\frac{1}{2}}(Vs^{-1}) - 3 \times 10^{-5}\ (R^2 = 0.997)$. Additionally, plot

of log i *vs* log υ showed a linear relationship (Fig. 3.14) with slope equal to 0.61 which is very close to theoretical value of 0.50 for a diffusion controlled process.[64] All these results suggest that oxidation of PG on surface of AuNP/poly(*p*-ABSA)/GCE is diffusion controlled.

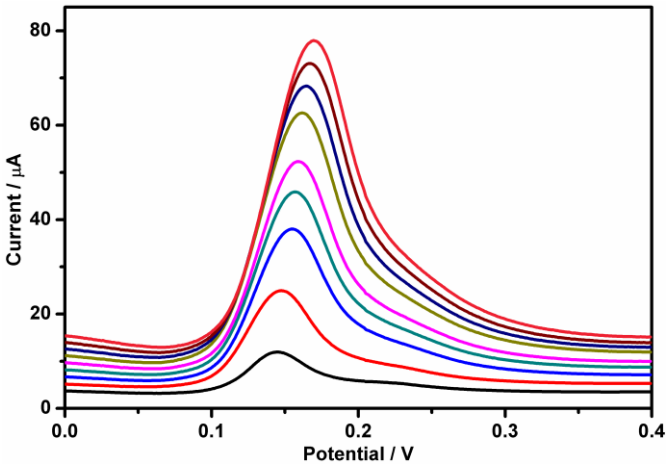

Figure 3.13a: Overlay of linear sweep voltammograms of PG on AuNP/poly(*p*-ABSA)/GCE at various scan rates

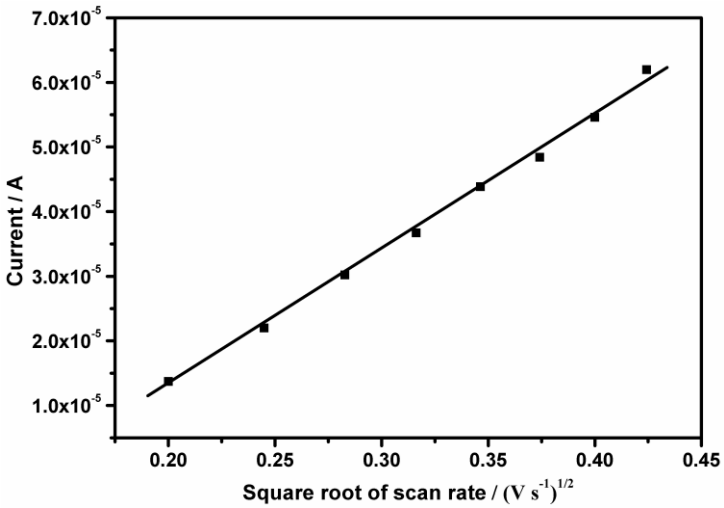

Figure 3.13b: Plot of anodic peak currents *vs* square root of scan rate of PG

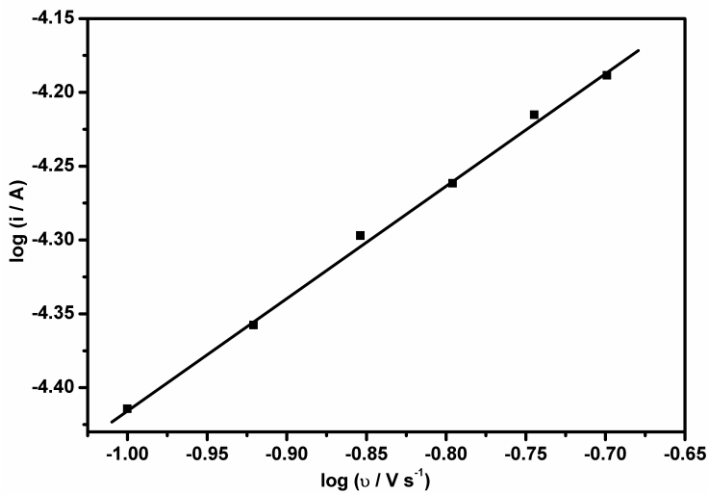

Figure 3.14: Plot of log i *vs* log υ

3.3.7 Analytical parameters

Differential pulse voltammograms for oxidation of PG at various concentrations are depicted in Fig. 3.15a. Adopting previously defined optimal conditions, an analytical calibration graph was constructed. From Fig. 3.15b it could be seen that a linear relationship between oxidation peak current and concentration of PG was obtained over the concentration range from 1.0×10^{-4} to 9.0×10^{-6} M. The linear regression equation was $I_p\ (A) = 0.38C\ (M) - 2 \times 10^{-6}$ with a correlation coefficient of 0.997 and a detection limit of 1.9×10^{-7} M. Performance of the developed sensor was compared (Table 3.2) with other reported works. The results showed that oxidation of PG on AuNP/poly(*p*-ABSA)/GCE possess an extremely lower oxidation potential and lower detection limit in comparison with other reported works.

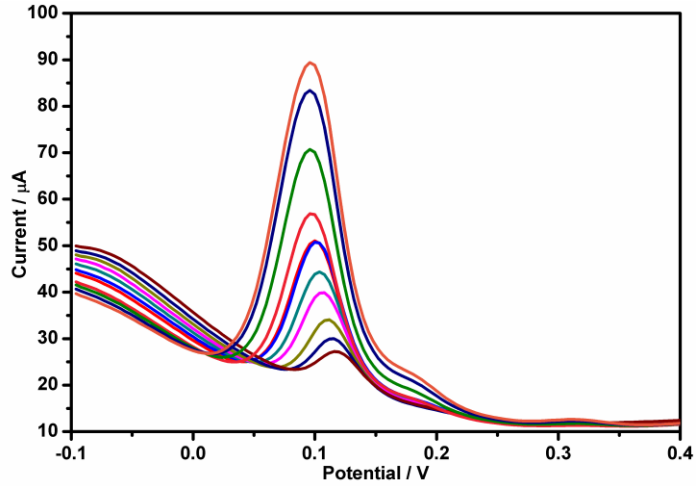

Figure 3.15a: Overlay of differential pulse voltammograms for oxidation of PG at various concentrations

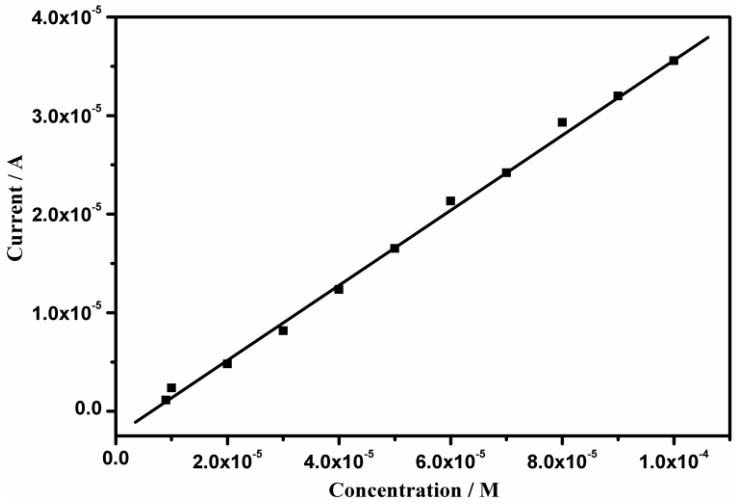

Figure 3.15b: Plot of peak current *vs* concentrations of PG in the range 1.0 × 10^{-4} to 9.0 × 10^{-6} M

3.3.8 Evaluation of kinetic parameters

Based on latest IUPAC recommendations,[183] charge transfer coefficient (α) of PG at the surface of AuNP/poly(*p*-ABSA)/GCE can be calculated from Tafel plot (Fig. 3.16). Anodic charge transfer coefficient α_a is given by the following equation,

$$\alpha_a = \frac{RT}{F}\frac{dlnj_a}{dE}$$

where j_a is anodic current density, E is applied potential and other terms have their usual scientific significance. Reciprocal of slope of Tafel plot (E *vs* ln j_a) will give the value of $\frac{dlnj_a}{dE}$. Based on the above equation, value of α_a was calculated to be 0.48; which is in good agreement with theoretical value of 0.50. [183]

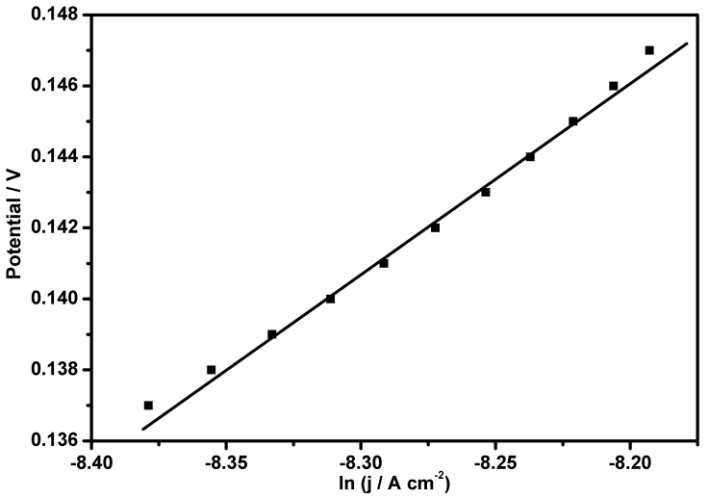

Figure 3.16: Tafel plot

Number of electrons (n) involved in reaction was calculated using the following equation[184]

$$(\mathbf{1}-\boldsymbol{\alpha_a})\boldsymbol{n}=\frac{\mathbf{47.7}}{(\boldsymbol{E_{pa}}-\boldsymbol{E_{p1/2}})}$$

where $E_{p1/2}$ is half peak potential. For irreversible oxidation of PG, number of electrons was calculated to be 2.3. It indicates that oxidation of PG involves two electrons per molecule, similar to oxidation of substituted phenols.[185] The suggested mechanism is shown in Scheme 3.2

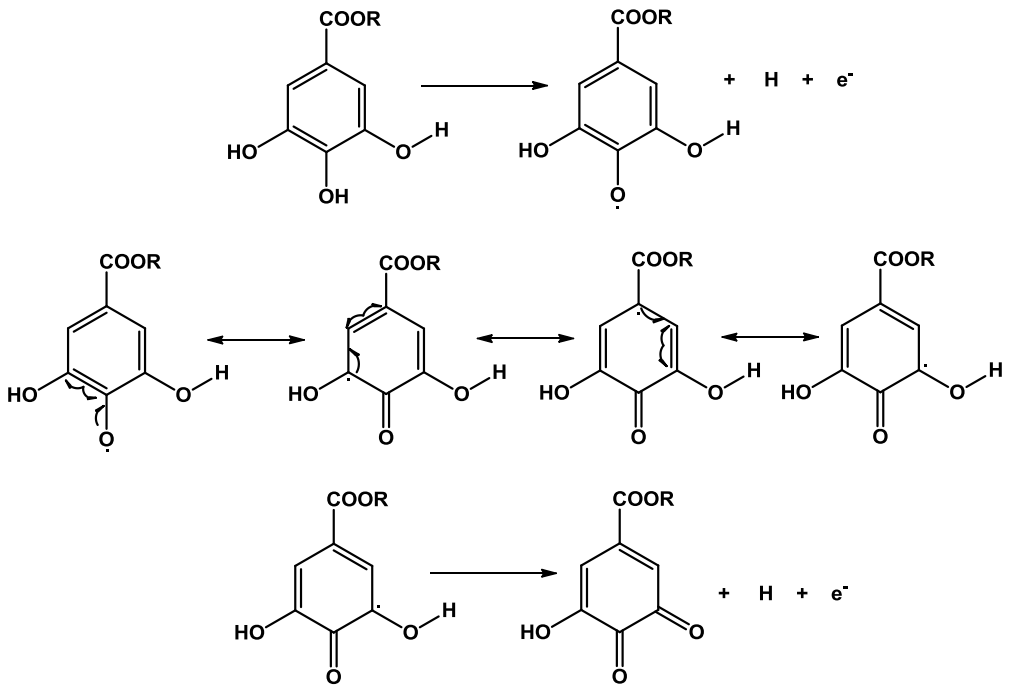

Scheme 3.2: Mechanism of electrooxidation of PG

Heterogeneous rate constant (k_s) for irreversible oxidation of PG at bare and AuNP/poly(*p*-ABSA)/GCE was estimated using Laviron equation[186]

$$E_{pa} = E^{0\prime} + \frac{RT}{(1-\alpha)nF}\left(\ln\frac{(1-\alpha)nF}{RTk_s} - \ln \upsilon\right)$$

where E_{pa} and $E^{0\prime}$ are anodic peak potential and formal potential respectively. The value of k_s was calculated from intercept of plot, E_{pa} *vs* ln υ (Fig. 3.17). Whereas $E^{0\prime}$ was obtained from intercept of E_{pa} *vs* υ graph by extrapolating to vertical axis at υ = 0 (Fig. 3.18). The k_s was found to be 2.99 and 3.21 s^{-1} for bare and AuNP/poly(*p*-ABSA)/GCE respectively. Comparatively higher value of k_s for AuNP/poly(*p*-ABSA)/GCE suggests better electrocatalytic ability of modified electrode for oxidation of PG.

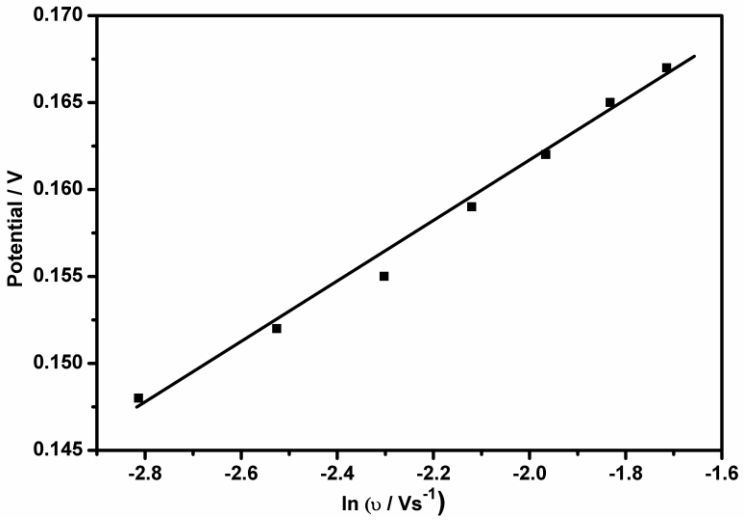

Figure 3.17: Variation of E_{pa} with ln υ

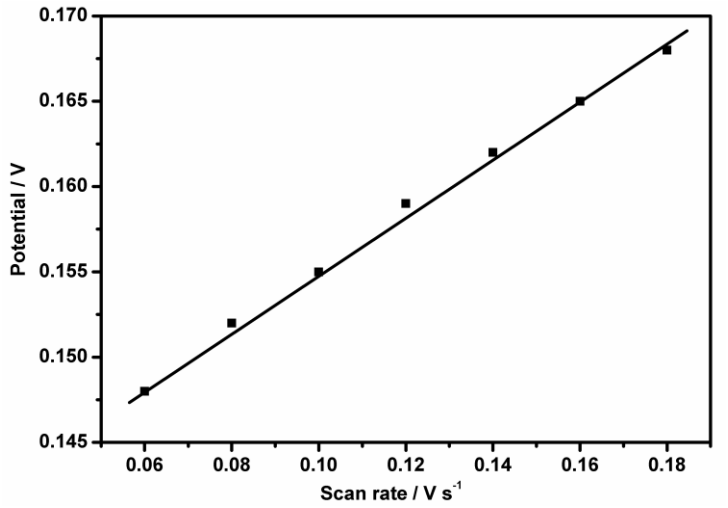

Figure 3.18: Variation of E_{pa} with scan rate

3.3.9 Chronoamperometric measurements

Chronoamperometry was employed to study the electrocatalytic oxidation of PG at AuNP/poly(*p*-ABSA)/GCE. Chronoamperograms obtained for various concentrations of PG (1.0×10^{-3} to 1.0×10^{-4} M) at AuNP/poly(*p*ABSA)/GCE is shown in Fig. 3.19a. The plot of I vs $t^{-1/2}$ for different concentrations of PG at the surface of AuNP/poly(*p*ABSA)/GCE depicted straight lines with different slopes (Fig. 3.19b). Diffusion coefficient (D) was calculated from slopes of resulting straight lines plotted *vs* various concentrations of PG (Fig. 3.19c). Electrochemical reaction (at a mass transport limited rate) of PG is described by Cottrell equation,[184]

$$\boldsymbol{I = nFAD^{1/2}C\pi^{-1/2}t^{-1/2}}$$

where C and D are bulk concentration (mol cm^{-3}) and diffusion coefficient (cm^2 s^{-1}), respectively. The plot of I *vs* $t^{-1/2}$ is linear under the diffusion controlled process and diffusion coefficient of 2.3×10^{-6} cm^2 s^{-1} was

estimated from its slope. The calculated value of diffusion coefficient is comparable with 3.9×10^{-6} cm^2 s^{-1}, which is reported for PG.[187]

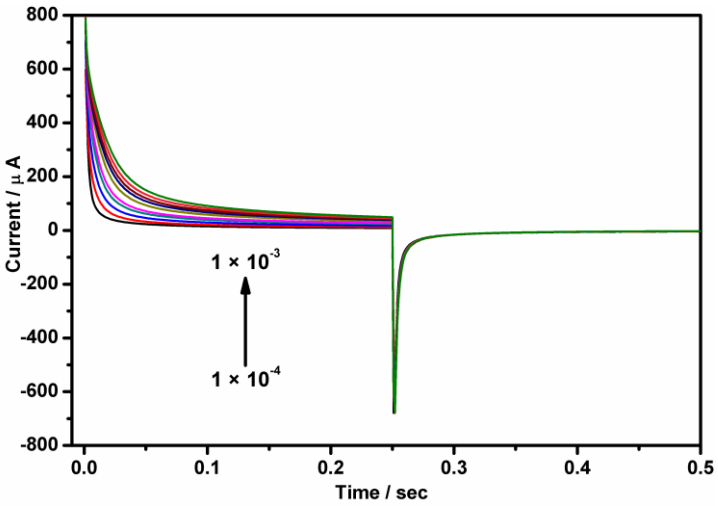

Figure 3.19a: Chronoamperograms obtained at AuNP/poly(*p*-ABSA)/ GCE in 0.1 M PBS (pH 7.0) for different concentrations of PG

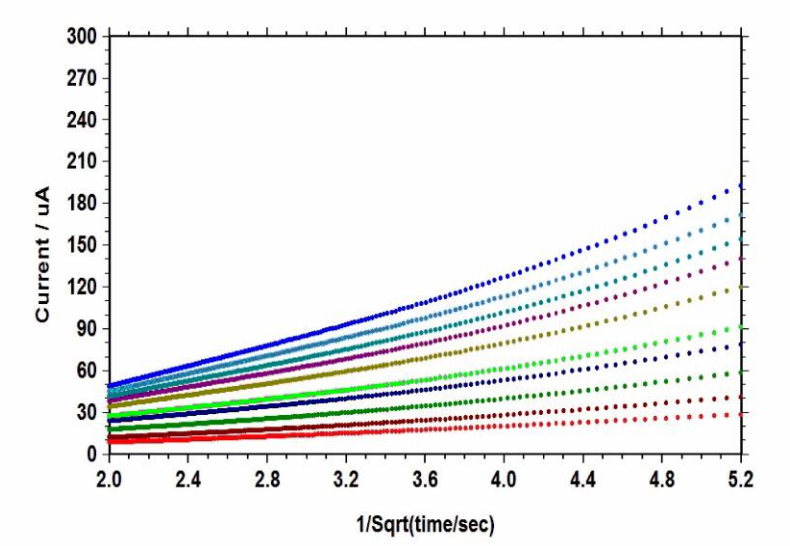

Figure 3.19b: Plots of current *vs* $t^{-1/2}$ derived from the chronoamperograms of Fig. 3.19a

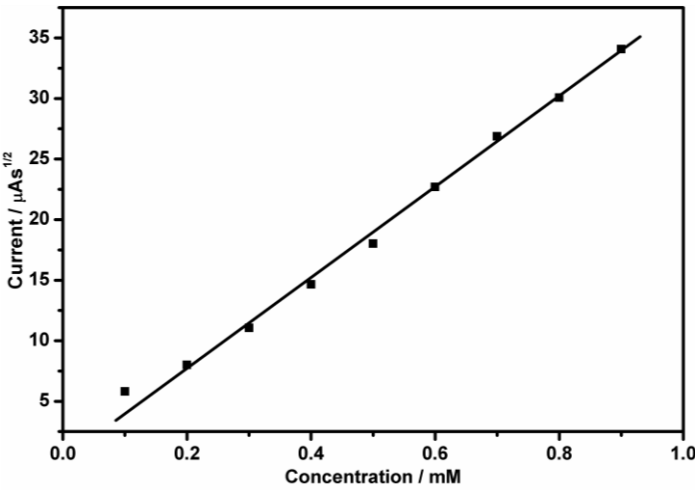

Figure 3.19c: Plot of slope of the straight lines against various concentration of PG

3.3.10 Interference study

Effect of other species on electro oxidation of PG at AuNP/poly(*p*-ABSA)/GCE was studied. It was observed that, up to 100 fold concentration of NaCl, Na_2SO_3, citric acid, CH_3COOH and EDTA have no influence on signals of 1.0×10^{-4} M PG with deviations below 5% (Table 3.3). However, peak current of PG changed significantly in presence of ascorbic acid.

3.3.11 Reproducibility and stability

To ascertain the reproducibility of modified electrode for determination of 1.0×10^{-4} M PG, AuNP/poly(*p*-ABSA)/GCE was prepared six times by using the same GCE. The relative standard deviation obtained was 1.1%. The results indicated that modified electrode has excellent reproducibility. The negligible change in oxidation peak current even after storage for seven days, points to excellent stability of developed sensor.

3.3.12 Application study

To evaluate the practical performance of proposed method, AuNP/poly(*p*-ABSA)/GCE was applied for determination of PG in coconut oil and sunflower oil. Oil samples were tested initially to check the absence of antioxidants and then different quantities of PG were added into the samples. The analysis of vegetable oil samples spiked with PG gave rise to results showed in Table 3.4. The recoveries ranged from 98.9 to 101.3% and observed results are in good agreement with the standard spectrophotometric method discussed in section 2.5.1.[146] Good accordance of two methods indicates reliability of developed sensor for determination of PG in vegetable oil samples. All these results strongly proves that AuNP/poly(*p*-ABSA)/GCE is a promising sensor for the determination of PG.

3.4 Conclusions

In the present study we have used AuNP/poly(*p*-ABSA) composite modified GCE for determination of PG. Proposed sensor demonstrated lowered oxidation potential and enhanced current response. Additionally, fabricated sensor exhibited high sensitivity, low detection limit, good reproducibility and stability. Electrochemical observation showed that the AuNP/poly(*p*-ABSA) composite allow determination of PG in edible vegetable oils with recoveries ranged between 98.9 and 101.3 %.

Table 3.1: Comparison of different modified electrodes for detection of PG

Modified electrode	Potential (V)	Current (μA)
[a]TBC4/GE	0.224	0.13
[b]MSA/GE	0.188	4.47
[c]AuNP/CPE	0.180	27.56
AuNP/poly(*p*-ABSA)/GCE	0.106	35.17

[a] *tert*-butylcalix[4]arene modified gold electrode
[b] Self assembled monolayer of mercaptosuccinic acid modified gold electrode
[c] Gold nanoparticle modified carbon paste electrode

Table 3.2: Comparison of different PG sensors

Electrode	Ep vs Ag/AgCl (V)	Linear range (M)	LOD (M)	References
GCE	0.599	0.70×10^{-3} - 4.71×10^{-6}	2.54×10^{-6}	176
NiPcTs/Ppy/Pt	0.550	4.00×10^{-3} - 4.00×10^{-4}	7.23×10^{-6}	159
P3MT/CFMEs	0.442	1.00×10^{-5} - 1.00×10^{-6}	4.00×10^{-7}	181
MWNT/GE	0.180	1.00×10^{-4} - 1.00×10^{-5}	6.30×10^{-7}	182
AuNP/poly(*p*-ABSA)/GCE	0.106	1.00×10^{-4} - 9.00×10^{-6}	1.90×10^{-7}	Present work

LOD - limit of detection
NiPcTs/Ppy/Pt - Platinum/polypyrrole electrode modified with tetrasulfonate nickel (II) phthalocyanine complex
P3MT/CFMEs - poly(3-methylthiophene)/cylindrical carbon fiber microelectrodes
MWNT- multiwalled carbon nanotube
GE- gold electrode

Table 3.3: Effect of possibly interfering species on the signal of 1.0×10^{-4} M PG

Species	Concentration (M)	Signal change (%)
Sodium chloride	1.0×10^{-2}	-1.28
Sodium sulphite	1.0×10^{-2}	-1.83
Citric acid	1.0×10^{-2}	1.40
EDTA	1.0×10^{-2}	3.14
Acetic acid	1.0×10^{-2}	-1.69
Ascorbic acid	1.0×10^{-4}	12.75

Table 3.4: Determination of PG in food samples

Samples	Added (M)	Spectrophotometric method			Proposed method		
		Found (M)	Recovery (%)[a]	RSD (%)	Found (M)	Recovery (%)[a]	RSD (%)
Coconut oil	2.00×10^{-5}	2.03×10^{-5}	101. 5	1.1	2.02×10^{-5}	101.3	1.5
	6.00×10^{-5}	6.05×10^{-5}	101.0	1.5	5.98×10^{-5}	99.8	4.1
	9.00×10^{-5}	9.08×10^{-5}	100.8	3.7	8.88×10^{-5}	98.9	1.3
Sunflower oil	2.00×10^{-5}	2.01×10^{-5}	100.5	0.8	1.99×10^{-5}	99.7	1.3
	6.00×10^{-5}	6.04×10^{-5}	100.8	2.7	6.02×10^{-5}	100.6	2.1
	9.00×10^{-5}	9.11×10^{-5}	101.2	2.1	9.06×10^{-5}	101.0	1.1

[a]Average of five replicates

*RSD – Relative standard deviation

Chapter 4

VOLTAMMETRIC SENSOR FOR TERTIARY BUTYLHYDROQUINONE BASED ON POLY BROMOPHENOL BLUE MODIFIED GLASSY CARBON ELECTRODE

Contents

4.1 Introduction
4.2 Experimental
4.3 Results and discussion
4.4 Conclusions

This chapter describes development of an electrochemical sensing platform using poly bromophenol blue (poly BPB) film modified glassy carbon electrode (GCE) for determination of tert-butylhydroquinone (TBHQ), a widely used synthetic phenolic antioxidant (SPA). A pair of well-defined quasi reversible peaks with formal potential $E^0 = -0.042$ V was obtained from cyclic voltammetry (CV). Influence of different experimental parameters on voltammetric response of TBHQ was investigated. Under optimal conditions, oxidation peak current of TBHQ was proportional to its concentration in the range 1.0×10^{-5} to 1.0×10^{-6} M using differential pulse voltammetry (DPV). Limit of detection (LOD) and limit of quantification (LOQ) were calculated to be 3.50×10^{-8} M and 1.17×10^{-7} M respectively. Kinetic parameters such as charge transfer coefficient (α) and heterogeneous rate constant (k_s) for bare and modified electrodes were evaluated. Diffusion coefficient (D) was calculated using chronoamperometry. To validate the practical applicability of proposed sensor, poly BPB/GCE was applied for determination of TBHQ in coconut and sunflower oils, which led to satisfactory results.

4.1 Introduction

Oxidation of oil and fats, resulting in quality deterioration, discoloration and rancidity is a major challenge faced by food industry.[188] Food additives such as antioxidants can effectively enhance shelf life of food products during their production and storage. Since natural antioxidants are often unstable and relatively expensive; SPAs are extensively used by the food industry.[189] The SPAs such as butylated hydroxyanisole (BHA), butylated hydroxytoluene (BHT) and butylated hydroquinone (TBHQ) retard the oxidative degradation process by scavenging the free radicals formed and are used either alone or in combinations.[190] Among SPAs, TBHQ (E 319, Fig. 4.1) has aroused considerable attention ever since its first approval as a food additive in USA during 1970s, due to its promising properties such as high thermal stability, low cost, easy availability, anti-lipid peroxidation and its inability to form complexes with either iron or copper.[191,192] However, risk and side effects of TBHQ has become a concern for consumers. Various studies have shown that excess use of TBHQ may lead to loss of nourishment and even carcinogenesis.[193] Association of TBHQ with attention deficit and hyperactivity disorder (ADHD) in human has been documented.[194] It has also been found that excessive use of TBHQ can cause liver enlargement, neurotoxic effects, seizures and paralysis in laboratory animals.[195] Permissible level of TBHQ in food products and edible oils vary greatly among countries. In European Union, TBHQ is banned as an antioxidant in vegetable oils, whereas in USA and China, TBHQ is allowed upto 200 ppm in vegetable oils.[196,197] Hence, a close monitoring of TBHQ levels in vegetable oils is essential to comply with export and import regulations in the globalized market for food stuffs.

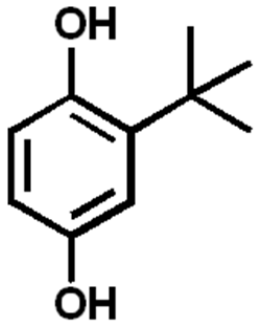

Figure 4.1: Structure of TBHQ

Till date, a variety of analytical methods have been reported for determination of TBHQ in food and oil samples, such as UV-visible spectrophotometry,[198] high performance liquid chromatography (HPLC),[199] HPLC-time-of–flight mass spectrometry (HPLC-TOFMS)[200] and gas chromatography-mass spectrometry (GC-MS).[201] Although these methods have been successfully applied for the determination of TBHQ, they still have some disadvantages such as expensive instrumentation, most require time consuming preliminary extraction steps and are inappropriate for field use also. Compared with the above mentioned methods, electroanalytical techniques are being recognized as an alternative tool because it combines the advantages of low operational cost, speed, simplicity and sensitivity.[185]

In electroanalytical chemistry, modification of electrodes has always been a field of interest. By reducing over potential, modifiers effectively channel electrons between electroactive species to electrode surface, thereby increasing the selectivity and sensitivity of electrode.[202] Use of conducting films as a material for electrode modification has attracted considerable scientific attention as the electropolymerized film is more uniform and by controlling the number of cycles of electropolymerization, thickness of

polymer film can be easily controlled compared to other conventionally adsorbed layer.[203] Dyes used for electropolymerization are acknowledged as one of the excellent electron acceptors or donors. Owing to its easy synthesis from aqueous solution and its stability in presence of air and water, 3′,3″,5′,5″-tetrabromophenolsulfonaphthalein, BPB, is used as electrode modifier for the present study. By potential cycling, BPB forms a polymeric film on the surface of GCE, which can act as an excellent electron mediating agent. The poly BPB/GCE possesses unique properties such as large surface area, effective electron transfer ability and good sensitivity.

Present study is aimed to develop an electrochemical sensing strategy for the determination of TBHQ using poly BPB as sensing material on the surface of GCE (Scheme 4.1), based on CV and DPV. Among various modified electrodes we have used for determination of TBHQ (Table 4.1), better oxidation signals were obtained with poly BPB/GCE, hence its choice is warranted. The as-prepared electrode (poly BPB/GCE) was characterized by atomic force microscopy (AFM), scanning electron microscopy (SEM), electrochemical impedance spectroscopy (EIS) and CV. The study also evaluates application of developed sensor for determination of TBHQ in edible vegetable oils.

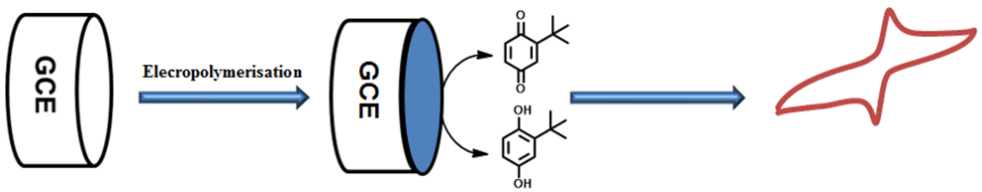

Scheme 4.1: Redox reaction of TBHQ on poly BPB/GCE

4.2 Experimental

4.2.1 Preparation of poly BPB film modified GCE

Prior to modification, GCE was cleaned as detailed in section 2.3. The poly BPB/GCE was fabricated by dipping bare GCE in 0.1 M PBS of pH 6.0 containing 5.0×10^{-4} M BPB and cyclic voltammetric sweeps were recorded between −1.0 to 1.8 V at the scan rate of 0.1 V s^{-1} for 20 cycles (Fig. 4.2). Finally, modified GCE was activated by six successive cycles in 0.1 M PBS of pH 7.0 between −1.0 to 0.9 V.[60]

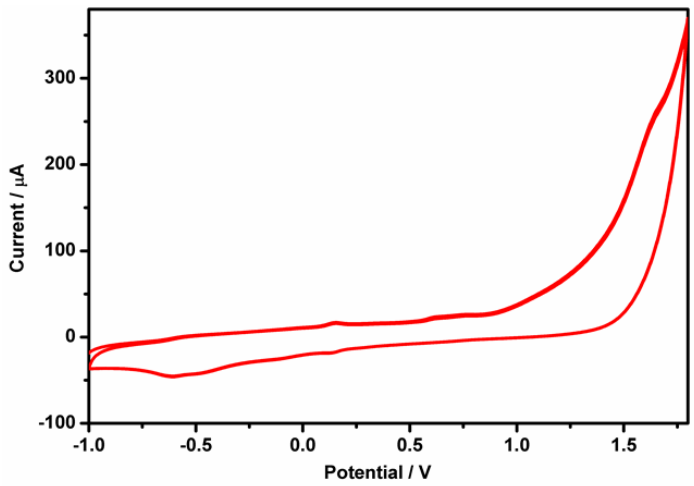

Figure 4.2: Cyclic voltammograms obtained for electropolymerization of BPB on GCE

An obvious oxidation peak at 0.748 V indicates the oxidation of hydroxyl group of BPB monomer. A reversible redox peak observed at about 0.140 V suggests formation of polymer film on the surface of GCE by electropolymerization.[59]

4.2.2 Experimental procedure

Prior to electrochemical measurements, buffer solutions were purged with nitrogen gas. For all voltammetric experiments, the three electrode system was immersed in 10 mL of 0.1 M PBS of pH 7.0 containing suitable amounts of TBHQ. Current measurements were done with DPV in the potential range −1.0 to 0.8 V with pulse period of 0.5 s, pulse amplitude of 0.05 V and pulse width of 0.05 s. Oxidation peak current obtained at −0.037 V was used for the determination of TBHQ.

4.2.3 Treatment of edible vegetable oil samples

Each edible oil (coconut and sunflower oils) sample (5.0 g) was placed in a 100 mL Erlenmeyer flask (with a screw cap) and anhydrous methanol (10 mL) was added into the flask. Mixture was then vigorously shaken for 30 minutes and centrifuged at 3000 rpm for 10 minutes. The extracts were transferred into a sample bottle after providing a settling time of three minutes.[176] Aliquot (100 μL) of obtained sample was subjected to analysis by recording its differential pulse voltammogram.

4.2.4 HPLC-UV as the standard method

Chromatographic determination of TBHQ was performed by adopting the procedure proposed by Lin *et al.*[147] with some minor modifications as detailed in section 2.5.2.

4.3 Results and discussion

4.3.1 Characterisation of electrode surface

SEM, AFM, CV and EIS were used to study the surface characteristics of bare and modified GCE

4.3.1.1 Surface morphology of bare GCE and poly(BPB)/GCE

Surface morphology of bare GCE and poly BPB/GCE was investigated by SEM (Fig. 4.3). Bare GCE (Fig. 4.3a) shows a smooth and uniform surface, however surface roughness is increased on modification with poly BPB (Fig. 4.3b). Based on SEM result, we could infer that BPB was successfully polymerized on electrode surface, resulting in an increased effective surface area of poly BPB/GCE. AFM images of bare and poly BPB/GCE is shown in Fig. 4.4. Compared to bare GCE, increased surface roughness of poly BPB/GCE (GCE: 22.56 nm, poly BPB/GCE: 35.13 nm) confirms the observations of SEM analysis.

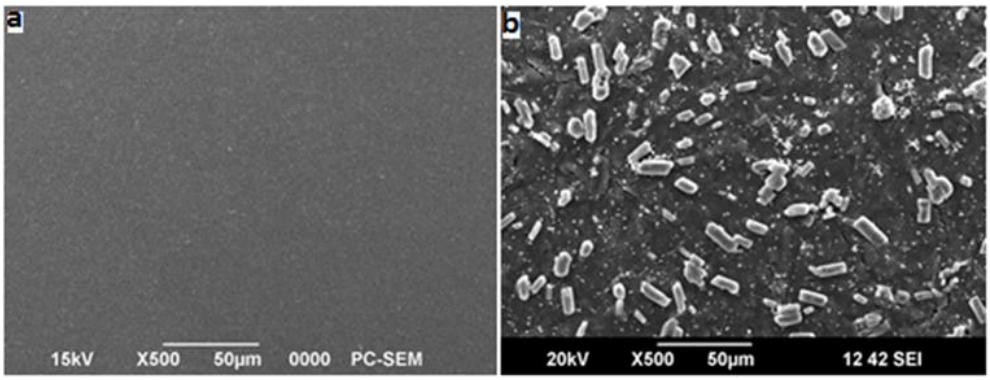

Figure 4.3: SEM images of (a) bare GCE (b) poly BPB/GCE

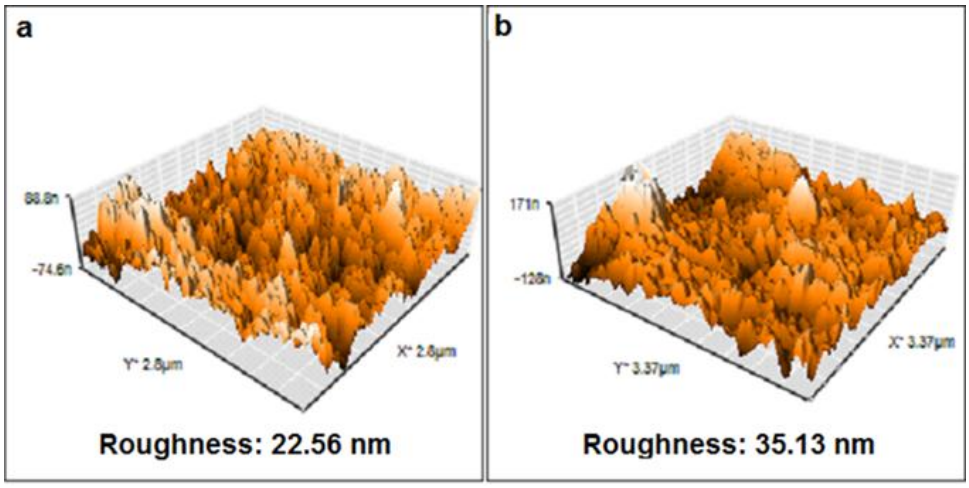

Figure 4.4: AFM images of (a) bare GCE (b) poly BPB/GCE

4.3.1.2 Surface area study

CV was employed to measure effective surface area of bare and modified electrodes using 2.0 × 10^{-3} M $K_3[Fe(CN)_6]$ as redox probe. Effective surface area of bare GCE (Fig. 4.5) and poly BPB/GCE (Fig. 4.6) was calculated by applying Randles–Sevcik equation for reversible systems.[179]

$$\boldsymbol{i_p = 2.69 \times 10^5 A D_R^{1/2} n^{3/2} v^{1/2} C}$$

where i_p is anodic peak current, A is effective surface area of electrode, n is number of electrons transferred, C refers to concentration of redox probe, D_R is diffusion coefficient and v is scan rate.

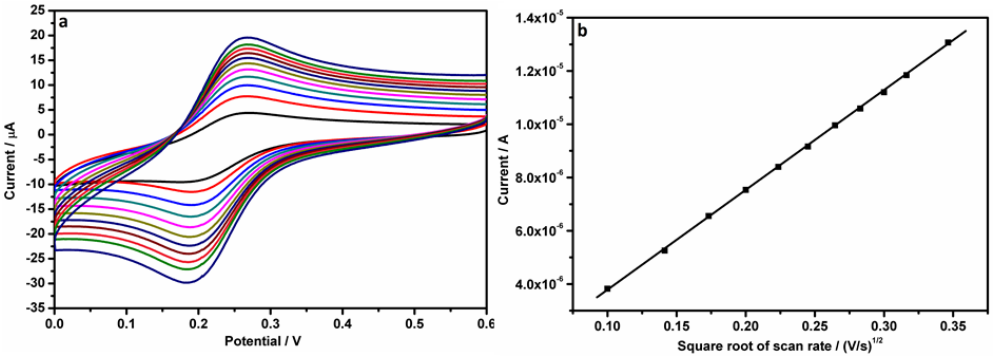

Figure 4.5: (a) Overlay of cyclic voltammograms of 2.0 × 10^{-3} M $K_3[Fe(CN)_6]$ on bare GCE at various scan rates (b) plot of current *vs* square root of scan rate for bare GCE

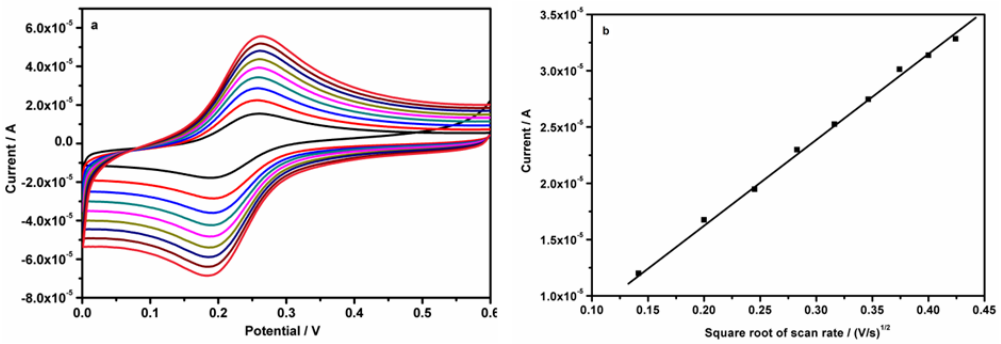

Figure 4.6: (a) Overlay of cyclic voltammograms of 2.0 × 10^{-3} M $K_3[Fe(CN)_6]$ on poly BPB/GCE at various scan rates (b) plot of current *vs* square root of scan rate for poly BPB/GCE

From the slope of i_p *vs* $\nu^{1/2}$, effective surface area of bare GCE and poly BPB/GCE was estimated to be 0.027 and 0.057 cm^2, respectively. It is evident from above result that apparent surface area of poly BPB/GCE has significantly increased compared to bare GCE, resulting in relatively better electrochemical performance of modified electrode.

4.3.1.3 Electrochemical impedance spectroscopic studies

EIS is an effective tool to explore interfacial properties of modified electrodes. In Nyquist plot, semi-circular portion observed at higher frequencies is attributed to charge transfer resistance of electrode surface.[204] From Fig. 4.7 it is clear that Nyquist diameter of bare GCE was smaller than poly BPB/GCE, explaining a higher electron transfer resistance between modified GCE and $[Fe(CN)_6]^{3-/4-}$ compared to bare GCE. An increase in charge transfer resistance of modified electrode indicates formation of poly BPB film over the electrode. The obtained result is consistent with those obtained from SEM images of both bare and modified electrodes.

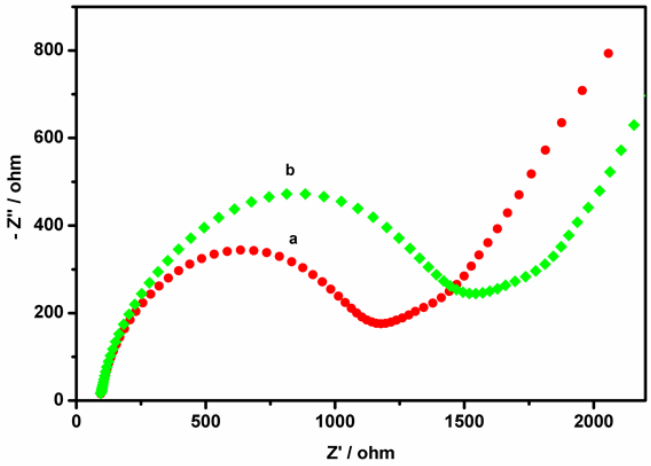

Figure 4.7: EIS spectra of (a) bare GCE (b) poly BPB/GCE in 5.0×10^{-3} M $[Fe(CN)_6]^{3-/4-}$ in 0.1 M KCl at the frequency range 1 -10^5 Hz

4.3.2 Electrochemical behaviour of TBHQ on bare and modified GCE

Electrochemical properties of TBHQ on bare and modified GCE were investigated using CV technique. Fig. 4.8 reveals behaviour of bare GCE

and poly BPB modified GCE in 0.1 M phosphate buffer solution (pH 7.0) containing 1.0×10^{-3} M TBHQ. As shown in Fig. 4.8, a pair of well defined, reproducible anodic (E_{pa}= 0.021 V, i_{pa}= 41.72 µA) and cathodic peaks (E_{pc}= −0.104 V, i_{pc}= 52. 81 µA) were observed at poly BPB/GCE. The obtained value of peak to peak separation ($\Delta E_p = (E_{pa} - E_{pc})$ = 0.125 V), was greater than that of a reversible process (ΔE_p = 0.059/n, n = 1). Above observations suggest that the electrochemical behaviour of TBHQ at poly BPB/GCE is quasi-reversible in nature. The formal potential, average of anodic and cathodic potential, was calculated to be −0.042 V.

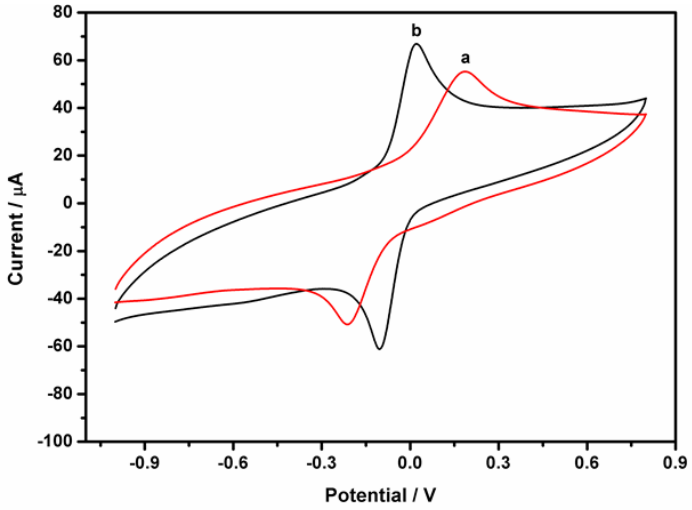

Figure 4.8: Cyclic voltammograms of 1.0×10^{-3} M TBHQ at (a) bare GCE (b) poly BPB/GCE in PBS of pH 7.0

On the other hand, for bare GCE, anodic and cathodic peaks were observed at 0.186 V (14.30 µA) and −0.212 V (29.30 µA) respectively. The peak separation observed was ΔE_p = 0.398 V, suggesting that electrochemical behaviour of TBHQ at bare GCE is an irreversible process where $\Delta E_p > 0.20$ V. Compared to bare GCE, oxidation potential of TBHQ at poly BPB/GCE has

lowered by a factor 0.165 V, with significant enhancement in anodic peak current. Excellent performance of the modified GCE compared to bare GCE could be due to hydrogen bonding interaction between hydroxyl group of TBHQ and sulfonic group of polymer film.[205] In addition, π-π interactions between the polymer film and TBHQ also played a major role in enhancing the electrochemical signal of TBHQ at poly BPB/GCE.[206]

Since oxidation of TBHQ occurs at a lower potential (−0.037 V) and produce significantly larger current compared to CV (Fig. 4.9), DPV technique was used for further studies.

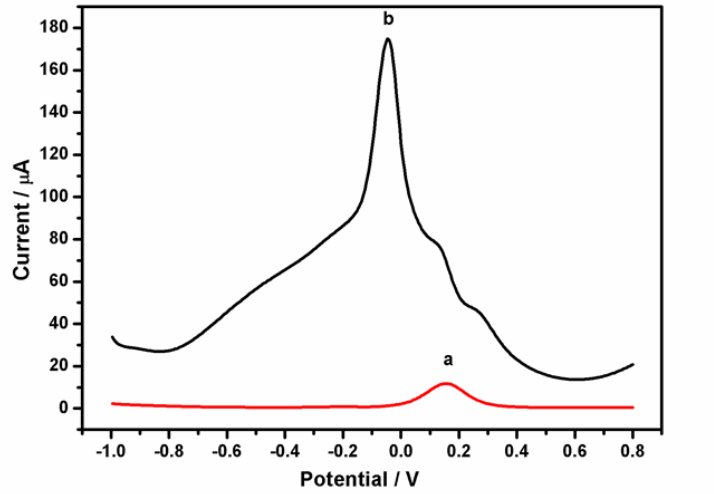

Figure 4.9: Differential pulse voltammograms of 1.0 × 10^{-3} M TBHQ at (a) bare GCE (b) poly BPB/GCE

4.3.3 Optimizing the variables of developed method

Effect of various factors such as supporting electrolyte, pH of medium, accumulation time and number of cycles of electropolymerization on the performance of sensor have been studied and conditions were optimized.

4.3.3.1 Influence of supporting electrolyte and pH

Electrochemical oxidation of 5.0 × 10^{-6} M TBHQ was probed and compared in various media such as phosphate buffer, citrate buffer, acetate buffer, KNO_3, NaOH, HCl and H_2SO_4 (each 0.1 M) using DPV. A well-defined peak and better oxidation response were obtained in 0.1 M PBS.

Furthermore, effect of pH on anodic peak current of 5.0 ×10^{-6} M TBHQ was carried out in 0.1 M PBS of pH in the range 4.0 to 9.0, graphical representation of which is presented in Fig.4.10. Oxidation peak current of TBHQ increased with increase in pH up to 7.0 with subsequent reduction at higher pH.

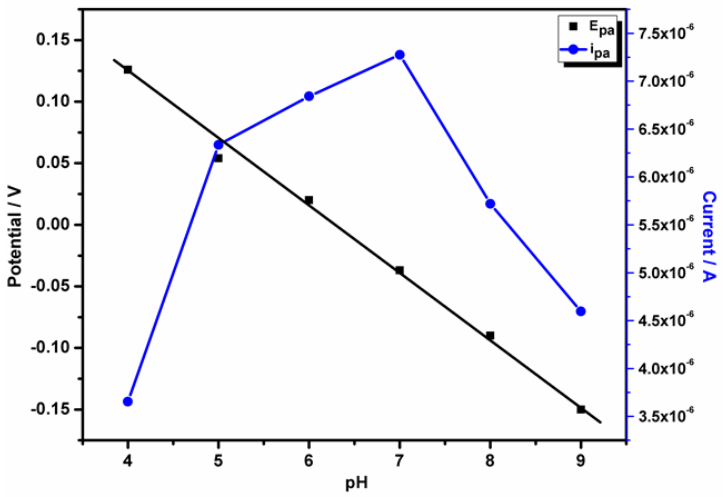

Figure 4.10: Influence of pH on oxidation peak current and peak potential of 5.0 × 10^{-6} M TBHQ

This can be correlated to the fact that when pH exceeds 7.0, most of the TBHQ molecules become ready to be deprotonated to form anions. Since electrochemical reaction process is associated with protonation, oxidation of TBHQ at pH > 7.0 was prevented by shortage of protons resulting in

decrease of peak current.[207,208] Hence, 0.1 M PBS of pH 7.0 was chosen as the supporting electrolyte for TBHQ.

Additionally, influence of pH on peak potential of TBHQ was also investigated. As evident from Fig. 4.10, oxidation peak potential decreases gradually and linearly on increasing pH, which clearly shows that oxidation of TBHQ is a proton leaving process. The plot of E_{pa} *vs* pH was linear with regression equation $E_p(V) = -0.053\,pH + 0.334$ ($R^2 = 0.995$), slope of which is very near to theoretical value of 0.059 V/pH, suggesting involvement of two protons and two electrons during the oxidation of TBHQ, which is in accordance with previous reports.[209,210] Hence, the observed peak could be due to oxidation of TBHQ to *tert*-butylquinone (TBQ)[211] and the plausible mechanism is shown in Scheme 4.2.

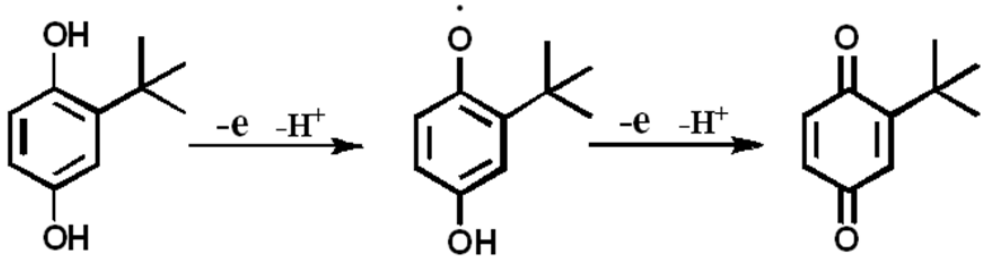

Scheme 4.2: Mechanism of electrooxidation of TBHQ

4.3.3.2 Effect of number of cycles of electropolymerization

DPV technique was used to analyse the effect of polymer film thickness on oxidation peak current of 5.0 $\times 10^{-6}$ M TBHQ. Fig. 4.11 illustrates the variation in oxidation peak current of TBHQ with different cycle numbers for electropolymerization of BPB at GCE. It is evident from Fig. 4.11 that the peak current has increased maximum up to 20 cycles and decreased

thereafter. An enhanced anodic peak current indicates the increase in specific surface area of modified electrode, resulting in more active catalytic sites on the electrode surface. Decrease in peak current above 20 cycles may be due to an increase in the thickness of polymer film, which will hinder electronic exchange between TBHQ and poly BPB/GCE. Therefore, optimal number of cycles for electropolymerization was fixed as 20 cycles.

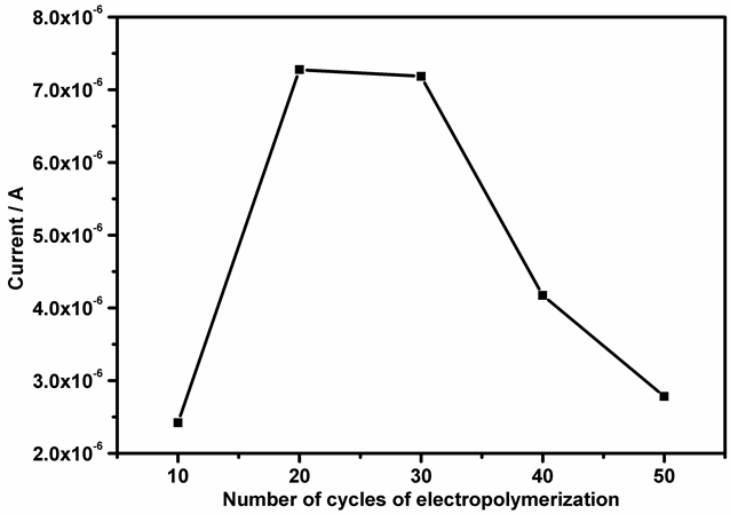

Figure 4.11: Influence of cycle number of electropolymerization on the peak current of 5.0 × 10^{-6} M TBHQ

4.3.4 Influence of scan rate

CV technique was employed to investigate the influence of scan rate on peak parameters of 1.0 × 10^{-3} M TBHQ at proposed sensor. As depicted in Fig. 4.12, anodic and cathodic peak potentials and peak currents increased as scan rate increased in the range from 0.02 to 0.38 V s^{-1}. Fig. 4.13 shows that redox peak current of TBHQ increased linearly with second root of scan rate ($\nu^{1/2}$) with regression equations $i_{\mathrm{pa}}(\mathrm{A}) = 1.0 \times 10^{-4}\, \nu^{1/2}\, \left(\mathrm{V}^{1/2}\mathrm{s}^{-1/2}\right) +$

3.0×10^{-6} ($R^2 = 0.990$) and $i_{pc}(A) = -2.0 \times 10^{-4}\, \nu^{1/2}(V^{1/2}\, s^{-1/2}) - 3.0 \times 10^{-6}$ ($R^2 = 0.995$), for the plot of i_{pa} *vs* $\upsilon^{1/2}$ and i_{pc} *vs* $\upsilon^{1/2}$ respectively. Above results imply that the reaction is controlled by rate of diffusion of TBHQ at the surface of poly BPB/GCE sensor. As observed from Fig. 4.14, there exist a good linear relationship between logarithm of peak current and logarithm of scan rate in the range 0.02 to 0.38 Vs^{-1} with regression equations $\log(i_{pa}/A) = 0.471 \log(\nu/V\, s^{-1}) - 3.91$ ($R^2 = 0.995$), for oxidation peak current and $\log(i_{pc}/A) = 0.484 \log(\nu/V\, s^{-1}) + 3.83$ ($R^2 = 0.997$), for reduction peak current. The obtained value of slopes for oxidation peak current and reduction peak current are 0.47 and 0.48 respectively, which is in agreement with theoretical value of 0.50 for a diffusion controlled process.[12]

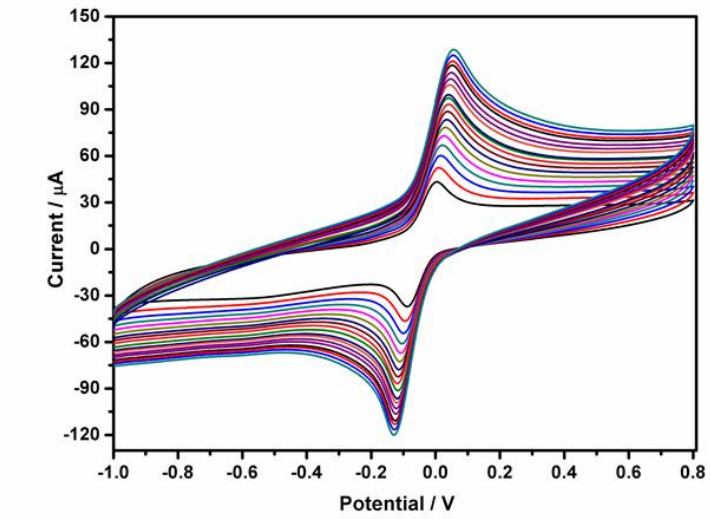

Figure 4.12: Overlay of cyclic voltammograms of 1.0×10^{-3} M TBHQ on poly BPB/GCE at various scan rates

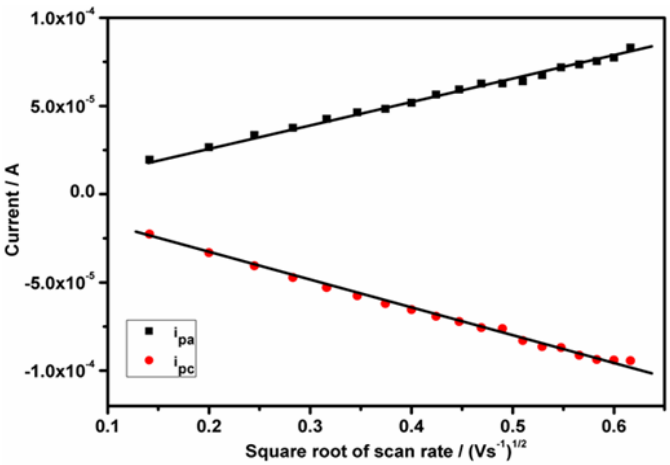

Figure 4.13: Plot of anodic and cathodic peak currents *vs* square root of scan rate for TBHQ

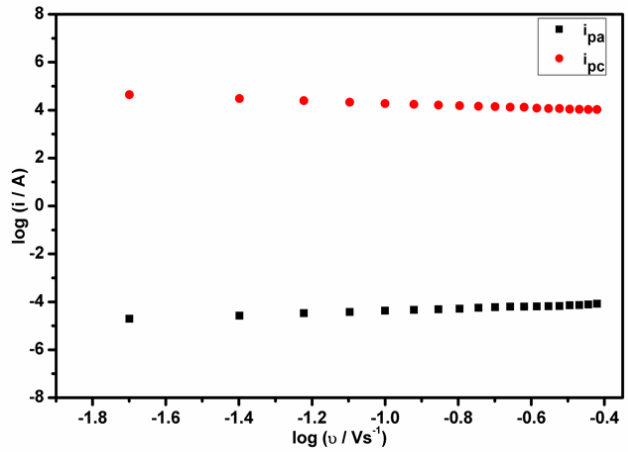

Figure 4.14: Plot of log i *vs* log υ

4.3.5 Determination of TBHQ

Fig. 4.15a shows the overlay of differential pulse voltammograms of TBHQ at various concentrations under optimal conditions. As depicted in Fig. 4.15b, the oxidation peak current is linearly proportional to concentration of TBHQ in the range 1.0×10^{-5} M to 1.0×10^{-6} M and following dependence was found, $i_{\mathrm{pa}}(A) = 0.558\, C\ (M) + 4.0 \times 10^{-6}\ (R^2 = 0.996)$.

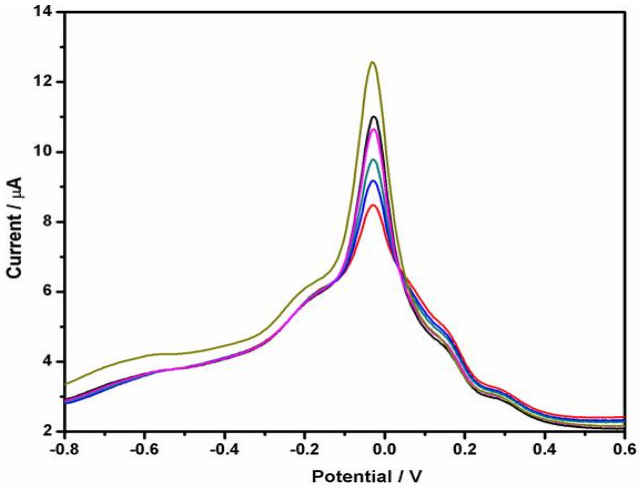

Figure 4.15a: Overlay of differential pulse voltammograms for oxidation of TBHQ at various concentrations

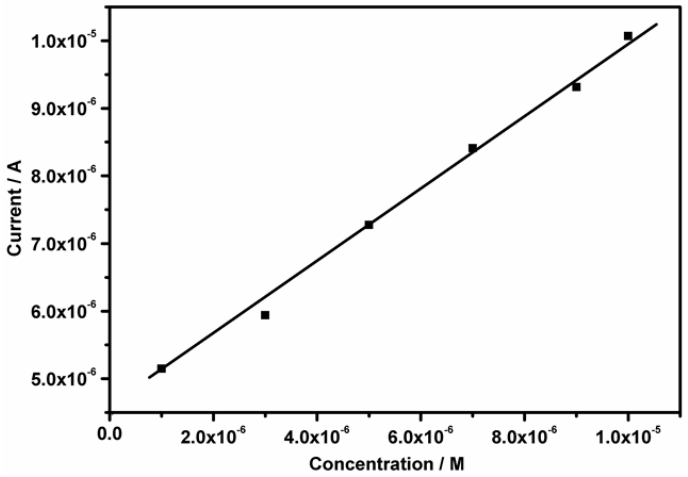

Figure 4.15b: Calibration curve for TBHQ in the concentration range $1.0 \times 10^{-5} - 1.0 \times 10^{-6}$ M

The limit of detection (LOD) and limit of quantification (LOQ) were estimated using equations 3 *S*/*m* and 10 *S*/*m* respectively, where *S* represents the standard deviation and *m* is slope of calibration curve. LOD and LOQ were calculated to be 3.50×10^{-8} M and 1.17×10^{-7} M respectively. Analytical

performance of proposed sensor is compared with other electrochemical sensors for TBHQ (Table 4.2). It is found that the proposed sensor exhibited relatively lower LOD and lower oxidation potential compared to other sensors.

4.3.6 Evaluation of kinetic parameters

Based on Laviron equation for quasi reversible process,[214] heterogeneous rate constant (k_s) and charge transfer coefficient (α) of TBHQ at the surface of poly BPB/GCE can be calculated from plot of anodic and cathodic peak potential *vs* log υ (Fig. 4.16). From linear part of above graph and from slope for cathodic peaks $\frac{2.303RT}{\alpha_c nF}$ and for anodic peaks $\frac{2.303RT}{(1-\alpha_a)nF}$, cathodic ($\alpha_c$) and anodic ($\alpha_a$) charge transfer co-efficients were calculated to be 0.528 and 0.599 respectively. Using α_a and α_c, value of average charge transfer co-efficient (α) was estimated to be 0.563. Heterogeneous electron transfer rate constant k_s of TBHQ on poly BPB/GCE was estimated by following Laviron equation,

$$\log k_s = \alpha\log(1-\alpha) + (1-\alpha)\log\alpha - \log\frac{RT}{nF\upsilon} - \frac{\alpha(1-\alpha)nF\Delta E_p}{2.3RT}$$

where n is number of electrons involved in reaction and other symbols represent their accepted scientific terms. The value of k_s for modified GCE was found to be 2.86 s^{-1}.

In the case of bare GCE, where ΔE_p > 0.20 V, following Laviron equation was used to calculate k_s.[186]

$$E_p = E^{0\prime} + \frac{RT}{(1-\alpha)nF}\left(\ln\frac{(1-\alpha)nF}{RTk_s} - \ln\upsilon\right)$$

where $E^{0\prime}$ is the formal potential whose value is obtained from intercept of plot of E_p *vs* υ by extrapolating to vertical axis at υ = 0. For bare GCE, value

of k_s was estimated to be 2.22 s^{-1}. Higher value of k_s for poly BPB/GCE implies that the modified electrode has a high electrocatalytic ability to promote electron transfer kinetics towards the redox reaction of TBHQ.

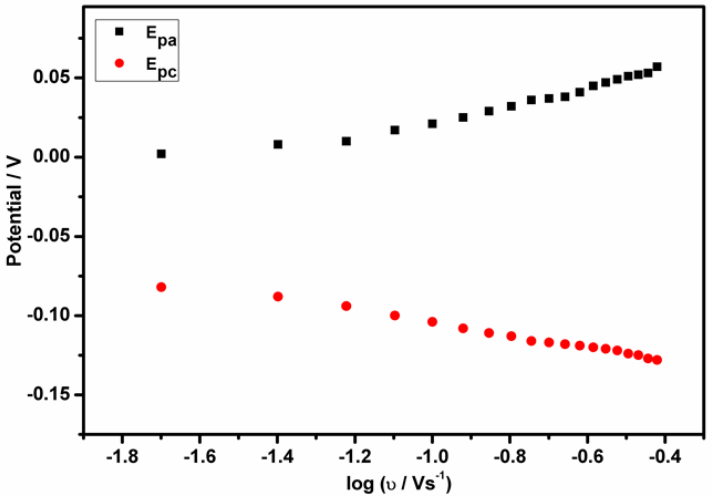

Figure 4.16: Variation of E_{pa} and E_{pc} with log υ

4.3.7 Chronoamperometry

Chronoamperometry was employed to investigate the electrocatalytic behaviour of TBHQ at poly BPB/GCE. Chronoamperograms obtained for various concentrations of TBHQ on modified electrode is depicted in Fig. 4.17a. Plots of electrocatalytic current *vs* $t^{-1/2}$ shows a near cottrellian behaviour, revealing that transient current is controlled by diffusion of TBHQ from bulk solution to surface of poly BPB/GCE (Fig. 4.17b). When slopes of the resulting straight lines were plotted against different concentrations of TBHQ, a straight line was resulted with $Slope\ (\mu A\ s^{-1/2}) = 24.8\ C\ (mM) + 6.23\ (R^2 = 0.996)$ (Fig. 4.17c). Using the slope of above obtained plot and

by applying Cottrell equation,[187] value of diffusion coefficient (*D*) is estimated to be 1.59×10^{-5} cm^2 s^{-1}.

$$I = nFAD^{1/2}C\pi^{-1/2}t^{-1/2}$$

where *C* is bulk concentration (mol cm^{-3}) and other symbols have their usual meanings.

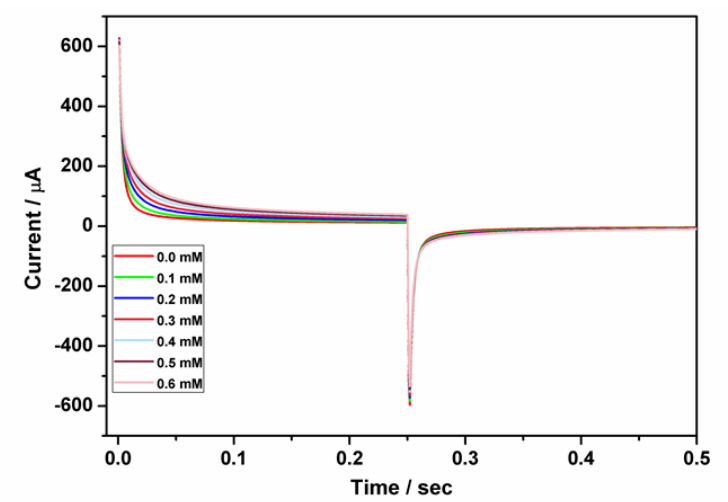

Figure 4.17a: Chronoamperograms obtained at poly BPB/GCE in 0.1 M PBS (pH 7.0) for different concentrations of TBHQ

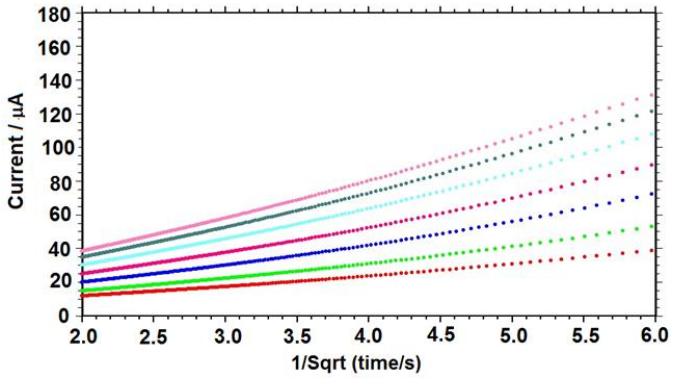

Figure 4.17b: Plots of I *vs* $t^{-1/2}$ derived from the chronoamperograms of Fig. 4.17a

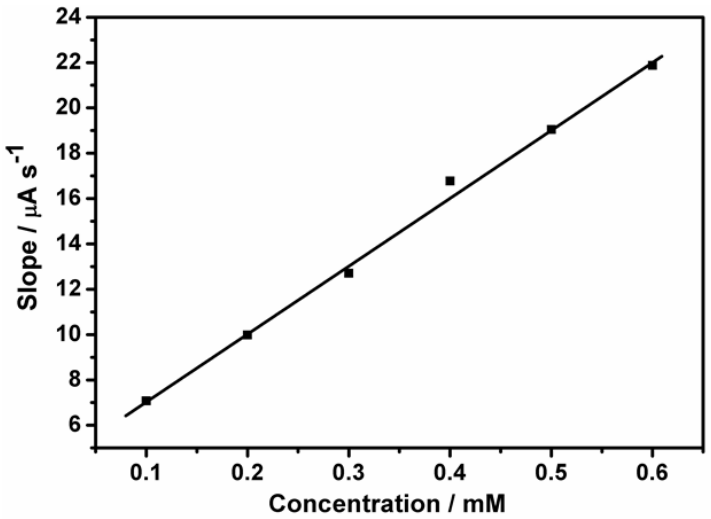

Figure 4.17c: Plot of slope of the straight lines against concentration of TBHQ

4.3.8 Interference study

In order to investigate the influence of foreign species on the oxidation peak current of TBHQ, effect of increasing concentrations of different coexisting species (such as sodium chloride, sodium sulphite, EDTA, citric acid, acetic acid and ascorbic acid) on anodic peak current of TBHQ was monitored. The obtained result showed that upto 100 fold excess concentration of sodium chloride, sodium sulphite, EDTA, citric acid and acetic acid have no influence on the oxidation peak current of 5.0×10^{-6} M TBHQ, with signal deviation below ±5% (Table 4.3). However, 1: 1 ratio of ascorbic acid interferes severely on the signal of 5.0×10^{-6} M TBHQ.

4.3.9 Reproducibility, repeatability and stability

Reproducibility of poly BPB/GCE was confirmed by examining the generation of a reproducible surface through repeated determination of

5.0×10^{-6} M TBHQ using separate poly BPB/GCE for five times. The relative standard deviation (RSD) was found to be 1.8%. Repeatability of the developed sensor was also checked by taking five successive measurements of 5.0×10^{-6} M TBHQ using same poly BPB/GCE and RSD was calculated to be 3.5%. The proposed sensor retained 95% of its initial response for one week, indicating its high stability.

4.3.10 Analytical performance

To evaluate analytical utility of the proposed sensor, poly BPB/GCE was employed to determine TBHQ in coconut and sunflower oil samples. The experimental results are presented in Table 4.4 and obtained results are in good agreement with the HPLC-UV method. The values of recovery ranged between 99.8 and 101.8% suggesting that the proposed method is reliable and effective for the determination of TBHQ in vegetable oils.

4.4 Conclusions

As part of the present investigations, a new electrochemical sensing method has been developed for monitoring TBHQ in coconut and sunflower oil samples. Under optimum analytical conditions, the proposed sensor exhibited good linear range, stability and repeatability. Various kinetic parameters such as charge transfer coefficient, heterogeneous rate constant and diffusion co-efficient were calculated. The poly BPB/GCE was successfully used for the determination of TBHQ in coconut and sunflower oils with recoveries ranged between 99.8 and 101.8%. Accuracy of the proposed method was compared with HPLC-UV method. Developed sensor thus opens a new opportunity for sensing of TBHQ in food samples.

Table 4.1: Comparison of different modified electrodes for detection of TBHQ

Modified electrode	Ep (V)	Current (µA)
[a] poly BPB /GE	0.058	5.59
[b] TMOPPMn(III)Cl/GE	-	-
[c]MWCNT/Pt	0.244	18.53
polyBPB/GCE	-0.037	24.41

[a] Poly bromophenol modified gold electrode

[b][5,10,15,20-tetrakis (4-methoxyphenyl) porphyrinato] manganese (III) chloride modified gold electrode

[c] Multiwalled carbon nanotube modified platinum electrode

Table 4.2: Comparison of different TBHQ sensors

Electrode	*Ep vs* Ag/AgCl (V)	Linear range (M)	LOD (M)	References
[a]MWNT-Brij ®35/GCE	0.270	1.00×10^{-3}-1.00×10^{-6}	2.60×10^{-7}	[211]
GCE	0.610	1.01×10^{-3}- 2.01×10^{-6}	2.30×10^{-7}	[212]
[b]Graphene/Ch/GCE	> 0.200	1.20×10^{-4}- 4.00×10^{-6}	1.40×10^{-7}	[207]
[c]CPE	> 0.100	1.15×10^{-5} - 1.05×10^{-6}	7.11×10^{-8}	[213]
Poly BPB/GCE	-0.037	1.00×10^{-5} - 1.00×10^{-6}	3.50×10^{-8}	Present work

[a] MWNT-Brij ®35/GCE – multiwalled carbon nanotube modified GCE in Brij ®35 micellar medium

[b] Ch - choline

[c] CPE- carbon paste electrode

Table 4.3: Effect of possibly interfering species on the signal of 5.0×10^{-6} M TBHQ

Species	Concentration (M)	Signal change (%)
NaCl	5.0×10^{-4}	-2.76
Sodium sulphite	5.0×10^{-4}	-3.39
EDTA	5.0×10^{-4}	1.60
Citric acid	5.0×10^{-4}	2.22
Acetic acid	5.0×10^{-4}	-2.03
Ascorbic acid	5.0×10^{-6}	-23.05

Table 4.4: Determination of TBHQ in food samples

Samples	Added (M)	HPLC-UV method[147]			Proposed method			
		Found (M)	Recovery (%)[a]	RSD (%)	Added (M)	Found (M)	Recovery (%)[a]	RSD (%)
Coconut oil	9.00×10^{-6} to 4.00×10^{-6}	8.99×10^{-6} to 3.89×10^{-6}	99.4	1.9	1.00×10^{-5} to 4.00×10^{-6}	1.02×10^{-5} to 3.90×10^{-6}	99.8	1.8
Sunflower oil	9.00×10^{-6} to 4.00×10^{-6}	9.12×10^{-6} to 4.11×10^{-6}	103.1	3.1	1.00×10^{-5} to 4.00×10^{-6}	1.03×10^{-5} to 4.02×10^{-6}	101.8	2.4

[a] Average of six replicates

RSD = Relative standard deviation

.....ꕥ.....

Chapter 5

VOLTAMMETRIC SENSOR FOR PONCEAU 4R BASED ON POLY L-CYSTEINE MODIFIED GLASSY CARBON ELECTRODE

Contents

5.1 Introduction
5.2 Experimental
5.3 Results and discussion
5.4 Conclusions

This chapter explores utility of poly(L-Cysteine) modified glassy carbon electrode [poly(L-Cys)/GCE] as a voltammetric sensor for determination of Ponceau 4R (P4R), a synthetic food colorant. On poly(L-Cys) modified electrode, P4R behaved as perfectly reversible redox system with E_{pa} = 0.031 V and E_{pc} = -0.001 V (ΔE_p = 0.032 V). Under optimal conditions, anodic peak current increased with concentrations of P4R in the linear range 1.0 × 10^{-5} to 1.0 × 10^{-6} M. Minimum detectable concentration and limit of quantification were found to be 3.73 × 10^{-8} M and 1.24 × 10^{-7} M, respectively. Kinetic parameters such as charge transfer coefficient (α) and heterogeneous rate constant (k_s) were estimated to be 0.570 and 2.56 s^{-1} respectively. Chronocoulometry was employed to calculate average surface concentration of P4R on poly(L-Cys)/GCE and diffusion coefficient (D) and values obtained were 5.54 × 10^{-9} mol cm^{-2} and 2.93 × 10^{-6} cm^2 s^{-1}, respectively. Proposed method was validated using commercial soft drink samples.

5.1 Introduction

Color is a vital sensory attribute perceived by human to evaluate food stuffs. Food colorants complement or enhance natural colours, which are lost or destroyed during food processing and storage. Synthetic food colorants are preferred over natural counterparts due to their superior qualities such as cost effectiveness, consistency of strength, range and brilliance of shade, stability and ease of application.[215-217] These synthetic dyes with extensive chemical diversity are represented by five major groups *viz.*, azo dyes, triarylmethanes, chinophthalon derivatives of quinine yellow, xanthenes and indigo colorants.[218] Among synthetic colorants, azo compounds such as P4R (E 124, Fig. 5.1), sunset yellow and tartrazine are characterized by presence of chromophoric azo bonds (-N=N-) which constitute around 65% of commercial dye market.[219]

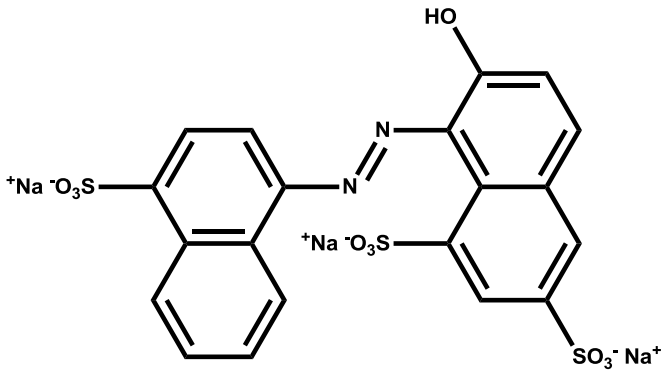

Figure 5.1: Structure of P4R

P4R, [1-(4-sulpho-1-napthylazo)-2-napthol-6,8-disulphonic acid, trisodium salt], is usually used in soft drinks, beverages, dry mix products, sugar confectioneries and bakery products to impart an attractive red color.[220]

However, scientific studies have shown that P4R can cause mutagenesis,[221] reproductive toxicity, neurotoxicity[222] and frequent headaches[223] when consumed in excess. Additionally, it is suspected to be a potential carcinogen.[224,225] Therefore, use of P4R has been strictly controlled by laws and regulations across the globe.[226,227] The European Food Safety Authority (EFSA) has revaluated safety of P4R in 2009 and reduced the acceptable daily intake from 0-4 to 0.7 mg per kg body weight.[228] Furthermore, it is not being approved as a food colorant by many countries including United States, Canada, Norway and Finland.[229] However, there have been reports on presence of excessive amounts of P4R in food products.[218,230] Thus, rapid, accurate and reliable methods for determination of P4R are necessary for ensuring the quality and safety of food stuffs.

Till date, various methods based on high performance liquid chromatography (HPLC),[231,232] capillary electrophoresis[233] and spectrophotometry[234,235] have been developed for determination of P4R. Though, these methods are well established and widely recognized, they require relatively costlier equipment, advanced technical knowledge and time-consuming processes. In contrast, electrochemical methods can be employed for on-site detection of synthetic food colorants due to their high sensitivity, short analysis time, good handling convenience and low cost.[236-240]

Owing to their properties such as good biocompatibility, excellent stability and ease of preparation, modification of electrodes with polymers of amino acids have gained much attention for the past few years.[241-243] L-cysteine, a sulphur containing amino acid, is commonly used for modification of electrodes as it contains amine, sulfhydryl and carboxyl

functional groups. The amine nitrogen atom of L-Cys can easily form a stable covalent bond with edge plane sites on surface of carbon electrodes during electropolymerization.[244]

Present study aims to develop a sensitive voltammetric sensor for the determination of P4R using poly L-Cys modified GCE. For determination of P4R, we have tried various chemical modifications on different electrodes (Table 5.1). From Table 5.1 it is clear that maximum peak current and lowest overpotential were obtained with poly(L-Cys)/GCE and its selection is thus justified. Due to greater electrocatalytic activity of polymer film modified GCE, oxidation signals of P4R were enhanced considerably compared to bare GCE. After optimizing experimental parameters, practical applicability of developed sensor was assessed by determining concentration of P4R in soft drink samples and results were validated with conventional spectrophotometric method detailed in section 2.5.3.[148]

5.2 Experimental

5.2.1 Preparation of poly(L-Cys)/GCE

GCE was cleaned as described in section 2.3 and cleaned GCE was immersed in 0.1 M PBS (pH 7.0) containing 5.0×10^{-3} M L-Cys. Electropolymerization of L-Cys on surface of GCE was performed by cycling potential between -0.8 to 2.0 V, at a scan rate of 0.1 V s^{-1} (Fig. 5.2).[245] After electropolymerization, physically adsorbed L-Cys monomers were removed from poly L-Cys/GCE by washing with ethanol and the electrode was dried in air.

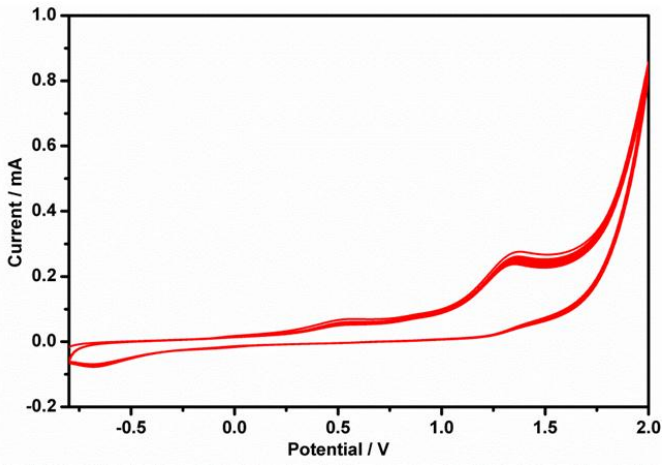

Figure 5.2: Cyclic voltammograms obtained for electropolymerization of L-Cys on GCE

During first anodic scan, an oxidation peak was obtained at 1.30 V and in reverse scan a reduction peak was obtained at -0.50 V.[245] As number of cycles of polymerization increases, cathodic peak current also increases, indicating formation of a polymer film on the surface of GCE.[246] Amine functionality in L-Cys undergoes one electron oxidation to form corresponding free radical during anodic scan, which then forms a nitrogen-carbon linkage at the surface of GCE.[244] Thickness of polymer film on electrode surface can be controlled by concentration of L-Cys and number of cyclic voltammetric scans.

5.2.2 Analytical procedure

All the electrochemical measurements were performed using 0.1 M PBS (pH 7.0) as supporting electrolyte. Desired volume of P4R solution was pipetted into an electrochemical cell containing 10 mL of PBS. Square wave voltammetric (SWV) measurements were recorded from -0.8 to 0.5 V with pulse amplitude of 0.025 V, quiet time of 2 s, scan rate of 0.1 V s^{-1},

increment of 0.004 V and frequency of 15 Hz. Prior to and after each electrochemical measurements, modified electrode was activated by potential cycling between -0.5 to 0.5 V in electrolyte solution until the voltammogram remains unchanged. Oxidation peak current measured at 0.031 V was used for determination of P4R.

5.2.3 Sample treatment

Soft drink samples of two commercial brands procured from local market were used without pre-treatment. One mL of sample solution was added into 9.0 mL of 0.1 M PBS (pH 7.0) and resultant solution was subjected to electrochemical analysis, following analytical procedure described in Section 5.2.2.

5.3 Results and discussion

5.3.1 Characterisation of electrode surface

Scanning electron microscopy (SEM), atomic force microscopy (AFM), cyclic voltammetry (CV) and electrochemical impedance spectroscopy (EIS) were used to explore surface characteristics of bare and modified GCE.

5.3.1.1 Surface morphology of bare GCE and poly(L-Cys)/GCE

SEM and AFM techniques were used to probe surface morphology of bare and modified GCE. From Fig. 5.3a, it is clearly evident that surface of bare GCE was smooth and uniform. Conversely, surface of poly(L-Cys)/GCE was relatively rough and possessed distinctive interstices (Fig. 5.3b), which increased number of active sites and was good for accumulation of more analytes. AFM images (Fig. 5.4) also support observations of SEM analysis. As revealed from Fig. 5.4, surface roughness of polymer modified

GCE (44.05 nm) is significantly increased compared to bare GCE (23.86 nm), which points to effective modification of GCE with polymer film.

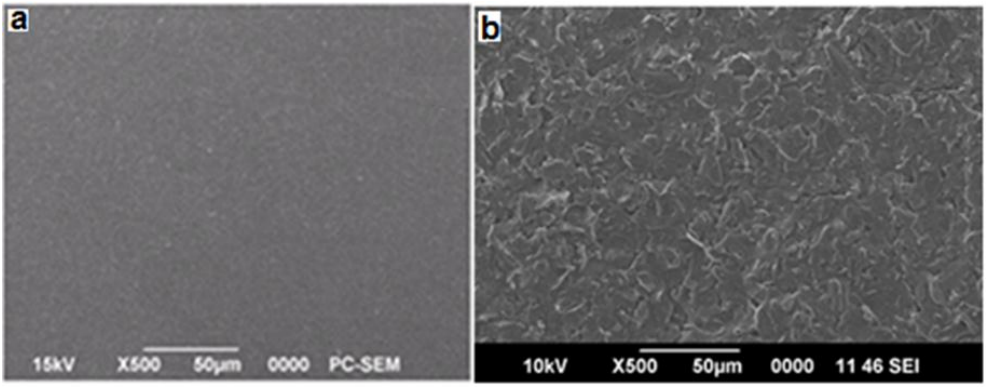

Figure 5.3: SEM images of (a) bare GCE (b) poly(L-Cys)/GCE

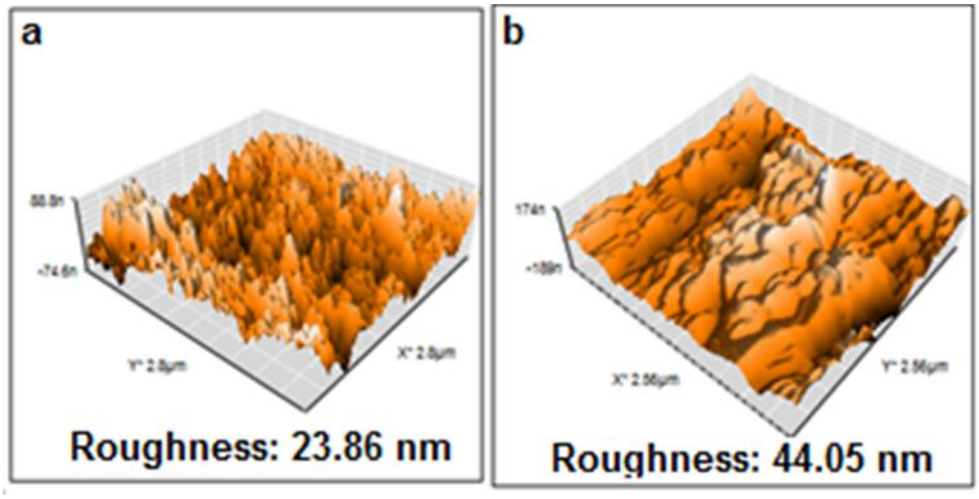

Figure 5.4: AFM images of (a) bare GCE (b) poly(L-Cys)/GCE

5.3.1.2 Surface area study

Cyclic voltammograms of 2.0×10^{-3} M $K_3Fe(CN)_6$ solution were recorded on both bare (Fig. 5.5) and poly(L-Cys)/GCE (Fig. 5.6) in the potential range 0 to 0.6 V at different scan rates. In both cases, peak current

(i_p) increased linearly with square root of scan rate ($v^{1/2}$). From the slope of plot i_p *vs* $v^{1/2}$, effective surface area of bare and polymer modified electrodes were estimated using Randles-Sevcik equation for reversible redox systems.[179]

$$i_p = 2.69 \times 10^5 A n^{3/2} D^{1/2} C v^{1/2}$$

where n is number of electron transferred, A is surface area of electrode, D is diffusion coefficient and C is concentration of $K_3Fe(CN)_6$ solution. For 2.0×10^{-3} M $K_3Fe(CN)_6$ redox probe, number of electrons transferred and diffusion coefficient were found to be n = 1 and D = 7.60×10^{-6} cm^2 s^{-1}. Based on above equation, effective surface area of GCE and poly(L-Cys)/GCE were found to be 0.027 and 0.047 cm^2, respectively. Higher electroactive surface area of poly(L-Cys)/GCE offered more binding sites, which results in excellent catalytic activity of modified electrode for determination of P4R.

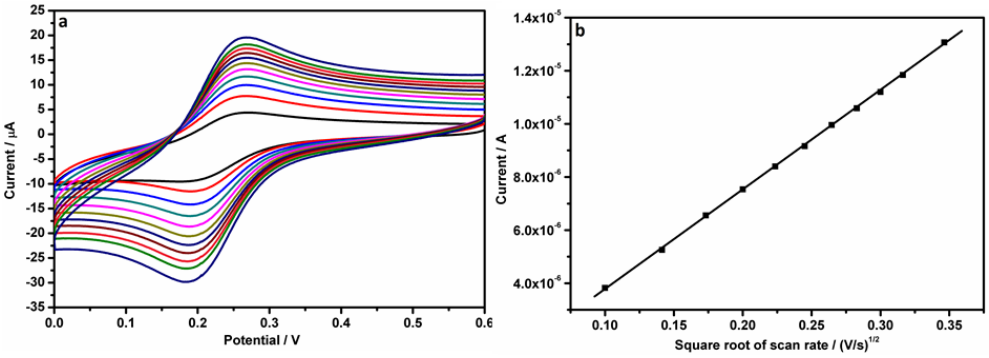

Figure 5.5: (a) Overlay of cyclic voltammograms of 2.0×10^{-3} M $K_3[Fe(CN)_6]$ on bare GCE at various scan rates (b) plot of current *vs* square root of scan rate for bare GCE

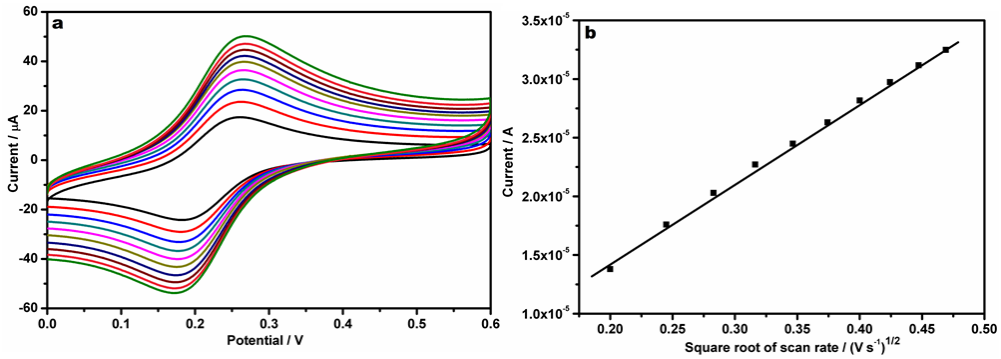

Figure 5.6: (a) Overlay of cyclic voltammograms of 2.0 × 10^{-3} M $K_3[Fe(CN)_6]$ on poly(L-Cys)/GCE at different scan rates (b) plot of current *vs* square root of scan rate for poly(L-Cys)/GCE

5.3.1.3 Electrochemical impedance spectroscopic studies

EIS is an important non-invasive and informative tool for learning interfacial properties of electrodes. Solution of 5.0 × 10^{-3} M $[Fe(CN_6)]^{3-/4-}$ containing 0.1 M KCl was used as redox probe for recording Nyquist plots of bare and modified GCE (Fig. 5.7). In the impedance spectra, semicircular portion observed at higher frequencies is related to electron transfer limited process and diameter of semicircle gives charge transfer resistance at electrode surface (R_{ct}).[26] Further, linear part of impedance spectra observed at lower frequency denotes diffusion limited process. For bare GCE, R_{ct} was found to be 1062 ohm and upon modification, R_{ct} decreased considerably (352 ohm). Higher value of R_{ct} for bare GCE indicates large hindrance to interfacial electron transfer, whereas a lower value for poly(L-Cys)/GCE shows superior electron transfer ability of modified electrode. Above results also confirm successful modification of GCE with polymer film.

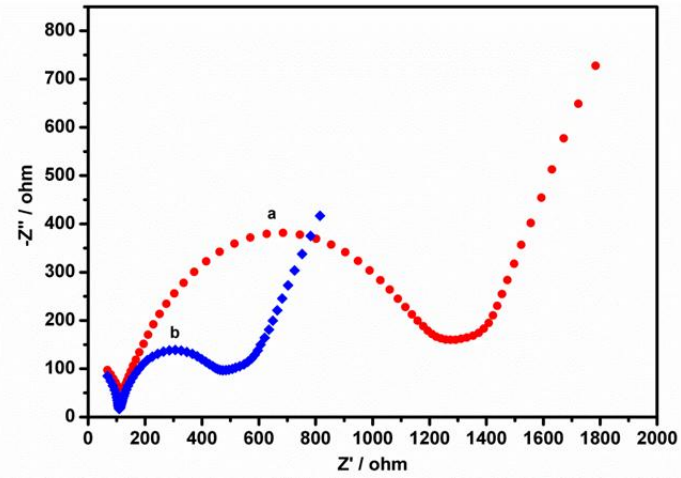

Figure 5.7: EIS spectra of (a) bare GCE (b) poly(L-Cys)/GCE in 5.0×10^{-3} M $[Fe(CN)_6]^{3-/4-}$ in 0.1 M KCl at the frequency range 1 - 10^5 Hz

5.3.2 Electrochemical behaviour of P4R on bare and poly(L-Cys) film modified electrode

Electrochemical behaviour of 1.0×10^{-4} M P4R on bare and poly(L-Cys)/GCE were explored by CV in 0.1 M PBS of pH 7.0. Weak irreversible oxidation peak (E_{pa} = 0.280 V, i_{pa} = 0.20 µA) was observed on bare GCE (Fig. 5.8) indicating feeble electrocatalytic activity of bare GCE towards oxidation of P4R. On the other hand, poly(L-Cys)/GCE showed stable well defined redox peaks, with anodic and cathodic peak potentials at 0.031 V (8.20 µA) and -0.001 V (-3.87 µA) respectively. Peak to peak separation of 0.032 V demonstrated a reversible electrochemical process. On modification with polymer film, oxidation over potential of P4R was decreased by 0.249 V, with remarkable increase in oxidation peak current. This could be ascribed to superior electrocatalytic activity of modified electrode towards electro oxidation of P4R. Greater electrocatalytic activity of poly(L-Cys)/GCE could be mainly attributed to its large surface area and fast electron transfer

ability. Polymer films having three dimensional structures with good chemical and physical stability can offer more active sites and effective potential for electrode reaction.[66]

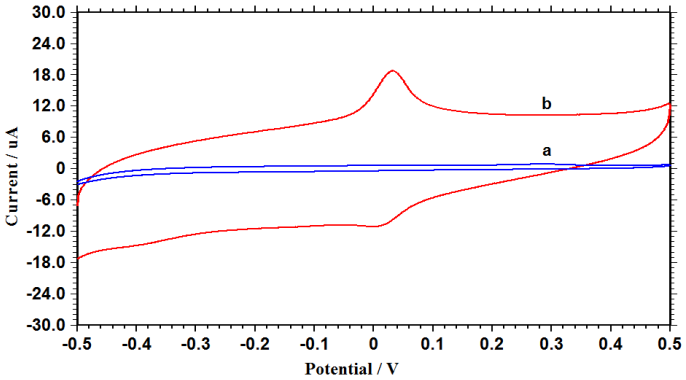

Figure 5.8: Cyclic voltammograms of 1.0 × 10^{-4} M P4R at (a) bare GCE and (b) poly(L-Cys)/GCE in 0.1 M PBS of pH 7.0

Since square wave voltammetric (SWV) technique could remarkably increase anodic peak current of P4R on poly(L-Cys)/GCE (56.18 μA) compared to CV, it was chosen for further voltammetric studies (Fig. 5.9).

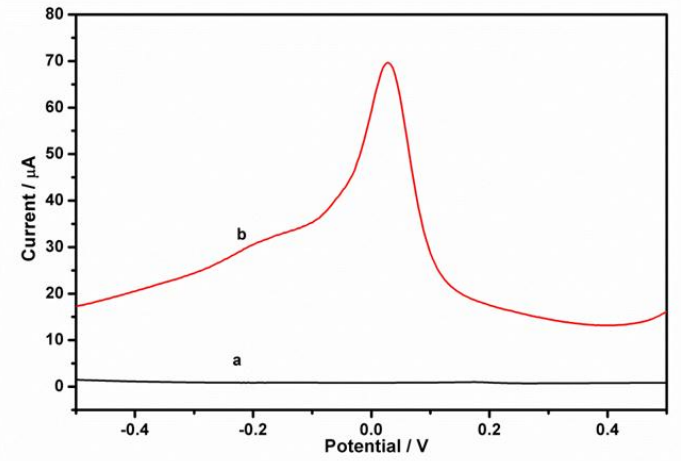

Figure 5.9: Square wave voltammograms of 1.0 × 10^{-4} M P4R at (a) bare GCE (b) poly(L-Cys)/GCE in 0.1 M PBS of pH 7.0

5.3.3 Optimization of experimental parameters

Performance of developed sensor was evaluated by studying the influence of different variables (supporting electrolyte, pH of medium, accumulation time and number of cycles of electropolymerization of L-Cys) and parameters were optimized.

5.3.3.1 Influence of supporting electrolyte and pH

Square wave voltammograms of 1.0×10^{-5} M P4R were recorded in 0.1 M solutions of various supporting electrolytes such as acetate buffer, phosphate buffer, citrate buffer, KNO_3, HCl and NaOH. Electrochemical behaviour of P4R in terms of peak shape, peak potential and peak height was found to be best when 0. 1 M PBS was used as supporting electrolyte. Therefore, 0.1 M PBS was chosen as supporting electrolyte for further experiments.

Influence of pH on anodic peak potential of 1.0×10^{-5} M P4R at poly(L-Cys)/GCE were studied in the pH range of 2.0 to 8.0 by SWV. It is observed that, on increasing pH of solution from 2.0 to 8.0, peak potential shifted linearly to negative values (Fig. 5.10), indicating involvement of protons in oxidation of P4R.[64] Plot of E_p *vs* pH was linear with regression equation, $E_{pa}(V) = -0.062p^H + 0.461$ ($R^2 = 0.990$). Based on equation[247] $\frac{dE_p}{dpH} = \frac{2.303mRT}{nF}$, where m and n corresponds to number of protons and electrons, value of $\frac{m}{n}$ for oxidation of P4R was found to be 1.03, which suggests participation of equal number of protons and electrons in the electrochemical process.[248,249]

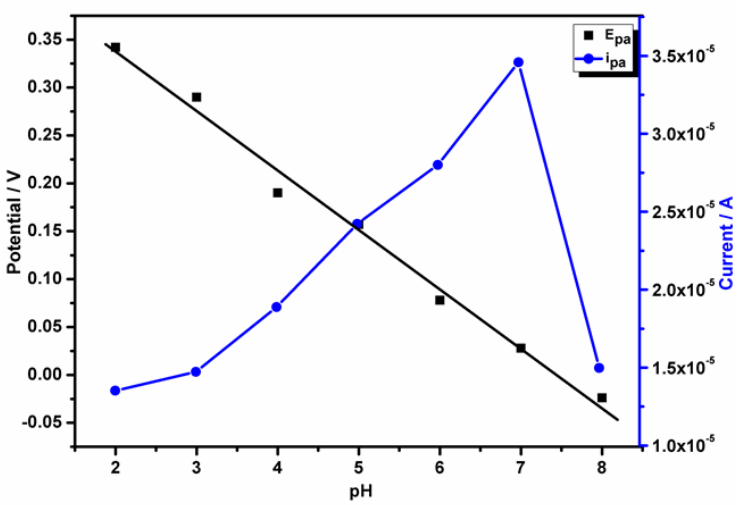

Figure 5.10: Influence of pH on the oxidation peak potential and peak current of 1.0×10^{-5} M P4R

Relationship between pH and anodic peak current of 1.0×10^{-5} M P4R was also explored in above mentioned pH range. As shown in Fig. 5.10, peak current showed an increase up to pH 7.0 and then decreased with further increase in pH. Based on these observations, 0.1M PBS of pH 7.0 was used for further studies.

5.3.3.2. Influence of accumulation time

Effect of accumulation time on electrochemical response of 1.0×10^{-5} M P4R at poly(L-Cys)/GCE was also examined. Oxidation current of P4R enhanced significantly when accumulation time was increased and Fig. 5.11 depicts variation of i_{pa} with accumulation time. It is observed that peak current increases up to 4 minutes and then remained almost stable. Considering sensitivity of developed sensor, an accumulation time of 4 minutes was chosen for determination of P4R.

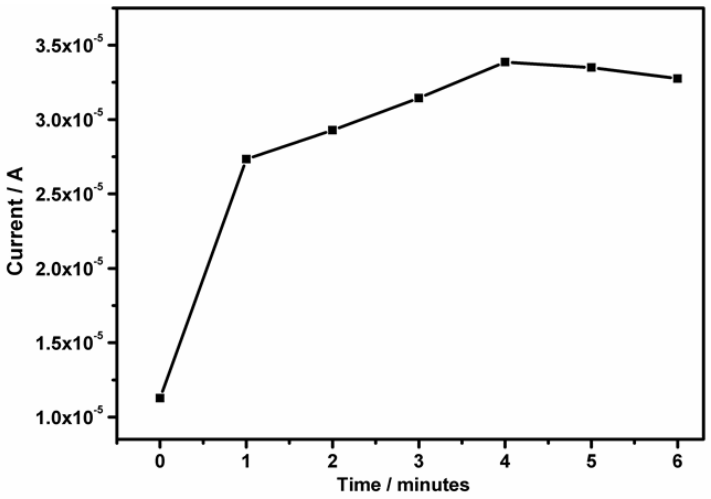

Figure 5.11: Influence of accumulation time on the anodic peak current of 1.0×10^{-5} M P4R

5.3.3.3. Influence of number of cycles of electropolymerization

In an electropolymerization process, number of cyclic voltammetric scans determines the thickness of as grown polymer film**.** Fig. 5.12 illustrates relationship between oxidation peak current of 1.0×10^{-5} M P4R and number of cycles of electropolymerization. It is clear that oxidation peak current increase with increase in number of cycles from 10 to 30 and decreases thereafter (Fig. 5.12). Reduction in oxidation peak current, on increasing number of cycles of electropolymerization from 30 to 50 imply that it is very difficult for the electrons to reach electrode surface through thick polymer film due to increase in the diffusion barrier.[250,251] Therefore, 30 was chosen as the optimum number of cycles for polymerization of L-Cys on GCE.

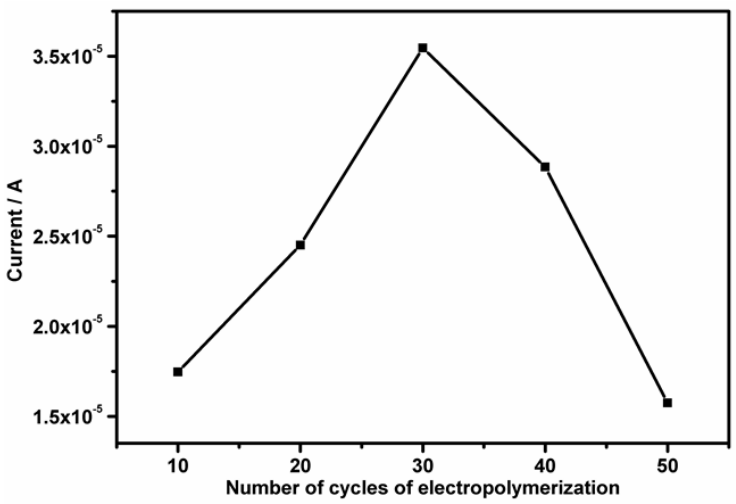

Figure 5.12: Influence of number of cycles of electropolymerization on the anodic peak current of 1.0 × 10^{-5} M P4R

5.3.4 Influence of scan rate

To elucidate underlying mechanisms involved in electrochemical process, cyclic voltammogramms of 1.0 × 10^{-4} M P4R at different scan rates were recorded and the results are shown in Fig. 5.13. As evidenced from Fig. 5.14, anodic and cathodic peak currents of P4R increased linearly with scan rate in the range 0.02 to 0.20 V s^{-1} with linear regression equations,

$$i_{pa}(A) = 7.0 \times 10^{-5} v\ (V\ s^{-1}) + 3.0 \times 10^{-7}\ (R^2 = 0.998)\ \text{and}$$
$$i_{pc}(A) = -4.0 \times 10^{-5} v\ (V\ s^{-1}) + 2.0 \times 10^{-7}\ (R^2 = 0.998)$$

respectively, suggesting that electrochemical process of P4R on poly(L-Cys)/GCE was adsorption controlled. Since there is no remarkable shift in oxidation and reduction peak of P4R with scan rate, redox process of P4R at poly(L-Cys)/GCE can be considered as reversible. Moreover, plot of log i_p *vs* log υ showed a linear relationship (Fig. 5.15) in the scan rate range 0.02 to 0.20 V s^{-1}, with slopes of anodic and cathodic peak currents

as 1.13 and 1.12, respectively. Closeness in values of slopes to theoretical value of 1.0 also confirms that the electrochemical behaviour of P4R on poly(L-Cys)/GCE is an adsorption controlled process.[252]

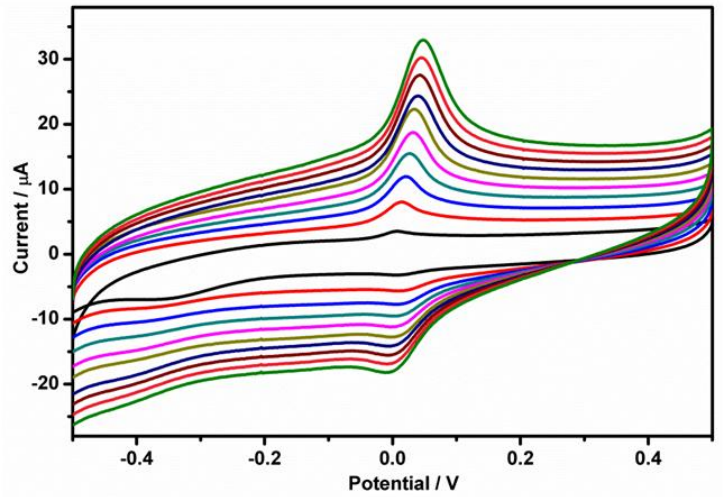

Figure 5.13: Overlay of cyclic voltammograms of 1.0×10^{-4} M P4R on poly(L-Cys)/GCE at various scan rates

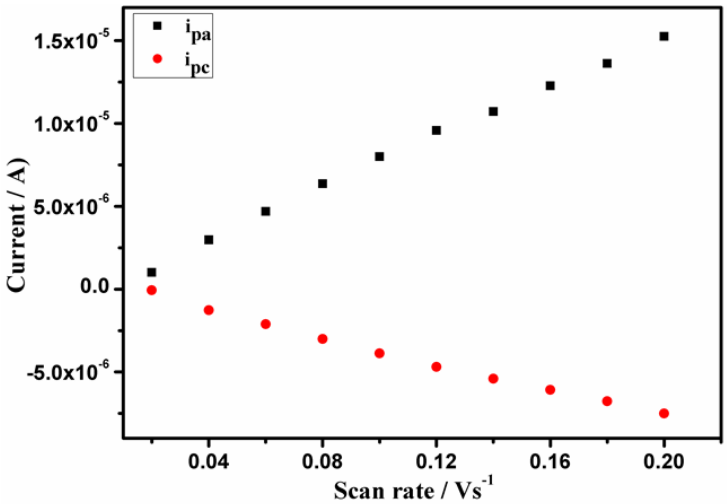

Figure 5.14: Variation of anodic and cathodic peak currents of 1.0×10^{-4} M P4R with scan rate

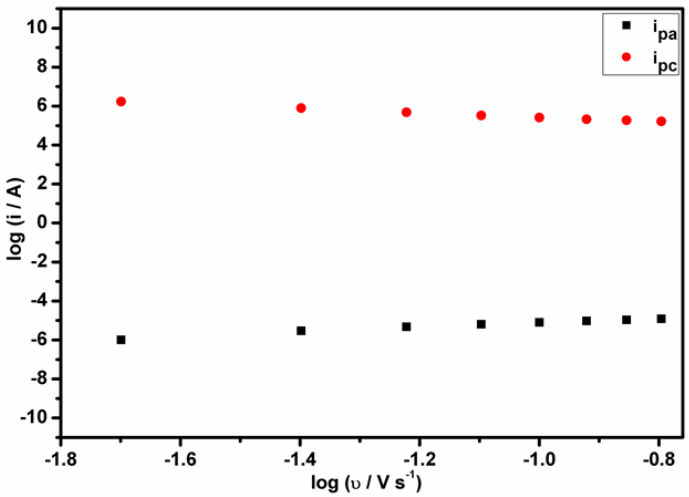

Figure 5.15: Plot of log i *vs* log υ

5.3.5 Calibration plot and limit of detection

Relationship between oxidation peak currents and different concentrations of P4R is given in Fig. 5.16a. Oxidation peak currents showed linear dependence to concentrations in the range 1.0×10^{-5} to 1.0×10^{-6} M and corresponding linear regression equation was $I_p\,(A) = 3.05C\,(M) + 4.94$ ($R^2 = 0.996$) (Fig. 5.16b). Limit of detection (LOD) and limit of quantification (LOQ) of P4R were found to be 3.73×10^{-8} M and 1.24×10^{-7} M, respectively. Lower detection limit and lower oxidation potential of P4R at poly(L-Cys)/GCE can be ascribed to better electrocatalytic property of polymer film on surface of GCE. Comparative performance of developed sensor reveals that electro oxidation of P4R takes place at a lower potential than other electrochemical sensors (Table 5.2).[253-256] This also confirms superior electrocatalytic property of L-Cys polymer film on surface of GCE.

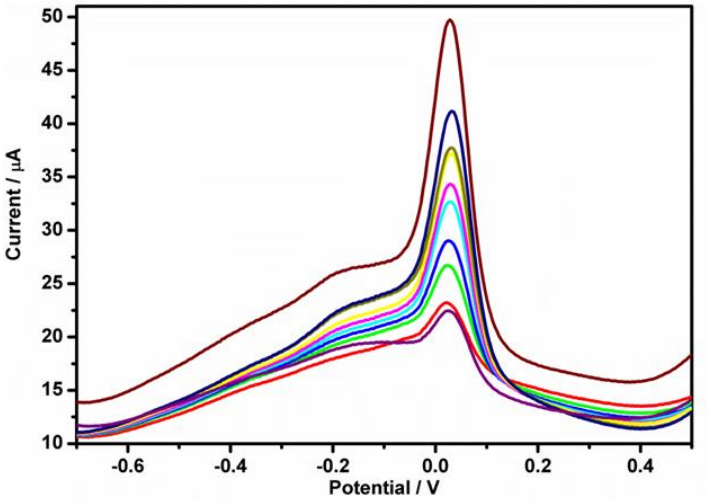

Figure 5.16a: Overlay of square wave voltammograms for electrooxidation of P4R on poly(L-Cys)/GCE at various concentrations in 0.1 M PBS of pH 7.0

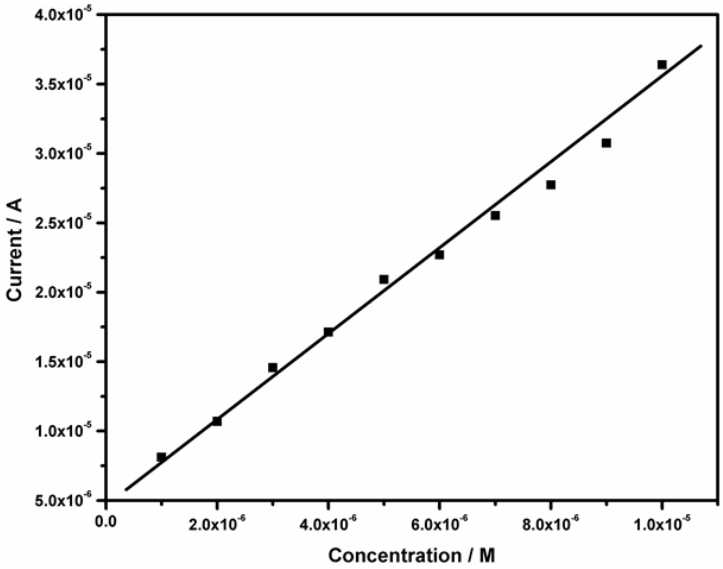

Figure 5.16b: Calibration curve of P4R in the concentration range $1.0 \times 10^{-5} – 1.0 \times 10^{-6}$ M

5.3.6 Number of electrons

Number of electrons (n) take part in electrochemical oxidation of P4R were calculated using the following equation.[257]

$$\boldsymbol{\Delta E = \frac{0.059}{n}}$$

Potential difference between redox peaks ($\Delta E = E_{pa} - E_{pc}$) of P4R on poly(L-Cys) modified GCE was found to be 0.032 V at a scan rate of 0.1 V s^{-1}. Thus, number of electrons take part in electrochemical oxidation of P4R was calculated to be 2 using above equation.

5.3.7 Reaction mechanism

From pH study, it can be inferred that electrochemical oxidation of P4R involves equal number of electrons and protons. Additionally, number of electrons taking part in the oxidation of P4R was also calculated to be two. On reviewing literature, oxidation of 2-naphthol result in the formation of 2,3-dihydroxynaphthalene through two electron-two protons transfer.[258]

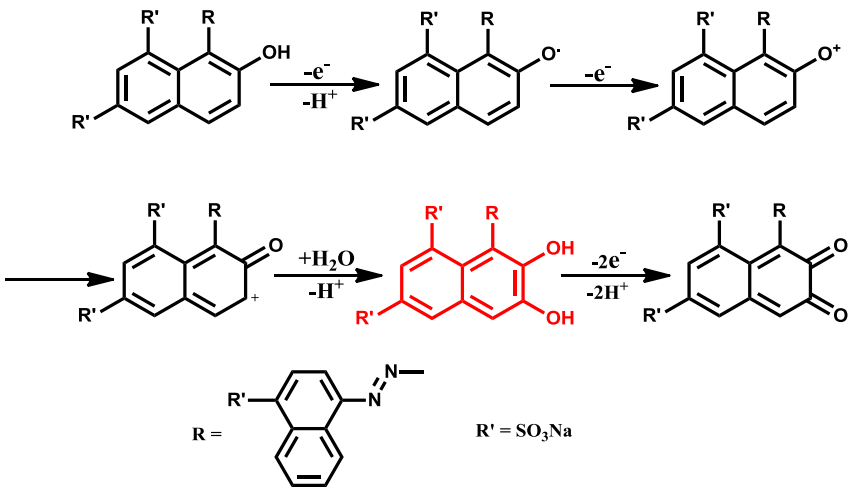

Scheme 5.1: Mechanism of electrochemical oxidation of P4R

Since P4R is a 2-naphthol derivative, observed oxidation peak could be due to formation of 2,3-dihydroxynaphthalene via oxidation of hydroxyl group present in P4R.[259] Naphthalene 1,2-diol is further oxidised to give quinone through non electrochemical process (Scheme 5.1).

5.3.8 Evaluation of kinetic parameters

Charge transfer coefficient (α), which explains precedence of electron transfer to either oxidation or reduction,[260] was also evaluated following Laviron's method.[214]

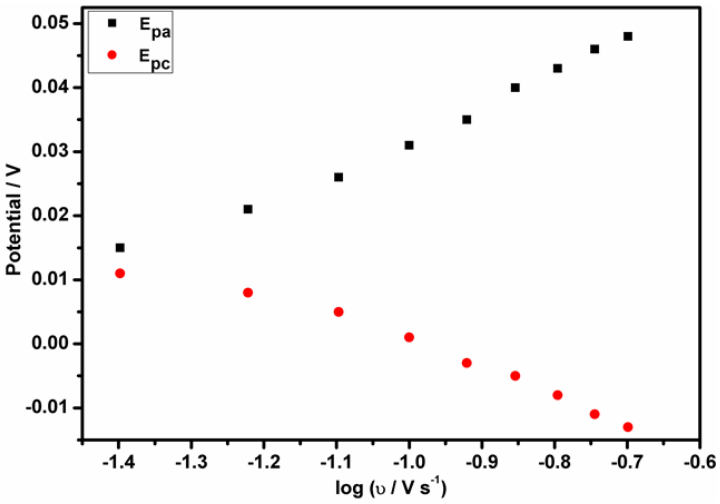

Figure 5.17: Variation of E_{pa} and E_{pc} with log υ

From Fig. 5.17, it is obvious that at higher scan rate, peak potential varies linearly with logarithm of scan rate. In the scan rate range 0.10 to 0.20 V s^{-1}, plot of E_{pa} and E_{pc} *vs* log υ shows linear behaviour with regression equations, $E_{pa}(V) = 0.059\,\upsilon(Vs^{-1}) - 0.088$ ($R^2 = 0.997$) and $E_{pc}(V) = -0.046\,\upsilon(Vs^{-1}) - 0.093$ ($R^2 = 0.996$). Based on slope of above plots and by following the equations given below,[261,262]

$$E_{pa} = a + \{2.303RT|(1-\alpha)nF\}log\upsilon$$

$$E_{pc} = b - \{2.303RT|\alpha nF\}log\upsilon$$

where a and b are constants, it is possible to calculate anodic (α_a) and cathodic charge transfer coefficients (α_c) and values were found to be 0.639 and 0.502 respectively. From α_a and α_c, value of α was calculated as 0.570.

For poly(L-Cys)/GCE, heterogeneous rate constant (k_s) can be estimated by following Laviron's equation for redox systems,[214]

$$\log k_s = \alpha\log(1-\alpha) + (1-\alpha)\log\alpha - \log\frac{RT}{nFv} - \frac{\alpha(1-\alpha)nF\Delta E_p}{2.3RT}$$

where ΔE_p is the potential difference and n is the number of electrons transferred. Value of k_s for poly(L-Cys)/GCE was estimated to be 2.56 s^{-1}.

Since electrochemical oxidation of P4R on bare GCE is an irreversible process, following Laviron equation is a suitable measure to calculate k_s[186]

$$E_{pa} = E^{0\prime} + \frac{RT}{(1-\alpha)nF}\left(\ln\frac{(1-\alpha)nF}{RTk_s} - \ln v\right)$$

where $E^{0\prime}$ or formal potential is obtained by extrapolating intercept of plot E_p *vs* v to vertical axis at $v = 0$ and other symbols have their usual significance. Heterogeneous rate constant for bare GCE was calculated to be 1.27 s^{-1}

Higher value of k_s for poly(L-Cys)/GCE could be attributed to faster electron transfer ability of modified electrode due to greater conductivity of polymer film and increased surface concentration of P4R on poly(L-Cys)/GCE.

5.3.9 Chronocoulometric studies

Chronocoulometry, a classical technique used in electrochemistry measure charge (coulombs) as a function of time (chrono) and it was used to estimate diffusion coefficient of P4R at poly(L-Cys)/GCE. Chronocoulograms of P4R were recorded in the range 1.1×10^{-3} to 4.0×10^{-4} M and is shown in Fig. 5.18a. Plot of Q *vs* $t^{1/2}$ showed linear dependence, which demonstrates that the transient current depends on adsorption of P4R on surface of poly(L-Cys)/GCE (Fig. 5.18b). Linear relationship between slopes of Q *vs* $t^{1/2}$ graph and concentration of P4R is depicted in Fig. 5.18c. The corresponding regression equation is, $Slope\left(\mu C\ s^{-\frac{1}{2}}\right) = 17.64\ (mM) + 84.00\ (R^2 = 0.998)$. Using slope of the above plot and by applying Anson equation,[23] value of D was calculated as 2.93×10^{-6} $cm^2\ s^{-1}$.

$$\boldsymbol{Q = \frac{2nFAC(Dt)^{1/2}}{\pi^{1/2}} + Q_{dl} + Q_{ads}}$$

where D is diffusion coefficient of analyte, n is number of electrons, Q_{dl} is double layer charge, Q_{ads} is adsorption charge, C is bulk concentration, A is effective surface area of electrode and other symbols have their standard meanings. Value of Q_{ads} was obtained from intercept of plot Q *vs* $t^{1/2}$.

Saturated adsorption capacity (Γ) could be calculated from following equation,

$$\boldsymbol{Q_{ads} = nFA\Gamma}$$

and value was found to be 5.54×10^{-9} mol cm^{-2}.

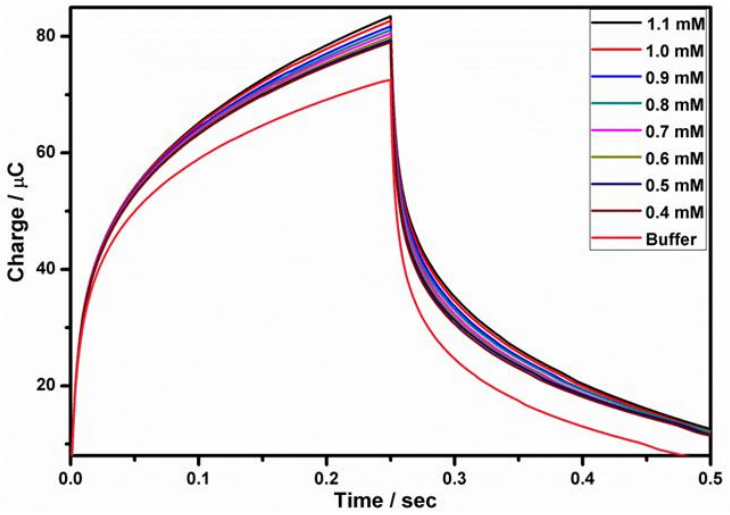

Figure 5.18a: Chronocoulograms obtained at poly(L-Cys)/GCE in 0.1 M PBS (pH 7.0) in the concentration range 1.1×10^{-3} - 4.0×10^{-4} M

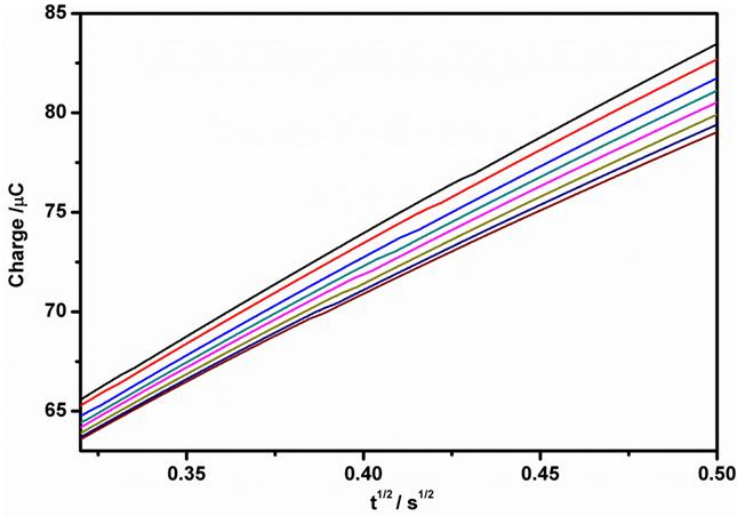

Figure 5.18b: Plot of Q *vs* $t^{1/2}$ derived from the chronocoulograms of Fig. 5.18a

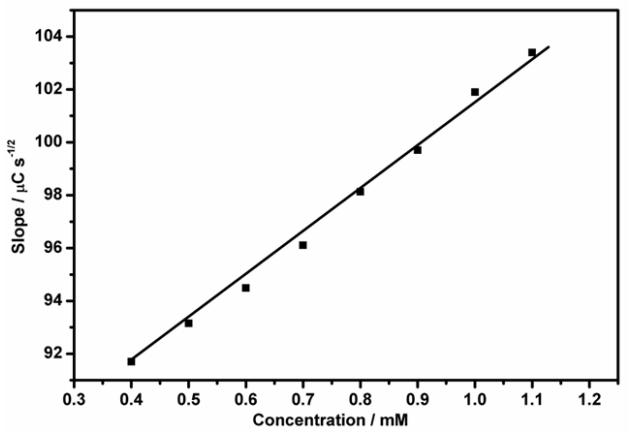

Figure 5.18c: Plot of slope of Q *vs* $t^{1/2}$ graph against concentration of P4R

5.3.10 Repeatability, reproducibility and stability of poly(L-Cys)/GCE

Cardinal features of a good sensor includes its repeatability, reproducibility and stability.[263] Repeatability and reproducibility of poly(L-Cys)/GCE modified electrode was appraised in PBS (pH 7.0) containing 1.0×10^{-5} M P4R. Relative standard deviation (RSD) of oxidation peak current was 1.1% for six successive measurements, indicating good repeatability of poly(L-Cys)/GCE. To evaluate the reproducibility of modified electrode, six poly(L-Cys)/GCE electrodes were prepared. Generation of reproducible surface was evaluated by SWV and RSD of 2.2% implies suitable reproducibility of developed sensor. Stability of developed sensor was observed by assessing its oxidation peak current after seven days. It was found that 96.6% of oxidation peak current was retained even after seven days, which shows good stability of proposed sensor.

5.3.11 Interference study

One of the major characteristics of a good sensor is its selectivity towards different coexisting substances. Selectivity of the proposed sensor was

examined using various coexisting species on the oxidation peak current of P4R. Square wave voltammograms of 1.0×10^{-5} M P4R were recorded to study the effect of interfering species *viz.*, sodium chloride, sodium sulphite, fructose, citric acid, aspartame and ascorbic acid under optimal conditions. From Table 5.3, it is evident that up to 100 fold excess concentrations of sodium chloride, sodium sulphite, fructose, citric acid and aspartame did not show any interference in determination of P4R (signal change less than ± 5 %). However, interference was observed when concentration of ascorbic acid was same as that of P4R.

5.3.12 Application study

Practical applicability and performance of proposed sensor was determined by quantitative analysis of P4R in two commercial soft drink samples and the results are summarized in Table 5.4. No matrix interferences were observed in analysis of samples. Recovery values were ranged from 102.4 to 103.7%, revealing good accuracy of proposed sensor. On comparing results, developed method showed consistent results with spectrophotometric method,[148] confirming practical utility and reliability of the developed method for determination of P4R.

5.4 Conclusions

Electrochemical behaviour of P4R on poly(L-Cys) modified GCE was explored. Polymer modified GCE exhibited better electrochemical activity for oxidation of P4R compared to bare GCE. Linear dynamic range of 1.0×10^{-5} to 1.0×10^{-6} M was obtained with LOD and LOQ as 3.73×10^{-8} M and 1.24×10^{-7} M, respectively. Catalytic efficiency of poly(L-Cys) modified GCE was explored by evaluating charge transfer coefficient, heterogeneous

rate constant and diffusion coefficient. Additionally, developed sensor showed better reproducibility and stability. Validation of developed sensor was done by analysing concentration of P4R in soft drink samples.

Table 5.1: Comparison of different modified electrodes for detection of P4R

Modified electrode	Ep (V)	Current (μA)
[a]DT/GE	0.608	2.78
[b]polyBPB/GCE	0.240	30.25
[c]AuNP/GCE	0.032	17.73
Poly(L-Cys)/GCE	0.031	56.18

[a] Self assembled monolayer of dodecane thiol modified gold electrode
[b] Poly bromophenol blue modified glassy carbon electrode
[c] Gold nanoparticle modified glassy carbon electrode

Table 5.2: Comparison of different P4R sensors

Electrode	Signal	Ep (V)	Linear range (M)	LOD (M)	References
[a]DME	Reduction	-0.728	$6.62 \times 10^{-6} - 0$	6.23×10^{-8}	[253]
DME	Reduction	-0.688	-	5.62×10^{-8}	[254]
[b]AB film/GCE	Oxidation	0.560	6.62×10^{-6}- 8.27×10^{-8}	4.96×10^{-8}	[255]
[c]MWCNT/GCE	Oxidation	0.560	2.48×10^{-6}- 4.14×10^{-8}	2.48×10^{-8}	[256]
Poly(L-Cys)/GCE	Oxidation	0.031	1.00×10^{-5}- 1.00×10^{-6}	3.37×10^{-8}	Present method

[a]DME – dropping mercury electrode
[b]AB film – acetylene black film
[c]MWCNT – multiwalled carbon nanotube

Table 5.3: Effect of possibly interfering species on signal of 1.0×10^{-5} M P4R

Species	Concentration (M)	Signal change (%)
Sodium chloride	1.0×10^{-3}	-1.38
Sodium sulphite	1.0×10^{-3}	-1.54
Fructose	1.0×10^{-3}	-1.91
Citric acid	1.0×10^{-3}	1.82
Ascorbic acid	1.0×10^{-5}	15.75

Table 5.4: Determination of P4R in soft drink samples

Samples	Spectrophotometric method				Proposed method			
	Added (M)	Found (M)	Recovery (%)[a]	RSD (%)	Added (M)	Found (M)	Recovery (%)[a]	RSD (%)
Sample I	9.00×10^{-6} to 4.00×10^{-6}	8.99×10^{-6} to 3.85×10^{-6}	98.0	1.7	9.00×10^{-6} to 2.00×10^{-6}	9.21×10^{-6} to 2.10×10^{-6}	103.7	1.9
Sample II	9.00×10^{-6} to 4.00×10^{-6}	9.12×10^{-6} to 4.11×10^{-6}	102.0	2.1	9.00×10^{-6} to 2.00×10^{-6}	9.19×10^{-6} to 2.08×10^{-6}	102.4	1.5

[a] Average of five replicates
RSD - Relative standard deviation

Chapter 6

VOLTAMMETRIC SENSOR FOR ACID GREEN 50 BASED ON POLY GLYCINE MODIFIED GLASSY CARBON ELECTRODE

Contents

6.1 Introduction
6.2 Experimental
6.3 Results and discussion
6.4 Conclusions

This chapter details design of a voltammetric sensor for determination of synthetic food colorant, acid green 50 (AG), using poly Glycine modified glassy carbon electrode (poly Gly/GCE). Surface characterization of developed sensor was achieved using techniques such as cyclic voltammetry (CV), scanning electron microscopy (SEM), atomic force microscopy (AFM) and electrochemical impedance spectroscopy (EIS). Experimental parameters affecting sensor response were optimized. Electroanalytical reaction of AG at biopolymer film modified electrode was an irreversible process controlled by adsorption. Oxidation peak potential of AG was linearly related to its concentration in the range 1.0×10^{-4} to 9.0×10^{-6} M using square wave voltammetry (SWV), with a limit of detection of 3.62×10^{-7} M. Heterogeneous electron transfer rate constant (k_s) for electro-oxidation of AG was also determined. Chronocoulometry was used for estimating saturated adsorption capacity (Γ) and diffusion coefficient (D) and values obtained were 4.98×10^{-9} mol cm^{-2} and 1.63×10^{-5} cm^2 s^{-1}, respectively. Practical utility of the developed sensor was validated by successful determination of AG in commercial soft drink samples.

6.1 Introduction

Color is a major quality attribute considered by consumers, especially children while appraising appearance of foodstuffs. Food colorants maintain or improve natural colors that are lost during production and storage. Synthetic colorants are widely used instead of natural ones because of several advantages including better stability to temperature, oxidation and pH, cost effectiveness and availability in wide range of colors.[264,227] Different synthetic colorants are added to foods, but their list varies greatly among countries. Triarylmethane constitute a major class among synthetic food colorants and are represented by patent blue V (E131), brilliant blue FCF (E133) and acid green 50 (E142).[265]

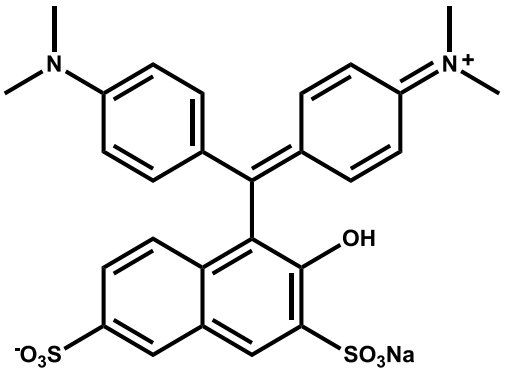

Figure 6.1: Structure of AG

Acid green 50 ($C_{27}H_{25}N_2O_7S_2Na$) (Fig. 6.1), can be used in variety of foodstuffs such as sweets, beverages, ice creams and tinned peas.[266] However, it poses potential risk to human health such as skin rash and bronchial asthma,[267] especially if consumed in excess. Hence, dietary levels of AG are subjected to regulation by standards such as Food and Agricultural

Organization, World Health Organization[268] and European Union directive 94/36/EC.[269] For AG, the EU Scientific Committee on Food has established an average daily intake of 5 mg/kg bw/day based on No-Observed-Adverse-Effect-Level.[270] Similarly, maximum permissible levels of AG for non-alcoholic flavored drinks were estimated to be 100 mg L^{-1}. Even though, adequate genotoxicity data is lacking for AG, European Commission to the European Food Safety Authority warns that the permitted dose may cause hypersensitivity reactions in susceptible individuals,[270] especially children. Currently, it is approved as a food additive in EU, Australia and New Zealand, but being prohibited in Canada, USA, Japan and Norway.[266]

Consequently, accurate and efficient methods of analysis need to be developed for ensuring safety of consumers and also to meet varying global regulatory frameworks. Several methods for determination of synthetic dyes are detailed in literature such as thin-layer chromatography,[271,272] derivative spectrometry[273,274] and spectrophotometric methods in combination with chemometrics,[275,276] but all of them require time-consuming pre-treatments. Capillary electrophoresis[277] and micellar electrokinetic capillary chromatography[278] have also been reported, but their major limitation is sensitivity problems resulting from small injection volumes. High-performance ion chromatography[279] and reversed-phase liquid chromatography[280,281] offer better resolution, sensitivity and selectivity. But, these methods face constraints such as lengthy analysis time and expensive solvents. In these aspects, voltammetry can be suggested as an alternative method due to its fastness, ease of use for on-site measurements, cost effectiveness and good reproducibility.

Though voltammetric techniques are well suited for the determination of synthetic food colorants, challenges such as fouling of electrode surface, higher overpotential, poor reproducibility and sluggish electron transfer kinetics, posed by conventional electrodes hamper its practical use in electrochemical sensing.[136,282] However, modification of electrodes with suitable electron transfer mediators alleviates above mentioned disadvantages and greatly promote their use for electrochemical sensing. They offer various advantages including homogeneity in electrochemical deposition, chemical stability of polymer film, strong adherence to electrode surface and high sensitivity.[283] Additionally, it is possible to control permeability of polymer film by changing polymerization time and by varying concentration of monomer used.[284] L- Glycine, the simplest amino acid is frequently used in electrode modification as it contains both carboxyl and amine functional groups.[285]

Present work is aimed to develop a voltammetric sensor for determination of food colorant, AG by employing poly Gly modified GCE. For electrochemical determination of AG, we have tried various chemical modifications on different electrodes (Table 6.1). From Table 6.1, it is clear that better oxidation signals were obtained with poly Gly/GCE and its selection is justified. Kinetic parameters such as heterogeneous rate constant and diffusion coefficient were also calculated. To our best knowledge, kinetic parameters for oxidation of AG have not been reported yet. The proposed method was also used for determining concentration of AG in commercial soft drink samples for validating its applicability.

6.2 Experimental

6.2.1 Preparation of poly Gly/GCE

GCE was cleaned as described in Section 2.3 and cleaned GCE was immersed in 0.1 M PBS (pH 7.0) containing 1.0×10^{-2} M Gly. Electropolymerization of Gly on surface of GCE was performed by cycling potential between -0.5 to 1.8 V, at a scan rate of 0.1 V s^{-1} (Fig. 6.2).[286] After electropolymerization, electrode was washed with water and dried in air.

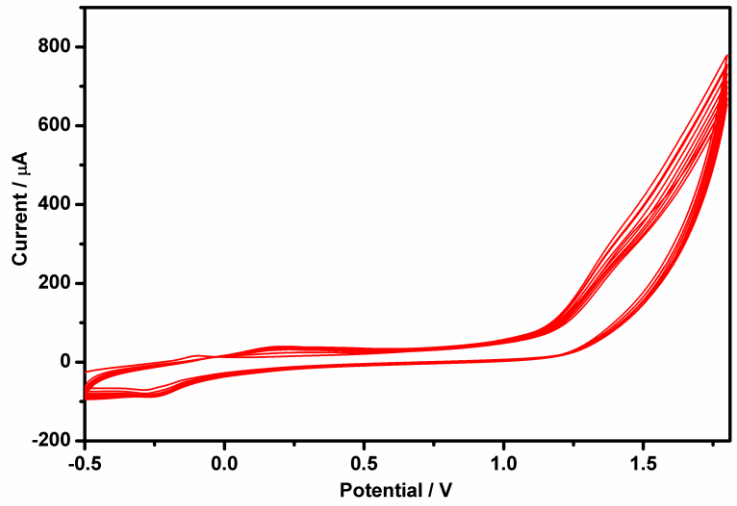

Figure 6.2: Cyclic voltammograms obtained for electropolymerization of Gly on GCE

During first anodic scan, an oxidation peak was obtained at 1.4 V. As number of cycles of polymerization increases, anodic peak current decreases, indicating formation of a polymer film on surface of GCE.[73] Amine functionality in Gly undergoes one electron oxidation to form corresponding free radical during anodic scan, which then forms a nitrogen-carbon linkage at the surface of GCE.[287]

6.2.2 Analytical procedure

All electrochemical measurements were carried out using 0.1 M PBS (pH 7.0) as supporting electrolyte. Desired volume of AG solution was pipetted into an electrochemical cell containing 10 mL of PBS. SWV measurements were recorded from 0 to 1.0 V, with pulse amplitude of 0.025 V, quiet time of 2 s, scan rate of 0.1 V s^{-1}, increment of 0.004 V and frequency of 15 Hz. Anodic peak current obtained at 0.640 V was used for determination of AG.

6.2.3 Sample treatment

Soft drink samples of two commercial brands procured from local market were used without pre-treatment. One mL of sample solution was added into 9.0 mL of 0.1 M PBS (pH 7.0) and resultant solution was subjected to electrochemical analysis, following the analytical procedure described in Section 6.2.2**.** Obtained results were compared with those from UV-visible spectrophotometric analysis, discussed in Section 2.5.3, under same conditions.[148]

6.3 Results and discussion

6.3.1 Characterisation of electrode surface

Surface characteristics of bare and poly Gly/GCE were studied using SEM, AFM, CV and EIS.

6.3.1.1 Surface morphology of bare GCE and poly Gly/GCE

Surface morphology of bare GCE and poly Gly/GCE were examined using SEM and AFM. As shown in SEM images (Fig. 6.3), surface topography of bare GCE was smooth, whereas polymer film modified

GCE had a flaky morphology, which proves surface modification of GCE during polymerization. Findings of SEM analysis were justified by observations obtained from AFM imaging. From AFM images of GCE and polymer film modified GCE (Fig. 6.4), it can be seen that relative to bare GCE (23.86nm), surface roughness of poly Gly/GCE (70.29 nm) has enhanced considerably, confirming modification of GCE on polymerization.

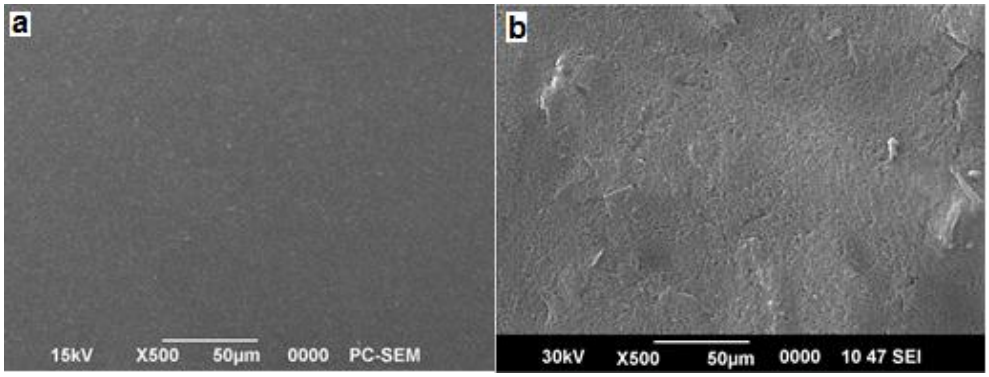

Figure 6.3: SEM images of (a) bare GCE (b) poly Gly/GCE

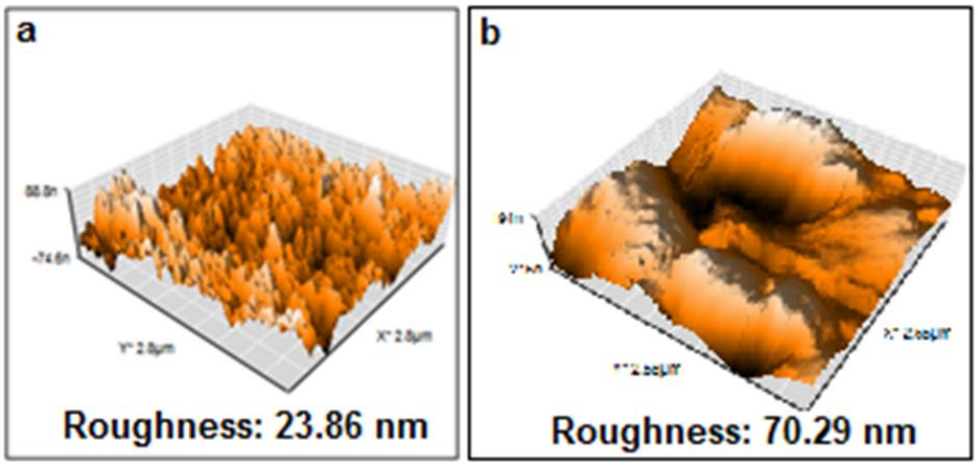

Figure 6.4: AFM images of (a) bare GCE (b) poly Gly/GCE

6.3.1.2. Surface area study

At various scan rates, cyclic voltammograms of 2.0 ×10^{-3} M $K_3Fe(CN)_6$ solution were recorded in the potential range 0 to 0.6 V on bare GCE (Fig. 6.5a) and poly Gly/GCE (Fig. 6.6a) to calculate effective surface area of electrodes. In both cases, peak current showed a linear increase to square root of scan rate (Fig. 6.5b and Fig. 6.6b), in accordance with Randles-Sevcik equation for reversible electrochemical reactions[179] and equation can be expressed as,

$$i_p = 2.69 \times 10^5 A n^{3/2} D^{1/2} C v^{1/2}$$

where C is concentration of $K_3Fe(CN)_6$ solution, D is diffusion coefficient, n is number of electron transferred and A is surface area of electrode. Based on Randles-Sevcik equation, effective surface area of bare and polymer modified electrodes were obtained as 0.027 and 0.068 cm^2, respectively. Compared to bare GCE, there is about threefold increase in electroactive surface area of modified electrode, indicating effective surface polymerisation resulting in increased number of catalytic sites for oxidation of AG.

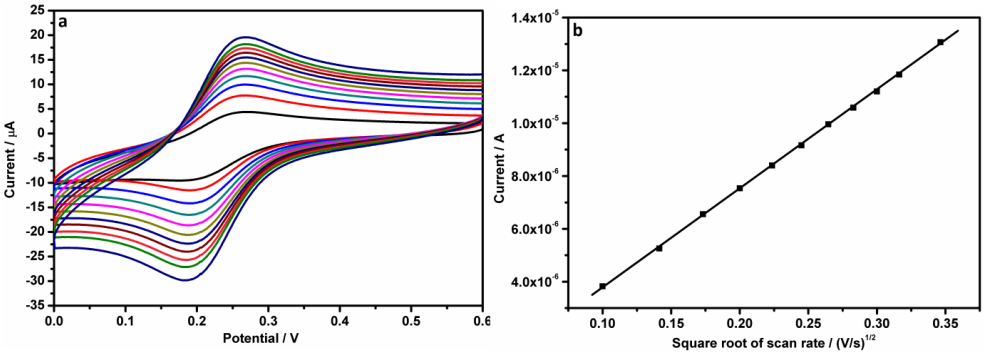

Figure 6.5: (a) Overlay of cyclic voltammograms of 2.0 × 10^{-3} M $K_3[Fe(CN)_6]$ on bare GCE at various scan rates (b) plot of current *vs* square root of scan rate for bare GCE

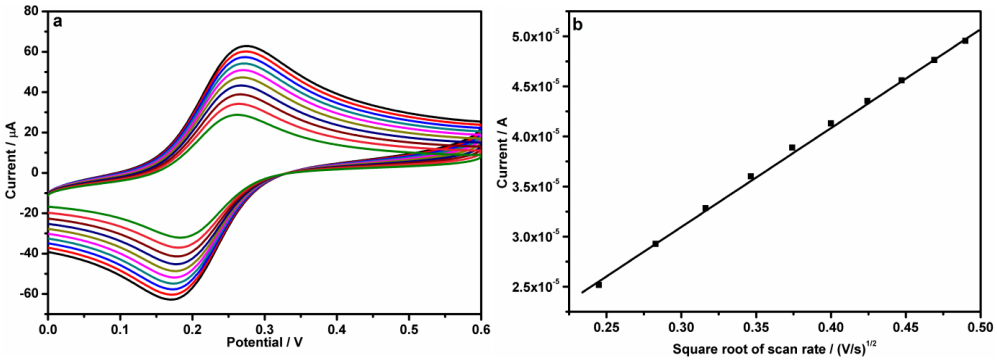

Figure 6.6: (a) Overlay of cyclic voltammograms of 2.0 × 10^{-3} M $K_3[Fe(CN)_6]$ on poly Gly/GCE at various scan rates (b) plot of current *vs* square root of scan rate for poly Gly/GCE

6.3.1.3 Electrochemical impedance spectroscopic studies

Electron transfer properties of bare and modified electrodes at electrolyte – electrode interface were probed by EIS. Fig. 6.7 depicts Nyquist plots of GCE and poly Gly/GCE, recorded in 0.1 M KCl containing 5.0 × 10^{-3} M $[Fe(CN)_6]^{3-/4-}$as redox probe, with in the frequency range of 1.0 - 10^5 Hz.

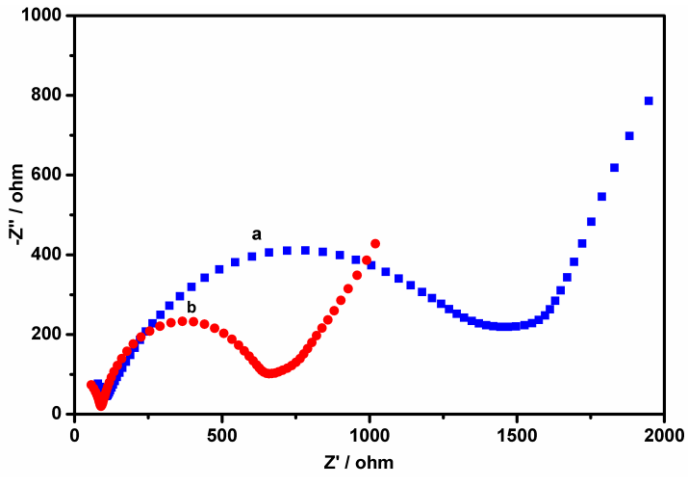

Figure 6.7: EIS spectra of (a) bare GCE (b) poly Gly/GCE in 5.0 × 10^{-3} M $[Fe(CN)_6]^{3-/4-}$ in 0.1 M KCl at the frequency range 1 - 10^5 Hz

Diameter of semi-circular part at higher frequency of Nyquist plot corresponds to charge transfer resistance (R_{ct}).[26] As depicted in Fig. 6.7, R_{ct} of bare GCE is high compared to polymer modified GCE. Lowered value of R_{ct} on poly Gly/GCE, points to effective modification of electrode surface with conducting polymer film. Above findings also endorse low charge transfer resistance and improved charge transfer kinetics at poly Gly/GCE.

6.3.1.4 Electrochemical behaviour of AG on poly Gly/GCE

Initially, electrochemical performance of GCE and poly Gly/GCE towards oxidation of 1.0×10^{-3} M AG were investigated by CV, in the potential range 0 to 1.0 V (Fig. 6.8). As depicted in Fig. 6.8, an irreversible oxidation peak was observed on both bare and polymer modified GCE. For bare GCE, a feeble oxidation signal was obtained at 0.754 V with a peak current of 0.78 µA (Fig. 6.8a), whereas on poly Gly/GCE (Fig. 6.8b), oxidation peak was shifted towards more negative potential (E_{pa} = 0.700 V), with a peak current of 6.99 µA. Compared to bare GCE, modified sensor showed better electrochemical behaviour for AG, in terms of lower oxidation potential and higher peak current. On poly Gly/GCE, peak potential has decreased by 0.054 V and peak current has increased by almost nine times. Enhanced oxidation peak current of AG at polymer modified GCE can be attributed to excellent electrical conductivity of poly Gly film, which accelerate electron transfer between electrode - electrolyte interfaces.

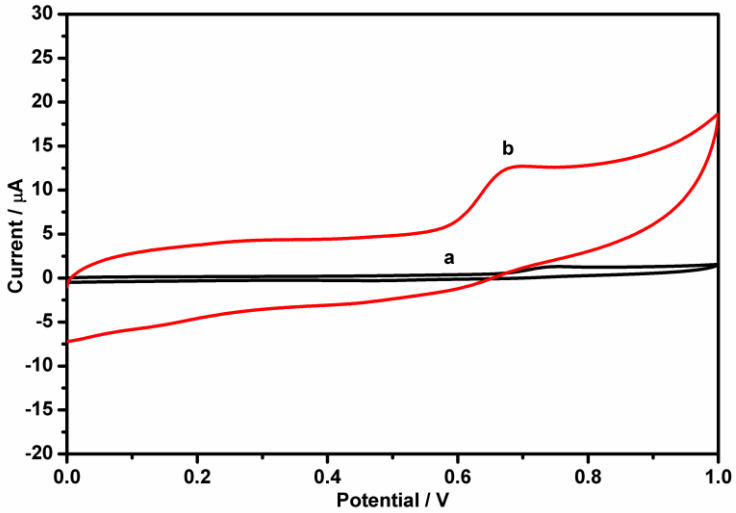

Figure 6.8: Cyclic voltammograms of 1.0 × 10^{-3} M AG at (a) bare GCE (b) poly Gly/GCE in PBS of pH 7.0

6.3.2 Optimization of experimental conditions

Parameters such as supporting electrolyte, pH of buffer, number of cycles of polymerization and accumulation time, which could have significant influence on oxidation of AG were investigated.

6.3.2.1 Influence of supporting electrolyte

Square wave voltammetric response of 5.0 × 10^{-5} M AG in 0.1 M concentration of various supporting electrolytes (acetate buffer, phosphate buffer, citrate buffer, hydrochloric acid, sulphuric acid, sodium hydroxide and sodium chloride) were assessed using developed sensor. Among aforementioned supporting electrolytes, lowest overpotential was obtained with PBS. Additionally, sensitivity of poly Gly/GCE towards AG was highest in 0.1 M PBS. Therefore, 0.1M PBS was chosen as supporting electrolyte for subsequent studies.

6.3.2.2 Influence of pH

Electrochemical behaviour of 5.0×10^{-5} M AG at poly Gly/GCE was probed in 0.1 M PBS, at pH ranges from 4.0 to 9.0, using SWV. From Fig. 6.9 it is clear that the oxidation peak current increases with increase in pH and highest peak current was recorded at pH 7.0. However, on further increasing the pH, the peak current decreased. Hence, 0.1 M PBS of pH 7.0 was selected for voltammetric determination of AG.

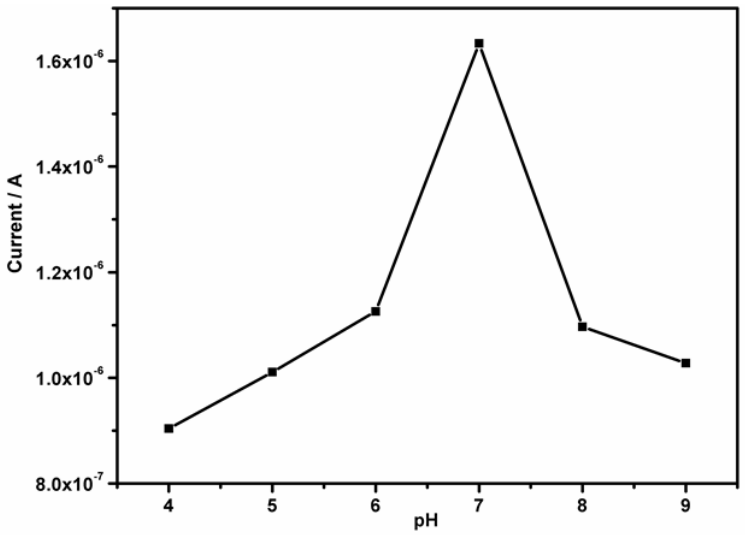

Figure 6.9: Influence of pH on the oxidation peak current of 5.0×10^{-5} M AG

6.3.2.3 Effect of number of cycles of electropolymerization

Sensitivity of modified electrode also depends on number of cycles of electropolymerization. Hence, further experiments were carried out to investigate electrochemical behaviour of 5.0×10^{-5} M AG on poly Gly/GCE by changing the number of cycles from 5 to 25. When number of cycles has increased from 5 to 10, oxidation peak current also increases simultaneously

(Fig. 6.10). However, on further increase in number of cycles from 10 to 25, reduction in oxidation peak current was observed. Further, oxidation current of AG was highest when number of cycles was 10. Reduction in peak current when number of cycles was increased above 10 could be attributed to the fact that, as thickness of polymer film increases, AG will take more time to diffuse into thicker layer of polymer film. Hence, electrodes modified by applying 10 cyclic scans, within the potential range of -0.5 to 1.8 V in solution containing 5.0×10^{-4} M Gly were used for further studies.

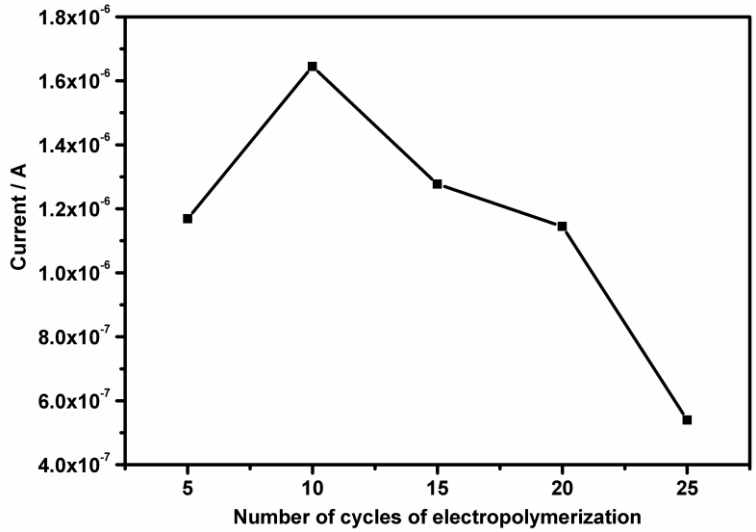

Figure 6.10: Influence of cycle number of electropolymerization on peak current of 5.0×10^{-5} M AG

6.3.2.4. Influence of accumulation time

Using SWV, oxidation peak current of 5.0×10^{-5} M AG was measured by varying accumulation time from 0 to 5 minutes. From Fig. 6.11, it is clear that peak current increases when accumulation time increases from 0 to 3 minutes, reaching the maximum value at 3 minutes, which indicates

that surface saturation of polymer film modified GCE by AG occurs at three minutes. Consequently, accumulation time of three minutes was selected for further studies.

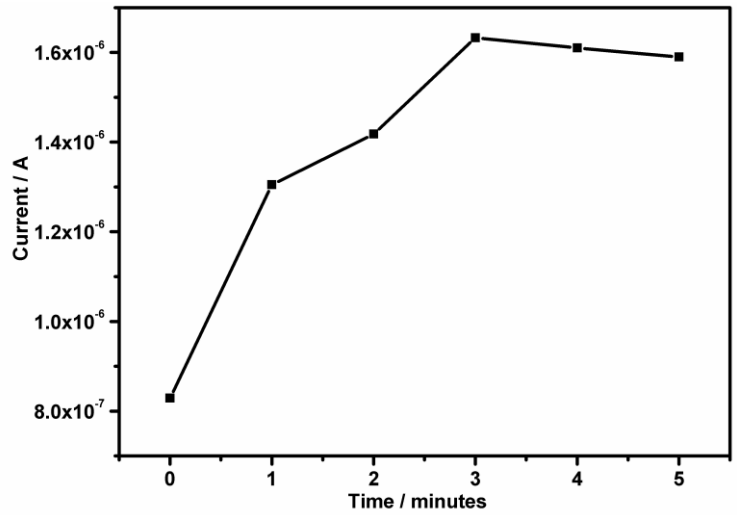

Figure 6.11: Influence of accumulation time on the peak current of 5.0 × 10^{-5} M AG

6.3.3 Effect of scan rate

Fig. 6.12a shows linear sweep voltammetric responses of 1.0 × 10^{-4} M AG at poly Gly/GCE over the scan rate range 0.10 to 0.36 V s^{-1}. In the above mentioned range, oxidation peak current shows linear response to scan rate and follows the equation, $i_p(A) = 6 \times 10^{-6}(Vs^{-1}) + 3 \times 10^{-6}(R^2 = 0.994)$. Based on the linear dependence between oxidation peak current (i_p) and scan rate (υ), it can be ascertained that the above process is adsorption controlled (Fig. 6.12b). Furthermore, a positive shift in oxidation peak potential of AG with scan rate confirms the irreversible nature of oxidation process.

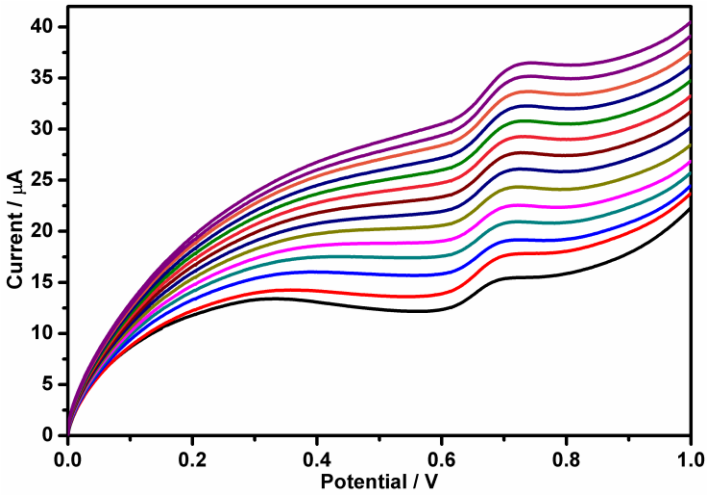

Figure 6.12a: Overlay of linear sweep voltammograms of 1.0×10^{-4} M AG on poly Gly/GCE at various scan rates

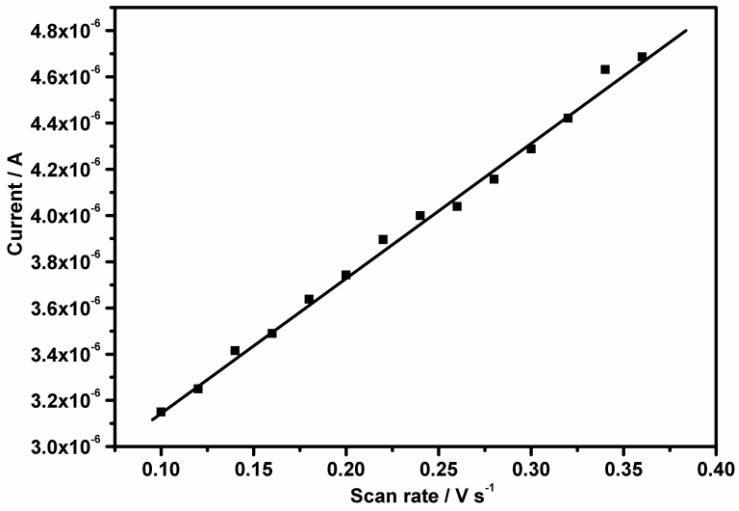

Figure 6.12b: Plot of anodic peak currents *vs* scan rate of 1.0×10^{-4} M AG

6.3.4 Calibration plot and limit of detection

Fig. 6. 13a shows square wave voltammograms of various concentrations of AG in 0.1 M PBS (pH 7.0) recorded at poly Gly/GCE. For the developed sensor, oxidation peak currents increased with increase in concentration of AG and peak currents were proportional to concentration in the range 1.0×10^{-4} to 9.0×10^{-6} M and follows equation, $i_p(A) = 0.029\ (M) + 5 \times 10^{-8}$ (0.995) (Fig. 6.13b). Limit of detection (LOD) and limit of quantification (LOQ) of developed sensor were estimated using equations, $3\frac{S}{m}$ and $10\frac{S}{m}$, where S and m are standard deviation of oxidation peak current for lowest concentration and slope of calibration curve respectively.[288] LOD and LOQ values were calculated as 3.62×10^{-7} and 1.21×10^{-6} M, respectively.

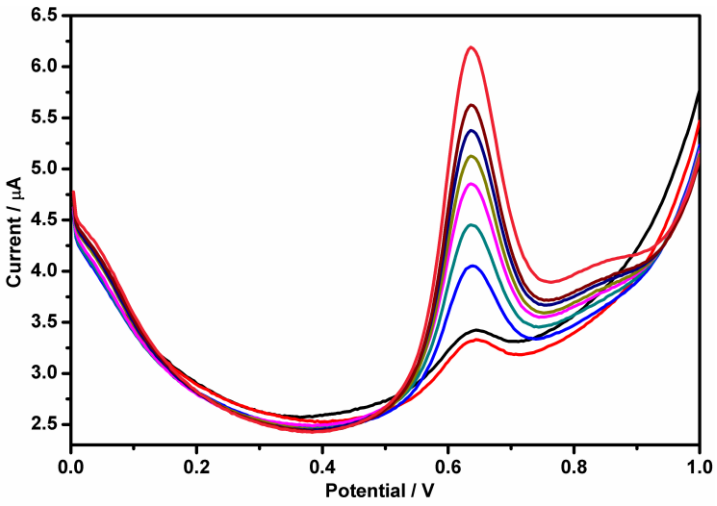

Figure 6.13a: Overlay of square wave voltammograms for oxidation of AG at various concentrations

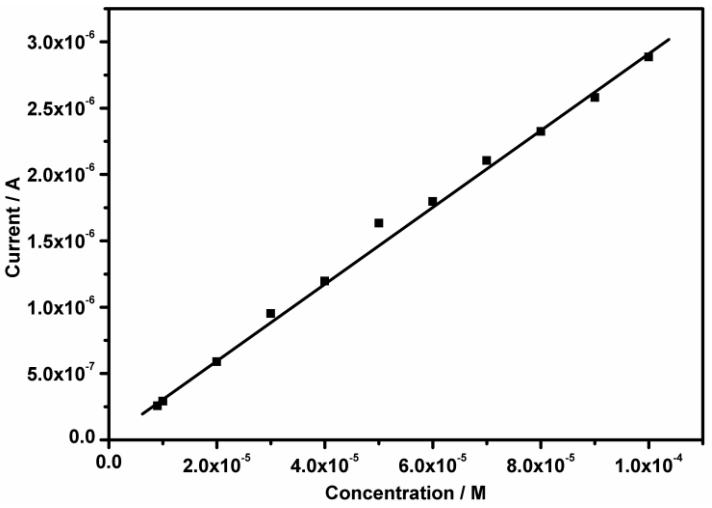

Figure 6.13b: Plot of concentrations of AG *vs* peak current in the range 1.0×10^{-4} to 9.0×10^{-6} M

Table 6.2 compares the performance of developed sensor with other methods for determination of AG.[289-292] Even though, LOD of present work is not the lowest, our method can be used as an alternative to other methods for determination of AG because other methods require sophisticated techniques, costly equipment and complicated operations. On contrast, the proposed method had its own unique features such as simplicity in operation, low cost and quick response, which makes it an ideal choice for determination of AG.

6.3.5 Number of electrons

Number of electrons (n) involved in totally irreversible electrode process can be calculated using equation,[184]

$$(\mathbf{1}-\boldsymbol{\alpha})\boldsymbol{n} = \frac{\mathbf{47.7}}{(\boldsymbol{E_p} - \boldsymbol{E_{p1/2}})}$$

where α is charge transfer coefficient and $E_{p1/2}$ is half peak potential. For an irreversible electrode process, value of α is 0.5. Based on above equation, number of electrons involved in irreversible electrochemical oxidation of AG was calculated as 1.3 (≈ 1). Number of electrons was also calculated by the following equation,[293,294]

$$i_p = \frac{nFQv}{4RT}$$

where Q is quantity of charge, R is gas constant, F is Faraday constant and T is absolute temperature in Kelvin. From slope of plot i_p *vs* υ, value of n is estimated to be 1.1 (≈ 1). Since AG is a triarylmethane dye, observed oxidation peak may be resulted due to formation of stable triarylmethane radical through one electron transfer.[295,296]

6.3.6 Evaluation of kinetic parameters

Heterogeneous rate constant (k_s) for irreversible oxidation of AG at bare and poly Gly/GCE was found using Laviron equation,[186]

$$E_{pa} = E^{0\prime} + \frac{RT}{(1-\alpha)nF}\left(\ln\frac{(1-\alpha)nF}{RTk_s} - \ln v\right)$$

where E_{pa} and $E^{0\prime}$ represent anodic peak potential and formal potential, respectively. Intercept of plot E_{pa} *vs* Napierian logarithm υ will give value for k_s (Fig. 6.14). Further, intercept of plot of E_p *vs* v obtained by extrapolating to v = 0 will give value of $E^{0\prime}$ (Fig. 6.15). Based on above equation, value of k_s for electrooxidation of AG on GCE and poly Gly/GCE was obtained as 3.54 and 4.08 s^{-1} respectively. An increase in magnitude of k_s suggests enhanced electron transfer ability of modified GCE for oxidation of AG.

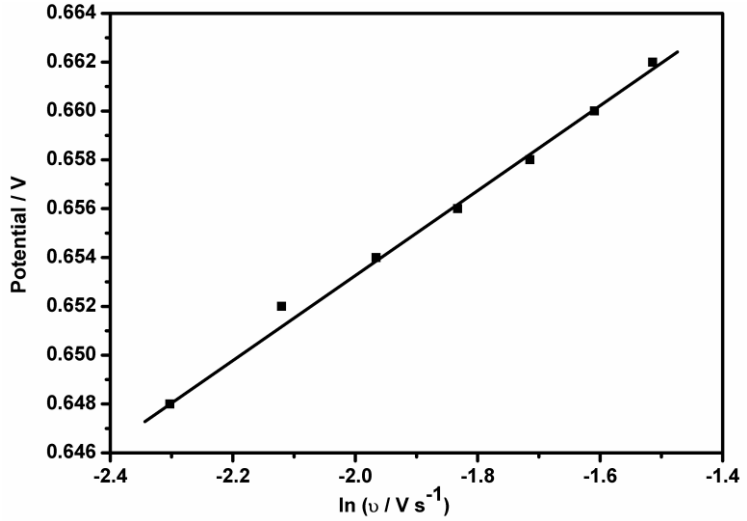

Figure 6.14: Variation of E_{pa} with ln υ

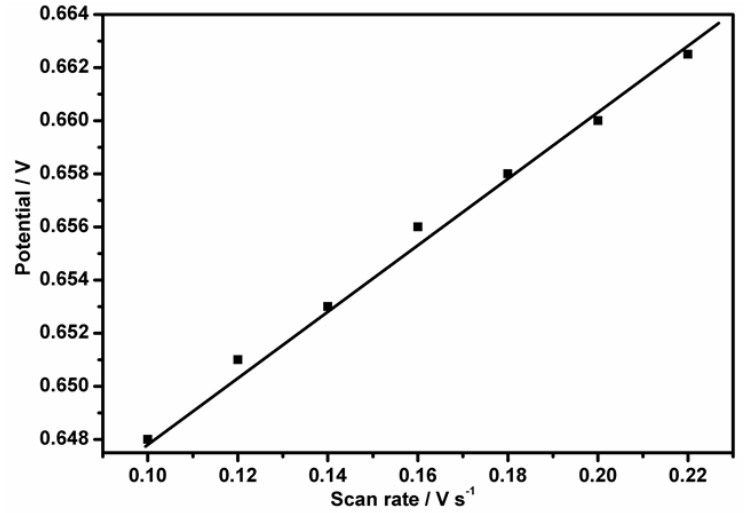

Figure 6.15: Variation of E_{pa} with υ

6.3.7 Chronocoulometric studies

Chronocoulometry was employed to measure diffusion coefficient (D) and saturated adsorption capacity (Γ) of polymer modified GCE. Fig. 6.16a displays overlay of charge (Q) – time (t) curves of AG recorded under optimum experimental conditions, over the concentration range 1.1×10^{-3} to 2.0×10^{-4} M. Linear relationship between Q and $t^{1/2}$ is shown in Fig. 6.16b and intercept of plot will give value of Faradaic charge resulting from oxidation of AG (Q_{ads}). Linear plot of slopes of Q - $t^{1/2}$ and concentrations of AG (Fig. 6.16c) can be described by regression equation, $Slope\left(\mu C s^{-\frac{1}{2}}\right) = 38.69\ C\ (\mu M) + 38.28$, ($R^2$ = 0.994), which was used for calculation of D by the following Anson equation,[23]

$$\boldsymbol{Q = \frac{2nFAC(Dt)^{1/2}}{\pi^{1/2}} + Q_{dl} + Q_{ads}}$$

where D is diffusion coefficient of analyte, Q_{dl} is double layer charge, C is bulk concentration, n is number of electrons, A is effective surface area of electrode and other symbols have their standard meanings. Value of D was obtained as 1.63×10^{-5} $cm^2\ s^{-1}$.

Also, saturated adsorption capacity (Γ) of poly Gly/GCE was calculated following equation,

$$\boldsymbol{Q_{ads} = nFA\Gamma}$$

and value was estimated to be 4.98×10^{-9} mol cm^{-2}.

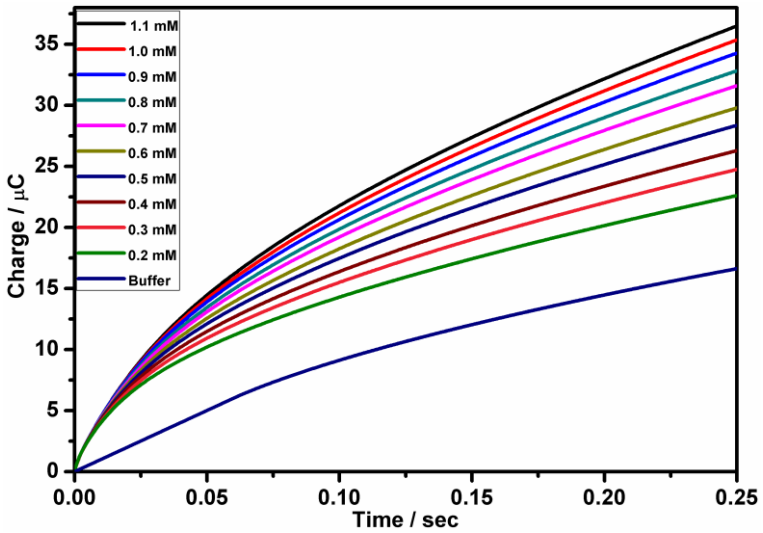

Figure 6.16a: Chronocoulograms obtained at poly Gly/GCE in 0.1 M PBS (pH 7.0) for different concentrations of AG

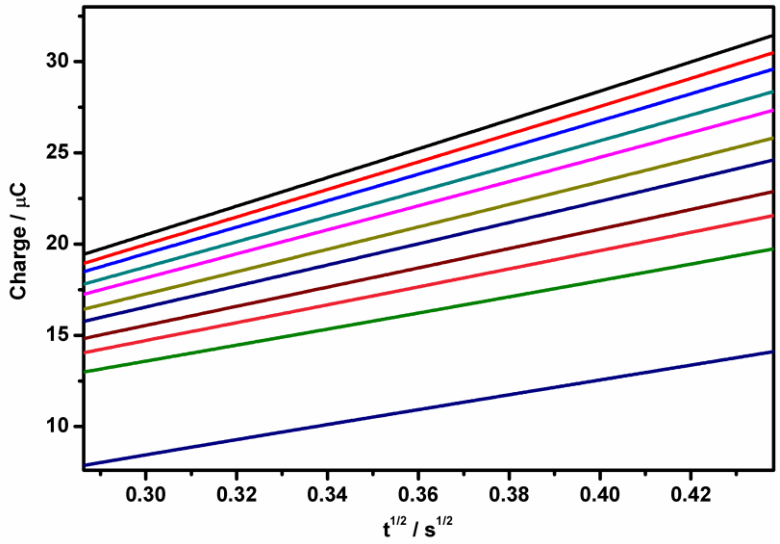

Figure 6.16b: Plots of Q *vs* $t^{1/2}$ derived from the chronocoulograms of Fig. 6.16a

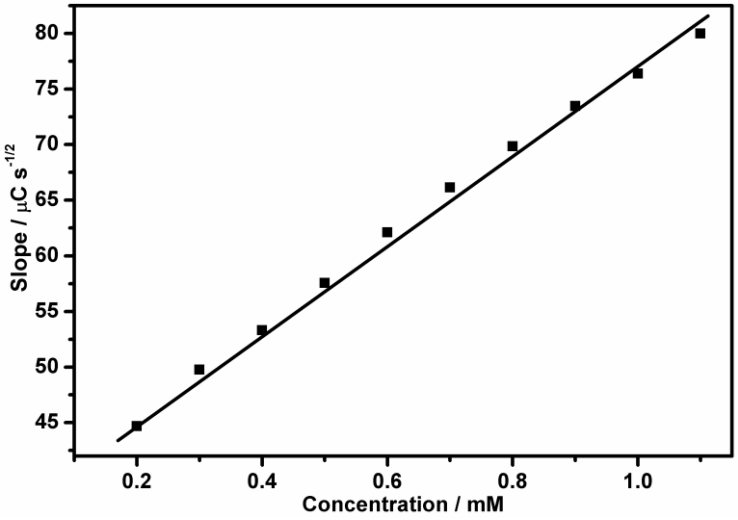

Figure 6.16c: Plot of slope of straight lines against concentrations of AG

6.3.8 Repeatability, reproducibility and stability of poly Gly/GCE

To study the repeatability of proposed method, oxidation peak current of 5.0×10^{-5} M AG at poly Gly/GCE was measured for five repetitive measurements. It is observed that oxidation peak current of 5.0×10^{-5} M AG was nearly constant with relative standard deviation (RSD) of 2.89%, indicating excellent stability of modified GCE for SWV measurements under optimum experimental conditions. Reproducibility of polymer modified GCE was also evaluated by recording oxidation peak current of AG at five different polymer film modified GCE, prepared by same fabrication procedure with RSD of 1.35%. Moreover, poly Gly/GCE retained 96% of its initial activity even after one week which indicates good stability of developed sensor. All these observations suggest that the developed sensor will provide accurate and consistent results for electrochemical determination of AG.

6.3.9 Interference study

Efficacy of developed sensor for determination of AG was studied using possibly interfering species by SWV. Table 6.3 presents results of interference study for 5.0×10^{-5} M AG in presence of up to 100 fold excess concentration of various interfering species such as citric acid, acetic acid, sodium sulphite, fructose, sodium chloride, EDTA and ascorbic acid under optimal conditions. Except ascorbic acid, all the other compounds did not interfere with the determination of AG (signal change less than ± 5 %). However, ascorbic acid significantly influences analysis of AG at concentration ratio of 1:1.

6.3.10 Application study

To verify analytical utility, poly Gly modified GCE was used for determination of AG in spiked soft drink samples. Before spiking, samples were tested to check presence of AG using SWV. No matrix interferences were found during analysis of samples. Recoveries were ranged from 99.2 to 103.5%, with RSD lower than 5%, signifies accuracy of developed method (Table 6.4). Furthermore, good agreement of obtained results with spectrophotometric method discussed in section 2.5.3.[148] shows consistency of developed sensor for the determination of AG in commercial soft drink samples.

6.4 Conclusion

Present work demonstrates effective use of biopolymer modified GCE for sensitive determination of AG. Proposed method allows determination of AG in the range 1.0×10^{-4} to 9.0×10^{-6} M, with LOD as 3.62×10^{-7} M. Kinetic parameters for oxidation of AG on poly Gly/GCE have also been evaluated. Developed sensor could successfully monitor concentration of

AG in spiked soft drink samples and accuracy of developed method was validated using spectrophotometric method.

Table 6.1: Comparison of different modified electrodes for detection of AG

Modified electrode	Ep (V)	Current (μA)
[a]BTB/GCE	0.948	0.24
[b]EBT/GCE	0.924	6.74
[c]BPB/GCE	0.668	1.07
PolyGly/GCE	0.644	9.82

[a]Poly bromothymol blue modified glassy carbon electrode
[b]Poly eriochrome black T modified glassy carbon electrode
[c]Poly bromophenol blue modified glassy carbon electrode

Table 6.2: Comparison of different methods for determination of AG

Determination Methods	Linear range (M)	LOD (M)	References
[a]Reversephased HPLC	5.54×10^{-5}- 8.67×10^{-9}	2.75×10^{-9}	[289]
HPLC with photodiode array	3.46×10^{-5}- 8.67×10^{-8}	2.25×10^{-8}	[290]
HPLC	3.46×10^{-4} - 8.67×10^{-7}	5.20×10^{-8}	[291]
UV-visible spectrophotometry	0 - 2.60×10^{-5}	-	[292]
Poly Gly/GCE	1.00×10^{-4} - 9.00×10^{-6}	3.62×10^{-7}	Proposed method

[a]HPLC – High Performance Liquid Chromatography

Table 6.3: Effect of possibly interfering species on the signal of 5.0×10^{-5} M AG

Species	Concentration (M)	Signal change (%)
Sodium chloride	5.0×10^{-3}	-2.36
Sodium sulphite	5.0×10^{-3}	3.39
Fructose	5.0×10^{-3}	-2.75
Citric acid	5.0×10^{-3}	3.58
Acetic acid	5.0×10^{-3}	3.83
EDTA	5.0×10^{-3}	1.36
Ascorbic acid	5.0×10^{-5}	18.26

Table 6.4: Determination of AG in soft drink samples

Samples	Added (M)	Spectrophotometric method			Proposed method			
		Found (M)	Recovery (%)[a]	RSD (%)	Added (M)	Found (M)	Recovery (%)[a]	RSD (%)
Coconut oil	9.00×10^{-5} to 2.00×10^{-5}	9.09×10^{-5} to 2.08×10^{-5}	101.1	1.8	9.00×10^{-5} to 2.00×10^{-5}	9.24×10^{-5} to 2.03×10^{-5}	103.5	2.8
Sunflower oil	9.00×10^{-5} to 2.00×10^{-5}	9.05×10^{-5} to 2.15×10^{-5}	102.3	2.1	9.00×10^{-5} to 2.00×10^{-5}	9.07×10^{-5} to 1.96×10^{-5}	99.2	2.4

[a]Average of six replicates

RSD – Relative standard deviation

Chapter 7

COLORIMETRIC SENSOR FOR TETRACYCLINE BASED ON GOLD NANOPARTICLE PROBE

Contents

7.1 Introduction
7.2 Experimental
7.3 Results and discussion
7.4 Conclusions

Present study reports the development of a simple, sensitive and rapid colorimetric method for determination of tetracycline (TET) using gold nanoparticles (AuNPs) as probe. The proposed assay relies upon formation of a stable complex between citrate and TET in presence of Cu^{2+}. Interaction of citrate/Cu^{2+}/TET complex rapidly induce aggregation of gold nanoparticles, resulting in red-to-blue (or purple) color change. Qualitative and quantitative detections of TET were achieved by colorimetric observations and UV-visible spectral measurements, respectively. Developed method showed a linear relation to concentration of TET in the range 9.0×10^{-6} to 9.0×10^{-7} M, in presence of 2.5×10^{-5} M Cu^{2+}. Calculated limit of detection (LOD) and limit of quantification (LOQ) were found to be 9.89×10^{-8} M and 3.29×10^{-7} M respectively. Proposed method was validated using pharmaceutical formulations.

7.1 Introduction

Tetracycline (Fig. 7.1), a polyketide[297] antibiotic with a broad spectrum of activity has been used for prophylaxis and therapy of human and animal diseases. Since it is relatively less expensive and easily available, it has also been used as an additive in animal feeds.[298] Researchers across globe have raised concerns that extensive use of TET can lead to emergence of resistance against human pathogens.[299] Additionally, antibiotics residues from foodstuffs of animal origin can cause allergic reactions in sensitized individuals.[300,301] Furthermore, TET in milk may potentially stain teeth of young children.[302] Thus, development of analytical method for determination of TET is very much vital for ensuring quality of food stuff and to safe guard public health. There have been lots of efforts to develop analytical tools for determination of tetracycline residues in animal products,[303-306] honey[307] and water.[308] Classical techniques that have been used so far includes high performance liquid chromatograohy,[309,310] capillary electrophoresis[311] and chemiluminescence.[312] However, above mentioned methods are often elaborative, expensive and always need authentic samples as reference standards. So development of a simple, cost effective, rapid and sensitive method for determination of TET is warranted.

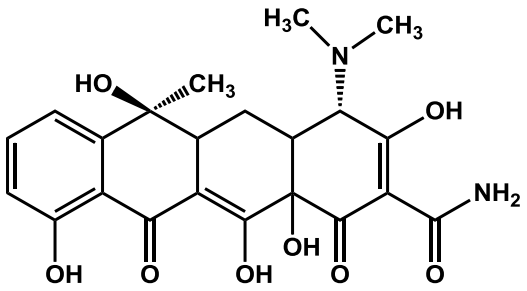

Figure 7.1: Structure of TET

Colorimetric sensing potential of AuNPs has received considerable attention owing to its properties such as on-site detection with high specificity and sensitivity, easy preparation, simple operation, flexibility to modification and ability for detection of analytes with naked eye. The colorimetric sensing property of AuNPs could be attributed to its high visible region extinction coefficient and also to its surface plasmon resonance (SPR), originating from coupling of conduction electrons with incident electromagnetic waves.[313] AuNPs based colorimeric methods have been devised for detection of proteins,[314] metal ions,[315,316] DNA[317] and small molecules.[318] When AuNPs are brought close to one another, absorbance at red region of UV-visible absorption spectra will increase. On observation with naked eye, a color change of solution from red to blue (or purple) is evident as a result of changes in inter-particle distance. This makes AuNPs an ideal marker for binding process.

In the present study, use of AuNPs as a colorimetric probe for rapid and sensitive determination of TET has been investigated. Trace metal ions such as Cu^{2+} can give rise to stable complexes with TET.[319] Moreover, Cu^{2+} can also form coordination complexes with various ligands such as citrate.[320] Considering above facts, a stable complex may be formed between citrate and TET in presence of Cu^{2+}, which can act as a cross linking agent based on their interactions. Moreover, formation of cross-network can be integrated with unique properties of gold nanoparticles for developing a colorimetric assay for TET that can be observed with naked eye. Thus, a simple and rapid colorimetric method for quantitative determination of TET has been developed utilizing unmodified gold nanoparticles as color indicator and Cu^{2+} as cross linker. Further, practical utility of developed method was confirmed by analysis of drug samples.

7.2 Experimental

7.2.1 Preparation of AuNPs

All glasswares used for the synthesis were cleaned with freshly prepared solution of aqua regia, followed by thorough rinsing with Milli-Q water and dried in air. The AuNPs were prepared according to published protocol as follows.[321] The sodium citrate solution (1%, 4.0 mL) was rapidly added to boiled $HAuCl_4$ solution under vigorous stirring. Mixed solution was boiled for 10 minutes, and further stirred for 15 minutes. The resulting solution was cooled to room temperature and filtered, which was stored in the refrigerator (4°C) until further use. Morphology of AuNPs was characterized by high resolution transmission electron microscopy (HRTEM) and dynamic light scattering (DLS) analysis. Stability of as-synthesized AuNPs were confirmed using zeta potential measurements.

7.2.2 Colorimetric determination of TET

Colorimetric analysis was performed at room temperature. Varying concentrations of TET were added into definite volume of AuNPs (1.0 mL) containing 2.5×10^{-5} M Cu^{2+} and resultant solutions were diluted with water to 2.0 mL. Absorption spectra of resultant solutions were studied with UV-visible spectrophotometer in wavelength ranging from 400 to 800 nm.

7.2.3 Analysis of pharmaceutical formulations

For analysis, stock solution was prepared by dissolving an adequate amount of pharmaceutical formulations (Resteclin, Abbott healthcare, India) in methanol, corresponding to a concentration of 1.0×10^{-4} M. Working

solutions were prepared by serial dilution of the stock solution. The solutions were subjected to spectrophotometric measurements.

7.3 Results and discussion

7.3.1 Characterisation of AuNPs

The as-synthesized citrate capped AuNPs were characterised by various techniques such as UV-visible absorption spectroscopy, TEM, DLS and zeta potential analysis. The absorption spectrum of AuNPs is depicted in Fig. 7.2. A sharp peak was centered at 520 nm, which corresponds to surface plasmon resonance (SPR) band of AuNPs. SPR band of AuNPs was resulting from coherent oscillation of free conducting electrons produced due to polarized electrons generated by incident light.[322,323] TEM images of AuNPs, reveals that as-synthesized AuNPs are nearly spherical in shape with an average diameter of 15 nm (Fig. 7.3a). The selected area electron diffraction (SAED) pattern of AuNPs is showed in Fig. 7.3b and the discrete dots seen in the pattern indicates crystalline character of AuNPs.[324] From DLS measurements (Fig. 7.4), hydrodynamic diameter of aqueous suspension of AuNPs was found to be 28.0 nm, which is slightly more than the mean dried state diameter of AuNPs obtained from TEM analysis. To further confirm the stability of AuNPs, zeta potential measurement was also performed (Fig. 7.5). A large negative value of zeta potential (-62.0 mV) indicates the excellent stability of aqueous suspension of AuNPs. The high negative value of zeta potential could be due to the presence of carboxyl groups on citrate capping agent.

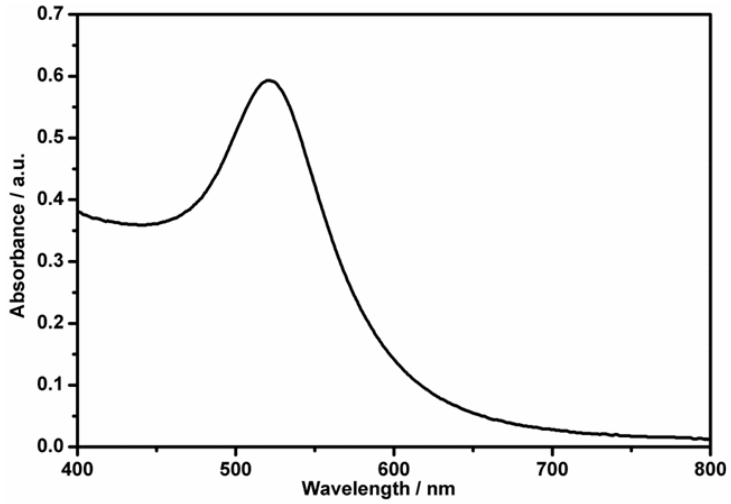

Figure 7.2: Absorption spectrum of AuNPs

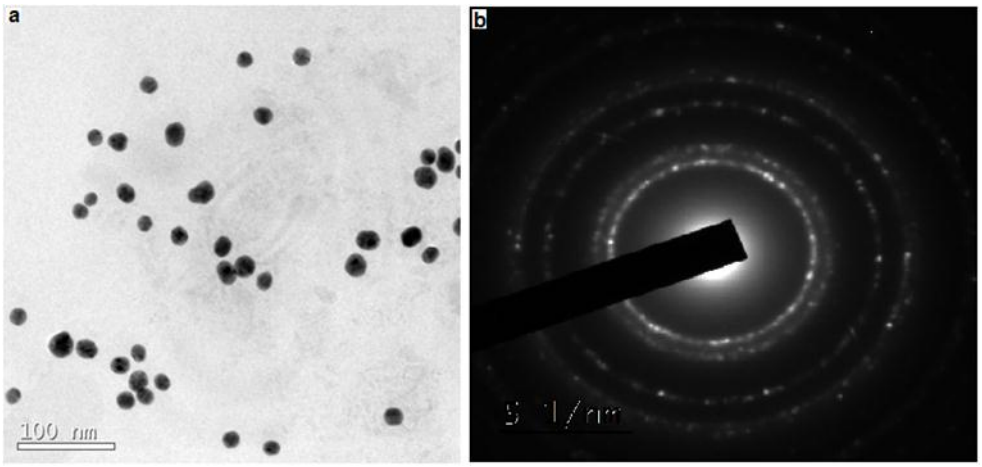

Figure 7.3: (a) TEM images of AuNPs (b) Selected area electron diffraction (SAED) pattern of AuNPs

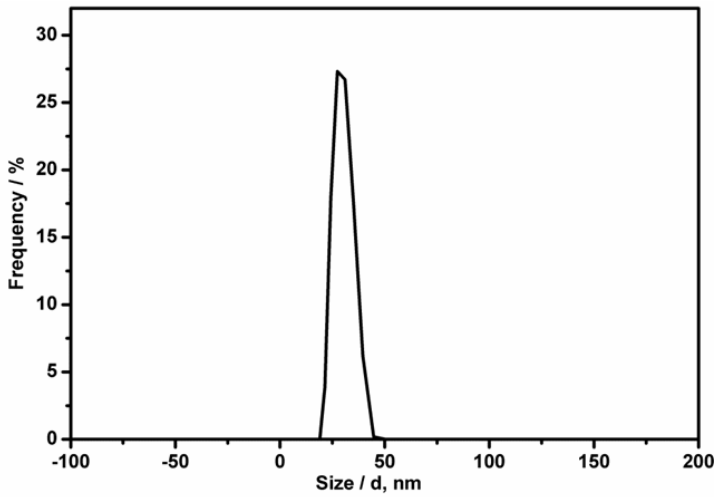

Figure 7.4: DLS spectrum of aqueous suspension of AuNPs

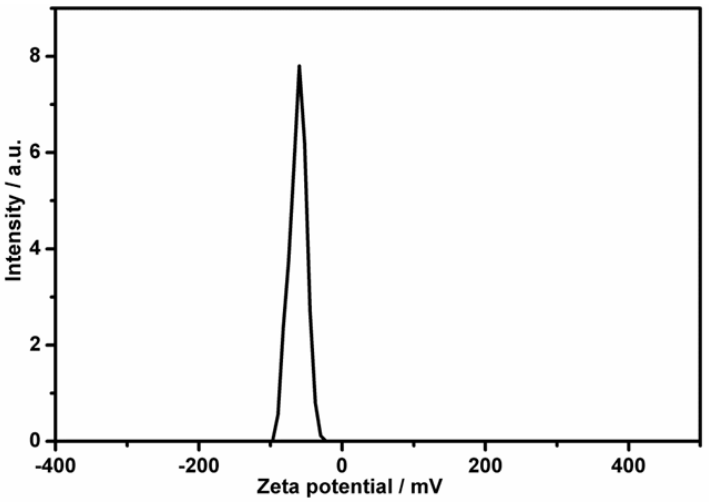

Figure 7.5: Zeta potential of AuNPs

7.3.2 Colorimetric assay of TET

It is noteworthy that aggregation of AuNPs in presence of TET is a sluggish process, which takes several hours for effective aggregation. Interestingly, it is also found that co-presence of Cu^{+2} as a crosslinking

agent stimulates the rapid aggregation of AuNPs (*ie*, in less than one minute). Absorption spectra of AuNPs recorded in the absence and presence of 1.0×10^{-4} M TET and 2.5×10^{-5} M Cu^{2+} is shown in Fig. 7.6. It can clearly been seen that addition of TET in presence of Cu^{2+} diminish the intensity of surface plasmon peak of AuNPs from its initial value at 520 nm and form a new absorption band at 630 nm. Subsequently, color of AuNPs has changed from red to blue when TET was added in presence of Cu^{2+} and is shown in the inset of Fig. 7.6. When 2.5×10^{-5} M Cu^{2+} ions were individually added to AuNPs, spectra remained unchanged. Utilizing this property, a probe was designed for colorimetric sensing of TET.

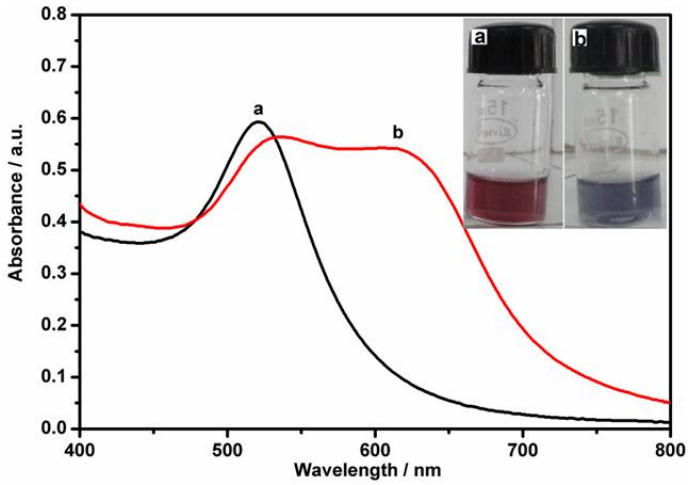

Figure 7.6: Absorption spectra of AuNPs solutions containing 2.5×10^{-5} M Cu^{2+} (a) in the absence and (b) presence of 1.0×10^{-4} M TET. Inset image shows corresponding colorimetric response

7.3.3 Influence of reaction media

Reaction media in which as-synthesized AuNPs showed maximum stability and intensity were studied. Among different media (water, acetate

buffer, citrate buffer and phosphate buffer), better results were obtained for water. Thus, water was selected as the suitable reaction medium for further studies.

7.3.4 Effect of various metal ions as cross-linking agents

It was found that TET could not rapidly stimulate aggregation of AuNPs in the absence of Cu^{2+}. Hence, rapid aggregation of AuNPs requires a cross linking reagent such as Cu^{2+}. In order to test specificity of Cu^{2+} as a cross-linker for detection of 1.0×10^{-4} M TET, impact of certain competing metal ions including Ba^{2+}, Co^{2+}, Ca^{2+}, Pb^{2+}, Mg^{2+} and Mn^{2+} were studied under the same conditions and concentration as that of Cu^{2+}. From the results, it was found that absorption ratio (A_{630}/A_{520}) was higher for same concentration of TET when Cu^{2+} was used as a cross-linker (Fig. 7.7). Hence, Cu^{2+} was selected as the cross-linking agent for further studies.

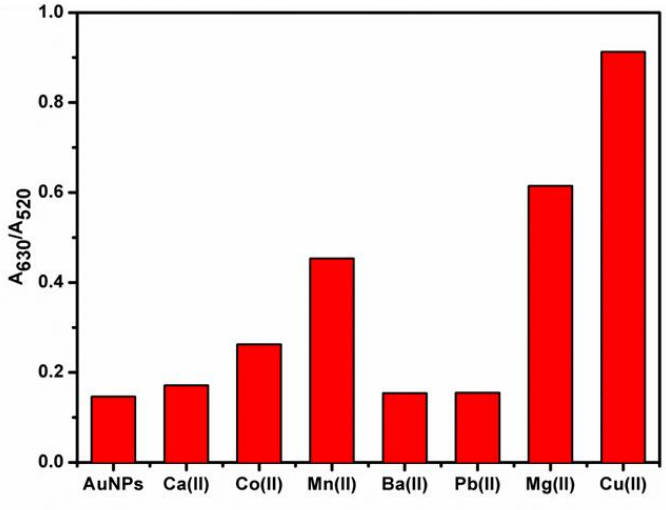

Figure 7.7: Effect of addition of various metal ions (Ca^{2+}, Co^{2+}, Mn^{2+}, Ba^{2+}, Pb^{2+}, Mg^{2+} and Cu^{2+}) on the absorption ratio of (A_{630}/A_{520}) AuNPs solution in presence of 1×10^{-4} M TET

7.3.5 Effect of concentration of Cu^{2+} on the absorbance of AuNPs

Aggregation of AuNPs is also sensitive to concentration of Cu^{2+}. From Fig. 7.8, it is clear that increase in concentration of Cu^{2+} from 5.0×10^{-6} to 2.5×10^{-5} M, did not cause any considerable change in absorbance of AuNPs at 520 nm. However, further increase in concentration of Cu^{2+} leads to a decrease in absorbance of AuNPs leading to aggregation. Based on above observations, it can be concluded that concentration of Cu^{2+} above 2.5×10^{-5} M is unsuitable for determination of TET because Cu^{2+} which does not form complexes could induce aggregation of AuNPs, so a concentration of 2.5×10^{-5} M Cu^{2+} was employed for further studies.

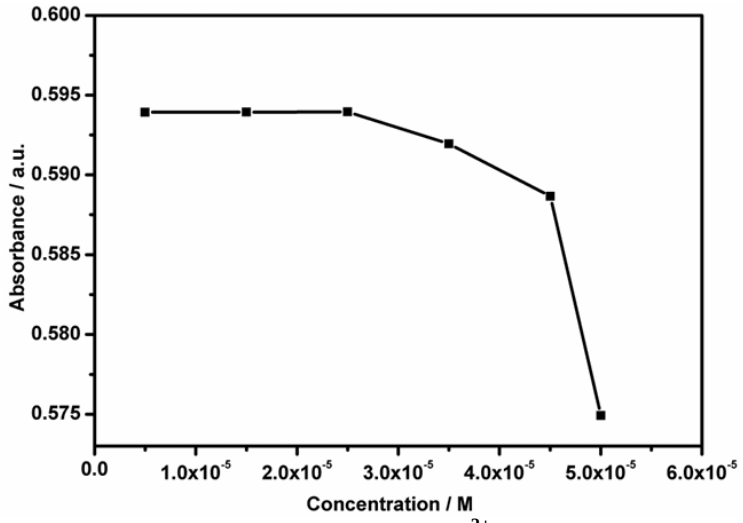

Figure 7.8: Effect of concentration of Cu^{2+} on absorption intensity of AuNPs

7.3.6 Influence of time on the absorption ratio of AuNPs

Effect of time on absorption ratio (A_{630}/A_{520}) of AuNPs, along with 2.5×10^{-5} M Cu^{2+} was examined in the absence and presence of varying

concentrations of TET. From Fig 7.9, it is evident that the absorption ratio of AuNPs remains unchanged for 20 minutes. Furthermore, TET stimulated aggregation of AuNPs in the presence of Cu^{2+} is very fast (binding time < 1 min) and absorption ratio become stable within one minute after addition of TET and remained stable for 20 minutes. From the above observations, it can be inferred that developed sensor showed a quick response for the determination of TET.

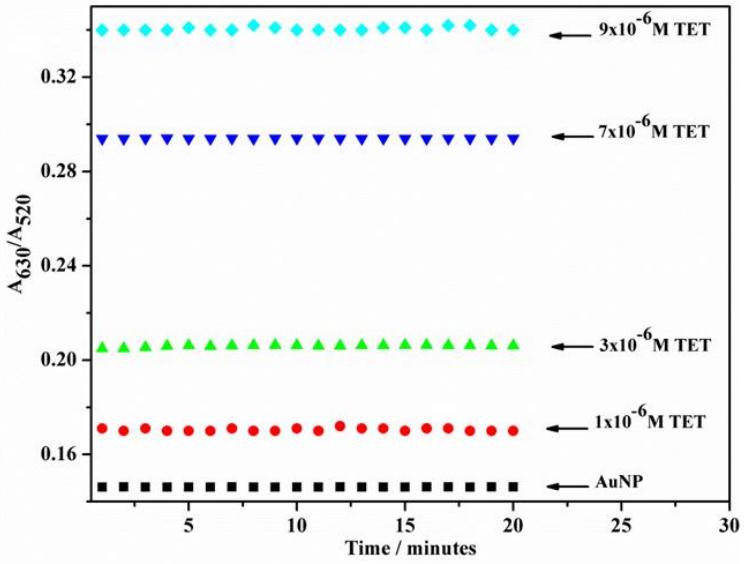

Figure 7.9: Absorption ratio (A_{630}/A_{520}) profiles of AuNPs solutions containing 2.5×10^{-5} M Cu^{2+} in the absence and presence of different concentrations of TET

7.3.7 Colorimetric determination of TET

To evaluate the sensitivity of developed system, UV-visible spectra of AuNPs at different concentrations of TET were recorded under optimized conditions. As seen in Fig. 7.10a, in presence of 2.5×10^{-5} M Cu^{2+}, absorbance of AuNPs at 520 nm gradually decreases whereas absorbance at

630 nm gradually increases when concentration of TET was increased. Thus, ratio of aggregated and dispersed AuNPs was reflected by the absorption ratio at 630 and 520 nm (A_{630}/A_{520}). The absorption ratio (A_{630}/A_{520}) exhibited a linear correlation to TET concentration in presence of 2.5 × 10^{-5} M Cu^{2+} in the range 9.0 × 10^{-6} M to 9 × 10^{-7} M (R^2 = 0.993) (Fig. 7.10b). For determination of 9.0 × 10^{-7} M TET, the relative standard deviation was found to be 0.45%, which imply that interaction between AuNPs and TET is highly reproducible. Using the equations, $\frac{3S}{m}$ and $\frac{10\,S}{m}$ (where m is slope of the calibration curve and S is standard deviation), LOD and LOQ were estimated as 9.89 × 10^{-8} M and 3.29 × 10^{-7} M respectively. In addition, TET induced aggregation of AuNPs in the presence of Cu^{2+} would result in color change from red to blue. As shown in Fig. 7.11, presence of TET up to 1.0 × 10^{-5} M can be viewed without the aid of any advanced instrument.

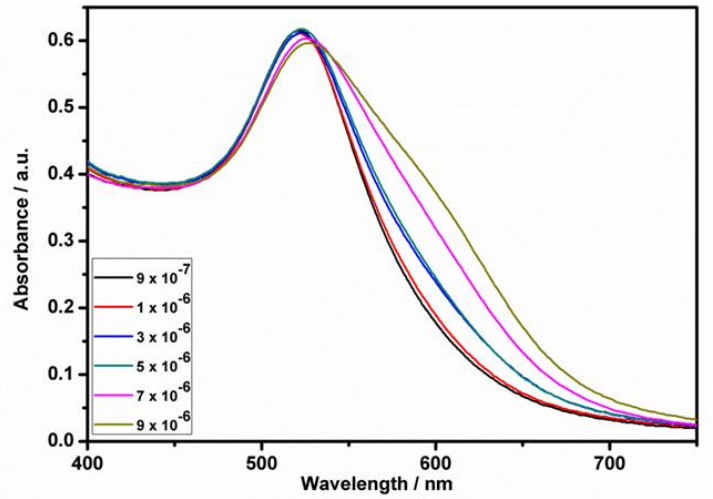

Figure 7.10a: Absorption spectra of AuNPs in the presence of 2.5 × 10^{-5} M Cu^{2+} and different concentration of TET in the range of 9.0 × 10^{-6} – 9.0 × 10^{-7} M

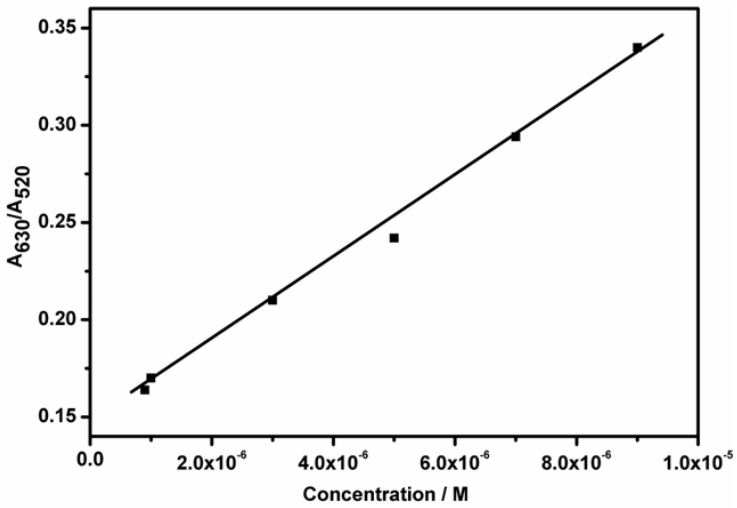

Figure 7.10b: Plot of absorption ratio ($A_{630/520}$) *vs* concentration of TET in the range of 9.0×10^{-6} – 9.0×10^{-7} M in presence of 2.5×10^{-5} M Cu^{2+}

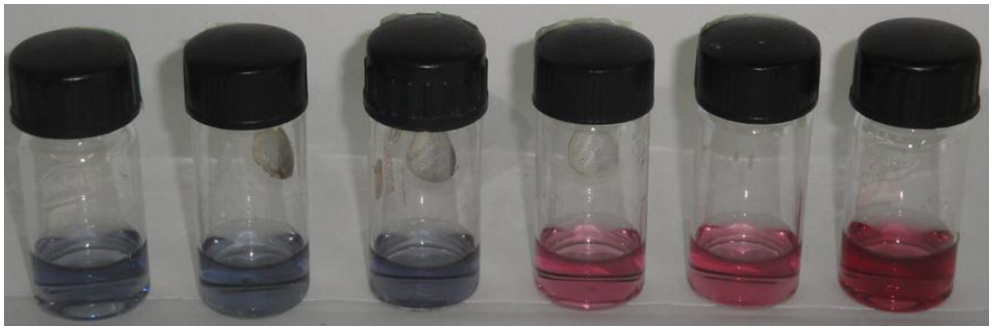

Figure 7.11: Photographs of a solution of (1) AuNPs + 1×10^{-4} M TET, (2) AuNPs + 5×10^{-5} M TET, (3) AuNPs + 1×10^{-5} M TET, (4) AuNPs + 5×10^{-6} M TET, (5) AuNPs + 1×10^{-6} M TET and (6) AuNPs in the presence of 2.5×10^{-5} M Cu^{2+} (from left to right)

Performance of the developed sensor for determination of TET was compared with other methods (Table 7.1). From the table, it is evident that the proposed sensor gives lowest detection limit for TET, which points to the superior performance of developed method for practical applications.

7.3.8 Mechanism of colorimetric assay

Synthesis of AuNPs was achieved by citrate reduction of gold salt to yield nanoparticles. An intense surface plasmon band formed by nanoparticles form the basis of citrate reduction method. AuNPs in aqueous solution are stabilized against aggregation due to citrate ion's (negative capping agent) electrostatic repulsion against van der Waals attraction between AuNPs. Red shift of absorption band from 520 to 630 nm was observed upon addition of TET ions in presence of Cu^{2+}, concomitant with a change in color of solution from red to purple. Since surface plasmon band of AuNPs is dependent to their inter-particle spacing, band at 520 nm becomes weaker with decrease in inter-particle distance. Second absorption band formed at longer wavelength can be ascribed to electric dipole-dipole interaction and to coupling between the plasmons of neighboring particles in the formed aggregates.[329,330] TET induced aggregation of AuNPs in presence of Cu^{2+} was further confirmed by TEM images. As shown in Fig. 7.12, AuNPs were mono-dispersed in the absence of TET; while in the presence of TET and Cu^{2+}, AuNPs aggregated together. This observation was consistent with red-shift of UV-visible absorption spectra and color change of AuNPs (from red to purple) in presence of TET and Cu^{2+} (Fig. 7.6). Also, as shown in Fig. 7.13, hydro dynamic diameter of AuNPs (28.0 nm) has increased when 1.0×10^{-4} M TET was added in the presence of 2.5×10^{-5} M Cu^{2+} (152.7 nm). From Fig. 7.14, it is obvious that addition of 2.5×10^{-5} M Cu^{2+} alone could not induce the aggregation of AuNPs because surface plasmon band of AuNPs at 520 nm did not show any change in absorbance upon addition of Cu^{2+}.

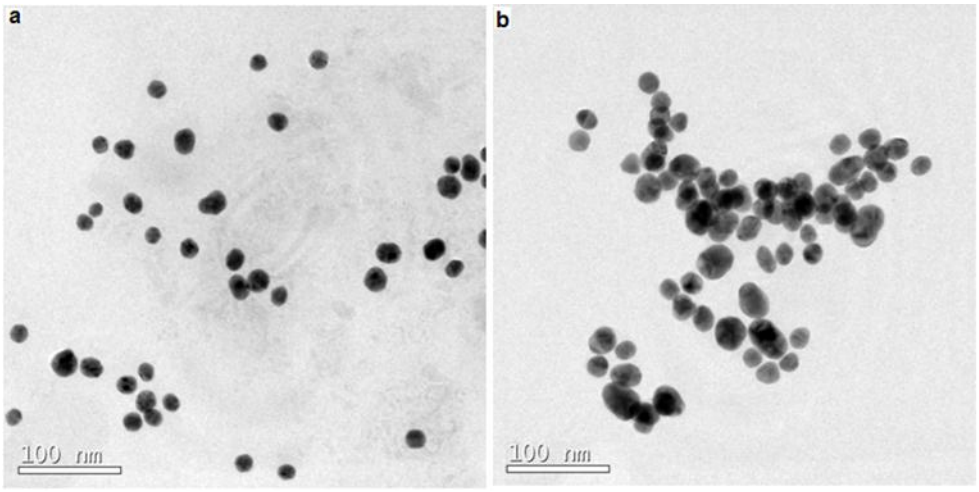

Figure 7.12: TEM images of AuNPs (a) in the absence and (b) presence of 1×10^{-4} M TET and 2.5×10^{-5} M Cu^{2+}

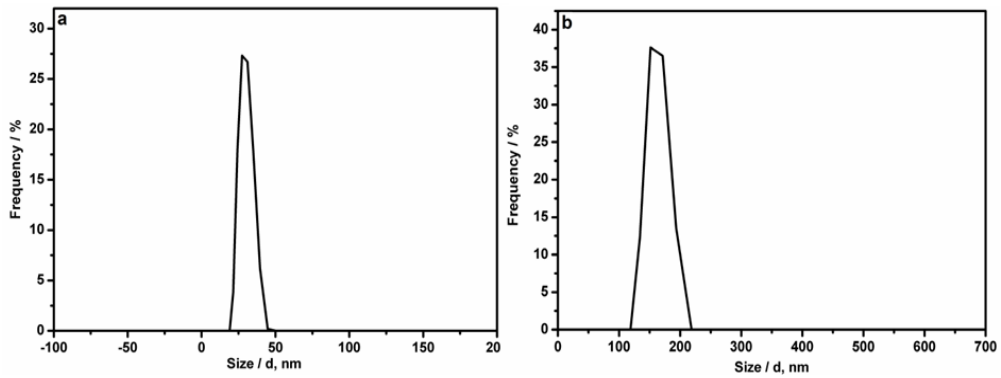

Figure 7.13: DLS spectra of AuNPs (a) in the absence and (b) presence of 1.0×10^{-4} M TET and 2.5×10^{-5} M Cu^{2+}

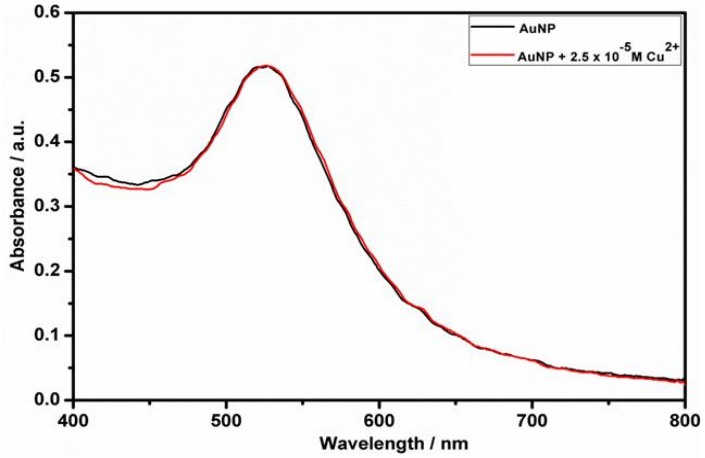

Figure 7.14: Absorption spectra of AuNPs in the absence and presence of 2.5 × 10^{-5} M Cu^{2+}

TET can bind Cu^{2+} by coordination with oxygen of hydroxyl and amide groups at ring A. It can also bind with oxygen of the hydroxyl group at ring B and oxygen of the carbonyl group at ring C.[331,332] Similarly, citrate ion can also bind Cu^{2+} by coordination with oxygen atoms of carboxyl groups.[333] Considering above facts, it is assumed that Cu^{2+} can act as a cross-linking agent for citrate capped AuNPs and TET. Furthermore, above assumption was confirmed by zeta potential analysis. Zeta potential of AuNPs was measured in the presence and absence of 1.0 × 10^{-4} M TET and was found to be -25 mV and -62 mV respectively (Fig. 7.15). Decrease in zeta potential value of AuNPs upon addition of TET suggests that the stability of AuNPs has decreased by the addition of TET in presence of Cu^{2+}. This may be due to the fact that cross-linking of citrate capped AuNPs and TET through Cu^{2+} ions decrease the surface charge of AuNPs leading to aggregation of AuNPs causing a rapid, red-to-blue (or purple) color change. Based on all these observations, plausible mechanism for the colorimetric determination of TET is depicted in Scheme 7.1.

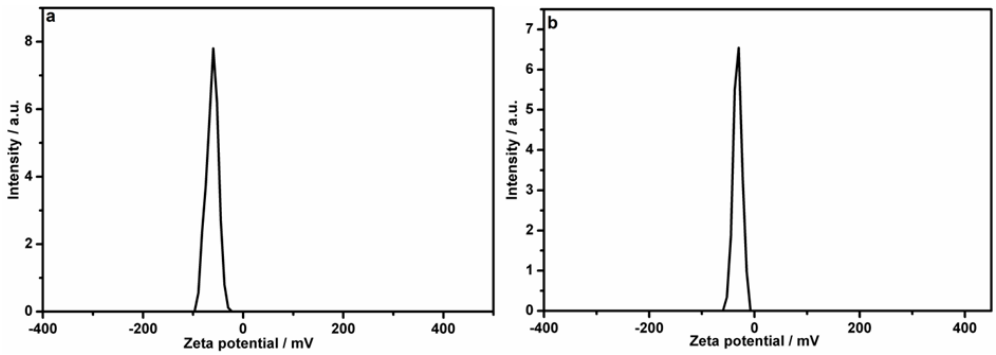

Figure 7.15: Zeta potential of AuNPs (a) in the absence and (b) presence of 1 × 10^{-4} M TET and 2.5 × 10^{-5} M Cu^{2+}

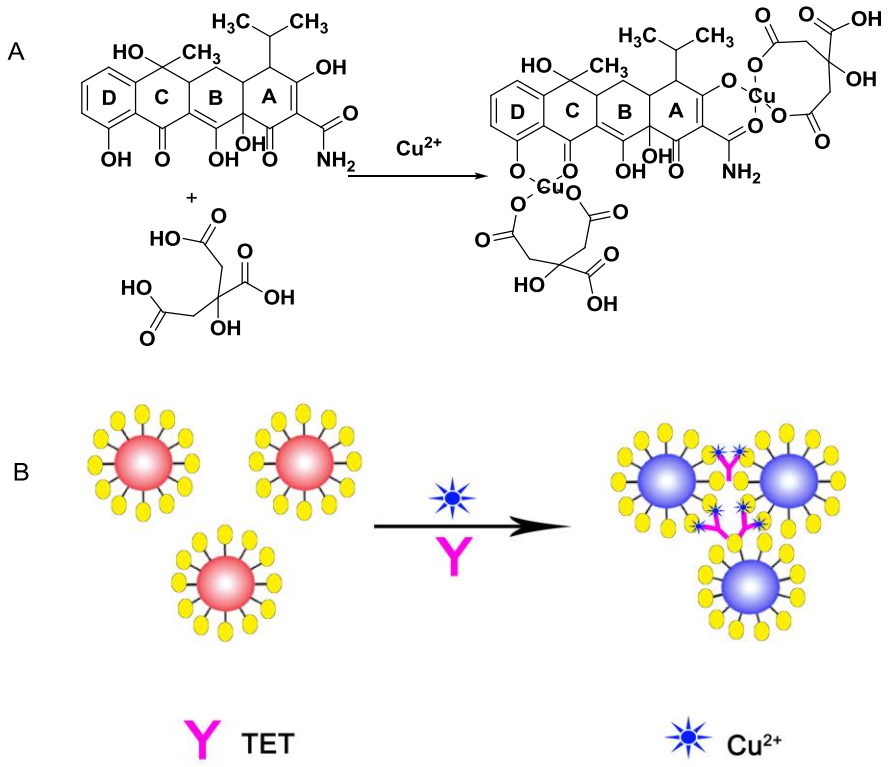

Scheme 7.1: (A) Cu^{2+} induced cross-linking recognition between citrate and TET. (B) Schematic representation of colorimetric detection of TET using citrate modified gold nanoparticles (AuNPs) cross-linked by Cu^{2+}

7.3.9 Selectivity

Selectivity of proposed method was evaluated by testing response of assay towards different drugs such as penicillins [ampicillin (AMP), amoxicillin (AMX)], ceftriaxone sodium (CFS), cefalexin (CFL), metronidazole (MTZ), tinidazole (TNZ) and sulfamethoxazole (SMZ). Under the same experimental conditions, only 1.0×10^{-4} M TET induces aggregation of AuNPs compared to other drugs under study (Fig. 7.16).

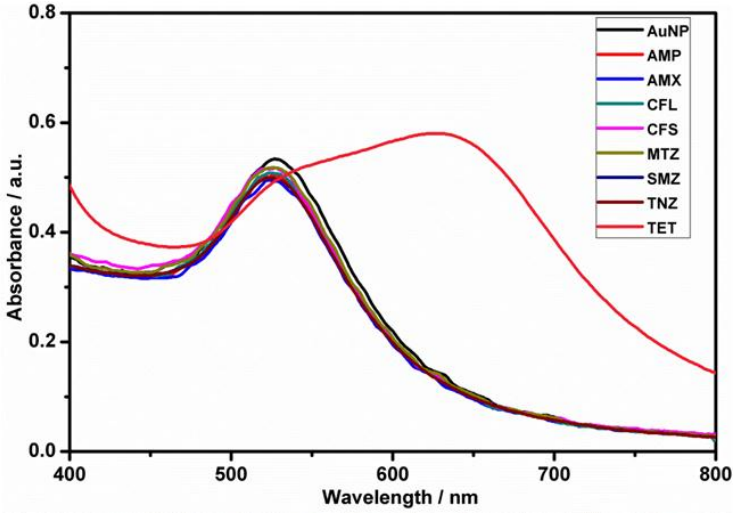

Figure 7.16: Selectivity of developed sensor

Furthermore, colorimetric response of AuNPs towards TET (5.0×10^{-6} M) in presence of aforementioned drugs at various concentrations (1:1, 1:10, 1:100) were examined. As shown in Fig. 7.17, presence of even 100 fold excess of above drugs does not cause any significant change in the absorption ratio of AuNPs (signal change below ± 5%). Hence, TET can be detected at trace levels even in the presence of these drugs.

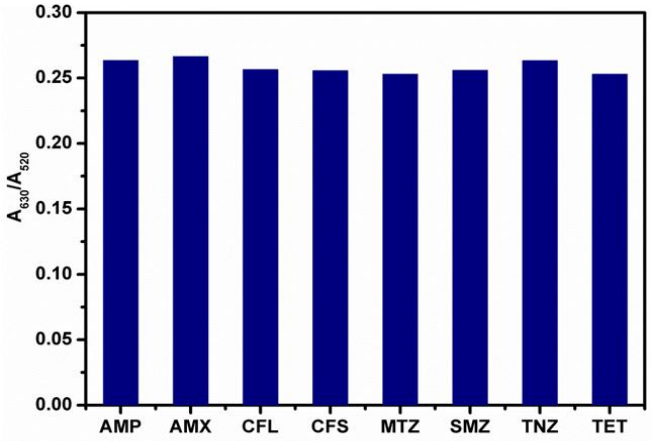

Figure 7.17: Effect of various drugs on absorption ratio of AuNPs for the determination of 5.0 × 10^{-6} M TET

7.3.10 Application study

Developed method was used for the determination of TET content of a pharmaceutical preparation (Resteclin, Abbott healthcare, India) and results are shown in Table 7.2. The obtained results are in good agreement with the TET content, labeled on the drug.

7.4 Conclusions

Present work describes a simple colorimetric assay for determination of TET using AuNPs. Proposed assay is based on the distance dependent optical properties of AuNPs and TET triggered self-assembly of AuNPs in presence of Cu^{2+}. Aggregation of AuNPs induces a color change from red-to-blue (or purple). Developed method showed a linear correlation between absorbance and concentration of TET in the range 9.0 × 10^{-6} to 9.0 × 10^{-7} M, in presence of 2.5 × 10^{-5} M Cu^{2+}. Calculated LOD and LOQ for TET were found to be 9.89 × 10^{-8} M and 3.29 × 10^{-7} M respectively. The developed method was used for determination of TET in pharmaceutical formulations.

Table 7.1: Comparison of different methods for determination of TET

Determination Methods	Linear range (M)	LOD (M)	References
Spectrophotometry	3.61×10^{-4}- 1.03×10^{-5}	1.69×10^{-6}	[325]
[a]AAS method	6.75×10^{-5}- 1.13×10^{-5}	2.24×10^{-7}	[326]
[b]HPLC-ED	1.00×10^{-4} - 2.50×10^{-6}	1.20×10^{-7}	[327]
[c]HPLC-PAD	2.25×10^{-4} - 2.24×10^{-7}	1.13×10^{-7}	[328]
AuNPs based colorimetry	9.00×10^{-6} - 9.00×10^{-7}	9.89×10^{-8}	Proposed method

[a] AAS - atomic absorption spectroscopic method
[b]HPLC-ED - High performance liquid chromatography with electrochemical detection
[c]HPLC-PAD - High performance liquid chromatography with pulsed amperometric detection

Table 7.2: Determination of TET in pharmaceutical formulation

Sample	Declared Amount (mg/tablet)	Found (mg/tablet)	RSD* (%)
Resteclin (Abbott healthcare, India)	500	501	1.9

RSD: Relative standard deviation
*average of four replicates

Chapter **8**

CARBON DOTS BASED FLUORESCENCE SENSOR FOR SUNSET YELLOW

Contents

8.1 Introduction
8.2 Experimental
8.3 Results and discussion
8.4 Fluorescence quenching of CDs by SY
8.5 Mechanism of fluorescence quenching
8.6 Selectivity
8.7 Application in real samples
8.8 Conclusion

A green, one step and low cost method to synthesize ethylenediamine (EDA) passivated carbon-dots (CDs) using hibiscus leaves as sole carbon source, via microwave irradiation process is reported here. The prepared CDs were found to be spherical in shape and blue emitting with a quantum yield (QY) of 38.7%. The CDs showed excellent water solubility and stability. Eventually, optical sensing aspects of CDs have been evaluated on food colorant, sunset yellow (SY). Since the fluorescence intensity of CDs was effectively quenched by SY via inner filter effect (IFE), CDs can act as a suitable sensing platform for determination of SY within the concentration range of 1.0×10^{-5} *to* 2.0×10^{-6} *M. Limit of detection and limit of quantification were estimated to be* 7.8×10^{-8} *M and* 2.6×10^{-7} *M, respectively. Practicality of developed sensor has been validated by determining the concentration of SY in soft drink samples.*

8.1 Introduction

Food colorants are widely used to improve the appearance and consumer acceptance of a variety of food products. Presently, synthetic dyes have replaced the natural ones owing to their properties such as easy and uniform coloring, stability to light, oxygen or pH, low microbial contamination and low cost.[334,264] SY (E 110, Fig. 8.1), one of the commonly used synthetic water soluble food colorant, is added to many foodstuffs such as cheese, candies and soft drinks.[335] It was recognized as food colorant by Joint FAO/WHO Expert Committee on Food Additives (JECFA) in 1982 and EU Scientific Committee for Food (SCF) in 1984.[336] The permissible level of SY in soft drinks was set by EU and China as 20 µg/ml[337] and 0.1 g/kg respectively.[338] However, excess intake of SY can cause serious health problems to consumers including allergies and asthmatic reaction, eczema, anxiety migraines, immune suppression and even cancer.[339,340] Hence, the presence and level of SY must be strictly controlled in all foodstuffs.

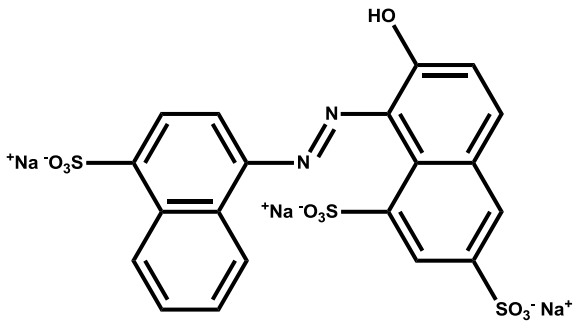

Figure 8.1: Structure of sunset yellow

Different methods such as high performance liquid chromatography-mass spectrometry (HPLC-MS),[341] fluorescence spectrometry,[342] capillary electrophoresis,[343] chromatography[344] and electrochemical methods[345] have

been reported for determination of SY. However, the above methods have many disadvantages such as expensiveness, complicated and long procedures and are unsuitable for field use.

For the past few years, fluorescent CDs, utilized as nascent 'nanolight', have garnered much interest due to their favourable attributes compared to traditional heavy metal based semiconductor quantum dots (QDs) and organic fluorophores. In spite of many advantages, vulnerability to photobleaching limits the use of organic fluorophores to large scale practical applications.[109] Although traditional QDs possess increased photostability and tunable fluorescence properties, their synthetic routes and storage are cumbersome. Compared with traditional QDs, CDs have advantages such as lower toxicity, easy functionalization, better biocompatibility and simple synthesis.[120] In addition, CDs possess unique optical properties arising from quantum confinement and edge effects and have excellent water solubility. All these properties make CDs as a cost effective and valuable candidate to be explored in a variety of fields including sensing,[346] bio-imaging,[347] clinical analysis[348] and catalysis.[349]

Much progress has been achieved in the synthesis of CDs including arc discharge,[113] electrochemical oxidation,[350] laser ablation[127] and hydrothermal method.[351] Most of the above mentioned methods always involve drawbacks such as low quantum yield, expensive precursor or intricate processes. However, a one pot, microwave irradiation provides a simple and efficient way of synthesizing highly fluorescent CDs within few minutes.[352]

Recently, significant efforts have been taken to develop green methodologies for preparing CDs using natural carbon precursors which are

easily available and harmless to environment.[346,353] However, most of these CDs have a relatively low QY of usually less than 10%, which limits their large-scale practical applications. A popular approach to enhance the fluorescence intensity of CDs is by surface passivation using small organic compounds such as EDA or other homologues.[354]

Herein, a novel and green method for synthesis of CDs by microwave irradiation of leaves of hibiscus plant (*Hibiscus rosasinensis*) have been discussed. Leaves of hibiscus plant were selected as carbon source and EDA as passivating agent. Formation of CDs involves dehydration and carbonization of Hibiscus leaves extract followed by surface passivation with EDA during microwave irradiation process. Structural and optical properties of the as-prepared CDs were studied by high resolution transmission electron microscopy (HRTEM), UV-visible and fluorescence spectroscopy. Surface characterization was done by X-ray photoelectron spectroscopy (XPS) as well as by Fourier transform infrared spectroscopy (FTIR). Prepared CDs can be used as an effective fluorescent probe for 'signal off' sensing of SY. Practical application was validated by measuring the concentration of SY in soft drink samples. To the best of our knowledge, it is the first fluorescence sensor for the determination of SY based on IFE.

8.2 Experimental

8.2.1 Synthesis of EDA passivated CDs

Microwave assisted method was used for the preparation of EDA passivated CDs using hibiscus leaves as the sole carbon source. Here, EDA was chosen as passivating agent since it improves the fluorescence intensity

of CDs.[355] The CDs were generated by microwave irradiation process (Scheme 8.1) as follows. Six grams of hibiscus leaves were added into 20 mL of deionized water, mixed and grinded using a domestic mixer grinder. The obtained hibiscus juice was filtered and 1 mL of the resultant solution was further diluted with 1 mL of deionized water. The above solution was mixed with 2.5 mL EDA at room temperature and the resultant solution was irradiated in a domestic microwave oven at 800 W for 4 minutes. The product was collected and 0.12 g of above product was dissolved in 20 mL deionized water, filtered and then centrifuged at 4000 rpm for 10 minutes. Supernatant solution containing CDs was subjected to purification by dialysis. The obtained solution of CDs was diluted to adjust the absorbance below 1 a. u.

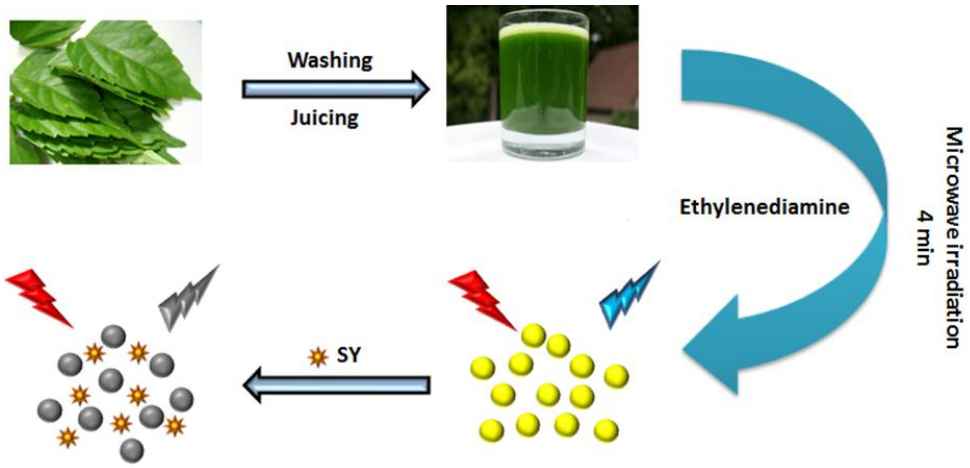

Scheme 8.1: Schematic illustration depicting one pot synthesis of CDs from hibiscus leaves

8.2.2 Analytical procedure

The CDs were excited using 400 nm laser and fluorescence spectra were recorded at $\lambda_{ex}/\lambda_{em}$ = 400/490 nm. Different concentrations of SY were added into definite volumes of CDs solution (0.5 mL of probe solution) and fluorescence intensity was measured in each case. The fluorescence intensity of CDs in the absence and presence of SY is designated as I_0 and I respectively.

8.2.3 Analysis of real samples

Soft drink samples were used directly (50 µL) without any extraction procedure. Standard addition method was used for the estimation of SY and the results were compared with those obtained from spectrophotometric analysis discussed in section 2.5.3[148]

8.3 Results and discussion

8.3.1 Optimization of synthetic condition of CDs

Effect of microwave irradiation time and amount of passivating agent on the fluorescence intensity of CDs were investigated and is discussed in the following sections.

8.3.1.1 Influence of microwave irradiation time on formation of CDs

The effect of microwave irradiation time on the photoluminescence properties of CDs is shown in Fig. 8.2. When the microwave irradiation time increased from 0 to 4 minutes, intensity and stability of CDs has also increased remarkably. However, further increase in irradiation time from 4 to 5 minutes did not enhance the stability and fluorescence intensity. Thus,

microwave irradiation time of four minutes was selected for the synthesis of CDs.

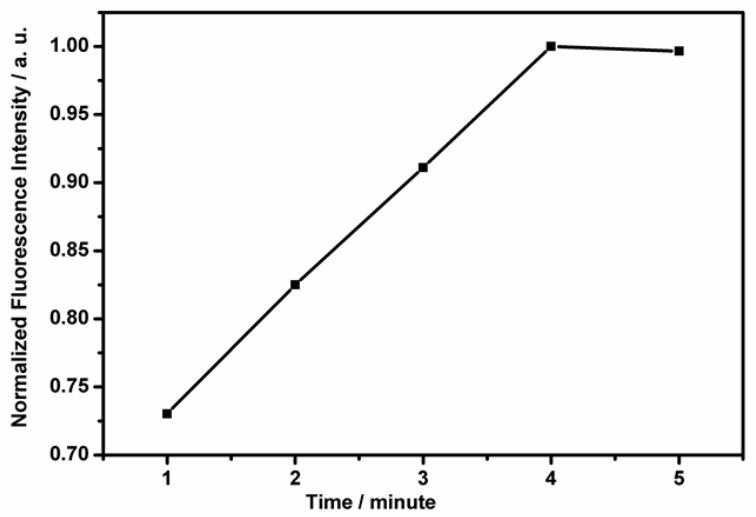

Figure 8.2: Effect of microwave irradiation time on the fluorescence intensity of CDs

8.3.1.2 Influence of amount of passivating agent on CDs

Effect of amount of EDA on fluorescence intensity and stability of CDs is illustrated in Fig. 8.3. When the volume of EDA increased gradually from 0.5 to 2.0 mL, photoluminescence properties of CDs has also been increased. Conversely, further increase in EDA did not alter the photoluminescence properties of CDs. These results support the notion that optimum amount of EDA required for formation of CDs is 2.0 mL.

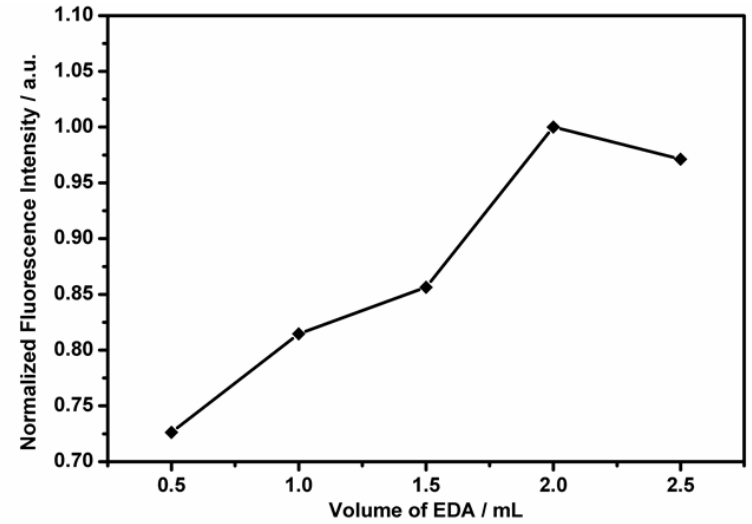

Figure 8.3: Effect of volume of EDA on the fluorescence intensity of CDs

8.3.2 Characterization of CDs

Optical properties of as-synthesized CDs were explored by absorption and emission spectral studies. As shown in Fig. 8.4a, UV-visible absorption spectrum showed two peaks at 280 and 338 nm, corresponding to n-π^* transition of C=O bonds and π- π^*transition of C=C bonds.[356,357] An intense emission peak at 490 nm was observed in the photoluminescence spectrum when CDs were excited at 400 nm (Fig. 8.4b). The CDs exhibited good solubility in water. The dispersed CDs were transparent and pale yellow in color under day light (Fig. 8.5a), while under UV light it emit bright blue photoluminescence (Fig. 8.5b), strong enough to observe with naked eye. As a result of surface passivation,[358] fluorescence intensity of EDA passivated CDs has remarkably increased compared to bare CDs (Fig. 8.6).

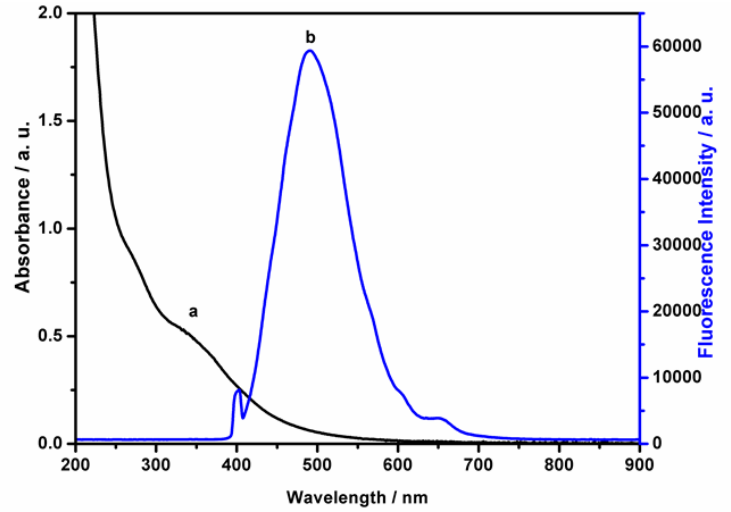

Figure 8.4: (a) Absorption and (b) emission spectrum of synthesized CDs

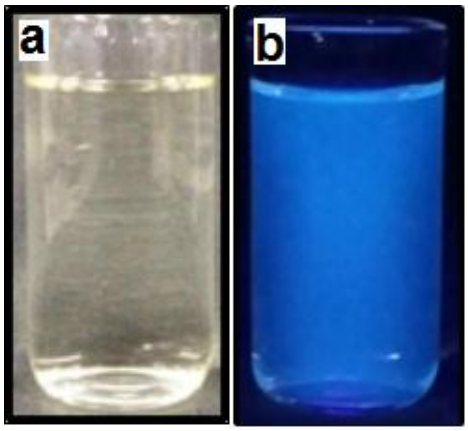

Figure 8.5: Solution of CDs under (a) visible and (b) UV light

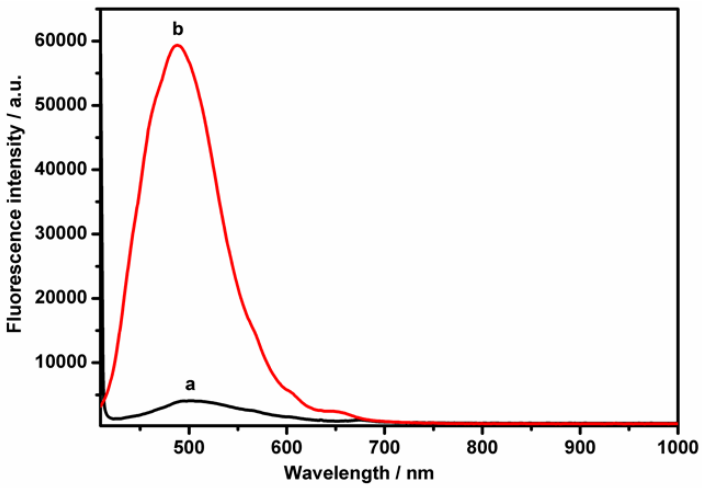

Figure 8.6: Fluorescence spectra of (a) bare CDs (b) EDA passivated CDs

Particle size and morphology of synthesized CDs were assessed by TEM analysis (Fig. 8.7). TEM images showed that the CDs were uniform in size and had nearly spherical morphology with an average diameter of about 9 nm. Furthermore, close observation of as-synthesized CDs by HRTEM analysis further suggests that the CDs have graphitic crystalline structure with lattice parameter of 0.32 nm (Inset of Fig. 8.7) which could be attributed to (002) planes of graphitic carbon[359,360]. Average hydrodynamic volume of aqueous suspension of CDs obtained from DLS analysis was found to be 21.49 nm (Fig. 8.8), which in turn is comparable with the mean dried state diameter obtained from TEM results.

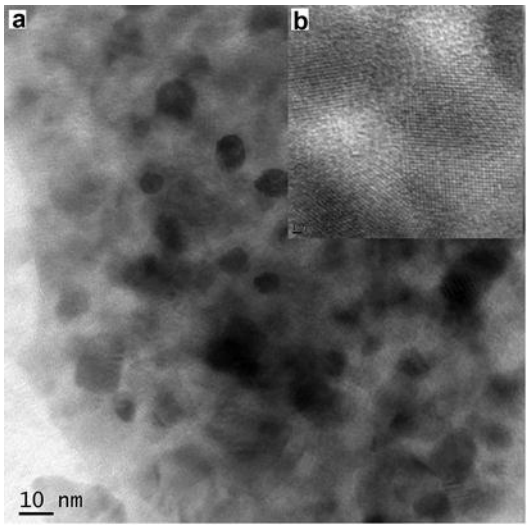

Figure 8.7: TEM image of synthesized CDs. Inset: Lattice spacing of one particle

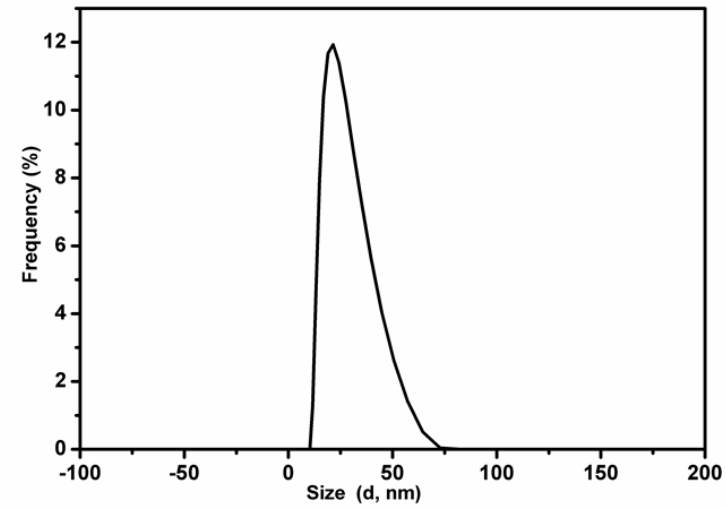

Figure 8.8: DLS spectrum of aqueous suspension of CDs

XPS and FTIR analysis were carried out to obtain clear information about surface states and surface functional groups of as-synthesized CDs. As shown in Fig. 8.9a, the XPS survey spectrum displayed a predominant graphitic C_{1s} peak at 284.6 eV, O_{1s} peak at 530.7 eV and an obvious N_{1s} peak at 399.7 eV. Deconvolution of high resolution XPS spectrum of C_{1s} peak gave four components at 284.6 eV, 285.9 eV, 286.6 eV and 287.5 eV which can be assigned to C-C/C=C, C-N, C-O (alkoxy) and C=O bonds respectively (Fig. 8.9b).[361] The O_{1s} spectrum in Fig. 8.9c is fitted with two peaks at 531.1 eV and 532.6 eV which are ascribed to C=O and C-OH/C-O-C bonds respectively.[362] Deconvolution of N_{1s} peak (Fig. 8.9d), gave three components with binding energies 399.6 eV, 400.9 eV and 401.7 eV and shows the presence of C-N-C, N-C_3 and N-H bonds indicating that CDs are partly doped with nitrogen atoms. [363]

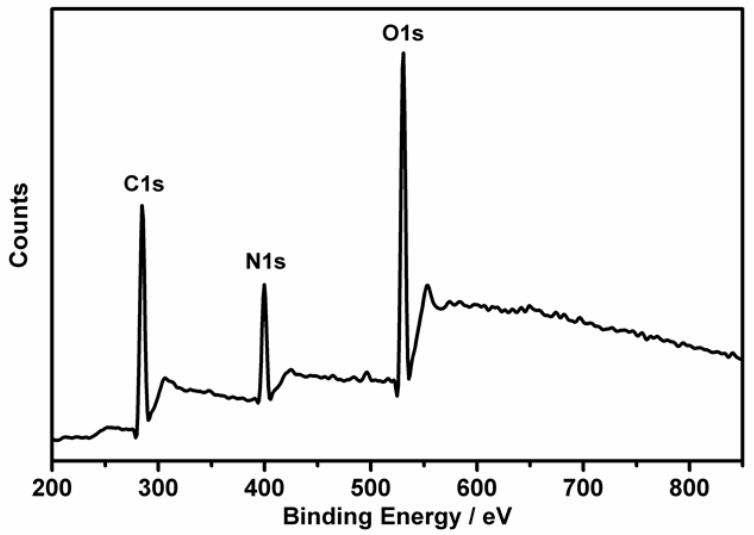

Figure 8.9a: XPS survey spectrum of CDs

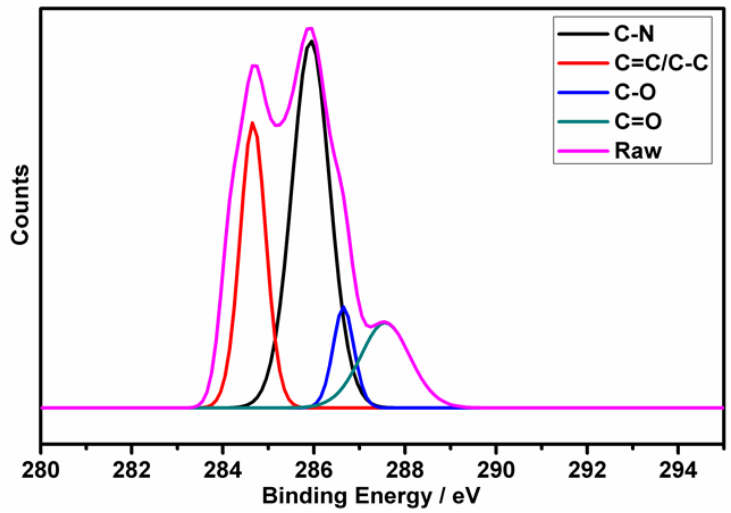

Figure 8.9b: High resolution C1s region of CDs

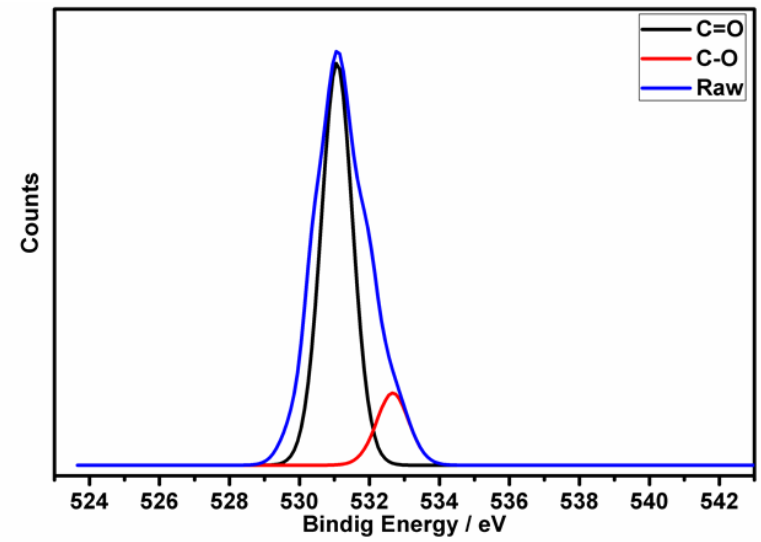

Figure 8.9c: High resolution O1s region of CDs

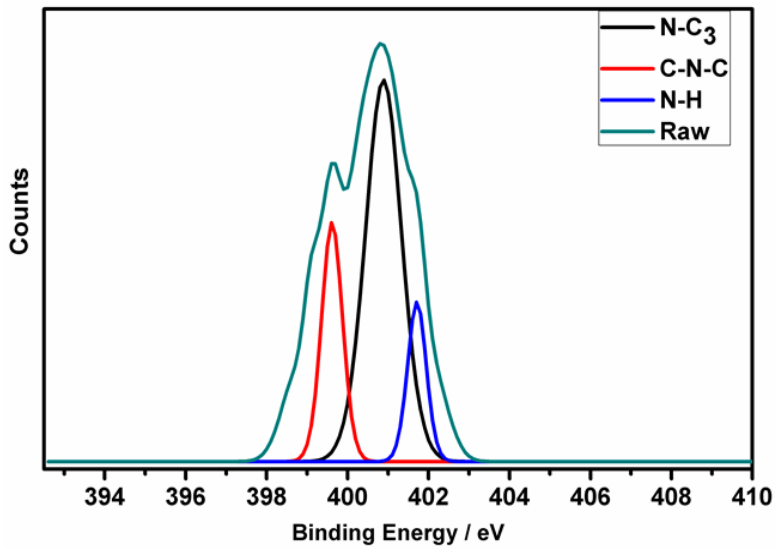

Figure 8.9d: High resolution N1s region of CDs

In the FTIR spectrum (Fig. 8.10), peaks at 3462 and 3194 cm^{-1} may be ascribed to O-H and N-H stretching vibrations, suggesting that the as prepared CDs possess strong hydrophilic properties, good stability and well dispersibility in water[362] The peak at 3008 cm^{-1} appears because of C-H bonds. Peaks emerged at 1587 and 1398 cm^{-1} may be due to asymmetric and symmetric stretching vibrations of COO^-.[352,357] The peaks at 1507 cm^{-1} corresponds to C-H bending vibrations[148,356] and the peak at 1348 cm^{-1} is identified as C-N stretching vibration.[347] Peaks at 1109 and 1039 cm^{-1} may be attributed to CO stretching and bending vibrations (CO bonds in carbonyl group) respectively.[354]

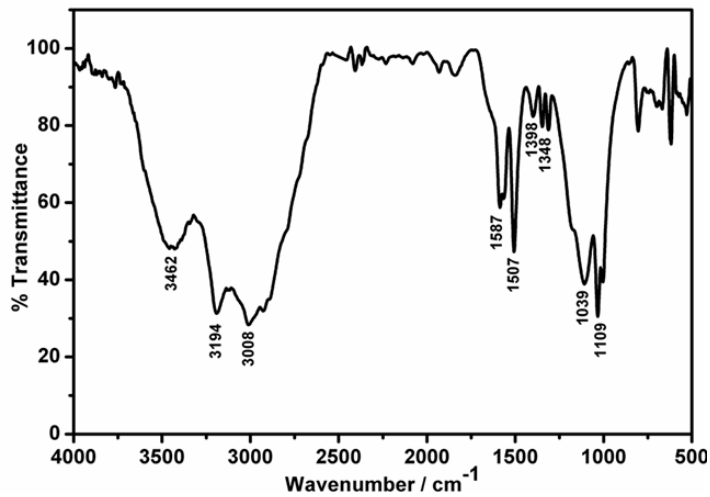

Figure 8.10: FTIR spectrum of CDs

In general XPS results of CDs showed satisfactory agreement with FTIR data which imply that the CDs derived from leaves of hibiscus plant are functionalized with –COOH, -C=O, -OH and $–NH_2$ groups, which facilitates their excellent water solubility. Presence of these functional groups improved the stability and hydrophilicity of as-synthesized CDs in aqueous systems, which help them to function as an excellent fluorescent probe for analytical applications.

8.3.3 Measurement of quantum yield

Emission and absorption spectra of different concentrations of CDs were recorded and are shown in Fig. 8.11a and Fig. 8.11b respectively. Further, the integrated fluorescence intensities of CDs were plotted against their absorbance (Fig. 8.11c). QY of the prepared CDs was calculated according to the following equation[97] using fluorescein (QY = 93%) as the reference.

$$Q_{CDs} = Q_R \frac{I_{CDs}}{I_R} \frac{A_R}{A_{CDs}} \frac{\eta_{CDs}^2}{\eta_R^2}$$

where 'Q' is the fluorescence QY, 'I' stands for integrated emission intensity, 'A' refers to absorbance at excited wavelength and 'η' is refractive index. The subscript CDs represent the carbon dots and 'R' is standard. From slopes of the plot of integrated fluorescence intensities and absorbance, quantum yield of as synthesized CDs was estimated to be 38.7%.

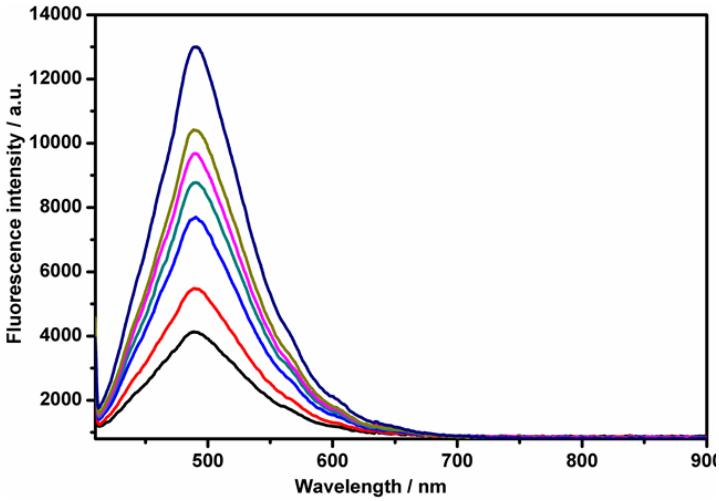

Figure 8.11a: Fluorescence spectra of different concentrations of CDs

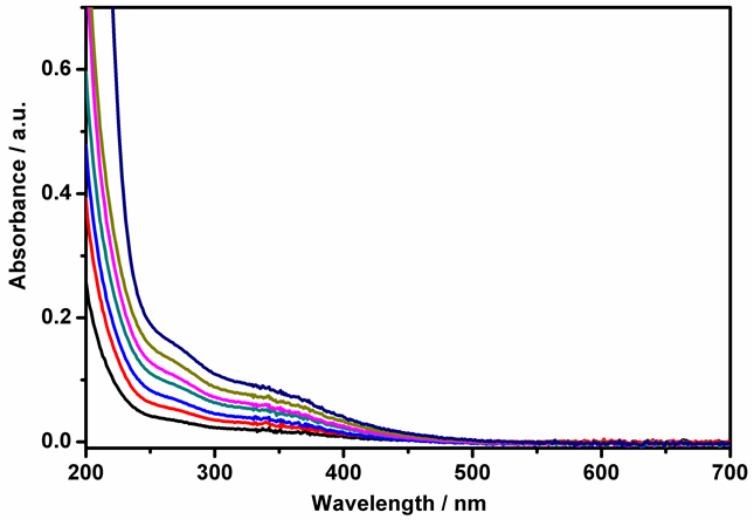

Figure 8.11b: Absorption spectra of different concentrations of CDs

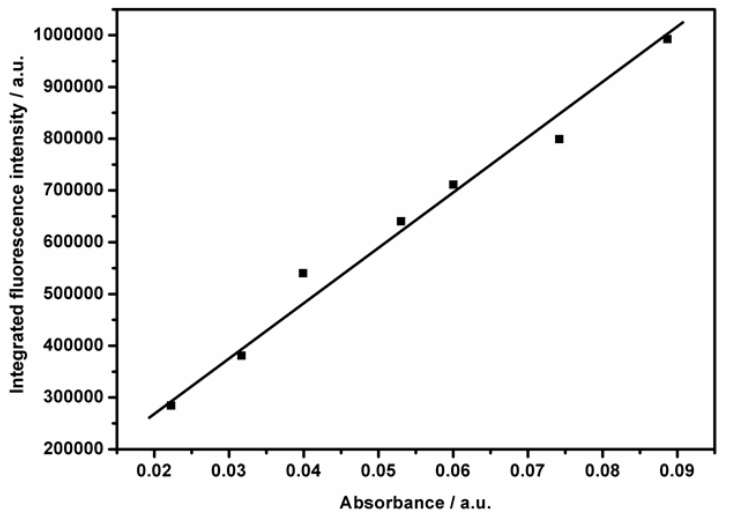

Figure 8.11c: Linear relationship between integrated fluorescence intensities and absorbance of CDs

8.3.4 Optimization of experimental parameters

Performance of developed sensor was assessed by studying the effect of different variables such as medium, pH of the medium and irradiation time on the fluorescence intensity of CDs and parameters were optimized

8.3.4.1 Effect of medium

Medium for which the as synthesized CDs showed maximum emission intensity was selected for further studies. Among different buffers (phosphate buffer, acetate buffer and citrate buffer) studied, maximum intensity and better stability was obtained for acetate buffer (ABS), which in turn resulted in selection of ABS as a suitable medium for further studies.

8.3.4.2 Effect of pH

The influence of pH on fluorescence intensity of CDs is shown in Fig. 8.12. As presented in Fig. 8.12, relative fluorescence intensity of CDs

increased with increase in pH from 2.0 to 4.0 and maximum intensity was obtained at pH 4.0. However, further increase in pH from 5.0 to 8.0 results in gradual reduction of fluorescence intensity. These findings suggest that pH value of the system strongly influence the emission property of CDs. Consequently 0.1 M ABS of pH 4.0 was selected for further studies.

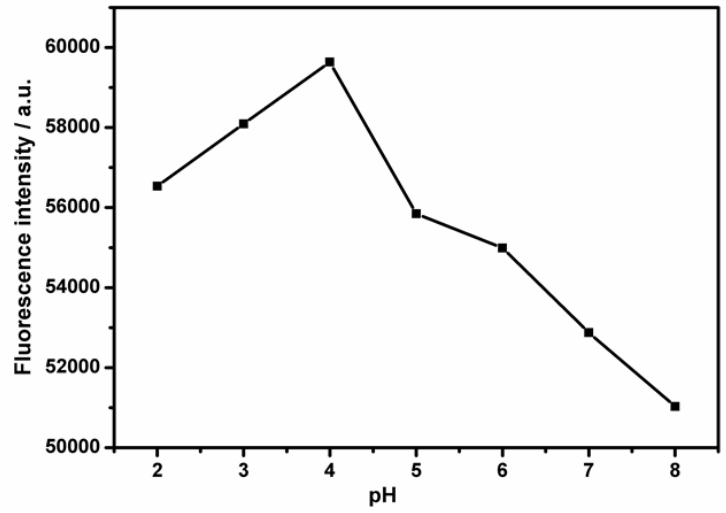

Figure 8.12: Effect of pH on fluorescence intensity

8.3.4.3 Effect of irradiation time on fluorescence intensity

Influence of irradiation time on fluorescence intensity of CDs in the absence and presence of SY was recorded. It can be ascertained from Fig. 8.13 that the fluorescence intensity of the probe remains unchanged upon continuous UV irradiation for 15 minutes. Furthermore, after addition of SY, fluorescence intensity of CDs was quenched and it became stable suddenly. This reveals the prompt response of developed sensor towards determination of SY, which augments the usefulness of sensor for real time analysis.

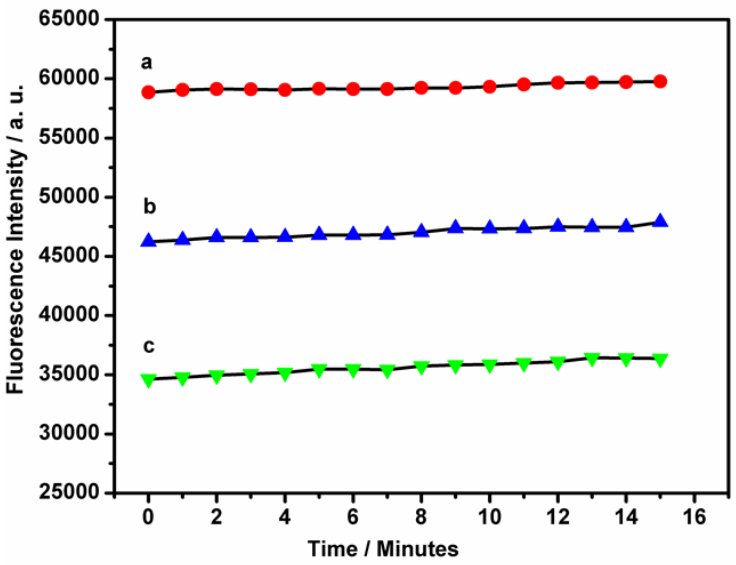

Figure 8.13: Effect of time on the fluorescence intensity of (a) CDs (b) CDs + 7.0 × 10^{-6} M SY (c) CDs + 1.5 × 10^{-5} M SY

8.4 Fluorescence quenching of CDs by SY

In order to explore the feasibility of CDs as a probe for determination of SY, we studied the dependence of I_0/I on different concentrations of SY. As shown in Fig. 8.14a strong emission of CDs was quenched gradually with increase in concentration of SY. Fig. 8.14b displays the linear correlation between decrease in fluorescence quenching efficiency and concentrations of SY in the range 1.0 × 10^{-5} to 2.0 × 10^{-6} M. The limit of detection and limit of quantifications were estimated to be 7.8 × 10^{-8} M and 2.6 × 10^{-7} M, respectively. Relative standard deviation was found to be 0.12 % through three parallel determinations at a fixed SY concentration of 2.0 × 10^{-6} M revealing excellent reliability of developed sensor.

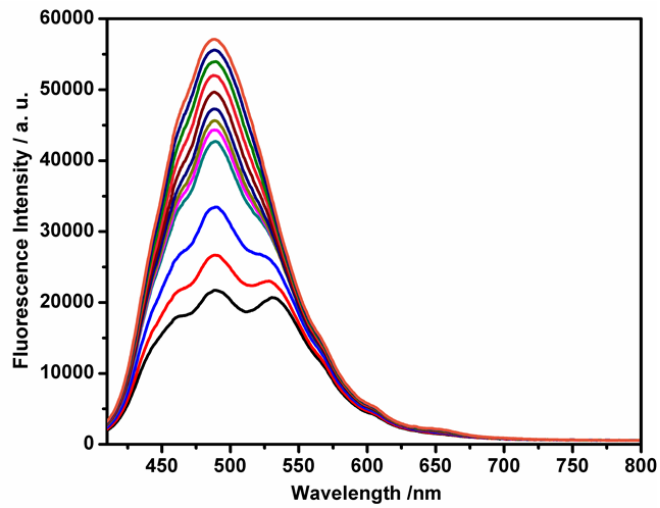

Figure 8.14a: Effect of concentration of SY on the fluorescence intensity of CDs (2.5×10^{-5} to 2.0×10^{-6} M SY)

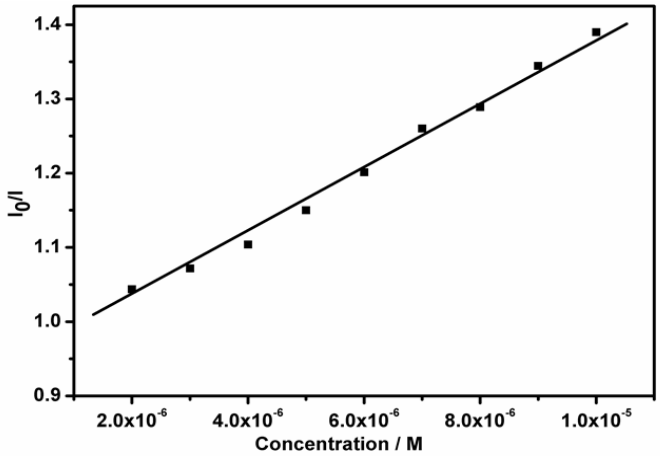

Figure 8.14b: Linear relationship between ratio of fluorescence intensities and concentrations of SY in the range 1.0×10^{-5} to 2.0×10^{-6} M

Table 8.1 compares the results of present experiment with previous reports for determination of SY. Even though, the limit of detection of present work is not the lowest, the proposed method can be used as an

alternative to other methods for the determination of SY in real sample analysis because most of reported sensors require sophisticated techniques, special equipment, complicated operations and toxic or expensive chemicals. On contrast, the present method had its own unique features such as green synthesis, simplicity in operation, low cost and quick response, which makes it an ideal choice for routine analysis of SY in soft drink samples.

8.5 Mechanism of fluorescence quenching

To understand the mechanism of fluorescence quenching of CDs by SY, absorption and fluorescence emission spectrum of CDs and SY were examined.

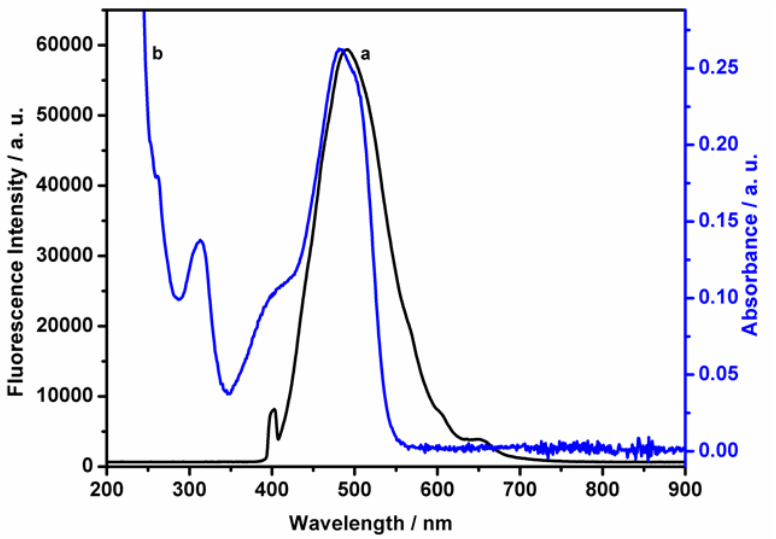

Figure 8.15: Overlay of (a) fluorescence spectrum of CDs (b) absorption spectrum of SY

From Fig. 8.15, it is clear that there exist a good spectral overlap between emission band of CDs and absorption band of SY, which imply that

the quenching of fluorescence emission intensity may arise from IFE or fluorescence resonance energy transfer (FRET). From measurements of zeta potentials of CDs and SY, it is found that both CDs and SY possess negative charge (-11.2 and -12.4 mV respectively), as a result there exist strong electrostatic repulsion which inhibits an efficient FRET process between CDs and SY.

Efficiency of IFE depends on complementary overlap between absorption spectrum of absorber with the excitation or emission spectrum of fluorophore.[367] Moreover, sensors based on fluorescence IFE did not require establishment of inter molecular interaction between fluorophore and target molecule. To confirm the mechanism, fluorescence lifetime measurements were carried out. As shown in Fig. 8.16, fluorescence decay time was found to be 3.78 and 3.97 ns before and after addition of SY. The fluorescence decay curve of CDs also has no variations in the presence and absence of SY. All these observations ruled out the possibility of electron transfer process in CDs – SY system, suggesting that the fluorescence quenching can be mainly ascribed to the IFE of SY on fluorescence of CDs.[368] Furthermore, up on addition of SY, there is a considerable change in shape of emission spectrum along with quenching which again confirms the mechanism as IFE.[137,369] In addition, absorption spectrum of SY did not show obvious change in presence of CDs, which imply that no complex was formed between CDs and SY in system (Fig. 8.17). All these results clearly suggest that the mechanism based on IFE can be accounted for decrease in fluorescence intensity of CDs rather than other possible process.

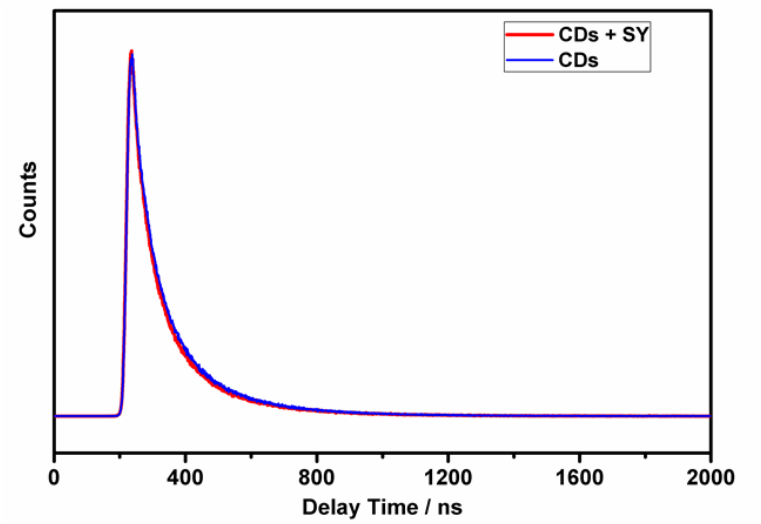

Figure 8.16: Fluorescence decay curves of CDs in the absence and presence of SY

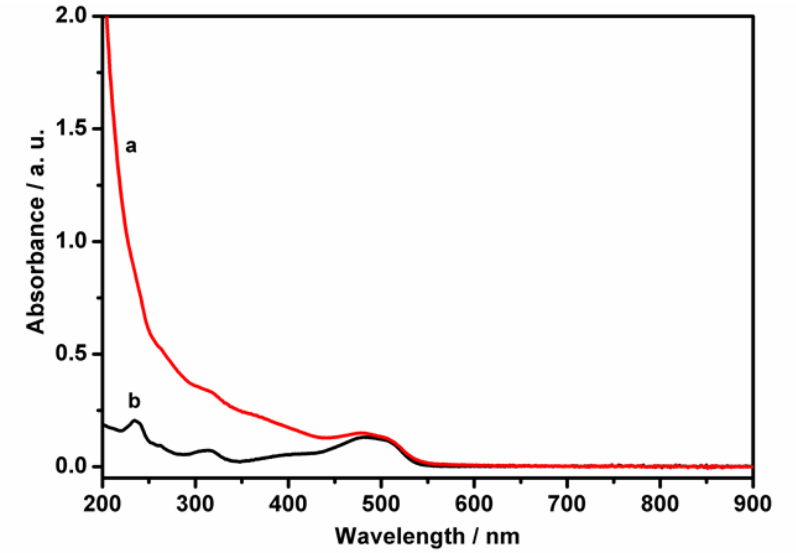

Figure 8.17: Absorption spectra of SY in the (a) presence and (b) absence of CDs

8.6 Selectivity

Selectivity of proposed sensing system was investigated by evaluating fluorescence response of interfering substances such as sugars (glucose, fructose) artificial sweeteners (aspartame, saccharin), ascorbic acid, NaCl and citric acid under same conditions (Fig. 8.18). It is evident from Fig. 8.18 that only SY can effectively quench the fluorescence intensity of CDs, suggesting a good selectivity of the developed probe towards the determination of SY.

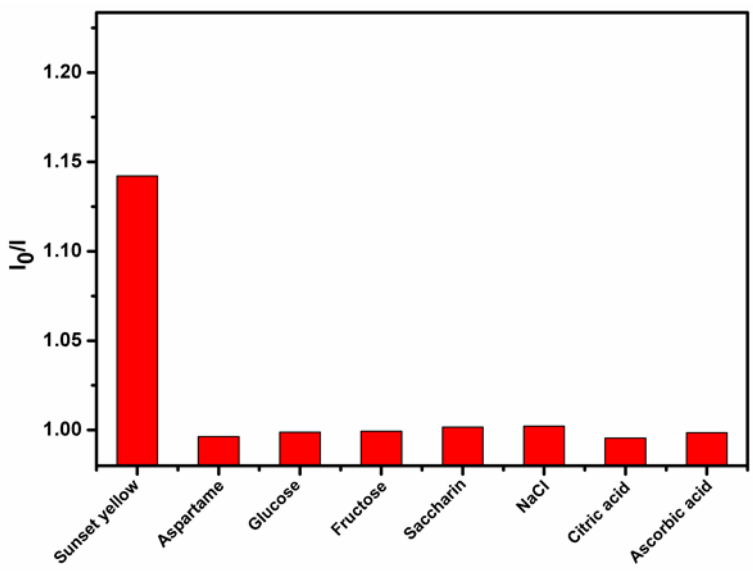

Figure 8.18: Selectivity of the developed sensor

We have also examined the fluorescence response of developed system to SY at concentration of 5.0×10^{-6} M in the presence of various concentrations (1:1, 1:10 and 1:100) of aforementioned substances and it was found that even 100 fold excess of interfering species does not cause any significant change in fluorescence intensity of probe (signal change

below ± 5%) (Fig. 8.19). Thus, it can be confirmed that most of common interfering species in foods could be tolerated at concentrations up to 100 times.

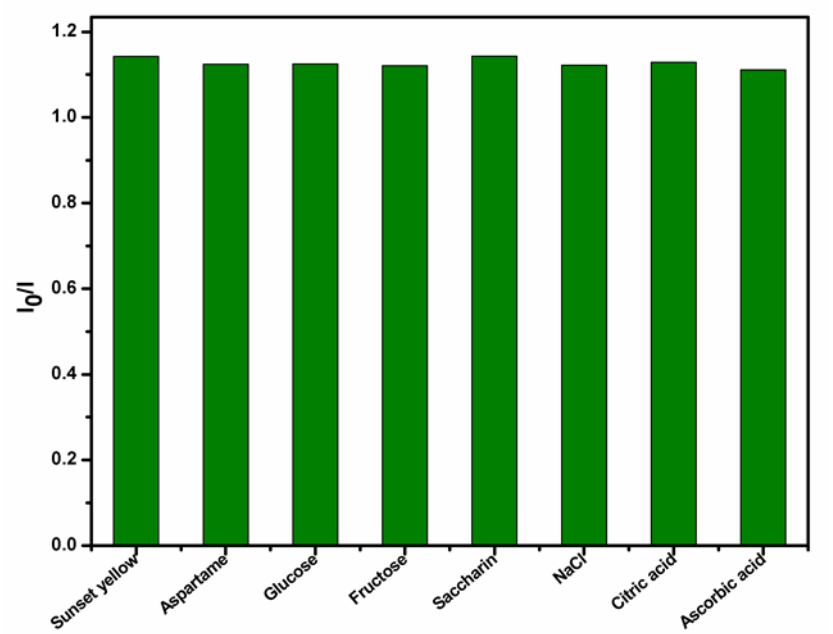

Figure 8.19: Effect of various substances on the fluorescence spectrum of CDs for the determination of 5.0×10^{-6} M SY

8.7 Application in real samples

Practical utility of developed sensor was evaluated by determining the concentration of SY in soft drink samples. The SY in two different commercial brands of soft drinks were found to be 2.3×10^{-7} and 3.6×10^{-7} M respectively which is in good agreement with the results obtained from spectrophotometric analysis detailed in section 2.5.3., in which the values were estimated to be 2.5×10^{-7} and 3.3×10^{-7} M respectively. The above results indicate reliability and accuracy of developed sensor for determination of SY in soft drink samples.

8.8 Conclusion

A novel, green and one step microwave irradiation method was successfully developed for synthesis of fluorescent CDs based on carbonization of Hibiscus leaves extract followed by passivation with EDA. Synthesized CDs showed strong fluorescence emission with high quantum yield (38.7%), good aqueous dispersibility, excellent chemical and photostability. Practical performance of developed sensor was assessed by determining concentration of SY in commercial soft drink samples. Use of eco-friendly hibiscus leaves as carbon source and simplicity of synthetic procedure will open up broad potential avenues in sensing and other purposes with further research.

Table 8.1: Comparison of different methods for determination of SY

Determination Methods	Linear range (M)	LOD (M)	References
Salting-out assisted liquid-liquid extraction	3.32×10^{-5}- 8.84×10^{-7}	1.54×10^{-7}	[364]
[a](HLA/GO) method	2.87×10^{-5}- 2.21×10^{-7}	1.32×10^{-7}	[365]
UV-visible spectrophotometry	3.86×10^{-4} - 2.21×10^{-6}	6.63×10^{-7}	[366]
Electrochemical sensor	1.00×10^{-5} - 1.00×10^{-6}	4.03×10^{-8}	[249]
CDs	1.00×10^{-5} - 2.00×10^{-6}	7.84×10^{-8}	Proposed method

[a]Hybrid linear analysis method

.....ꕥ.....

Chapter 9

SUMMARY

Contents

9.1 Objectives of work
9.2 Summary of work done
9.3 Future outlook

Objectives of the present investigation, summary of work done and future outlook are given in this chapter.

9.1 Objectives of work

1) Development of chemical sensors for determination of food additives and pharmaceuticals.

2) Chemical modification of electrodes using polymers and nanomaterials.

3) Surface characterization of developed sensors using scanning electron microscopy, atomic force microscopy, cyclic voltammetry and electrochemical impedance spectroscopy.

4) Optimization of various experimental parameters for development of sensors.

5) Evaluating kinetic parameters of electrode reactions using electroanalytical techniques.

6) Prediction of plausible mechanism for oxidation of target species at the surface of electrode.

7) Synthesis of gold nanoparticles (AuNPs) and its development as a colorimetric sensor for pharmaceutical

8) Characterization of synthesized AuNPs by transmission electron microscopy, X-ray photoelectron spectroscopy, UV-vis absorption spectroscopy, dynamic light scattering and zeta potential measurements.

9) Green synthesis of fluorescence probe, carbon dots (CDs) and its characterization by transmission electron microscopy, UV-vis absorption spectroscopy, fluorescence spectroscopy, dynamic light scattering and zeta potential measurement.

10) Development of CDs based fluorescence sensor for food additive.

11) Validating the practical utility of developed sensors using spiked/real samples and pharmaceutical formulations.

9.2 Summary of work done

In the present investigations, six chemical sensors comprising four electrochemical and two optical sensors (colorimetric and fluorescence sensor each) were developed for quantification of food additives and pharmaceutical. Significant features of developed sensors are enlisted below.

Sl No	Type of sensor developed	Sensing probe	Linear range (M)	Limit of detection (M)	Analyte
1	Electrochemical sensors	AuNP/poly(*p*-ABSA)/GCE	1.0×10^{-4} - 9.0×10^{-6}	1.9×10^{-7}	Propyl gallate
2		Poly BPB/GCE	1.0×10^{-5} - 1.0×10^{-6}	3.5×10^{-8}	*Tert*-butylhydroquinone
3		Poly(L-Cys)/GCE	1.0×10^{-5} - 1.0×10^{-6}	3.7×10^{-8}	Ponceau 4R
4		Poly Gly/GCE	1.0×10^{-4} - 9.0×10^{-6}	3.6×10^{-7}	Acid green 50
5	Colorimetric Sensor	Citrate capped AuNPs	9.0×10^{-6} - 9.0×10^{-7}	9.9×10^{-8}	Tetracycline
6	Fluorescence Sensor	EDA - CDs	1.0×10^{-5} - 2.0×10^{-6}	7.8×10^{-8}	Sunset yellow

9.3 Future outlook

World of sensors has unveiled numerous applications for monitoring almost everything around us. Future research in sensor technology will be focussed to innovate and improvise sensor devices for *in-vivo* use. Significant progress in this regard can be achieved only by a team of multi-disciplinary researchers from chemistry, physics, biology, materials science, electronics and other related fields. Commercial mass production of portable hand-held, cheap and reliable sensing devices will help to address emerging concerns in medical diagnostics, food quality control, environmental monitoring, defense and industrial manufacturing process. Thus, rapid advancements in field of sensors will improve safety and quality of life.

.....ꕥ.....

References

[1] A.P. Demchenko, *Introduction to Fluorescence Sensing*, 2nd Edn., Springer, Switzerland, 1 (2015).

[2] G.G. Cammann, E.A. Guilbault, H. Hal, R. Kellner, O.S. Wolfbeis, *The Cambridge Definition of Chemical Sensors, Cambridge Workshop on Chemical Sensors and Biosensors*, Cambridge University Press, New York (1996).

[3] A.M. Bond, F.Z. Scholz, *Chemie.*, **30**, 117 (1990).

[4] J. Heyrovsky, J. Kuta, *Principles of Polarography,* Academic press, New York (1996).

[5] J.O.M. Bockris, S.U.M. Khan, *Surface Electrochemistry*, Plenum Press, New York (1993).

[6] R.L. McCreery, *Carbon Electrode Surface Chemistry*; *In: Neuro Methods, Vol. 27: Voltammetric Methods in Brain Systems*, A.A. Boulton, G.B. Baker, R.N. Adams (Eds.), Humana Press Inc., New York (1995).

[7] C.G. Zoski, *Handbook of Electrochemistry*, Elsevier B.V., UK, 121 (2007).

[8] K. Kinoshita, *Carbon: Electrochemical and Physicochemical Properties*, Wiley, New York (1988).

[9] B. Uslu, S.A. Ozkan, *Anal. Lett.,* **40**, 817 (2007).

[10] P.J.F. Harris, *Crit. Rev. Solid State Mater. Sci.*, **30**, 235 (2005).

[11] A.J Bard, L. Faulkner, *Electrochemical Methods: Fundamentals and Applications*, 2nd Edn., Wiley, New York (2001).

[12] J. Wang, *Analytical Electrochemistry*, 2nd Edn., Wiley-VCH, USA (2000).

[13] https://en.wikipedia.org/wiki/Cyclic_voltammetry

[14] P.M.S. Monk, *Fundamentals of Eletroanalytical Chemistry*, Wiley, Chichester, (2001).

[15] C.M.A. Brett, A.M.O. Brett, *Electroanalysis*, Oxford Science Publications, New York (1998).

[16] H.H. Willard, L.L. Merritt, J.A. Dean, F.A. Settle, *Instrumental Methods of Analysis*, 6th Edn., D. Van Nostrand Co, New York (1981).

[17] F.A. Settle, *Handbook of Instrumental Techniques for Analytical Chemistry*, Prentice Hall PTR, **1**, 720 (1997).

[18] B.D. Topal, S.A. Ozkan, B. Uslu, *The Open Chemical and Biochemical Methods Journal*, **3,** 56 (2010).

[19] D. Grieshaber, R. MacKenzie, J. Vörös, E. Reimhu, *Sensors*, **8**, 1400 (2008).

[20] P. Kissinger, W.R. Heineman, *Laboratory Techniques in Electroanalytical Chemistry*, 2nd Edn., CRC press, Marcel Dekker, New York (1996).

[21] Z. Galus, *Fundamentals of Electrochemical Analysis*, Ellis Horwood Ltd., England, 25 (1976).

[22] F.C. Anson, *Anal. Chem*., **38**, 54 (1966).

[23] F.C. Anson, *Anal. Chem*., **36**, 932 (1964).

[24] E.P. Randviir, C.E. Banks, *Anal. Methods*, **5**, 1098 (2013).

[25] F. Patolsky, M. Zayats, E. Katz, I. Willner, *Anal. Chem.*, **71**, 3171 (1999).

[26] L. Mirmoghtadaie, A.A. Ensafi, M. Kadivar, M. Shahedi, M.R. Ganjali, *Int. J. Electrochem. Soc.*, **8**, 3755 (2013).

[27] G.N.S. Quasi, E. Deutsch, R.J. Windgassen, *J. Am. Chem. Soc.*, **90**, 2441 (1968).

[28] P.R. Moses, L. Wier, R.W. Murray, *Anal. Chem.*, **47,** 1882 (1975).

[29] R.A. Durst, A.J. Baumner, R.W. Murray, R.P. Buck, C.P. Andrieux, *Pure Appl. Chem.*, **69,** 1317 (1997).

[30] D.C. Tiwari, R. Jain, S. Sharma, *J. Sci. Ind. Res.*, **66**, 1011 (2007).

[31] https://www.intechopen.com/books/aspects-on-fundaments-and-applications-of-conducting-polymers/application-of-conducting-polymers-in-electroanalysis-

[32] A. Volkov, G. Tourillon, P.C. Lacaze, J.E. Dubois. *J. Electroanal. Chem.*, **115,** 279 (1980).

[33] C.M.A. Brett, G. Inzelt, V. Kertesz, *Anal. Chim. Acta*, **385,** 119 (1999).

[34] Y.X. Sun, B.X. Ye, Y. Wang, X.R. Tang, X.Y. Zhou, *Microchem. J.*, **58,** 182 (1998).

[35] A.S.N. Murthy, K.S. Reddy, *Electrochim. Acta*, **28**, 473 (1983).

[36] N.J. Yang, X.X. Wang, *Electrochim. Acta*, **52,** 6962 (2007).

[37] M. Yuqing, C. Jianrong, W. Xiaohua, *Trends Biotechnol.*, **22**, 227 (2004).

[38] J.C. Vidal, E. Garcia-Ruiz, J.R. Castillo, *Microchim. Acta*, **143**, 93 (2003).

[39] M. Gerard, A. Chaubey, B.D. Malhotra, *Biosens. Bioelectron.*, **17**, 345 (2002).

[40] A.N. Shipway, M. Lahav, I. Willner, *Adv. Mater.*, **12**, 993 (2000).

[41] J. Li, X. Lin, *Sens. Actuators B*, **126**, 527 (2007).

[42] S. Guo, E. Wang, *Anal. Chim. Acta*, **598**, 181 (2007).

[43] Y.W. Tan, Y.F. Li, D.B. Zhu, *Langmuir*, **18**, 3392 (2002).

[44] J. Zhang, M. Oyama. *Anal. Chim. Acta*, **540**, 299 (2005).

[45] M. Fukushima, H. Yanagi, S. Hayashi, N. Suganuma, Y. Taniguchi, *Thin Solid Films*, **39**, 438 (2003).

[46] X. Dai, O. Nekrassova, M.E. Hyde, R.G. Compton, *Anal. Chem.*, **76**, 5924 (2004).

[47] M.S. El-Deab, T. Okajima, T. Ohsaka, *J. Electrochem. Soc.*, **150**, A851 (2003).

[48] G.G. Wildgoose, C.E. Banks, R.G. Compton, *Small*, **2,** 182 (2006).

[49] U.S. Mohanty, *J. Appl. Electrochem.*, **41,** 257 (2011).

[50] W. Cai, T. Gao, H. Hong, J. Sun, *Nanotechnol. Sci. Appl.*, **1,** 17 (2008).

[51] A. Cavicchioli, M.A. La-Scalea, I.G.R. Gutz, *Electroanalysis*, **16**, 697 (2004).

[52] D. Hernandez-Santos, M.B. Gonzalez-Garcia, A.C. Garcia, *Electroanalysis*, **4**, 1225 (2002).

[53] C.M. Welch, C.E. Banks, A.O. Simm, R.G. Compton, *Anal. Bioanal. Chem.*, **382**, 12 (2005).

[54] S.A. Kumar, S.M. Chen, *Sens. Actuators, B*, **123**, 964, (2007).

[55] L. Zhang, C. Zhang, J. Lian, *Biosens. Bioelectron.*, **24**, 690 (2008).

[56] Z. Zhu, F. Wang, F. Wang, L. Xi, *J. Electroanal. Chem.*, **708**, 13 (2013).

[57] B.L. Li, J.H. Luo, H.Q. Luo, N.B. Li, *Food Chem.*, **173**, 594 (2015).

[58] S. Jesny, K. Girish Kumar, *Electroanalysis*, **27**, 1828 (2017)

[59] G.J. Yang, X.L. Qu, A.P. Zhu, C.Y. Wang, Q.S. Qu, X.Y. Hu, *J. Electroanal. Chem.*, **604**, 48 (2007).

[60] P. Yang, W. Wei, C. Tao, J. Zeng, *Bull. Environ. Contam. Toxicol.*, **79**, 5 (2007).

[61] H. Xu, W. Zhang, D. Wang, W. Zhu, L. Jin, *J. Chromatogr. B*, **846**, 14 (2007).

[62] Y. Peng, C. Hu, D. Zheng, S. Hu, *Sens. Actuators B*, **133**, 571 (2008).

[63] G. Yang, Y. Wang, F. Qi, *Microchim. Acta*, **177**, 365, (2012).

[64] U. Sivasankaran, A. Thomas, A.R. Jose, K. Girish Kumar, *J. Electrochem. Soc.*, **164**, B292 (2017).

[65] Y. Gu, W. Liu, R. Chen, L. Zhang, Z. Zhang, *Electroanalysis*, **25**, 1209 (2013).

[66] K. Zhang, P. Luo, J. Wu, W. Wang, B. Ye, *Anal. Methods*, **5**, 5044 (2013).

[67] D. Thomas, Z. Rasheed, S. Jesny, K. Girish Kumar, *J. Food Sci. Technol*., **52**, 6719, (2015).

[68] T. Jos, A.R. Jose, U. Sivasankaran, K. Girish Kumar, *J. Electrochem. Soc.*, **162,** B94, (2015).

[69] B.R.L. Ferraz, F.R.F. Leite, A.R. Malagutti, *Talanta*, **154**, 197 (2016).

[70] A. Yu, H. Zhang, H. Chen, *Electroanalysis*, **9**, 788 (1997).

[71] L. Wang, P. Huang, H. Wang, J. Bai, L. Zhang, Y. Zhao, *Int. J. Electrochem. Sci.*, **2**, 216 (2007).

[72] P.V. Narayana, T.M. Reddy, P. Gopal, G.R. Naidu, *Anal. Methods*, **6**, 9459 (2014).

[73] B.R.L. Ferraz, F.R.F. Leite, A.R. Malagutti, *J. Solid State Electrochem.*, **20**, 2509 (2016).

[74] G. Zhang, P. He, W. Feng, S. Ding, J. Chen, L. Li, H. He, S. Zhang, F. Dong, *J. Electroanal. Chem.*, **760**, 24 (2016).

[75] P. Gründler, *Chemical Sensors: An Introduction for Scientists and Engineers*, Springer-Verlag, Berlin, Heidelberg (2007).

[76] P.C.A. Jerónimo, A.N. Arau´jo, M. Conceicão, B.S.M. Montenegro, *Talanta*, **72**, 13 (2007).

[77] W.R. Seitz, *Optical Ion Sensing*; *In: Fiber Optic Chemical Sensors and Biosensors II*, CRC press, Boca Raton, Florida (1991).

[78] E.C. Dreaden, A.M. Alkilany, X. Huang, C.J. Murphy, M.A. El-Sayed, *Chem. Soc. Rev.*, **41**, 2740 (2012).

[79] M. Faraday, *Philos. Trans. R. Soc.*, London, **147**, 145 (1857).

[80] R. Elghania, J.J. Storhoff, R.C. Mucic, R.L. Letsinger, C.A. Mirkin, *Science*, **277**, 1078 (1997).

[81] R. Klajn, J.F. Stoddart, B.A. Grzybowski, *Chem. Soc. Rev*., **39**, 2203 (2010).

[82] S.K. Ghosh, T. Pal, *Chem. Rev*., **107**, 4797 (2007).

[83] M.C. Daniel, D. Astruc, *Chem. Rev*., **104**, 293 (2004).

[84] D. Liu, Z. Wang, X. Jiang, *Nanoscale*, **3**, 1421 (2011).

[85] J. Yguerabide, E.E. Yguerabide, *Anal. Biochem*., **262**, 137 (1998).

[86] P.K. Jain, K.S. Lee, I.H. El-Sayed, M.A. El-Sayed, *J. Phys. Chem. B*, **110**, 7238 (2006).

[87] B. Sepu´lveda, P.C. Angelome´, L.M. Lechuga, L.M. Liz-Marza´n, *Nano Today*, **4**, 244 (2009).

[88] U. Kreibig, M. Vollmer, *Optical Properties of Metal Clusters*, Springer, Berlin, **25**, 532 (1995).

[89] K.L. Kelly, E. Coronado, L.L Zhao, G.C. Schatz, *J. Phys. Chem. B*, **107**, 668 (2003).

[90] M.E. Stewart, C.R. Anderton, L.B. Thompson, J. Maria, S.K. Gray, J.A. Rogers, R.G. Nuzzo, *Chem. Rev*., **108**, 494 (2008).

[91] Z. Tan, J. Liu, R. Liu, Y. Yin, G. Jiang, *Chem. Commun*., 7030 (2009).

[92] Q. Cao, H. Zhao, Y. He, X. Li, L. Zeng, N. Ding, J. Wang, J. Yang, G. Wang, *Biosens. Bioelectron.,* **25**, 2680 (2010).

[93] L. Li, B. Li, D. Cheng, L. Mao, *Food Chem.*, **122**, 895 (2010).

[94] S.K. Tripathy, J.Y. Woo, C.S. Han, *Anal. Chem.*, **83**, 9206 (2011).

[95] Y. Hu, C. Du, Y. Li, L. Fan, X. Li, *Analyst*, **140**, 4662 (2015).

[96] A.P. Demchenko, *Introduction to Fluorescence Sensing*, 2nd Edn., Springer, Switzerland (2015).

[97] J.R. Lakowicz, *Principles of Fluorescence Spectroscopy*, Kluwer Academic and Plenum Publishers, New York (2000).

[98] H. Kim, B.I. Lee, S.H. Byeon, *Chem. Commun.*, **51**, 725 (2015).

[99] J. Li, X. Li, X. Shi, X. He, W. Wei, N. Ma, H. Chen, *ACS Appl. Mater. Interfaces*, **5**, 9798 (2013).

[100] X. Yan, H. Li, X. Han, X. Su, *Biosens. Bioelectron.*, **74**, 277 (2015).

[101] L. Shang, S. Dong, *Anal. Chem.*, **81**, 1465 (2009).

[102] T. Liu, Y. Zhang, T. Hou, Q. Xue, L. Wang, S. Wang, *RSC Adv.*, **7**, 23422 (2017).

[103] L. Shang, S. Dong, *Anal. Chem*., **81**, 1465 (2009).

[104] P. Dutta, D. Saikia, N.C. Adhikary, N.S. Sarma, *ACS Appl. Mater. Interfaces*, **7**, 24778 (2015).

[105] G. Li, H. Fu, X. Chen, P. Gong, G. Chen, L. Xia, H. Wang, J. You, Y. Wu, *Anal. Chem*., **88**, 2720 (2016).

[106] M. Rong, L. Lin, X. Song, T. Zhao, Y. Zhong, J. Yan, Y. Wang, X. Chen, *Anal. Chem*., **87**, 1288 (2015).

[107] M. Lin, H.Y. Zou, T. Yang, Z.X. Liu, H. Liu, C.Z. Huang, *Nanoscale*, **8**, 2999 (2016).

[108] H. Kim, B. Lee, S. Byeon, *Chem. Commun*., **51**, 725 (2015).

[109] U.R. Genger, M. Grabolle, S.C. Jaricot, R. Nitschke, T. Nann, *Nat. methods*, **5**, 763 (2008).

[110] G.G. Guilbault, *Practical Fluorescence*, 2nd Edn., Marcel Dekker, New York (1990).

[111] https://en.wikipedia.org/wiki/Stokes_shift

[112] Y. Wang, A. Hu, *J. Mater. Chem. C*, **2**, 6921 (2014).

[113] X. Xu, R. Ray, Y. Gu, H.J. Ploehn, L. Gearheart, K. Raker, W.A. Scrivens, *J. Am. Chem. Soc.*, **126**, 12736 (2004).

[114] H. Li, Z. Kang, Y. Liu, S.T. Lee, *J. Mater. Chem*, **22**, 24230 (2012).

[115] S.N. Baker, G.A. Baker, *Angew. Chem. Int. Ed*., **49**, 6726 (2010).

[116] A.L. Himaja, P.S. Karthik, S.P. Singh, *Chem. Rec*., **15**, 595 (2015).

[117] Z. Kang, Y. Liu, C.H.A. Tsang, D.D.D. Ma, X. Fan, N.B. Wong, S.T. Lee, *Adv. Mater*., **21**, 661 (2009).

[118] Z. Kang, Y. Liu, S.T. Lee, *Nanoscale*, **3**, 777 (2011).

[119] Y. Zhang, X. Han, J. Zhang, Y. Liu, H. Huang, H. Ming, S.T. Lee, Z. Kang, *Nanoscale*, **4**, 7760 (2012).

[120] S.Y. Lim, W. Shen, Z. Gao, *Chem. Soc. Rev*., **44**, 362 (2015).

[121] G. Eda, Y.Y. Lin, C. Mattevi, H. Yamaguchi, H.A. Chen, I.S. Chen, C.W. Chen, M. Chhowalla, *Adv. Mater*., **22**, 505 (2010).

[122] K. Krishnamoorthy, M. Veerapandian, R. Mohan, S.J. Kim, *Appl. Phys. A: Mater. Sci. Process*., **106**, 501 (2012).

[123] J.H. Shen, Y.H. Zhu, C. Chen, X.L. Yang, C.Z. Li, *Chem. Commun*., **47**, 2580 (2011).

[124] J.H. Shen, Y.H. Zhu, X.L. Yang, J. Zong, J.M. Zhang, C.Z. Li, *New J. Chem*., **36**, 97 (2012).

[125] P. Zuo, X. Lu, Z. Sun, Y. Guo, H. He, *Microchim. Acta*, **183**, 519 (2016).

[126] G. Oza, M. Ravichandran, V.I. Merupo, S. Shinde, A. Mewada, J.T. Ramirez, S. Velumani, M. Sharon, M. Sharon, *Sci. Rep*., **6**, 21286 (2016).

[127] J. Wang, C.F. Wang, S. Chen, *Angew. Chem., Int. Ed*., 9297 (2012).

[128] Y.H. Yang, J.H. Cui, M.T. Zheng, C.F. Hu, S.Z. Tan, Y. Xiao, Q. Yang, Y.L. Liu, *Chem. Commun.*, **48**, 380 (2012).

[129] B. De, N. Karak, *RSC Adv.*, **3**, 8286 (2013).

[130] A. Prasannan, T. Imae, *Ind. Eng. Chem. Res*., **52**, 15673 (2012).

[131] S. Pandey, A. Mewada, G. Oza, M. Thakur, N. Mishra, M. Sharon, M. Sharon, *Nanosci. Nanotechnol. Lett*., **5**, 775 (2013).

[132] J. Zhou, Z. Sheng, H. Han, M. Zou, C. Li, *Mater. Lett.*, **66**, 222 (2012).

[133] M. Tan, L. Zhang, R. Tang, X. Song, Y. Li, H. Wu, Y. Wang, G. Lv, W. Liu, X. Maa, *Talanta*, **115**, 950 (2013).

[134] H. Xu, X. Yang, G. Li, C. Zhao, X. Liao, *J. Agric. Food Chem*., **63**, 6707 (2015).

[135] Y. Yuan, X. Zhao, M. Qiao, J. Zhu, S. Liu, J. Yang, X. Hu, *Spectrochim. Acta A Mol. Biomol. Spectrosc*., **167**, 106 (2016).

[136] S. Jesny, S. Menon, K. Girish Kumar, *RSC Adv*., **6**, 75741 (2016).

[137] U. Sivasankaran, S.T. Cyriac, S. Menon, *J. Fluores*., **22**, 69 (2017).

[138] D. Thomas, A.E. Vikraman, T. Jos, K. Girish Kumar, *LWT Food Sci. Technol*., **63**, 1294 (2015).

[139] T. Jos, L. Lonappan, Z. Rasheed, A.E. Vikraman, K. Girish Kumar, *Electrochem. Lett.*, **3**, B23 (2014).

[140] S. Menon, A.R. Jose, S. Jesny, K. Girish Kumar, *Anal. Methods*, **8**, 5801 (2016).

[141] A.E. Vikraman, A.R. Jose, M. Jacob, K. Girish Kumar, *Anal. Methods*, **7**, 6791 (2015).

[142] R. Leena, A.K. Jissy, K. Girish Kumar, A. Datta, *J. Phys. Chem. C*, **115**, 21858 (2011).

[143] S. Jesny, K. Girish Kumar, *J. Electroanal. Chem*., **801**, 153 (2017).

[144] A. Thomas, U. Sivasankaran, K. Girish Kumar, *Spectrochim. Acta A Mol. Biomol. Spectrosc*., Doi: 10.1016/j.saa.2017.06.040 (2017).

[145] A.R. Jose, A.E. Vikraman, K. Girish Kumar, *New J. Chem*., Doi: 10.1039/C7NJ00795G (2017).

[146] AOAC, *Official Methods of Analysis of the Association of Official Analytical Chemists*, 15th Edn., K. Helrich, Editor, Arlington, Virginia, 1140 (1990).

[147] X. Lin, Y. Ni, S. Kokot, *Anal. Chim. Acta*, **765**, 54 (2013).

[148] AOAC, *Official Methods of Analysis of the Association of Official Analytical Chemists*, 15th Edn., K. Helrich, Editor, Arlington, Virginia, 1125 (1990).

[149] S. Michalkiewicz, M. Mechanik, J. Malyszko, *Electroanalysis*, **16**, 588 (2004).

[150] S.P. Kochhar, J. B. Rossel, *Food Antioxidant*, Elsevier, London, **19** (1990).

[151] L. Guo, M.Y. Xie, A.P. Yan, Y.Q. Wan, Y.M. Wu, *Anal. Bioanal. Chem.*, **386**, 1881 (2006).

[152] J.L. Zurita, A. Jos, A. Peso, M. Salguero, M. López-Artíguez, G. Repetto, *Water Res.*, **41**, 2599 (2004).

[153] JECFA, Joint FAO/WHO Expert Committee on Food Additives from: http://www.inchem.org/documents/jecfa/jecmono/v32je02.htm (accessed, June 5, 2016).

[154] C. Perrin, M. Meyer, *Food Chem.*, **77**, 93 (2002).

[155] D.W.M. Sin, Y.C. Wong, C.Y. Mak, S.T. Sze, W.Y. Yao, *J. Food Comp. Anal.*, **19**, 784 (2006).

[156] J.Y. Wang, H.L. Wu, Y.M. Sun, H.W. Gu, Z. Liu, Y.J. Liu, R.Q. Yu, *J. Chromatogr. B*, **947,** 32 (2014).

[157] L.F. Cápitan-Vallvey, M.C. Valencia, E.A. Nicolás, *J. Food Sci*., **68**, 1595 (2003).

[158] L.F. Cápitan-Vallvey, M.C. Valencia, E.A. Nicolás, *Anal. Chim. Acta*, **503**, 179 (2004).

[159] C. De la Fuenta, J.A. Acuña, M.D. Vázquez, M.L. Tascón, M.I. Gómez, P.S. Batanero, *Talanta*, **44**, 685 (1997).

[160] Y. Guan, Q. Chu, L. Fu, T. Wu, J. Ye, *Food Chem.*, **94**, 157 (2006).

[161] E. Bakker, *Anal. Chem.*, **76**, 3285 (2004).

[162] A. Malinauskas, J. Malinauskiene, A. Ramanavicius, *Nanotechnology*, **16**, R51 (2005).

[163] Y. Ohnuki, T. Ohsaka, H. Matsuda, N. Oyama, *J. Elecroanal. Chem.*, **158**, 55 (1983).

[164] A. Volkov, G. Tourillon, D.C. Lacaze, J.E. Dubois, *J. Elecroanal. Chem.*, **115**, 279 (1980).

[165] Y. Sahin, K. Pekmez, A. Yildiz, *J. Appl. Polym. Sci.*, **90**, 2163 (2003).

[166] J. Yue, A.J. Epstein, Z. Zhong, P.K. Gallogher, A. G. MacDiarmid, *Synth. Met.*, **41**, 765 (1991).

[167] Y. Hu, Y. Song, Y. Wang, J. Di, *Thin Solid Films*, **519**, 6605 (2011).

[168] J. Li, H. Xie, L. Chen, *Sens. Actuators, B*, **153**, 239 (2011).

[169] G.Z. Hu, L. Chen, Y. Guo, X.L. Wang, S.J. Shao, *Electrochim. Acta*, **55**, 4711 (2010).

[170] M. Moreno, E. Rincon, J.M. Pèrez, V.M. González, *Biosens. Bioelectron.*, **25**, 778 (2009).

[171] Y.M. Zhang, H. Chen, X. Gao, Z.C. Chen, X.F. Lin, *Biosens. Bioelectron.*, **35**, 277 (2012).

[172] R.N. Goyal, V.K. Gupta, M. Oyama, N. Bachheti, *Talanta*, **72**, 976 (2007).

[173] H. Guan, P. Zhou, X. Zhou, Z. He, *Talanta*, **77**, 319 (2008).

[174] H. Xu, L.P. Zeng, S.J. Xing, G.Y. Shi, Y.Z. Xian, L.T. Jin, *Electrochem. Commun.*, **10**, 1839 (2008).

[175] X. Dai, R.G. Comston, *Anal. Sci.*, **25**, 1221 (2009).

[176] Y. Ni, L. Wang, S. Kokot, *Anal. Chim. Acta*, **412**, 185 (2000).

[177] F. Fusalba, P. Gouérec, D. Villers, D. Bélanger, *J. Electrochem. Soc.*, **148**, A1 (2001).

[178] E. Laviron, *J. Elecroanal. Chem.*, **100,** 263 (1979).

[179] J.E.B. Randles, *Trans. Farady Soc.*, **44**, 322 (1948).

[180] A.H. Shah, W. Zaid, A. Shah, U.A. Rana, H. Hussain, M.N. Ashiq, R. Qureshi, A. Badshah, M.A. Zia, H.B. Kraatzb, *J. Electrochem. Soc.*, **162,** H115 (2015).

[181] L. Agui, M.A. Lopez-Huertas, P. Yanez-Sedeno, J.M. Pingarron, *J. Elecroanal. Chem.*, **414**, 141 (1996).

[182] A.E. Vikraman, Z. Rasheed, L. Rajith, L.A. Lonappan, K. Girish Kumar, *Food Anal. Methods*, **6**, 775 (2013).

[183] R. Guidelli, R.G. Compton, J.M. Feliu, E. Gileadi, J. Lipkowski, W. Schmickler, *Pure Appl. Chem*., **86**, 245 (2014)

[184] A.J. Bard, L.R. Faulkner, *Electrochemical Methods: Fundamentals and Applications*, 2nd Edn., Wiley, New York, **163** (2001).

[185] R.A. Mederos, C. Romeu, R. Filho, O.F. Filho, *Food Chem.*, **123**, 886 (2010).

[186] E. Laviron, *J. Elecroanal. Chem.*, **101**, 19 (1974).

[187] A.E. Vikraman, *Novel Electrochemical and Fluorescence Sensors for Food Additives and Neurotransmitters*, Ph. D. Thesis, CUSAT, Kerala, India, 90 (2015).

[188] E.R. Sherwin, *J. Am. Oil Chem. Soc*., **55**, 809 (1978).

[189] J. Sanhueza, S. Nieto, A. Valenzuela, *J. Am. Oil Chem. Soc.*, **77**, 933 (2007).

[190] O. Bruggemann, A. Visnjevski, R. Burch, P. Patel, *Anal. Chim. Acta*, **504**, 81 (2004).

[191] D.L. Madhavi, R.S. Singhai, P.R. Kulkarni, *Technological aspects of food antioxidants; In: Food Antioxidants: Technological, Toxicological and Health Perspectives,* D.L. Madhavi, S.S. Deshpande, D.K. Salunkhe (Eds.), Marcel Dekker, New York, 159 (1996).

[192] R.D. O'Brien, *Fats and oils: Formulating and processing for applications*, 2nd Edn. CRC press, Florida (1998).

[193] M.Z. Ding, J.K. Zou, *Food Chem.*, **131**, 1051 (2012).

[194] P. Lavin, *Elementary School Guidance and Counselling*, **26**, 115 (1991).

[195] G.J. Van Esch, *Food Chem. Toxicol.*, **24**, 1063 (1986).

[196] Food and Drug Administration, *Food additives permitted for direct addition to food for human consumption* (2013). http://www.accessdata.fda.gov/scripts/cdrh/cfdocs/cfcfr/CFRSearch.cfm?fr=72.185./.

[197] GB2760, *National food safety standard on food additive*, China (2011).

[198] L.F. Captian-Vallvey, M.C. Valencia, E.A. Nicolas, *Analyst*, **126**, 897 (2001).

[199] H.W. Wang, W.M. Liu, *J. Sep. Sci.*, **27**, 1189 (2004).

[200] M. Chen, Q. Xia, M. Liu, Y. Yang, *J. Food Sci*., **76**, 98 (2011).

[201] R. Rodil, J.B. Quintana, G. Basaglia, M.C. Pietrogrande, R.J. Cela, *J. Chromatogr. A*, **1217**, 6428 (2010).

[202] A. Afkhami, A. Shirzadmehr, T. Madrakian, H. Bagheri, *Talanta*, **131**, 548 (2015).

[203] C. Xiaowei, W. Fang, C. Zilin, *Anal. Chim. Acta*, **623**, 213 (2008).

[204] J. Bobacka, A. Lewenstam, A. Ivaska, *J. Electroanal. Chem.*, **489**, 7 (2000).

[205] Z. Wang, F. Yang, H. Zheng, X. Qin, J. Luo, Y. Li, *Analyst*, **139**, 3622 (2014).

[206] D. Lin, B. Xing, *Environ. Sci. Technol.*, **42**, 7254 (2008).

[207] P. Wang, C. Han, F. Zhou, J. Lu, X. Han, Z. Wang, *Sensor. Actuat. B-Chem.*, **224**, 885 (2016).

[208] J. Tang, W. Wang, S. Zheng, Y. Zhang, J. Wei, J. Wang, *Food. Anal. Methods*, **9**, 3044 (2016).

[209] R.P. Caramit, A.S.A. Ara´ujo, D.K. Fogliatto, L.H. Viana, M.A.G. Trindadeb, V.S. Ferreira, *Anal. Methods*, **7**, 3764 (2015).

[210] A. Thomas, A.E. Vikraman, D. Thomas, K. Girish Kumar, *Food Anal. Methods*, **8**, 2028 (2015).

[211] G. Ziyatdinova, K. Os'kina, E. Ziganshina, H. Budnikov, *Anal. Methods*, **7,** 8344 (2015).

[212] G.K. Ziyatdinova, E.R. Ziganshina, K.S. Os'kina, H.C. Budnikov, *J. Anal. Chem.*, **69**, 750 (2014).

[213] T.A. de Araújo, A.M. Barbosa, L.H. Viana, V.S. Ferreira, *Colloids Surf. B Biointerfaces*, **79**, 409 (2010).

[214] E. Laviron, *J. Elecroanal. Chem.*, **101**, 19 (1979).

[215] C.F. Timberlake, P. Bridle, J. Walford, *Developments in food colours I*, J. Walford Edn., Elsevier Applied Science Publishers, London, 115 (1980).

[216] J. Coulson, *Synthetic organic colours for food: Developments in food colours*, J. Walford Edn., Elsevier Applied Science Publishers, London, 47 (1980).

[217] J.L. Love, *N. Z. J. Sci*., **27**, 113 (1984).

[218] K.S. Minioti, C.F. Sakellariou, N.S. Thomaidis, *Anal. Chim. Acta*, **583**, 103 (2007).

[219] L.H. Ahlström, C.S. Eskilsson, E. Björklund, *Trends Anal. Chem*., **24**, 49 (2005).

[220] J. Zhang, M.L. Wang, C. Shentu, W.C. Wang, Z.D. Chen, *Food Chem.*, **160,** 11 (2014).

[221] P. Mpountoukas, A. Pantazaki, E. Kostareli, P. Christodoulou, D. Kareli, S. Poliliou, *Food Chem. Toxicol.*, **48**, 2934 (2010).

[222] T.N. Nagaraja, T. Desiraju, *Food Chem. Toxicol.*, **31**, 41 (1993).

[223] C. Hawley, R.E. Buckley, *J. Orthomolecular Psychiatry*, **5**, 129 (1976).

[224] G. Talaska, M. Al-Zoughoo, *J. Environ. Sci. Health C Environ. Carcinog. Ecotoxicol. Rev.*, **21**, 133 (2003).

[225] M.S. Khehra, H.S. Saini, D.K. Sharma, B.S. Chadha, S.S. Chimni, *Dyes Pigm.*, **70**, 1 (2006).

[226] E.C. Vidotti, J.C. Cancino, C. Oliveira, M. Rollemberg, *Anal. Sci.*, **21,** 149 (2005).

[227] N. Yoshioka, K. Ichihashi, *Talanta*, **74**, 1408 (2008).

[228] EFSA, Scientific Opinion on the Re-evaluation of Ponceau 4R (E 124) as a Food Additive, *EFSA J.* **7,** 1328 (2009).

[229] http://www.fda.gov/ForIndustry/ColorAdditives/ColorAdditiveInventories/ ucm115641. htm.

[230] P. Wang, X. Hu, O. Cheng, X. Zhao, X. Fu, K. Wu, *J. Agric. Food. Chem.*, **58**, 12112 (2010).

[231] F. Feng, Y. Zhao, W. Yong, L. Sun, G. Jiang, X. Chu, *J. Chromatogr. B*, **879**, 1813 (2011).

[232] M. Ma, X. Luo, B. Chen, S. Su, S. Yao, *J. Chromatogr. A*, **1103**, 170 (2006).

[233] M. Ryvolova, P. Taborsky, P. Vrabel, P. Krasensky, J. Preisler, *J. Chromatogr. A*, **1141**, 206 (2007).

[234] Y. Ni, Y. Wang, S. Kokot, *Talanta*, **7**, 432 (2009).

[235] A. Zalacain, S. Ordoudi, I. Blazquez, E. Diaz-Plaza, M. Carmona, M. Tsimidou, *Food Addit. Contam.*, **22**, 607 (2005).

[236] T. Wei, X. Huang, Q. Zeng, L. Wang, *J. Electroanal. Chem.*, **743,** 105 (2015).

[237] J. Han, Y. Zhuo, Y.Q. Chai, Y. Xiang, R. Yuan, *Anal. Chem*., **87,** 1669 (2015).

[238] T. Zheng, Q. Zhang, S. Feng, J.J. Zhu, Q. Wang, H. Wang, *J. Am. Chem. Soc*., **136**, 2288 (2014).

[239] Y. Lin, Q. Zhou, Y. Lin, D. Tang, R. Niessner, D. Knopp, *Anal. Chem*., **87,** 8531 (2015).

[240] Y.S. Fang, X.J. Huang, L.S. Wang, J.F. Wang, *Biosens. Bioelectron*., **64**, 324 (2015).

[241] S. Jesny, Z. Rasheed, K. Girish Kumar, *Ionics*, **23**, 1533 (2017).

[242] L. Zhang, X. Lin, *Anal. Bioanal. Chem*., **382**, 1669 (2005).

[243] W. Ma, D.M. Sun, *Acta Phys. Chim. Sin.*, **23,** 332 (2007).

[244] R.S. Deinhammer, M. Ho, J.W. Anderegg, M.D. Porter, *Langmuir*, **10**, 1306 (1994).

[245] C. Wang, C. Li, F. Wang, C. Wang, *Microchim. Acta*, **155,** 365 (2006).

[246] J. Wang, S. Zhang, Y. Zhang, *Anal. Biochem*., **396**, 304 (2010).

[247] E. Laviron, *J. Electroanal. Chem. Interfacial Electrochem*., **52**, 355 (1974).

[248] S.T. Cyriac, D. Thomas, A.E. Vikraman, K. Girish Kumar, *J. Electrochem. Soc*.**, 163**, B683 (2016).

[249] A.E. Vikraman, D. Thomas, S.T. Cyriac, K. Girish Kumar, *J. Electrochem. Soc*., **161**, B305 (2014).

[250] W.M. Si, W. Lie, Y.X. Zanga, M.Z. Xia, F.Y. Wang, Q.L. Hao, *Electrochim. Acta*, **85**, 295 (2012).

[251] L. Chen, C. Yuan, H. Dou, B. Gao, S. Chen, X. Zhang, *Electrochim. Acta*, **54**, 2335 (2009).

[252] E. Laviron, L. Roullier, C. Degrand, *J. Electroanal. Chem*., **112**, 11 (1980).

[253] S. Combeau, M. Chatelutu, O. Vottori, *Talanta*, **56**, 115 (2002).

[254] S. Chanlon, L. Joly-Pottuz, M. Chatelutu, O. Vottori, J.L. Cretier, *J. Food Comp. Anal*., **18**, 503 (2005).

[255] X. Yang, H. Qin, M. Gao, H. Zhang, *J. Sci. Food Agri*., **91**, 2821 (2011).

[256] Y. Zhang, X. Zhang, X. Lu, J. Yang, K. Wu, *Food Chem*., **122**, 909 (2010).

[257] Y. Tao, W.E. Bentley, T.K. Wood, *Biotechnol. Bioeng*., **90**, 85 (2005).

[258] M. Panizza, G.Cerisola, *Electrochim. Acta*, **48**, 3491 (2003).

[259] P.F. Salazar, S. Kumar, B.A. Cola, *J. Electrochem. Soc*., **159**, B483 (2012).

[260] https://en.wikipedia.org/wiki/Charge_transfer_coefficient.

[261] M. Chao, X. Ma, *Int. J. Electrochem. Sci*., **7**, 6331 (2012)

[262] Z. Mai, X. Zhao, X. Zou, *Talanta*, **81**, 167 (2010)

[263] S. Zhu, H.J. Li, W.X. Niu, G.B. Xu, *Biosens. Bioelectron*., **25**, 940 (2009).

[264] S.P. Alves, D.M. Brum, É.C.B. de Andrade, A.D.P. Netto, *Food Chem.*, **107**, 489 (2008).

[265] J. Kirschbaum, C. Krause, S. Pfalzgraf, H. Bruckner, *Chromatographia*, **57**, S-115 (2003).

[266] https://en.wikipedia.org/wiki/Green_S

[267] F.I. De Andrade, M.I.F. Guedes, I.G.P. Vieira, F.N.P. Mendes, P.A.S. Rodrigues, C.S.C. Maia, M.M.M. Ávila, R.L. de Matos, *Food Chem.*, **157**, 193 (2014).

[268] A. Downham, P. Collins, *Int. J. Food Sci. Technol*., **35**, 5 (2000).

[269] EC, *Directive of the European Parliament and of the Council 94/36/EC of June 30, 1994 on Colors for Use in Foodstuffs*, *Official J*., L237, 13, 10/9/1994.

[270] European food safety authority, *EFSA J.*, **8**, 32 (2010).

[271] H. Oka, Y. Ikaia, N. Kawamura, M. Yamada, H. Inoue, *J. Chromatogr*. **411**, 437(1987).

[272] H. Oka, Y. Ikaia, T. Ohno, N. Kawamura, J. Hayakawa, K. Harada, M. Suzuki, *J. Chromatogr. A,* **674,** 301 (1994).

[273] C.C. Blanco, A.M.G. Campana, F.A. Barrero, *Talanta*, **43**, 1019 (1996).

[274] V. Gianotti, S. Angioi, F. Gosetti, E. Marengo, M.C. Gennaro, *J. Liq. Chromatogr. Relat. Technol*,. **28**, 923 (2005).

[275] Y. Ni, X. Gong, *Anal. Chim. Acta*, **354,** 163 (1997).

[276] E. Dinc, E. Baydan, M. Kanbur, F. Onur, *Talanta*, **58**, 579 (2002).

[277] H. Liu, T. Zhu, Y. Zhang, S. Qi, A. Huang, Y. Sun, *J. Chromatogr. A*, **718**, 448 (1995).

[278] C.O. Thompson, V.C. Trenerry, *J. Chromatogr. A*, **704**, 195 (1995).

[279] Q.C. Chen, S.F. Mou, X.P. Hou, J.M. Riviello, Z.M. Ni, *J. Chromatogr. A*, **827**, 73 (1998).

[280] M.A. Prado, H.T. Godoy, *J. Liq. Chromatogr. Relat.Technol.*, **25**, 2455 (2002).

[281] J. Kirschbaum, C. Krause, S. Pfalzgraf, H. Bruckner, *Chromatographia*, **57**, S115 (2003).

[282] E. Palecek, *Nature*, **188**, 656 (1960).

[283] J. Wang, T. Golden, R. Li, *Anal. Chem*., **60** 1642 (1988).

[284] J. Wang, *Electroanalysis*, **3**, 255 (1991).

[285] F. Zhang, S. Gu, Y. Ding, L. Zhou, Z Zhang, L. Li, *J. Electroanal. Chem*., **698**, 25 (2013).

[286] A.M. Yu, H.L. Zhang, H.Y. Chen, *Electroanalysis*, **9**, 788 (1997).

[287] Y. Li, X. Liu, W. Wei, *Electroanalysis*, **23**, 2832 (2011).

[288] J. Inczedy, T. Lengyel, A. M. Ure, In; *Compendium of Analytical Nomenclature*, H. Freiser, G. H. Nancollas (Eds), 3rd Edn., Blackwell Science, Oxford, **18**, 41 (1998)

[289] K.S. Minioti, C.F. Sakellariou, N.S. Thomaidis, *Anal. Chim. Acta.*, **583**, 103 (2007).

[290] N. Yoshioka, K. Ichihashi, *Talanta*, **74**, 1408 (2008).

[291] I. Stachová, I. Lhotská, P. Solich, D. Satínský, *Food Addit. Contam. Part A*, **33**, 1139 (2016).

[292] O.W. Lau, M.M.K. Poon, S. Mok, F.M.Y. Wong, S.F. Luk, *Int. J. Food Sci. Technol*., **30**, 793 (1995).

[293] Y. Li, Z. Ye, P. Luo, B. Ye, *Anal. Methods*, **6**, 1928 (2014).

[294] E. Laviron, *J. Electroanal. Chem.*, **100**, 263 (1979).

[295] D.A. Hall. M. Sakuma, P.J. Elving, *Electrochim. Acta*, **11**, 337 (1966).

[296] I. Němcová, I. Němec, *Chem. Zvesti.*, **26**, 115 (1972).

[297] C. Khosla, Y. Tang, *Science***, 308**, 367 (2005).

[298] I. Chopra, M. Roberts, *Microbiol. Mol. Biol. Rev*., **65**, 232 (2001).

[299] W.A. Moats, R.H. Khan, *J. Agric. Food Chem.*, **43**, 931 (1995).

[300] A.D. Dayan, *Vet. Microbiol*., **35**, 213 (1993).

[301] A.E. Vandenbogaard, E.E. Stobberingh, *Int. J. Antimicrob. Agents*, **14**, 327 (2000).

[302] P. Navratilova, I. Borkovkova, M. Drackova, B. Janstova, L. Vorlova, *Czech J. Food Sci.*, **27**, 379 (2009).

[303] F.K. Muriuki, W.O. Ogara, F.M. Njeruh, E.S. Mitema, *J. Vet. Sci*., **2**, 97 (2001).

[304] K. De Wasch, L. Okerman, H. De Brabander, J.V. Hoof, P.D. Backer, *Analyst*, **123**, 2737 (1998).

[305] A.L. Pena, C.M. Lino, L.N. Silveria, *J. AOAC Int.*, **82**, 55 (1999).

[306] S.M. Croubels, K.E. Vanoosthyze, C.H. Vanpeteghem, *J. Chrom. B*, **690**, 173 (1997).

[307] M. Jeon, I.R. Paeng, *Anal. Chim. Acta*, **626**, 180 (2008).

[308] Z. Ye, H.S. Weinberg, M.T. Meyer, *Anal. Chem.*, **79**, 1135 (2007).

[309] L. Monser, F. Darghouth, *J. Pharm. Biomed. Anal*., **23**, 353 (2000).

[310] K. Ng, S.W. Linder, *J. Chromatogr. Sci.*, **41**, 460 (2003).

[311] P. Kowalski, *J. Pharm. Biomed. Anal*., **47**, 487 (2008).

[312] S. Han, E. Liu, H. Li, *Luminescence*, **21**,106 (2006).

[313] P. Mulvaney, *Langmuir*, **12**, 788 (1996**)**.

[314] H. Li, L. Rothberg, *J. Am.Chem. Soc*., **126**, 10958 (2004).

[315] X.J. Xue, F. Wang, X.G. Liu, *J. Am. Chem. Soc*., **130**, 3244 (2008).

[316] L. Li, B. Li, Y. Qi, Y. Jin, *Anal. Bioanal. Chem*., **393**, 2051 (2009).

[317] J.J. Storhoff, A.A. Lazarides, C.A. Mirkin, R.L. Letsinger, R.C. Mucic, G.C. Schatz, *J. Am. Chem. Soc*., **122**, 4640 (2000**)**.

[318] L. Li, B. Li, *Analyst*, **134**, 1361 (2009).

[319] W.R. Chen, C.H. Huang, *Environ. Sci. Technol*., **43**, 401 (2009).

[320] D. Mastropaolo, D.A.Powers, J.A. Potenza, H. Schugar, *J. Inorg. Chem*., **15**, 1444 (1976).

[321] P.M. Arnal, M. Comotti, F. Schiith, *Angew. Chem. Int. Ed*., **45**, 8224 (2006).

[322] F.X. Zhang, L. Han, L.B. Israel, J.G. Daras, M.M. Maye, N.K. Ly, C. Zhong, Analyst, **127**, 462 (2002).

[323] A.C. Templeton, W.P. Wuelfing, R.W. Murray, *Acc. Chem. Res*., **33**, 27 (2000).

[324] P. Kannan, S.A. John, *Nanotechnology*, **19**, 85602 (2008).

[325] J.L. Rufino, F.C.B. Fernandes, M.S. Ruy, H.R. Pezza, L. Pezza, *Ecl. Quim, São Paulo*, **35**, 139 (2010).

[326] A.J. Abdulghani, H.H. Jasim, A.S. Hassan, *Int. J. Anal. Chem.*, DOI:org/10.1155/2013/305124 (2013)

[327] D. Vega, L. Agüí, A. González-Cortés, P. Yáñez-Sedeño, J.M. Pingarrón, *Anal. Bioanal. Chem.*, **389**, 951 (2007).

[328] T. Charoenraks, S. Chuanuwatanakul, K. Honda, Y. Yamaguchi, O. Chailapakul, *Anal. Sci.*, **21**, 241 (2005).

[329] N.T.K. Thanh, Z. Rosenweig, *Anal. Chem*., **74**, 1624 (2002).

[330] L. Xu, B. Li, Y. Jin, *Talanta*, **84**, 58 (2011).

[331] N.P. Sachan, C.M. Gupta, *Talanta*, **27**, 457 (1980).

[332] P.P. Silva, W. Gerra, J.N. Silveira, A.M.C. Ferreira, T. Bortolotto, F.L. Fischer, H. Terenzi, A. Neves, E.C. Maia, *Inorg. Chem*., **50**, 6414 (2011).

[333] http://www.chemspider.com/Chemical-Structure.4953985.html

[334] X. Chen, K. Wu, Y. Sun, X. Song, *Sens. Actuator B Chem*., **185**, 582 (2013).

[335] J. Li, X.J. Wang, H. Duan, Y. Wang, Y. Bu, C. Luo, *Talanta*, **147**, 169 (2016).

[336] ESFA, *ESFA Panel on Food: Scientific Opinion on the Re-evaluation of Sunset Yellow FCF (E 110) as Food Additive on Request from the European Commission*, *EFSA*, *J* **7** 1330 (2009).

[337] M. Gomez, V. Arancibia, C. Rojas, E. Nagles, *Int. J. Electrochem. Sci*., **7**, 7493 (2012).

[338] L. Yu, M. Shi, X. Yue, L. Qu, *Sens. Actuator B Chem*., **209**, 1 (2015).

[339] J. Wang, B. Yang, H. Wang, P. Yang, Y. Du, *Anal. Chim. Acta*, **893**, 41 (2015).

[340] R. Sarıkaya, M. Selvi, F. Erkoç, *Chemosphere*, **88**, 974 (2012).

[341] X. Pan, P. Qin, R. Liu, J. Wang, *J. Agric. Food. Chem*., **59**, 6650 (2011).

[342] E. Dinc, E. Baydan, M. Kanbur, F. Onur, *Talanta*, **58**, 579 (2002).

[343] A.V. Jager, F.G. Tonin, M.F.M. Tavares, *J. Sep. Sci*., **28**, 957 (2005).

[344] R. Sahraei, A. Farmany, S.S. Mortazavi, *Food Chem*., **138**, 1239 (2013).

[345] Y.Z. Song, J.M. Xu, J.S. Lv, H. Zhong, Y. Ye, J.M. Xie, *Russ. J. Phys. Chem. A*., **86**, 303 (2012).

[346] R. Bandi, B.R. Gangapuram, R. Dadigala, R. Eslavath, S.S. Singh, V. Guttena, *RSC Adv*., **6**, 28633 (2016).

[347] S. Sahu, B. Behera, T.K. Maiti, S. Mohapatra, *Chem. Commun*., **48**, 8835 (2012).

[348] L. Bao, Z.L. Zhang, Z.Q. Tian, L. Zhang, C. Liu, Y. Lin, B. Qi, D.W. Pang, *Adv. Mater*., **23**, 5801 (2011).

[349] S. Zhuo, M. Shao, S.T. Lee, *ACS Nano.*, **6**, 1059 (2012).

[350] Q.L. Zhao, Z.L. Zhang, B.H. Huang, J. Peng, M. Zhang, D.W. Pang, *Chem. Commun*., **41**, 5116 (2008).

[351] V.N. Mehta, S. Jha, S.K. Kailasa, *Mater. Sci. Eng. C*., **38**, 20 (2014).

[352] Y. Liu, N. Xiao, N. Gong, H. Wang, X. Shi, W. Gu, L. Ye, *Carbon*, **68,** 258 (2014).

[353] A. Sachdev, P. Gopinath, *Analyst*, **140**, 4260 (2015).

[354] W. Dong, S. Zhou, Y. Dong, J. Wang, X. Ge, L. Sui, *Luminescence*, **30**, 867 (2015).

[355] U. Sivasankaran, S. Jesny, A.R. Jose, K. Girish Kumar, *Anal Sci*., 33, 281 (2017).

[356] X. Yang, Y. Zhuo, S. Zhu, Y. Luo, Y. Feng, Y. Dou, *Biosens. Bioelectron.*, **60**, 292 (2014).

[357] H. Xu, X. Yang, G. Li, C. Zhao, X. Liao, *J. Agric. Food. Chem*., **63**, 6707 (2015).

[358] Y.P. Sun, B. Zhou, Y. Lin, W. Wang, K.A.S. Fernando, P. Pathak, M.J. Meziani, B.A. Harruff, X. Wang, H. Wang, P.G. Luo, H. Yang, M.E. Kose, B. Chen, L.M. Veca, S. Xie, *J. Am. Chem. Soc*., **128**, 7756 (2006).

[359] J. Lu, J.X. Yang, J. Wang, A. Lim, S. Wang, K.P. Loh, *ACS Nano*., **3**, 2367 (2009).

[360] H. Ming, Z. Ma, Y. Liu, K. Pan, H. Yu, F. Wang, Z. Kang, *Dalton Trans*., **41**, 9526 (2012).

[361] C. Wang, D. Sun, K. Zhuo, H. Zhang, J. Wang, *RSC Adv*., **4,** 54060 (2014).

[362] Y. Liu, Y. Liu, S.J. Park, Y. Zhang, T. Kim, S. Chae, M. Park, H.Y. Kim, *J. Mater. Chem. A*., **3,** 17747 (2015).

[363] J. Hou, J. Li, J. Sun, S. Ai, M. Wang, *RSC Adv*., **4**, 37342 (2014).

[364] R.S. Razmara, A. Daneshfar, R. Sahrai, *J. Ind. Eng. Chem.*, **17,** 533 (2011).

[365] Y.S. Al-Degs, *Food Chem.*, **117,** 485 (2009).

[366] A.H. El-Sheikh, Y.S. Al-Degs, *Dyes Pigm.*, **97** 330 (2013).

[367] C.A. Parker, *Photoluminescence of Solutions*, Elsevier, New York (1968).

[368] N. Shao, Y. Zhang, S.M. Cheung, R.H. Yang, W.H. Chan, T. Mo, K. Li, F. Liu, *Anal. Chem.*, **77**, 7294 (2005).

[369] A.R. Jose, U. Sivasankaran, S. Menon, K. Girish Kumar, *Anal. Methods*, **8**, 5701 (2016).

.....ꕥ.....

List of Publications and Presentations

[1] **S.T. Cyriac**, D. Thomas, A.E. Vikraman, K. Girish Kumar, Electrochemical sensor for propyl gallate, based on synergic effect of gold nanoparticles and poly (p-aminobenzenesulfonic acid), *Journal of the Electrochemical Society*, **14**, B683 (2016).

[2] U. Sivasankaran, **S.T. Cyriac**, S. Menon, K. Girish Kumar, Fluorescence turn off sensor for brilliant blue FCF - an approach based on inner filter effect, *Journal of Fluorescence,* **27,** 69 (2017).

[3] A.E. Vikraman, D. Thomas, **S.T. Cyriac**, K. Girish Kumar, Kinetic and thermodynamic approach in the development of a voltammetric sensor for sunset yellow, *Journal of the Electrochemical Society*, **161**, B305 (2014).

[4] D. Thomas, L. Lonappan, L. Rajith, **S.T. Cyriac**, K. Girish Kumar, Quantum Dots (QDs) based fluorescent sensor for the selective determination of nimesulide, *Journal of Fluorescence*, **23**, 473 (2013).

[5] T. Jos, D. Thomas, **S.T. Cyriac**, M. Jacob, K. Girish Kumar, Effect of anionic surfactant on the reduction of tinidazole at a gold nanaoparticle modified glassy carbon electrode. *Indo American Journal of Pharmaceutical Research*, **3**, 8434 (2013).

Conference papers

[1] One-pot synthesis of carbon dots for fluorescence turn-off detection of sunset yellow (International Symposium on New Trends in Applied Chemistry, Sacred Heart College, Thevara, February 2017).

[2] Development of voltammertic sensor for the determination of green S using poly (glycine) modified glassy carbon electrode (Current trends in Chemistry, CUSAT, February 2017).

[3] Determination of a synthetic food colorant cochineal red A using poly (L-cysteine) modified glassy carbon electrode (Recent Advances in Chemistry, Vimala College, Thrissur, January 2017).

[4] Development of voltammertic sensor for the determination of ponceau 4R using poly (L-cysteine) modified glassy carbon electrode (International Conference on Material for the Millennium, CUSAT, January 2016).

[5] Electroanalytical determination of a synthetic antioxidant propyl gallate (Current trends in Chemistry, CUSAT, January 2014).

[6] Development of poly (bromophenol blue) modified glassy carbon electrode based sensors for the determination of synthetic antioxidant *tert*-butylhydroquinone (23rd Swadeshi Science Congress, Mahatma Gandhi University, Kottayam, November 2013).

[7] Nanoparticle probe for the detection of tetracycline (International Conference on Biologically Active Molecules, Gandhigram Rural Institute – Deemed University, Tamil Nadu, March 2012).

.....ഠാര.....